AD-A248 336

(1)

Department of the Navy

Office of Naval Research

Electrochemistry in Colloids and Dispersions

DTIC
ELECTE
MAR 27 1992
S D
D

Volume II

SOLUTE DISTRIBUTION, DIFFUSION, AND TRANSPORT

COLLOIDAL METALS

This document has been approved for public release and sale; its distribution is unlimited.

A final report to the Department of the Navy, compiled by the

Division of Colloid and Surface Chemistry

of the American Chemical Society

4 February 1992

GRANT NO. N00014-91-J-1616
MODIFICATION NO. P00001

92-06923

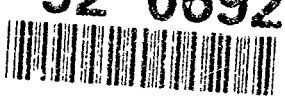

92 3 17 045

Best
Available
Copy

ABSTRACT

This report summarizes the current status of experimental and theoretical studies which address fundamental and applied aspects of electrochemistry in colloids and dispersions. The range of such microheterogeneous fluids examined includes micellar solutions, microemulsions, emulsions, latexes, and dispersions of solids in liquids. Several broad subtopics are described. These topics include electroanalytical methods and applications, solute distribution, diffusion, and transport, electrosynthesis and electrocatalysis, polymers and latexes, and colloidal metals and semiconductors.

This report is presented in three volumes, I, II, and III.

Accesion For	
NTIS CRA&I	☑
DTIC TAB	☐
Unannounced	☐
Justification	
By	
Distribution /	
Availability Codes	
Dist	Avail and / or Special
A-1	

Statement A per telecon
Dr. Robert Nowak ONR/Code 1113
Arlington, VA 22217-5000

NWW 3/26/92

CONTENTS

CONTENTS

CONTENTS

(11) ELECTROCHEMICAL FORMATION OF ORGANIC PIGMENT THIN FILMS BY DISRUPTION OF MICELLES

T. SAJI, M. GOTO, F. TAKEO, T. SUGIMOTO and T. OHNUMA
Department of Chemical Engineering, Tokyo Institute of Technology, Tokyo 152, Japan

ABSTRACT

Mechanism of the formation of organic pigment thin films by controlled potential electrolysis of an aqueous solution containing non-ionic surfactant with a ferrocenyl moiety and dispersed organic pigment was examined. The amount of β-type copper phthalocyanine film was proportional to the root of electrolysis time, which suggests that the rate of film growth is controlled by diffusion of the pigment particles. The results of the adsorption isotherms of the surfactants and the effect of electrolysis potential on film formation shows that electrolysis of the surfactant plays to decrease free surfactant (not adsorbed on the surface of pigment) to less than the critical micelle concentration (cmc) and to cause desorption of adsorbed surfactant on the pigment surface, which leads to the depositon of the pigment particles on the electrode.

INTRODUCTION

Recently, we have presented a novel technique for electrochemical formation of organic thin films by disruption of micellar aggregates by cationic surfactants having a ferrocenyl moiety (micelle disrution method, MD method).[1-3] Furthermore, we have presented the preparation of organic pigment thin films by this method using nonionic surfactant with ferrocenyl moiety (FPEG600, Fig. 1).[4] Later studies show that these organic pigments dispersing by the surfactant and not being incorporated in the micelles.[5,6] The pigment particles are released when the surfactants adsorbed on the particles are electrochemically oxidized and finally the particles deposit on the electrode (Fig. 2). Adsorption behavior of the surfactant has suggested that these films are prepared by the desorption of the surfactant from the pigment surface due to the oxidation of unadsorbed surfactant.[6] However, the direct evidence for this mechanism and the rate of film formation have not been reported. In the present paper, we have measured the amount of copper phthalocyanine film versus electrolysis time and electrolysis potential to clarify the details of the film-formation mechanism.

EXPERIMENTAL PROCEDURE

Film formation

having differnt length of poly(oxyethlene) chain were used (Fig. 1). As a pigment, β-type copper phthalocyanine (Dainichiseika Color & Chemicals, β-CuPc) was used. The transmission microscopy image of this pigment particles is given in Fig. 3. The size of this particle is approximately 0.1-0.2 μm in length. The solutions of this pigment were prepared in the following manner. An aqueous solution containing 2.0 mM surfactant, 0.1 M LiBr, and known amounts of the organic pigment was sonicated for 10 min and stirred for three days. The amount of pigment deposited on ITO electrode in film growth experiment was estimated by the absorption of the aqueous solution which was obtained by redispersing the film into an aqueous solution of 3 mM Brij 35. Film formation was undertaken by the controlled-potential electrolysis of this solution. The potential of the ITO was maintained at +0.50 V vs SCE for FPEG solution by considering the half-wave potentials of these surfactants (Table I). The obtained films were washed with distilled water just after electrolysis.

Adsorption isotherm.

68.9 mg of CuPc(10 mM) was added to 12 mL of FPEG solution. This solution was sonicated for 15 min, stirred for three days and centrifuged (Hitachi SCP 70H) at 40000 rpm (110000g) for 40 min. The surfactant concentration in the supernatant (C_{eq}) was detemined by the colorimetric

technique.[7]

The values of critical micelle concentration (cmc) were determined by the surface tension method (Table I).

RESULTS AND DISCUSSION

Properties of surfactants

Table I shows the physicochemical properties of the three surfactants. The cyclic voltammograms of these solutions showed a reversible one-electron step. Half-wave potentials, $E_{1/2}$, of the surfactants were obtained by rotating disk electrode. The cmc value was in the order of FPEG1540 < FPEG600 < FPEG1000 (Table I).

Typical representative photograph and scanning electron micrograph of β-CuPc thin film prepared by this method are shown in Fig. 4 and 5, which show that this film is transparent and has uniform thickness.

Rate of film growth

Film thickness of β-CuPc increases with electrolysis time (Fig. 6). The amount of film is proportinal to the amount of pigment added to the solution. The log plot analysis shows that it depends approximately on root of electrolysis time, which suggests that the rate is controlled by the diffusion of pigment particles.[8] Most of

organic pigment films become more than 1 um in thickness after 30 - 60 min electrolysis.[6] The thickness increased to more than 10 μm during overnight electrolysis.

Adsorption isotherm of surfactants

A type of adsorption isotherm commonly observed in adsorption from solutions of surfactants is the Langumuir--type isotherm, expressed by the equation:[9]

$$\Gamma = (\Gamma_M \cdot K \cdot C_{eq})/(1 + K\, C_{eq})$$

where Γ is the surface concentration of free (equilibrium) surfactant, in moles m^{-2}, Γ_M the surface concentration of the maximum adsorbed surfactant at monolayer adsorption, C_{eq} the concentration of the free surfactant in the liquid phase at adsorption equilibrium, K an equilibrium constant of the surfactant between the surface and the liquid phase.

Adsorption behaviour of FPEG on β-CuPc has been reported by us.[6] Figure 7 shows adsorption isotherm of FPEG on β-CuPc(1) particles, where the amount of the pigment are kept at 10 mM all through this experiment. The pigment particles in low concentration of FPEG600 (closed circle in Fig. 7) are sedimented without centrifugation. This sedimentation suggests that the pigment particles deposite when the concentration of free surfactant (C_{eq}) decreases to less than the cmc. The surface coverage is seen to increase

with increasing concentration of the free surfactant until a saturation value of 2.0 umol m^{-2} (Γ_M) is attained at slightly above the critical micelle concentration of FPEG (8 uM). The value of Γ_M gives an area per molecule of 83 A^2 $molecule^{-1}$. This value approximately closes to those for similar surfactants[10-14], which provides an evidence for monolayer adsorption at saturation.

The isotherms of FPEG1000 and 1500 were similar with that of FPEG600.

Effect of electrolysis potential on film formation

Amount of β-CuPc film deposited on the ITO electrode during 20 min electrolysis was plotted against the electrolysis potential (Fig. 8). The formation of the film starts at more positive potential than the half-wave potential of the surfactant by approximately 0.1 V.

It is reasonable to prsume that only free surfactant is oxidized to its cation at the electrode. Following equation is derived by Nernst equation based on the above assumption:

$$E_f = E_{1/2} - (RT/nF)\ln[C_{eq}/(C_{eq}^{o} - C_{eq})]$$

where E_f is electrolysis potential, $E_{1/2}$ half-wave potential of free surfactant, C_{eq}^{o}, C_{eq} the concentration of free surfactant in the vicinity of the electrode before and after

electrolysis, respectively. The diffusion coefficient of the surfactant is assumed to be equal to that of its oxidant.

The critical concentration of free surfactant at film formation (C_{eq}) can be calculated by the most negative (critical) electrolysis potential where film formation starts using above equation. The value of C_{eq}^{o} was estimated by the difference between total concentration of the surfactant (C_o) and the maximum adsorbed surfactant. The values of C_{eq} are colse to those of the cmc (Table I). The order of FPEG1540 < FPEG600 < FPEG1000 is the same as that of the cmc. These results gives the direct evidence that electrolysis of sufactant plays to decrease free surfactant to less than the cmc and to desorb adsorbed surfactant, which leads to deposition of the pigment particles. This conclusion is consistent with the results of adsorption isotherm of the surfactant

These results support following mechanism of the film formation:[6]

(i) The free surfactant (FPEG) diffuses to the electrode surface and is oxidized to its cation ($FPEG^{+}$). The concentration of the free surfactant in the vicinity of electrode decreases to less than the cmc.

(ii) The surfactants adsorbed on the pigment are desorbed from the pigment surface in order to satisfy the adsorption equilibrium. This desorption leads to the deposition of pigment on the electrode, which occurs

efficiently when the concentration of the free surfactant decreases to less than approximately the cmc.

(iii) After the electrode is covered with the pigment film, the free surfactant diffuses in the film, owing to the existence of small apace among the particles in the film, eventually reaches the electrode surface, and is electrolyzed. The concentration of the free surfactaactant in the vicinity of the film is kept at less than the cmc so that the film continues to grow for a long period to respectable thickness.

ACKNOWLEDGEMENTS

We thank R. Ohoki for the electron micrograph data. This work partially supported by a Grant-in-aid for Scientific Research from the Ministry of Education, Science and Culture (nos: 01604540 and 02205046), The Kurata Foundation, and Matsuda Foundation.

REFERENCES

1. Hoshino, K.; Saji, T. J. Am. Chem. Soc. 1987, 109, 5881-5883.
2. Hoshino, K.; Saji, T. Chem. Lett. 1987, 1439-1442.
3. Hoshino, K.; Goto, M.; Saji. Chem. Lett. 1987, 547-550.
4. Saji, T. Chem. Lett. 1988, 693-696.
5. Saji, T; Ishii, Y. J. Electrochem. Soc. 1989, 136,

2953-2956.

6. Saji, T; Hoshino, K; Ishii, Y; Goto, M. J. Am. Chem. Soc. 1991, 113, 450-456.

7. Baleux, B, C. R. Acad. Sci. Ser.B. 1972, 72, 1617.

8. Bard, A.J.; Faulkner, L.R. Electrochemical Methods; Wiley; New York, 1980, p200.

9. Rosen, M. J. In Surfactants and Interfacial Phenomina; Wiley, New York, 1978; pp. 36-38.

10. Kronberg, B.; Kall, L.; Stenius, P. J. Disp. Sci. Tech, 1981, 2, 215-232.

11. Furlong, D.N.; Aston, J.R. Colloids and Surfaces, 1982, 4, 121-129.

12. Kronberg, B.; Stenius, P.; Thorssell, Y. Colloids and Surfaces, 1984, 12, 113-123.

13 Partyka, S.; Zaini, S.; Lindheimer, M.; Brun, B. Colloids and Surfaces, 1984, 12, 255-270.

14. Boomgaard, Th.V.D.; Tadros, Th.F.; Lyklema, J. J. Colloid Interface Sci., 1987, 116, 8-16.

Table 1. Critical micelle concentration (cmc), half-wave potential ($E_{1/2}$) and total concentration of (C_o) of surfactants, and critical electrolysis potential of film formation (E_f) and critical concentration of free surfactant (C_{eq}) to lead deposition of β-CuPc particles

Surfactant	cmc (μM)	$E_{1/2}$ (V vs. SCE)	C_o (mM)	E_f (V vs. SCE)	C_{eq} (μM)
FPEG600	8	0.210	2.0	0.310	22
			3.0	0.330	20
FPEG1000	18	0.202	1.2	0.278	27
			1.5	0.290	27
			2.0	0.308	21
FPEG1500	6	0.166	0.5	0.230	7
			0.7	0.265	10
			1.0	0.290	2

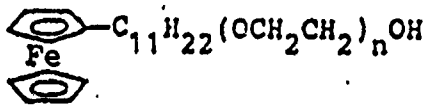

n = 12.3 FPEG600

n = 23.6 FPEG1000

n = 34.2 FPEG1500

Fig. 1

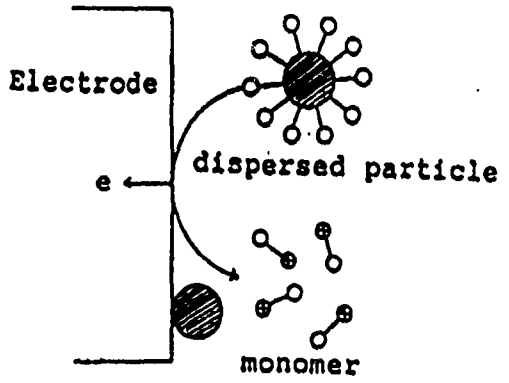

Fig. 2

Fig. 1. Molecular structures of non-ionic surfactants with a ferrocenyl moiety.

Fig. 2. Mechanism of formation of pigment film.

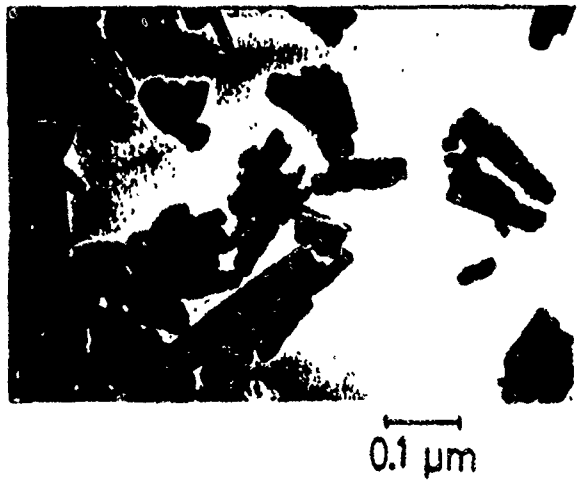

Fig. 3. Transmission electron micrograph of β-type copper phthalocyanine (β-CuPc) particles.

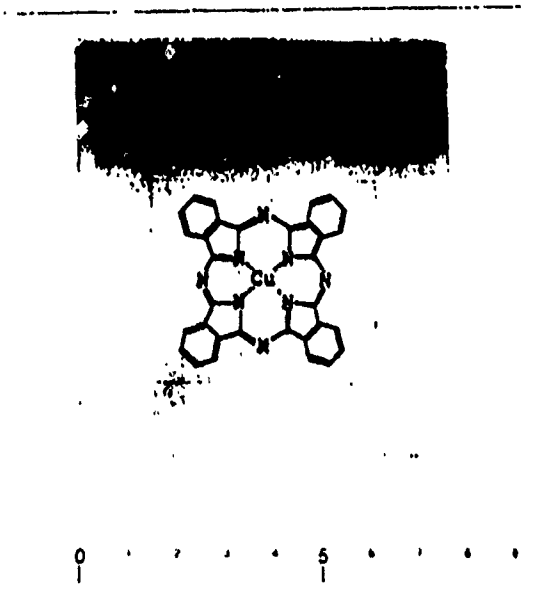

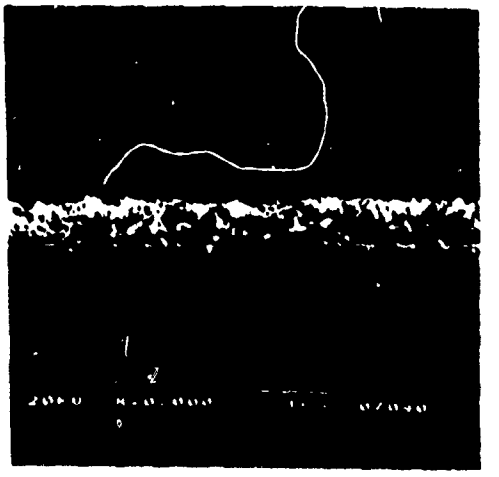

Fig. 4 Fig. 5

Fig. 4. Photograph of -CuPc film prepared by electrolysis of an aqueous solution containing 10 mM β-CuPc, 2 mM FPEG600, and 0.1 M LiBr for 20 min.

Fig. 5. Scanning electron micrograph of cross section of β-CuPc film prepared by the electrolysis of the same solution with Fig. 4 for 15 min.

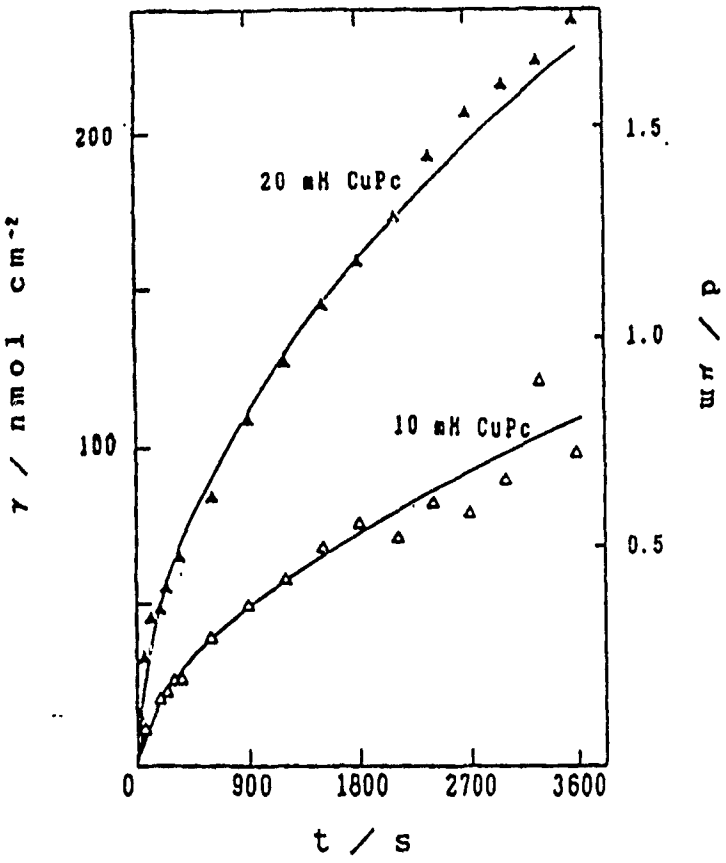

Fig. 6

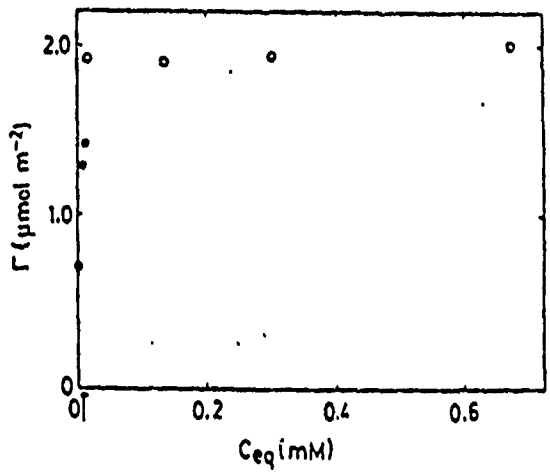

Fig. 7

Fig. 6. The amount of β-CuPc film versus electrolysis time. These films were prepared by electrolysis of an aqueous solution containing β-CuPc, 2.0 mM FPEG600 and 0.1 M LiBr at the ITO.

Fig. 7. Adsorption isotherm of FPEG600 on β-CuPc particles (10 mM). Closed circles indicate that β-CuPc particles were sedimented without centrifugation. The arrow indicates the cmc of FPEG600.

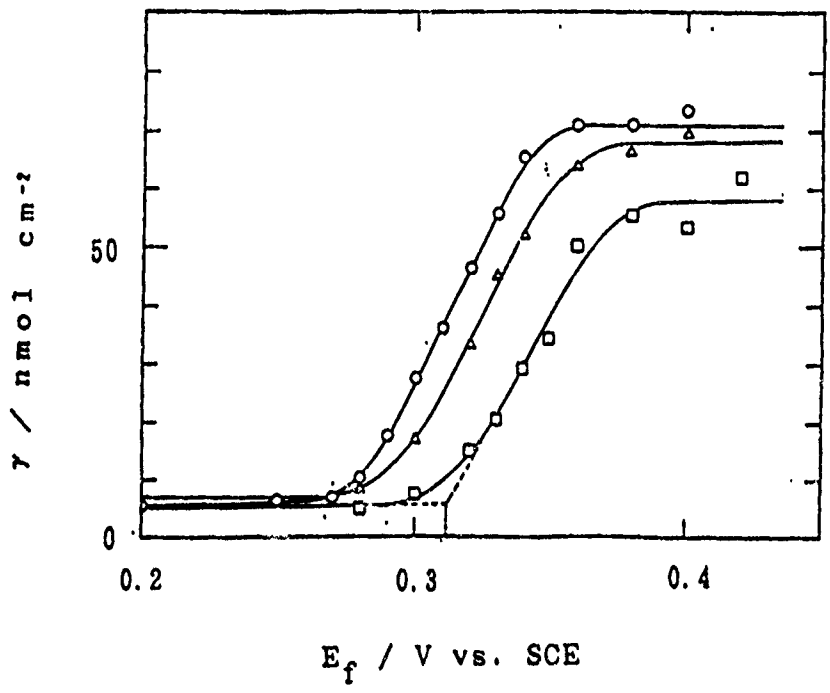

g. 8. The amount of β-CuPc film versus electrolysis potential (E_f). Concentration of β-CuPc: 10 mM.

(12) Redox-Switched Molecular Aggregates

Julio C. Medina, Timothy T. Goodnow,
Angel E. Kaifer, and George W. Gokel*
Department of Chemistry, University of Miami,
Coral Gables, Florida 33124 U.S.A.

1. Introduction

Macrocyclic molecules such as crown ethers have been known for a very long time.[1] The crown ethers and their relatives are not important only because they are large rings but because they can complex with cations,[2] anions,[3] and even molecular species.[4] The versatility of the crown ethers is remarkable and the field continues to burgeon.[5] In this short article, we describe the evolution of our work to develop compounds that can bind and transport cations[6] and, ultimately, molecules. This work has also led us to explore novel membrane-forming crown ether systems.[7]

2. Lariat Ethers

Crown ethers can be characterized as compounds containing a two-dimensional, cyclic array of heteroatom donor groups. The best known example is 18-crown-6 which has the structure $(CH_2CH_2O)_6$.[8] The cryptands[9] can be characterized similarly except that the donor array is three-dimensional. The best known of the cryptands is [2.2.2]-cryptand which has the structure $N(CH_2CH_2OCH_2CH_2OCH_2CH_2)_3N$. In essence, the latter is 18-crown-6 with a third strand attached. A cation is thus presented in each case with a cyclic donor array about 2.5-3Å across but the donors may be in a plane in the crown and in a spherical arrangement in the cryptand. The difference in

Received 6-24-91

II-15

binding exhibited by these two compounds is significant: the crowns tend to be weaker but more dynamic and the cryptands are stronger binders but have slower complexation and decomplexation rates.

Insert Figure 1 here

Cation complexation is characterized by the equilibrium

$$K_S = k_1/k_{-1} = k_{complex}/k_{release}.$$

Thus, a strong cation binder may have a high equilibrium binding constant because k_1 is very fast and k_{-1} is slow. On the other hand, if k_1 is slow but k_{-1} is much slower, K_S will still be large but the dynamics of the system will be reduced overall.

Transport of a cation by a carrier through a membrane depends on the binding constants and the rates. At the external boundary of the membrane (source phase), both K_S and k_1 should be large. Inside the membrane, when the carrier•cation complex is present, only the magnitude of K_S is important. Paradoxically, at the exit boundary (receiving phase), K_S should be small and k_{-1} should be large. Clearly the binding constants and rates cannot simultaneously be large and small. Our first solution to this problem was to develop the lariat ethers.[10] These are crown ethers having both a macrocyclic polyether ring and a donor-group-containing sidearm. Complexation of the cation involves cooperation between the macroring and sidearm. Since the crown ethers generally have fast complexation rates, the initial encounter between cation and ring is at or near the diffusion-controlled rate. Additional binding by the sidearm is merely a conformational

change so the system retains dynamics. Indeed, this two-step process has been studied by Eyring and Petrucci[11] and shown to have the hoped-for kinetic attributes.

Insert Figure 2 here

---

3. Redox Switching

3.1 Redox-switched lariat ethers

The lariat ethers show excellent cation binding strengths and form three-dimensional, cryptand-like complexes in solution[12] and in the solid state.[13] Even so, the dynamics of these systems with respect to membrane transport must inevitably be a compromise. One way around this difficulty is to alter some molecular property of the system so that binding and/or dynamics differs on one side of the membrane or the other. Thus, the carrier system could be a strong binder at one membrane surface and be switched to a weaker binder on the other. Alternatively, a weak binder could be switched to a higher binding strength state for cation binding and then returned to its normal, weakly binding state when release was required.[6b]

Two systems that have been exploited in this context are the nitroaromatic lariat ethers[14] and the anthraquinone-derived podands and lariat ethers.[15] Both nitrobenzene and anthraquinone have oxygen donor groups that can coordinate to the ring-bound cation but binding tends to be weak. Reduction of each system increases the electron density and, in turn, the binding ability of these systems. The drawback of the nitrobenzene radical anion is that it is unstable in water. The anthraquinone radical anion, on the other

hand, is quite stable in aqueous solution.

Insert Figure 3 here

Transport of cations through either a bulk liquid[16] or polymer-based membrane[17] could be effected by reducing anthraquinone to its high binding state at the source phase. Oxidation at the receiving phase side in the polymer-based membrane further enhances the overall transport rate.

3.2 Ferrocenyl cryptands

Ferrocene is a redox-active residue that offers the possibility of switching[18] but is converted from neutral to cation on oxidation (binding → weaker binding) whereas anthraquinone converts from neutral to anion on reduction (binding → stronger binding). Ferrocene differs from both nitrobenzene and anthraquinone in the sense that it contains no focussed donor group such as the ketone in anthraquinone and the N-O residue in the nitro group. Our choice was thus to incorporate the ferrocene molecule into a cryptand. As with most cryptands, cation binding ($k_{complex}$) was expected to be fairly rapid. Generation of the positive charge within the cavity would cause a general repulsion of the bound cation, presumably reducing overall binding and perhaps enhancing exit kinetics.

Previous studies of ferrocenyl cryptands have been undertaken by Hall and coworkers[19] and by Beer and coworkers.[20] In virtually all of the systems previously reported, ferrocene was incorporated as an amide. The presence of an amide in this system has two consequences. First, it rigidifies the

entire cryptand because each amide (–CO–NH–) functional group enjoys 20 kcal of resonance energy. Thus, the driving force for this portion of the molecule to remain planar is high. When two or four amides are present, the cumulative resonance energy is 40 or 80 kcal/mol, a substantial energy by any assessment. Second, –CO–NH– is electron withdrawing relative to $–CH_2–NH–$ so the redox potential of ferrocene will be altered accordingly.

We prepared the previously known[21] ferrocenyl-[2.2]-cryptand diamide and then reduced it to Fc[2.2][22] by using a six-fold excess of lithium aluminum hydride in THF solution.[23] This somewhat obvious step had been reported only once before but the resulting Fc[2.2] was characterized only as an oil.[22] After a rather cumbersome purification involving slow recrystallization after column chromatography in the final step, we obtained the crystalline hydrate of the ferrocenyl cryptand. The product, $Fc[2.2]•H_2O$ was recrystallized from Et_2O-hexane. The hydrate structure was obtained by x-ray methods and proved to be interesting in the sense that the water molecule was bound on the outside of the diaza-18-crown-6 portion of the cryptand by two bridging hydrogen bonds.

Insert Figure 4 here

Cation binding for this compound was fairly strong and substantially superior to the amide precursor and to other ferrocenyl amide cryptands. Indeed, the previously known ferrocenyl amide systems had been able to bind transition metals, presumably through the amide carbonyl groups.[19,20] Because these amide groups were planar and turned outward, it was not

the cavity *per se* that was holding the cation. Thus, redox switching would be less effective than for a saturated analog.

Cyclic voltammetry of the ferrocenyl system permitted an assessment of the change in binding strength that occurred when the system's oxidation state changed. The peak potentials for lithium, sodium, potassium, and calcium cations are recorded in Table 1 along with the ratio K/K_+. The reduction in binding strength as a result of an intra-cavity positive charge ranged from about 10^3 to $>10^4$.

Table 1. Electrochemical data for the ferrocenyl cryptand Fc[2.2].

		Redox Potential			
Cation	Equiv.	E_f^o	E_c^o	ΔE^o	K/K_+
None	0	0.216	–	–	–
Li^+	0.5	0.210	–	–	–
Na^+	0.5	0.214	0.402	0.188	$1.5x10^3$
K^+	0.5	0.224	0.348	0.124	$1.2x10^2$
Ca^{2+}	0.5	0.214	0.488	0.274	$4.3x10^4$

Conversion of Fc[2.2] into the dimethyldiammonium dication by reaction with CH_3I was expected to afford a system having a positively charged cavity that could accommodate an anion. It would have the further advantage that electrochemical or other oxidation of the system could convert the dication into a trication having a fairly rigid, nearly spherical cavity. Electrochemical oxidation proved successful, but no evidence was obtained

that the trication served as a receptor for halogen anions.

4. Lipophilic Lariat Ethers

The principle on which lariat ethers were designed involves cation complexation by the macroring in cooperation with donor groups in the sidearm. After working with these systems for a number of years, we came to view lariat ethers as any crown having a sidearm, whether or not it was likely to serve as a donor group. An excellent example is the steroidal lariat ether[24] shown in figure 5.

Insert Figure 5 here

4.1 Steroidal lariat ethers

We recognized early in this work that steroids are present in natural membranes and that they provide rigidity and order.[25] This is due in part to their ability to aggregate. Our original notion was that the steroid portion of a cholesteryl lariat ether might form ordered arrays of the liquid crystal type and this would, in turn, organize the crown ether macrorings. If the systems stacked, the macrorings might also stack to form a channel within the membrane. Adjusting the pitch of the helical steroidal array could, in principle, adjust the internal dimension of the channel. Alas, this notion has never had a satisfactory experimental test in our laboratory.

We did find, however, that the steroidal lariat ethers aggregate into vesicles.[26] As one might expect, these vesicles (technically niosomes) are quite

similar to those formed by phosphatidyl choline (pc, egg lecithin vesicles). They are large, unilamellar systems about 3000Å in diameter. Their volume entrapments are also similar to those of egg lecithin vesicles: 1-2%. As might be expected for an amphiphile comprised 100% of cholesteryl tails, the vesicles are extremely rigid (*ca.* 300-fold that of pc vesicles).[27]

4.2 Redox-switched vesicle formation

The fact that we could form a variety of vesicles from novel monomers suggested to us that the electrochemical switching principles referred to above might be applied in the vesicle case as they had been in the carrier case. The principle was somewhat different in this new case, however.

Crown ethers bind cations by replacing solvent molecules in the cation's solvation shell. Thus, the neutral, macrocyclic head group is replaced by a supramolecular cation. The new head group is more polar than the neutral macroring but there is no obvious mechanism for changing the oxidation state of an alkali or alkaline earth cation. Both Na^+ or K^+ can be reduced to the neutral metal (Na^0 or K^0) but the metal would not be bound in the macroring as is the cation. Moreover, the neutral metal is a potent chemical reducing agent and could not be formed in aqueous solution. Oxidation of K^+ to K^{++} is also not a useful approach.

We thus turned our consideration from alkali metals to transition metals. Other work in our group involved the ferrocene nucleus. Ferrocene has several important advantages. These are as follows. (i) Ferrocene is a well-known, readily available, iron-containing complex. (ii) The Fe(II)→Fe(III) potential is readily accessible. (iii) The ferrocinium cation is stable and

survives exposure to water. (iv) Numerous reactions are known that permit ferrocene to be incorporated into novel organic structures.

The most obvious means to attach a steroid to ferrocene was to use commercially available 1,1'-dicarboxyferrocene. Conversion of the acid into the acid chloride followed by reaction of the chloride with an alcohol or amine afforded a family of ferrocene derivatives as shown in figure 6. In addition, dimethylaminomethylferrocene was treated with cholestanol and CH_3I. This somewhat unusual reaction gave first a trimethylammonium salt which decomposed to the ferrocenylmethyl carbocation. The cation then was quenched by cholestanol in a normal Williamson ether synthesis to afford cholestanyl ferrocenylmethyl ether.

Insert Figure 6 here

Several novel ferrocene derivatives were prepared.[28] They are shown in Table 2.

Table 2. Redox-switched Membrane Precursors

No	*Site*	*Sidearm identity*	*Yield*	$[\alpha]_D$ (°)	mp °C	$E^\circ_{1/2}$
1	1	CH_2–O–cholestanyl	7	11.8	134-136	509
2	1,1'	$COOC_{17}H_{35}$	69	—	65-67	972
3	1,1'	COOcholestanyl	27	24.4	287-291	941
4	1,1'	COOcholesteryl	45	-0.44	267-269	945
5	1,1'	$CONHC_{18}H_{37}$	64	—	105-107	806
6	1,1'	$CON(C_{18}H_{37})_2$	77	—	32-34	711

Several structural features are represented by these compounds. Thus far, only one example of a monosubstituted lipophilic ferrocene derivative has been prepared. By virtue of the fact that the steroid is connected to the ferrocene through an aliphatic linkage, the redox potential of ferrocene differs little from its normal value of ≈400 mV.[29] In all of the other cases shown, the lipophilic residue was connected to ferrocene by an ester or amide residue. The electron withdrawing effect of ester is greater than that of amide in this case. Thus, the redox potential for the ester-bearing ferrocenes is in the range 950-1000 mV. The amides fall in a lower and braoder range: *ca.* 700-800 mV.

As the ferrocene portion of the molecule is neutral, we expected these systems to exhibit no amphipathic behavior in the absence of reduction. In general, this proved to be true. Compounds **1**, **3**, **4**, and **5** did not appear to aggregate. Surprisingly, light scattering suggested that **2** (particle size 67±19 nm) and **6** (89±23 nm) did aggregate even in the neutral state.

Compound **5** has been reported recently to be surface active so these results are not as surprising as they might otherwise appear.[30]

When compounds **1-6** were reduced, all appeared to aggregate into spherical particles. We were, however, unable to obtain good electron micrographs for any but **1**. In the latter case, somewhat irregular, multilamellar vesicles formed. We were able to estimate that individual membranes having a thickness of about 45Å had formed.

Oxidation of the monomers was accomplished either by bulk electrolysis or chemically using Ce^{4+} ion. In either case, the oxidized species was sonicated and then characterized by dynamic laser light scattering and electron microscopy. After formation and characterization of the vesicles, they were treated with dithionite to effect the Fe(III)→Fe(II) conversion, returning ferrocene to its neu · l state. When this was done, the vesicles collapsed and the monomers could be isolated in good yield, unchanged from their original condition.

At the present time, too few examples of this compound class are available for us to conclude anything definite. The fact that only the monosubstituted ferrocene formed stable vesicles when reduced may be due to monosubstitution or to the low redox potential. Experiments are currently underway to determine which of these factors is most important. In any event, the demonstration of reversible redox formation of vesicle systems offers a promising new approach to supramolecular systems.

Acknowledgments We thank the NIH for grants GM 33940, GM 36262,

and the NSF for a grant to AK (CHE 900053) that supported portions of this work. Support of JCM on a Patricia Roberts Harris fellowship administered by the University of Miami is also gratefully acknowledged. Portions of this work were conducted in collaboration with L. Echegoyen and Z. Chen whose important contributions are gratefully acknowledged.

References

1. Luettringhaus, A.; Ziegler, K.; *Liebigs Ann. Chem.* **1937**, *528*, 155.
2. Pedersen, C.J.; *J. Am. Chem. Soc.* **1967**, *89*, 2495, 7077.
3. Dietrich, B.; Lehn, J.-M.; Sauvage, J.P.; *Tetrahedron Lett.* **1969**, 2885.
4. Van Staveren, C.J.; van Erden, J.; van Veegel, C.J.M.; Harkema, S.; Reinhoudt, D.N.; *J. Am. Chem. Soc.* **1988**, *110*, 4994.
5. Gokel, G.W. *Crowns and Cryptands*, Royal Society of Chemistry Press, London, 1991.
6. (a) Gokel, G.W.; Trafton, J.E.; "Cation Binding by Lariat Ethers" in Y. Inoue and G. W. Gokel (Eds.) *Cation Binding by Macrocycles*, Marcel Dekker, New York, 1990, p. 253. (b) Kaifer, A. E.; Echegoyen, L. A.; "Redox Control of Cation Binding by Macrocyclic Systems," in Y. Inoue and G. W. Gokel (Eds.) *Cation Binding by Macrocycles*, Marcel Dekker, New York, 1990, p. 363.
7. Gokel, G.W. and Echegoyen, L. *Bio-organic Chemistry Frontiers*, **1990**, *1*, 115.
8. Gokel, G.W.; Korzeniowski, S.H.; *Macrocyclic Polyether Syntheses*, Springer Verlag, Berlin, 1982.
9. Lehn, J. M.; *Science*, **1985**, *227*, 849.
10. (a) Gokel, G.W.; Dishong, D.M.; Diamond, C.J.; *J. C. S. Chem. Commun.* **1980**, 1053; (b) Dishong, D.M.; Diamond, C.J.; Cinoman,

M.I.; Gokel, G.W.; *J. Am. Chem. Soc.* **1983**, *105*, 586. (c) Schultz, R.A.; White, B.D.; Dishong, D.M.; Arnold, K.A.; Gokel, G.W.; *J. Am. Chem. Soc.* **1985**, *107* 6659. (d) Gatto, V.J.; Gokel, G.W.; *J. Am. Chem. Soc.* **1984**, *106*, 8240.

11. (a) Echegoyen, L.; Gokel, G.W.; Kim, M.S.; Eyring, E.M.; Petrucci, S.; *J. Phys. Chem.* **1987**, 3854. (b) Gokel, G.W.; Echegoyen, L.; Kim, M.S.; Eyring, E.M.; Petrucci, S.; *Biophysical Chemistry* **1987**, *26*, 225.
12. (a) Kaifer, A.; Echegoyen, L.; Durst, H.; Schultz, R.A.; Dishong, D.M.; Goli, D.M.; Gokel, G.W.; *J. Am. Chem. Soc.* **1984**, *106*, 5100. (b) Kaifer, A.; Echegoyen, L.; Gokel, G.W.; *J. Org. Chem.* **1984**, *49*, 3029.
13. Gandour, R.D.; Fronczek, F.R.; Gatto, V.J.; Minganti, C.; Schultz, R.A.; White, B.D.; Arnold, K.A.; Mazzocchi, D.; Miller, S.R.; Gokel, G. W.; *J. Am. Chem. Soc.* **1986**, *108*, 4078.
14. Kaifer, A.; Gustowski, D.A.; Echegoyen, L.; Gatto, V.J.; Schultz, R.A.; Cleary, T.P.; Morgan, C.R.; Rios, A.M.; Gokel, G.W.; *J. Am. Chem. Soc.* **1985**, *107*, 1958.
15. Gustowski, D.A.; Delgado, M.; Gatto, V.J.; Echegoyen, L.; Gokel, G.W.; *J. Am. Chem. Soc.* **1986**, *108*, 7553.
16. Echeverria, L.; Delgado, M.; Gatto, V.J.; Gokel, G.W.; *J. Am. Chem. Soc.* **1986**, *108*, 6825.
17. Chen, Z.; Gokel, G.W.; Echegoyen, L.; *J. Org. Chem.* **1991**, *in press.*
18. Beer, P. D.; *Chem. Soc. Rev.* **1989**, *18*, 409.
19. (a) Hall, C.D.; Sharpe, N.W.; Danks, I.P.; Sang, Y.P.; *J. C. S. Chem. Commun.* **1989**, 419. (b) Hall, C.D.; Sharpe, N.W.; *J. Organomet. Chem.* **1991**, *405*, 365. (c) Hall, C.D.; Danks, I.P.; Nyburg, S.C.; Parkins, A.W.; Sharpe, N.W.; *Organometallics*, **1990**, *9*, 1602.
20. (a) Beer, P.D.; Keefe, A.D.; Sikanyika, H. *J. Chem. Soc. Dalton Trans.*

1990, 3289. (b) Beer, P.D.; Bush, C.D.; Hamor, T.; *J. Organomet. Chem.* **1988**, *339*, 133. (c) Beer, P.D.; Blackburn, C.; McAleer, J.F.; Sikanyika, H.; *Inorg. Chem.* **1990**, *29*, 378.

21. Hammond, P.J.; Bell, A.P.; Hall, C.D.; *J. Chem. Soc. Perkin Trans. 1*, **1983**, 707.
22. Oepen, G.; Voegtle, F.; *Liebigs Ann. Chem.* **1979**, 1094.
23. Medina, J.C.; Goodnow, T.T.; Bott, S.; Atwood, J.L.; Kaifer, A.E.; Gokel, G.W.; *J. C. S. Chem. Commun.* **1991**, 290.
24. Gokel, G.W.; Hernandez, J.C.; Viscariello, A.M.; Arnold, K.A.; Campana, C.F.; Echegoyen, L.; Fronczek, F.R.; Gandour, R.D.; Morgan, C.R.; Trafton, J.E.; Minganti, C.; Eiband, D.; Schultz, R.A.; Tamminen, M.; *J. Org. Chem.* **1987**, *52*, 2963.
25. Yeagle, P.; *The Membranes of Cells*, Academic Press, New York, 1987.
26. Echegoyen, L.E.; Hernandez, J.C.; Kaifer, A.; Gokel, G.W.; Echegoyen, L.; *J. C. S. Chem. Commun.* **1988**, 836.
27. Fasoli, H.; Echegoyen, L.E.; Hernandez, J.C.; Gokel, G.W.; Echegoyen, L.; *J. C. S. Chem. Commun.* **1989**, 578.
28. Medina, J.C.; Gay, I.; Chen, Z.; Echegoyen, L.; Gokel, G.W.; *J. Am. Chem. Soc.* **1991**, *113*, 365.
29. Bard, A.J.; *Electrochemical Methods: Fundamentals and Applications*; John Wiley, New York, 1980, p. 701.
30. (a) Fujihara, M.; Nishiyama, K.; Yamada, H.; *Thin Solid Films*, **1985**, *132*, 77 [*Chem. Abstracts* **1986**, *105*, 106687f]. (b) Nakahara, H.; Katoh, T.; Sato, M.; Fukuda, K.; *Thin Solid Films* **1988**, *160*, 153 [*Chem. Abstracts* **1989**, *110*, 102442c].

List of figures

Redox-Switched Molecular Aggregates

Figures

Figure 1. Structures of 18-crown-6 and [2.2.2]-cryptand

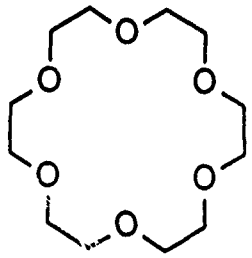

18-crown-6

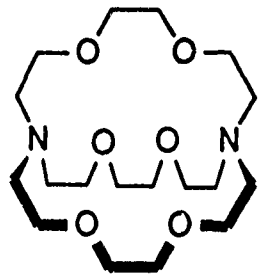

[2.2.2]-cryptand

Figure 2. Lariat ether scheme and carbon- and nitrogen-pivot lariat ethers

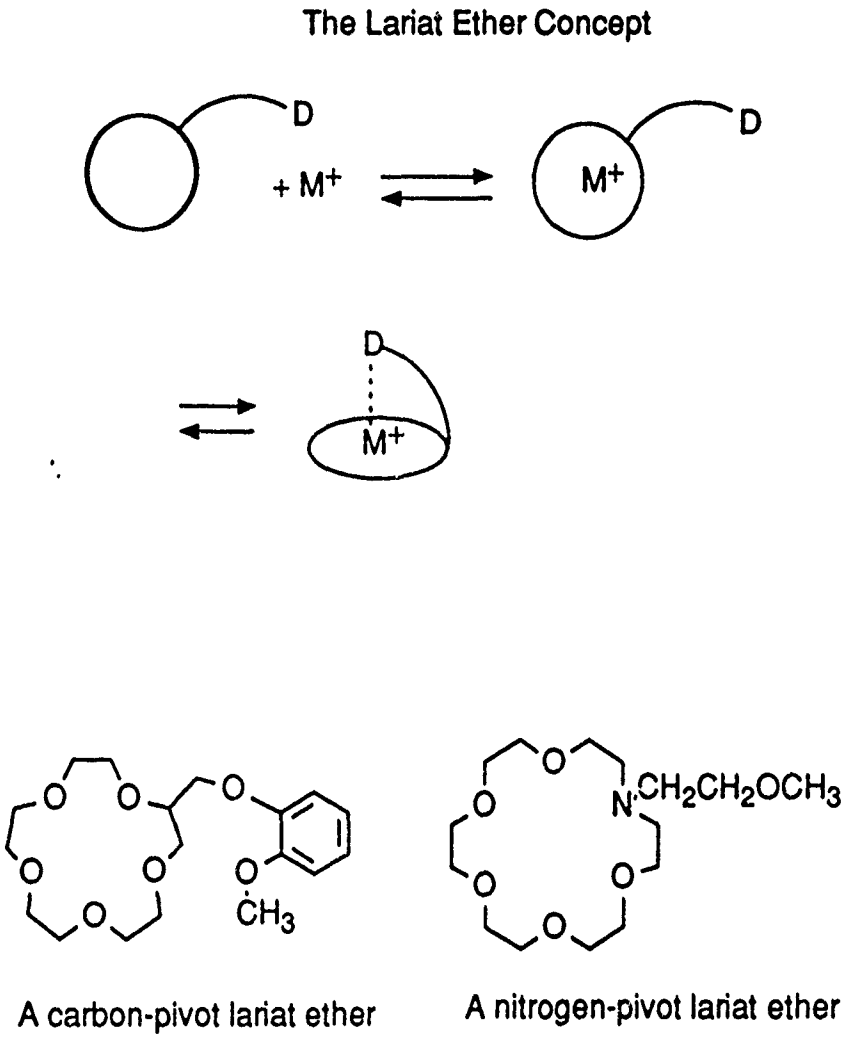

Figure 3. Nitroaromatic- and anthraquinone-derived lariat ethers

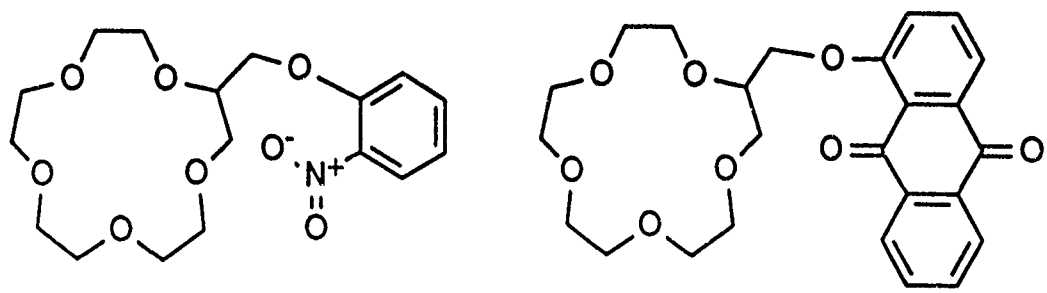

Figure 4. Synthesis of ferrocenyl-[2.2]-cryptand

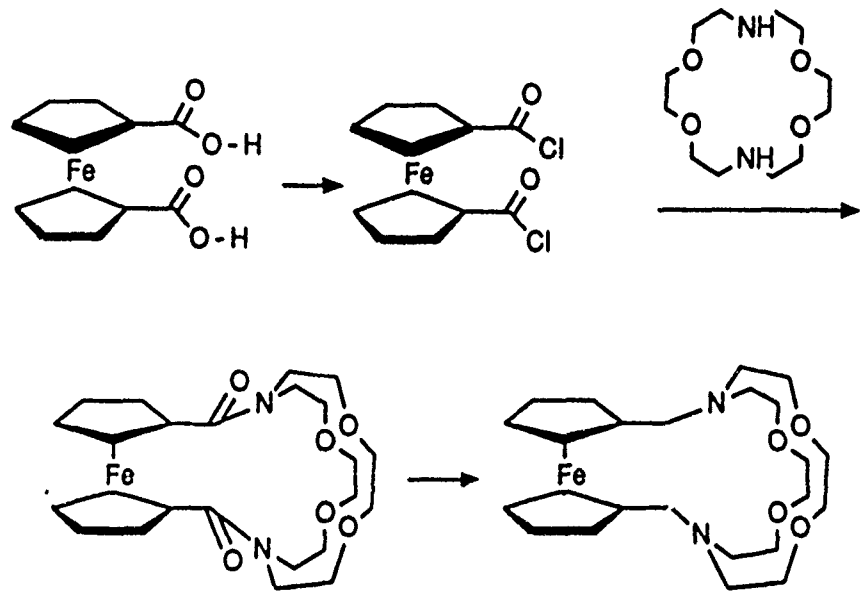

Figure 5. A steroidal lariat ether

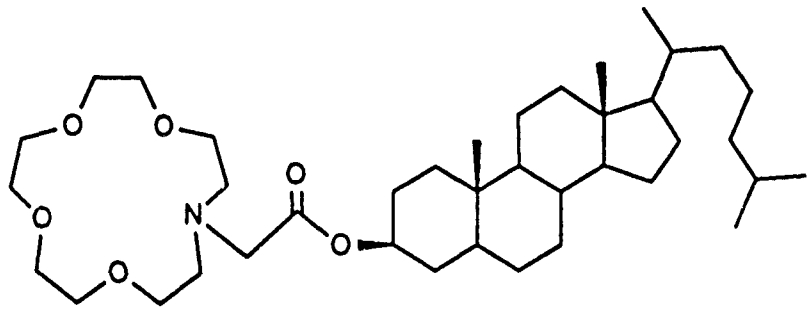

Figure 6. Syntheses of ferrocenyl steroids

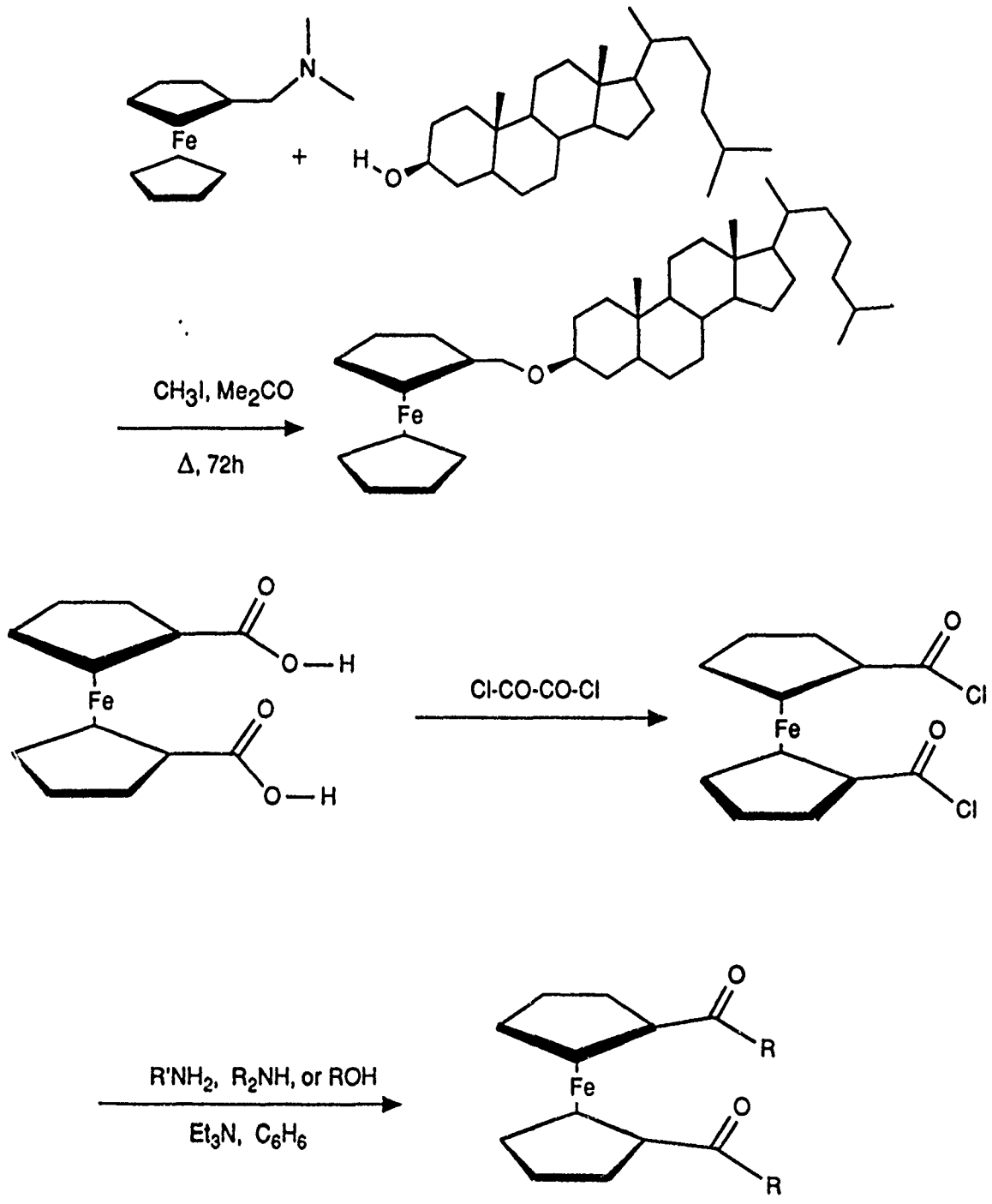

(13) # ELECTROCHEMICAL STUDIES OF REDOX PROBES IN MEMBRANE MIMETIC ASSEMBLIES: LIPOSOMES AND CAST LIPID FILMS

MEI HAN AND ANGEL E. KAIFER*

Chemistry Department, University of Miami, Coral Gables, FL 33124, U.S.A.

INTRODUCTION

The importance of electron transfer processes in biological systems cannot be overemphasized. In particular, many researchers have shown substantial interest in the electron transfer relay systems that occur in various types of biomembranes because of the high efficiency and directionality with which these systems operate. Two obvious examples are mitochondrial respiration and photosynthesis. The fact that these vectorial electron transfer processes occur in biomembranes adds to the difficulties encountered in their study because of the heterogeneity of membranes. The backbone of biological membranes is indeed composed of phospholipids, but the bilayer structure that they adopt creates sharp polarity gradients near both surfaces of the membrane. Thus, it is essentially impossible to mimic membrane environments with homogeneous solutions.

This is a significant problem in the application of electrochemical techniques to the investigation of biologically relevant redox species since many electrochemical properties can be substantially affected by the composition of the reaction medium. Let us consider, for example, the reduction potential of a redox couple, X/X^-. Its value is determined by the relative stabilities of the species involved, X and X^-, in the medium of interest. If the medium

Received 6-20-91

preferentially stabilizes X^- vs X, the reduction potential will shift to more positive values. Conversely, if X is stabilized vs the reduced form X^-, the reduction potential will shift in the negative direction.

Let us assume that one is to perform electrochemical studies on a redox species known to participate in a relevant biological electron transfer process. One can dissolve the redox center in an appropriate solvent and investigate its electrochemistry by a variety of techniques. If this procedure is followed, the results may or may not reflect closely the behavior of that redox center in the highly structured membrane environment. In any instance, much valuable information has been obtained through this approach. But, how can one investigate the electrochemistry of the redox center under conditions that resemble the biomembrane environment more closely? The obvious answer lies in membrane reconstitution techniques *(1)*. In his landmark book, Fendler has extensively reviewed the various approaches that can be used to mimic biological membranes. Micelles, monolayers, multilayers, vesicles, and other assemblies based on amphiphilic molecules have been utilized for this purpose. In the last few years we have used phospholipid vesicles (liposomes) and cast phospholipid multilayers as membrane mimetic assemblies for electrochemical studies. In our work we have investigated the electrochemical behavior of amphiphilic 4,4'-bipyridinium (viologen) derivatives incorporated into these lipid assemblies. We chose viologens *(2)* as model redox centers for the following reasons: (i) viologens exhibit fast rates of homogeneous and heterogenous electron transfer, (ii) their electrochemical and spectral behavior in a variety of media is well characterized, (iii) they can easily be modified with substituents of variable lipophilicity. We summarize here the results of our efforts in this area and establish comparisons between the two membrane mimetic systems concerning their general usefulness for electrochemical work.

EXPERIMENTAL

Materials. N,N'-diheptyl-4,4'-bipyridinium bromide (**1**·Br_2) was purchased from Aldrich and used without further purification. N-ethyl-N'-octadecyl-4,4'-bipyridinium bromide (**2**·Br_2) was synthesized as reported elsewhere *(3).* Crystalline egg phosphatidylcholine (PC) was purchased from Princeton Lipids or Sigma. No measurable difference was found between these two materials. L-α-distearoyl-PC (DSPC) and L-α-dioleoyl-PC (DOPC) were purchased from Sigma. All aqueous solutions were prepared with distilled water further purified with a Barnstead Nanopure four-cartridge system. All other chemicals were of the best quality commercially available.

(INSERT VIOLOGEN STRUCTURES HERE)

Equipment. Electrochemical experiments were performed with standard Princeton Applied Research instrumentation. Absorption spectra were recorded with a Hewlett-Packard 8452A spectrophotometer.

Procedures. Liposomes were prepared according to well-established procedures. Namely, 1 mL of a 100 mg/mL PC ethanolic solution (Sigma) was slowly evaporated under a stream of purified argon. The resulting lipid film was dried overnight under vacuum at 40°C. The dried film was then suspended in 10 mL of 50 mM phosphate buffer (pH 7) and sonicated under argon, in an ice-water bath, to constant turbidity with a Branson Model 185 probe sonifier. The resulting vesicle dispersion was then centrifuged to remove titanium particles released by the tip of the probe. The viologen probe was added either before or after sonication of the lipid but this did not seem to affect the electrochemical results.

Cast lipid films were prepared by a simple procedure. A measured microliter volume of a PC chloroform solution was deposited at the tip of a glassy carbon (GC) electrode. The electrode was rotated (200 rpm for 5-10 min)

to allow the evaporation of the chloroform in air. When the electrode was cast with pure PC, the viologen probe was incorporated by immersing the lipid-covered electrode in a millimolar solution of the redox-active viologen. More commonly, the viologen was preincorporated in the lipid film by dissolving it in the PC/chloroform solution used for casting. In this case, the electrode was equilibrated prior to any voltammetric measurements by immersing it in 0.100 M phosphate buffer solution (pH = 7.0) for 5-10 min. Immediately afterwards, the electrode was cycled at 100 mV/s between 0.0 and -1.2 V vs SSCE during 10 min. Voltammetric measurements were always recorded immediately after this pretreatment protocol was completed.

For variable temperature voltammetric experiments, the cell was immersed in a constant temperature bath. The reference calomel electrode was kept at room temperature and connected to the electrochemical cell through a salt bridge.

Absorption spectra of the lipid films were recorded by casting lipid films on indium-doped SnO_2-covered glass slides (transmittance 80%, Delta Technologies). The slide was then affixed to one of the optical windows of a 1.0-cm visible cell in such a way that the lipid film faced the solution side. The cell was filled with buffer solution and placed in the open cell holder of the spectrophotometer. This experimental arrangement permits recording the absorption spectrum of the lipid film as a function of the potential applied to the SnO_2 strip which acts as the working electrode.

All solutions for electrochemical experiments were purged with purified nitrogen or argon.

RESULTS AND DISCUSSION

The main goal of this work is to develop methodology to investigate the

electrochemistry of redox centers under conditions resembling as much as possible the intricate environment of a biological membrane. We will first discuss our work utilizing liposomes to provide the membrane mimetic environment. The second and longer section of this chapter will be devoted to our investigations of electrodes modified with cast posphatidylcholine films.

ELECTROCHEMISTRY IN THE PRESENCE OF LIPOSOMES

Several years ago our group was active in the investigation of micellar effects on the electrochemistry of methylviologen *(4-7)*. The results were greatly affected by the highly dynamic nature of the micellar aggregates and, more importantly, by the partitioning of methylviologen between the micellar aggregates and the bulk aqueous phase. To overcome these difficulties we thought that two changes would be desirable in order to further anchor the viologen probe in the membrane mimetic assembly: (i) an increase in the rigidity of the membrane mimetic assemblies, and (ii) a decrease of the solubility of the viologen probes in the bulk aqueous phase. Thus, we reasoned that vesicles were the logical next step after micelles, since they are known to be much more rigid than micelles from the standpoint of exchange dynamics between bound and free surfactant monomers. Concerning the viologen probe, $\mathbf{1}^{2+}$ appeared to be appropriate since it is soluble in water but its reduced forms, $\mathbf{1}^{+}$ and **1**, are quite insoluble. As a matter of fact, the insolubility of $\mathbf{1}^{+}$ and **1** has been utilized to prepare electrochromic films *(8,9)*. Therefore, we started to investigate the electrochemistry of $\mathbf{1}^{2+}$ in the presence of single unilamellar vesicles made by sonication of egg PC dispersions.

In the presence of PC liposomes, a cyclic voltammogram of $\mathbf{1}^{2+}$ displays two reduction and two corresponding oxidation peaks (see Figure 1) whose shape approximates that for purely diffusional behavior and is free from the

sharp redissolution peaks observed, on the positive-going scan, in the absence of liposomes *(10)*. This clearly indicates that the liposomes solubilize $\mathbf{1}^{+}$ and **1**, preventing their precipitation on the electrode surface. The peak current for the first reduction of $\mathbf{1}^{2+}$ in the presence of liposomes is linearly related to the square root of the scan rate in the 10-200 mV/s range. The measured half-wave potentials for the $\mathbf{1}^{2+}/\mathbf{1}^{+}$ and $\mathbf{1}^{+}/\mathbf{1}$ redox couples were -0.53 and -0.83 V vs SSCE, respectively. These values suggest that the liposomes provide a rather hydrophobic environment for viologen reduction. However, the interpretation of the potential values is hampered by the certain partitioning of $\mathbf{1}^{2+}$ between the bulk aqueous phase and the liposome aggregates which does affect the observed values.

Partitioning also affects the observed diffusion coefficient for $\mathbf{1}^{2+}$. In fact, the diffusional problem in this system is far from simple and, perhaps as a reflection of this, the ratios of anodic/cathodic peak currents are larger than unity in the voltammogram of Figure 1. Deviations from the theoretical ratios for multistep electron-transfer processes have also been noted in micellar solutions *(11)*.

In an effort to completely eliminate the partitioning of the electroactive probe into the bulk aqueous phase, we decided to use asymmetrically substituted viologens, such as $\mathbf{2}^{2+}$, which are expected to be more strongly anchored to the vesicle membrane due to their surfactant properties. However, this idea did was not very productive since the observed voltammetric behavior consisted of quite small waves which were difficult to measure. Similar results were also reported by another group *(12)*.

At this point, the use of vesicles as membrane models in aqueous electrochemical experiments did not seem to be highly promising. We thus looked for alternatives and decided to use a novel electrode modification

II-42

scheme, attaching the membrane mimetic assembly to the electrode surface. This approach appeared advantageous since it removed the partitioning problems that had always affected our previous work with micelles and vesicles.

ELECTRODES MODIFIED WITH CAST LIPID FILMS

Cast lipid films have been studied by several Japanese authors *(13-16)*. They are easy to prepare and, when immersed in water, adopt predominantly a multilayer organization. Interestingly, their use as electrode modifying films was essentially unexplored when we started our work. Only Tanaka et al. had investigated the barrier properties of palmitic acid films on electrodes *(17)*. They found that these films largely reduce the access of hydrophilic redox active species to the electrode surface thus partially passivating the electrode surface. We found similar results with PC films *(18)*. In fact, the films exhibited permselective properties, *i.e.*, $\mathbf{2}^{2+}$ readily permeates the PC film and undergoes electrochemical reduction inside the lipid matrix, while the more hydrophilic analogue methylviologen does not. Similar selectivity in favor of the more hydrophobic species was also observed in our experiments with ferrocene derivatives *(18)*. The permselective properties of these electrodes have generated interest in the field of pharmaceutical analysis *(19,20)*.

Once the selective permeability of the cast PC films had been demonstrated by these experiments we turned to loading the hydrophobic viologen probe into the lipid film by co-dissolving appropriate amounts of $\mathbf{2}\cdot Br_2$ and PC in the chloroform casting solution. Most electrodes prepared in this way exhibit stable voltammetric waves after the pretreatment described in the Experimental Section. A typical cyclic voltammogram obtained on a glassy carbon electrode covered with a PC/$\mathbf{2}^{2+}$ film (4.1×10^{-7} and 4.1×10^{-8}

mol/cm^2 of PC and $\mathbf{2}^{2+}$, respectively) is shown in Figure 2. This level of coverage results in a lipid film having an estimated thickness of 3.7 μm. Two redox processes are clearly visible corresponding to the two consecutive monoelectronic reductions of the viologen nucleus ($\mathbf{2}^{2+}/\mathbf{2}^{+}$ and $\mathbf{2}^{+}/\mathbf{2}$). The two half-wave potentials are -0.50 V and -0.80 V vs SSCE, respectively. The first cathodic peak current is linearly related to the square root of the scan rate indicating that the current is controlled by diffusion -- or diffusion-like processes -- of the viologen probe inside the PC film. In aqueous media the precipitation *(12,21)* of the reduced forms $\mathbf{2}^{+}$ and **2** and the interfacial self-assembly *(3)* of the dicationic form $\mathbf{2}^{2+}$ complicate the electrochemical behavior of the viologen probe. The fact that no precipitation effects are observed in the voltammogram of Figure 2 argues strongly in favor of the molecular organization of the cast PC/$\mathbf{2}^{2+}$ film. Cast phospholipid films formed by similar procedures exhibit organized multilayer structures *(13-16)*. It seems then that the amphiphilic dication $\mathbf{2}^{2+}$ (at a level of 9.1% mol) does not disrupt the multilayer organization of the PC molecules.

An important aspect of viologen chemistry is the tendency of the cation radical to dimerize in aqueous environments *(2,7,22)*. We reasoned that the extent of dimerization of $\mathbf{2}^{+}$ inside the PC film could be related to the degree of molecular organization of the film. A disorganized film would not be effective in preventing the dimerization of the cation radical *(7)*. Conversely, an organized multilayer arrangement should keep the cation radicals apart (if their concentration is not too large) resulting in little or no dimerization. For instance, in the bilayer system described by Majda and coworkers *(23)* which consisted of an octadecyltrichlorosilane monolayer, prepared on an alumina surface, and a second monolayer of an amphiphilic viologen, dimerization is extensive. Of course, in this system the cation radicals are in intimate contact

II - 44

with each other and dimerization is the expected result. In our multilayer system, with 2^{2+} at the 9.1% mol level, one would anticipate that dimerization should be much less favorable. This prediction agrees very well with the experimental findings. The electronic absorption spectrum of an exhaustively reduced PC film containing 9.1% mol of 2^{2+} is shown in Figure 3B. The reduction of the film was performed at a potential value of -0.7 V vs SSCE that insures complete conversion to the cation radical state. The spectral shape indicates a low level of dimerization. Furthermore, if the loading of viologen is decreased to 4.8% mol, the spectrum observed is almost identical to that exhibited by monomeric viologen cation radicals (see Figure 3A). Therefore, these experiments indicate that the viologen probes, at least when they are in the form of cation radicals, are distributed rather homogenously throughout the PC film. Aggregation or dimerization do not dominate the behavior of the cation radicals, suggesting that substantial molecular organization prevails in the film.

The fact that the reductive electrochemistry of the viologen probe exhibits diffusion controlled characteristics implies that substantial ionic currents can flow across the lipid film in order to maintain electroneutrality. Reduction of the viologen probe entails a decrease in its positive charge. Therefore, for every electron injected in the lipid film from the electrode surface, either an anion must be expelled out of the film or a cation has to move in from the solution. It is surprising that these ionic movements take place through a lipid film which is several micrometers thick since lipid bilayers effectively prevent the flow of ions across them in the absence of ionophoric carriers or channels. We believe that the fast ionic flow across the lipid films is due to the presence of defective regions in the multilayer arrangement. The lipid film can thus be visualized as a collection of organized multilayer domains containing small disorganized

regions.

The actual mechanism of charge propagation across the lipid films is of substantial interest. Charge propagation across modified films on electrodes is usually seen as the result of two contributions: (i) actual diffusion of the redox probe and (ii) electron hopping between neighboring redox sites having different oxidation states. The overall process is characterized by an apparent diffusion coefficient, D_{app}, which is given by the Dahms-Ruff equation *(24,25)*:

$$D_{app} = D + (\pi/4)\, k_{ex}\, \delta^2\, C \qquad (1)$$

where D is the actual diffusion coefficient of the redox probe, k_{ex} represents the electron self-exchange rate constant, δ is the average distance between neighboring redox sites, and C is the concentration of redox-active species. In order to discern the relative importance of these two mechanisms it is customary to measure D_{app} as a function of probe concentration. A linear dependence indicates predominance of electron hopping while a concentration independent D_{app} means that the actual diffusion of the probe is the dominant mechanism of charge propagation. We have measured the apparent diffusion coefficient of $\mathbf{2}^{2+}$ as a function of its concentration inside films made of PC and DSPC (molar ratio 8:2). To insure that the diffusion layer would always be confined within the lipid film in the time scale of these experiments, we cast films with 1.7×10^{-6} and 4.7×10^{-7} mol/cm^2 of PC and DSPC, respectively, plus varying amounts of $\mathbf{2}^{2+}$ resulting in lipid films with an estimated thickness of 17 μm. The results are given in Table 1. The observed variations in the D_{app} values are rather small, with a range from 4.4 to 6.5×10^{-9} cm^2/s. Because of the approximations involved in the estimation of the probe concentration inside the lipid film, it is difficult to assign any significance to the small changes observed. The reality of the slight decrease in D_{app} values with increasing probe concentration is questionable and thus we would not

II-46

speculate about possible causes. One can definitely say that the D_{app} values do not increase with the concentration of the probe, thus discarding electron hopping as the predominant charge propagation mechanism. The data seem to support actual diffusion of the viologen probes as the main contribution to the overall charge propagation.

LIPID COMPOSITION STUDIES IN PC/2^{2+} FILMS

Egg phosphatidylcholine is a convenient choice as the material for the cast lipid films because of its general availability. However, we decided to assess the effect of the nature of the lipid's fatty acid chains on the electrochemical behavior of the viologen probe. We were particularly interested in the possible effect of unsaturations in these chains since it is well known that chains having double bonds foster more disorganized structures *(26)*. Therefore, we investigated the behavior of 2^{2+} in pure DSPC (saturated) and DOPC (unsaturated) films. In these experiments the glassy carbon electrode was covered with 3.3×10^{-8} mol/cm^2 of $2{\cdot}Br_2$ and 3.3×10^{-7} mol/cm^2 of either DSPC or DOPC. Such coverage results in films having estimated thickness of 3.0 μm. Figure 4 shows the voltammetric responses observed with these films. Interestingly, the voltammetric currents are fairly small for the saturated DSPC film, while large, well-developed currents are observed with the unsaturated DOPC films. These results clearly demonstrate that DSPC forms a more compact multilayer arrangement through which the diffusional motion of the viologen probe is extremely hampered. On the other hand, the unsaturated lipid, DOPC, allows much faster diffusion of 2^{2+} and, thus, larger voltammetric currents. This is also in good agreement with the respective gel-to-fluid phase transition temperatures of both lipids, which are 61 and -10°C for DSPC and DOPC, respectively *(27)*. Therefore, since our experiments were performed at

room temperature, the DSPC film is in the gel state and the DOPC film is in the fluid state. The much higher fluidity of the latter explains the larger currents observed in the voltammetric experiments. We prepared mixed films using varying proportions of DOPC and DSPC. As expected (see Figure 5), the level of current observed increases with the molar fraction of the unsaturated lipid, DOPC. This is a very encouraging result because it suggests that our lipid multilayer films respond like biological membranes in that structural fluidity is controlled by the degree of unsaturation of the lipid's fatty acid chains. Thus it is possible to use this control on film fluidity to determine the extent of electrochemical conversions in the modified lipid film.

These results prompted us to look for phase transition temperatures that may manifest themselves in breaking points in current vs temperature plots. Figure 6 shows the first cathodic peak current for reduction of the viologen probe plotted as a function of temperature for several types of phospholipid films containing varying DSPC/DOPC molar ratios. It is clearly evident that increasing the temperature results in higher voltammetric currents. This is the case for all lipid compositions. However, no breaking points are seen, *i.e.*, no defined phase transitions were detected from the voltammetric behavior of our amphiphilic viologen probe. This is probably due to the mixed composition of these lipid films as well as to the likely presence of defective regions in the multilayer arrangement of the film. Nonetheless, the data of Figure 6 show that, at any of the surveyed temperatures, the voltammetric currents increase monotonically with the DOPC/DSPC ratio. Thus, both the lipid's degree of saturation and the temperature can be used as parameters to control the extent of the electrochemical conversions in the modified films. These properties, typical of biological membranes, confer a unique character to these modified electrodes.

All these experiments with cast lipid films were performed with the lipid film immersed in a pH 7 buffer solution. Under these conditions, PC is in its zwitterionic form, and the lipid film has no formal charge. Therefore, it is possible to modify gradually the nominal charge of the film by introducing varying amounts of anionic or cationic surfactants. We selected dicetyl phosphate (DCP), dioctadecyldimethylammonium bromide (DODAB), and cardiolipin (CARDI) as suitable charge modifiers of the lipid film owing to the resemblance of their charged head groups with those of PC.

(INSERT SURFACTANT STRUCTURES HERE)

How is the electrochemical behavior of 2^{2+} affected by the presence of charged surfactants in the film? Our results *(28)* indicate that the half-wave potentials for both viologen reductions shift monotonically with the molar ratio of charged surfactant in a direction which can be easily predicted from simple electrostatic effects. For instance, the data of Figure 7 shows that both the $2^{2+}/2^{+}$ and $2^{+}/2$ half-wave potentials shift to more positive values when DODAB is added to the film. This can be explained by the electrostatic destabilization of the unreduced forms (2^{2+} and 2^{+}) relative to the corresponding reduced forms (2^{+} and **2**, respectively) in both redox couples which is brought about by the presence of the cationic surfactant in the lipid film. As expected, the incorporation of the negatively charged surfactants CARDI and DCP causes the opposite effect, that is, negative shifts in both half-wave potentials (see Figure 7). This can be rationalized by the relative stabilization of the unreduced over the reduced forms in each one of the two viologen couples.

The magnitude of these effects is determined by the molar fraction of the charged surfactant in the film. CARDI shows a stronger effect than DCP since it has two negatively charged phosphate groups while DCP has only one.

Generally, the incorporation of charged surfactants to the lipid film tends to decrease the magnitude of the voltammetric currents associated with the redox couples of the viologen probe. This is consistent with our findings on the effects of saturated vs unsaturated chains in the electrochemistry inside the film (vide supra). Indeed, the addition of DODAB, DCP, or CARDI to a PC film increases the fraction of saturated chains and decreases the fluidity of the film, thus, causing a decrease in the observed volatmmetric currents. Nonetheless, these experiments demonstrate that the first and second half-wave potentials for the monoelectronic reductions of an amphiphilic viologen inside a PC film cast on a glassy carbon electrode can be adjusted over a range of about 200 mV by incorporating appropriate ratios of charged surfactants into the lipid film composition. The observed half-wave potentials are controlled by simple electrostatic interactions between the charged surfactants and the various redox forms of the viologen probe. These findings demonstrate the possibility of "fine tuning" the redox potentials of an electroactive compound immobilized in the lipid film, a relevant goal for applications involving electrocatalysis or mediation of electron transfer reactions by the film. Furthermore, these results clearly suggest possible mechanisms for the environmental control of redox potentials in biological membranes.

CONCLUSIONS

We have performed electrochemical investigations of redox probes in membrane mimetic environments using two different approaches. The probe can be solubilized in a solution containing membrane mimetic aggregates, like micelles and vesicles, and its electrochemical behavior can then be studied. Alternatively, a membrane mimetic film -- incorporating the redox probe -- can be attached to the electrode surface. Our work clearly suggests that the

ZT-50

second approach is more versatile and productive. Both approaches require the use of amphiphilic redox probes to enable their stable incorporation into the membrane mimetic assembly. However in the first approach, partitioning of the probe to the bulk aqueous phase may give rise to complicated voltammetric behavior involving adsorption, precipitation, and other phenomena. In the second approach, partitioning of the redox probe into the bulk aqueous phase may result only in decreased currents but the aqueous probe cannot interfere with the electrochemical experiment in any fundamental way. Thus, we have been able to perform a substantial amount of work with electrodes modified with lipid films incorporating an amphiphilic viologen probe. Our experimental results have verified that the lipid film is fairly well organized in a multilayer arrangement and exhibits several properties reminiscent of biological membranes.

ACKNOWLEDGEMENTS

The authors gratefully acknowledge the partial support of this research by the National Science Foundation (CHE-9000531).

REFERENCES

1. Fendler, J.H. *Membrane Mimetic Chemistry*; Wiley: New York, 1982.
2. Bird, C.L.; Kuhn, A.T. *Chem. Soc. Rev.* **1981**, *10*, 49.
3. Gomez, M.E.; Li, J.; Kaifer, A.E. *Langmuir*, in press.
4. Kaifer, A.E.; Bard, A.J. *J. Phys. Chem.* **1985**, *89*, 4876.
5. Kaifer, A.E.; Bard, A.J. *J. Phys. Chem.* **1987**, *91*, 2006.
6. Quintela, P.A.; Kaifer, A.E. *Langmuir* **1987**, *3*, 769.
7. Quintela, P.A.; Diaz, A.; Kaifer, A.E. *Langmuir* **1988**, *4*, 663.
8. Van Dam, H.T.; Ponjee, J.J. *J. Electrochem. Soc.* **1974**, *121*, 1555.
9. Jasinski, R.J. *J. Electrochem. Soc.* **1977**, *124*, 637.
10. Kaifer, A.E. *J. Am. Chem. Soc.* **1986**, *108*, 6837.
11. Eddowes, M.J.; Gratzel, M. *J. Electroanal. Chem.* **1983**, *152*, 143.
12. Lu, T.; Cotton, T.M.: Hurst, J.K.; Thompson, D.H.P. *J. Electroanal. Chem.* **1988**, *246*, 337.
13. Okahata, Y.; Taguchi, K.; Seki, T. *J. Chem. Soc., Chem. Commun.* **1985**, 1122.
14. Okahata, Y.; Ebato, H.; Taguchi, K. *J. Chem. Soc., Chem. Commun.* **1987**, 1363.
15. Okahata, Y.; Shimizu, O. *Langmuir* **1987**, *3*, 1171.
16. Okahata, Y.; Ye, X. *J. Chem. Soc., Chem. Commun.* **1989**, 1147.
17. Tanaka, K.; Tamamushi, R. *J. Electroanal. Chem.* **1987**, *236*, 305.
18. Garcia, O.J.; Quintela, P.A.; Kaifer, A.E. *Anal. Chem.* **1989**, *61*, 979.
19. Chastel, O.; Kauffman, G.J.; Patriarche, G.J.; Christian, G.D. *Anal. Chem.* **1989**, *61*, 170.
20. Wang, J.; Lu, Z. *Anal. Chem.* **1990**, *62*, 826.
21. Diaz, A.; Quintela, P.A.; Schuette, J.M.; Kaifer, A.E. *J. Phys. Chem.* **1988**, *92*, 3537.

II-52

22. Kosower, E.M.; Cotter, J.L.; *J. Am. Chem. Soc.* **1964,** *86,* 5524.

23. Miller, C.J.; Widrig, C.A.; Charych, D.H.; Majda, M. *J. Phys. Chem.* **1988,** *92,* 1928.

24. Dahms, H. *J. Phys. Chem.* **1968,** *72,* 362.

25. Ruff, I.; Friedrich, V.J. *J. Phys. Chem.* **1971,** *75,* 3297.

26. Stryer, L. *Biochemistry,* 3rd ed.; Freeman: New York, 1988; Chapter 12.

27. Bretscher, M.S. *Science* **1973,** *181,* 622.

28. Han, M.; Kaifer, A.E. *J. Chem. Soc., Chem. Commun.* **1990,** 1698.

VIOLOGEN STRUCTURES

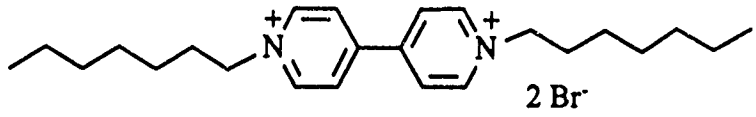

1·Br_2

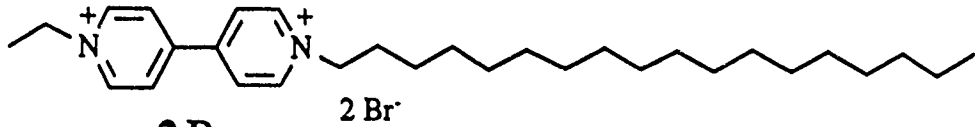

2·Br_2

SURFACTANT STUCTURES

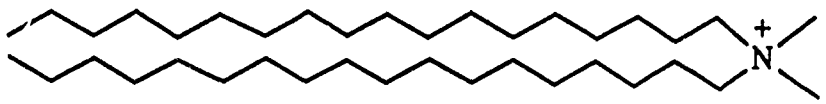

DODAB

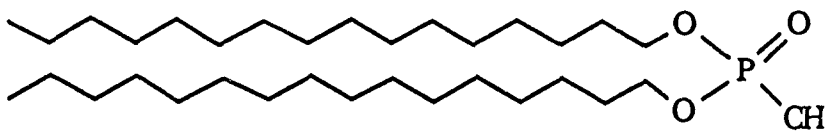

DCP

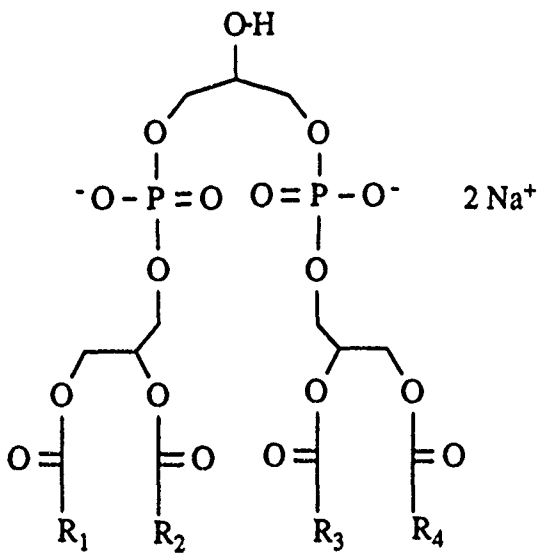

CARDI

TABLE 1. Dependence of the diffusion coefficient of **2**·Br_2 on its concentration inside lipid films made by casting 1.7 x 10^{-6} mol/cm^2 of PC and 4.7 x 10^{-7} mol/cm^2 of DSPC. Temperature: 22°C.

Concentration of **2**·Br_2 (mol/L) x 10^2	Diffusion coefficient (cm^2/s) x 10^9
2.9	6.0
4.6	6.5
6.5	5.4
7.9	5.0
10.0	4.4

II-56

FIGURE CAPTIONS

Figure 1. Cyclic voltammogram (50 mV/s) at a glassy carbon electrode (area = 0.08 cm^2) of 0.5 mM **1**·Br_2 in 50 mM phosphate buffer (pH = 7) also containing 12 mM PC in the form of vesicles.

Figure 2. Cyclic voltammogram (50 mV/s) in 0.100 M phosphate buffer (pH = 7.0) of a GC electrode (0.08 cm^2) covered with 4.1 x 10^{-8} mol/cm^2 **2**·Br_2 and 4.1 x 10^{-7} mol/cm^2 egg PC.

Figure 3. Absorption spectra of $\mathbf{2}^{+}$ inside PC films. (A) 4.8% mol of **2**·Br_2 in egg PC film. Absorbance scale: 0-0.16. (B) 9.1% mol of **2**·Br_2 in egg PC film. Absorbance scale: 0-0.42.

Figure 4. Cyclic voltammetric response (50 mV/s) in 0.100 M phosphate buffer (pH = 7.0) of a GC electrode (0.08 cm^2) covered with 4.1 x 10^{-8} mol/cm^2 of **2**·Br_2 and 4.1 x 10^{-7} mol/cm^2 of lipid. (A) The lipid is pure DOPC. (B) The lipid is pure DSPC.

Figure 5. Effect of the molar fraction of DSPC on the first reduction peak current for $\mathbf{2}^{2+}$ inside mixed DSPC/DOPC films.

Figure 6. Temperature effects on the first cathodic peak current for $\mathbf{2}^{2+}$ inside mixed DSPC/DOPC films. The molar ratios pf DSPC are (■) 0, (◇) 0.2, (●) 0.4, (▲) 0.6, and (○) 0.8.

Figure 7. Dependence of the half-wave potentials (V vs. SSCE) for the couples (A) $\mathbf{2}^{2+}/\mathbf{2}^{+}$ and (B) $\mathbf{2}^{+}/\mathbf{2}$ on the molar fraction of charged surfactant in the lipid film: (■) DODAB, (◇) DCP, and (○) CARDI.

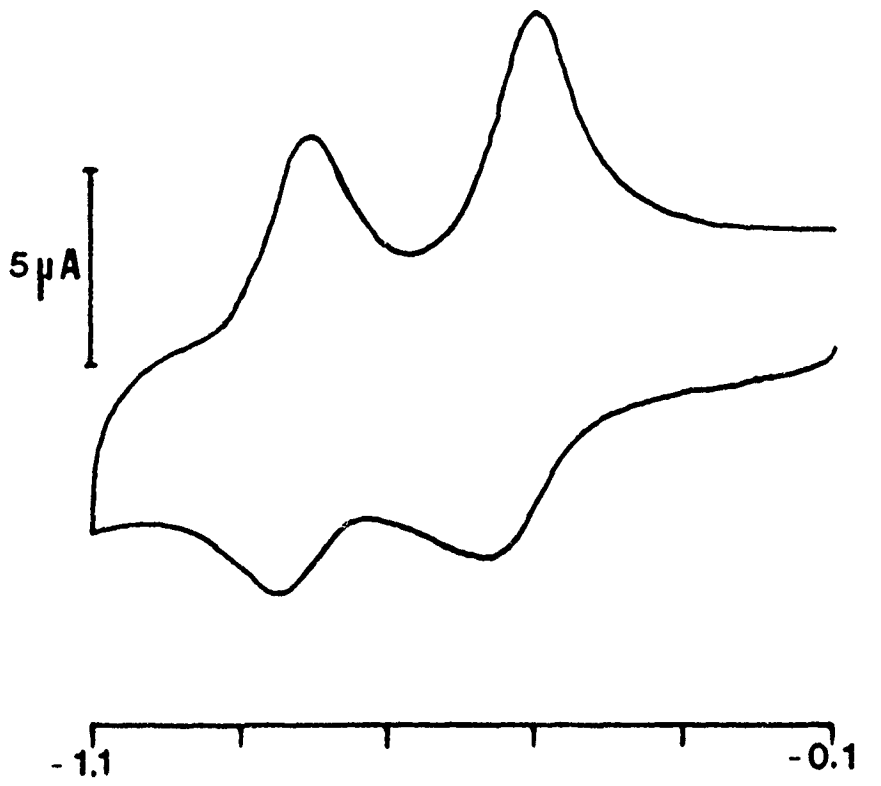

FIG. 1 HAN & KAIFER

II-58

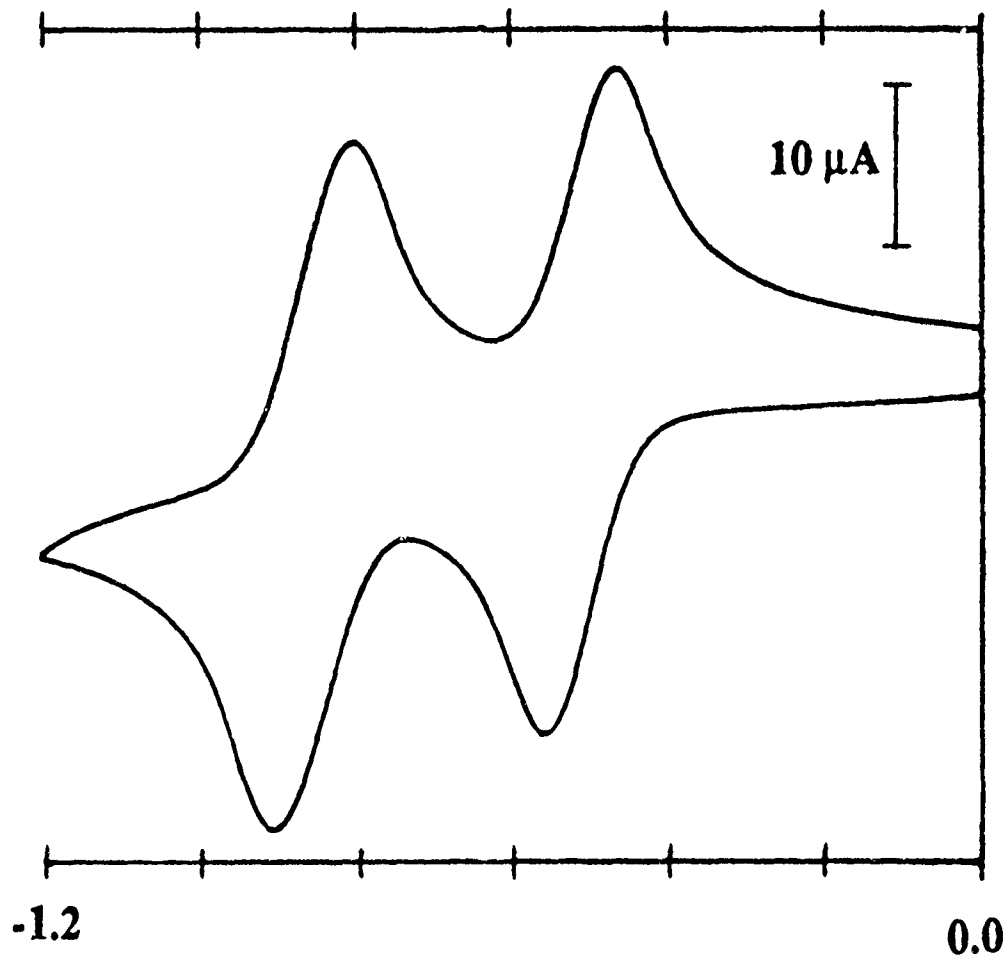

FIG. 2 HAN & KAIPER

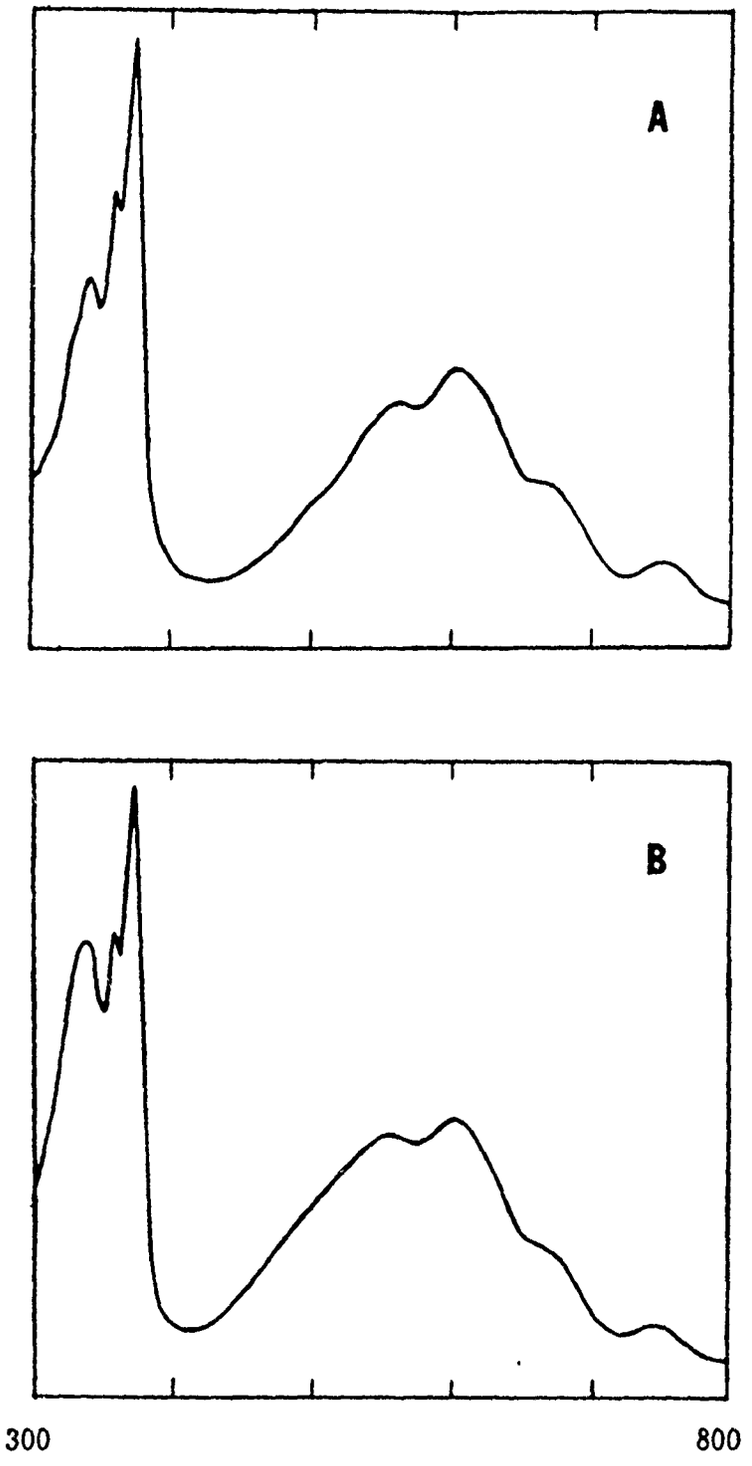

FIG. 3

HAN & KAIFER

IT-60

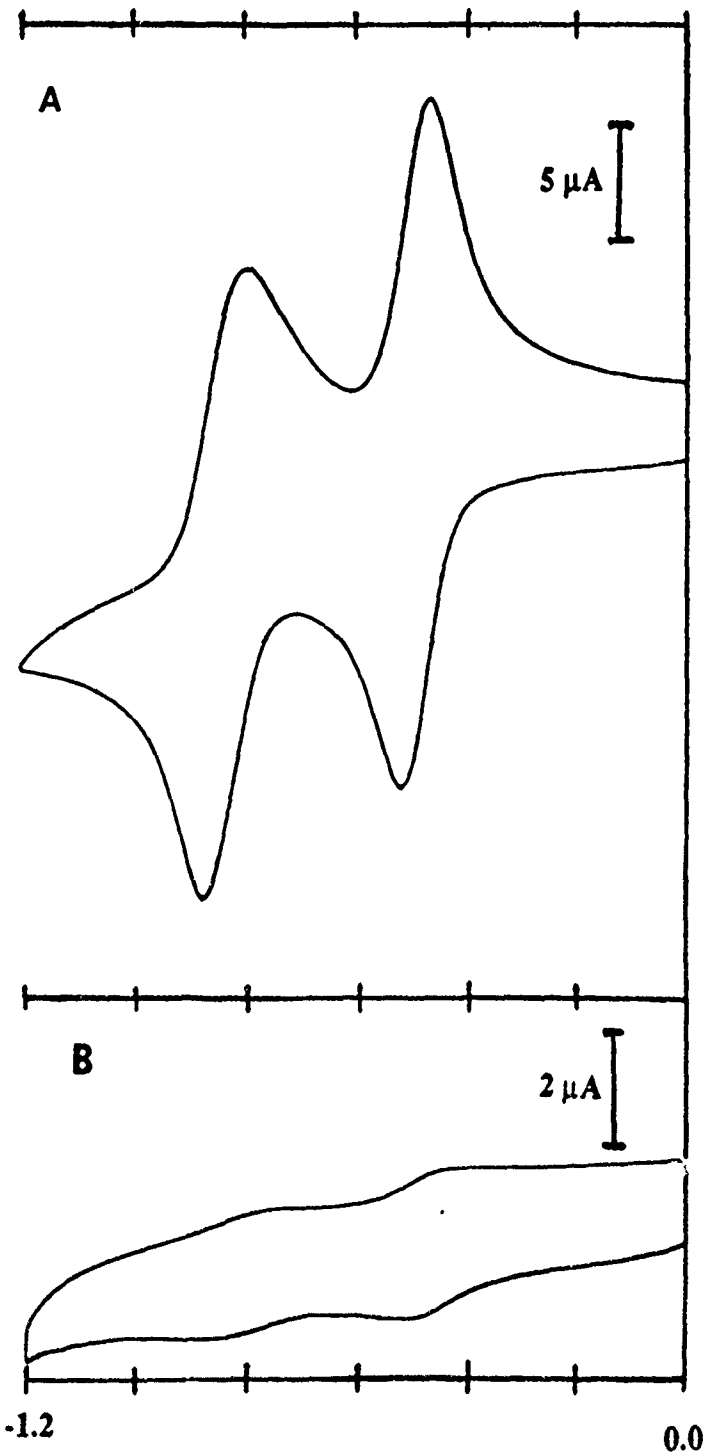

FIG. 4 HAN & KAIFER

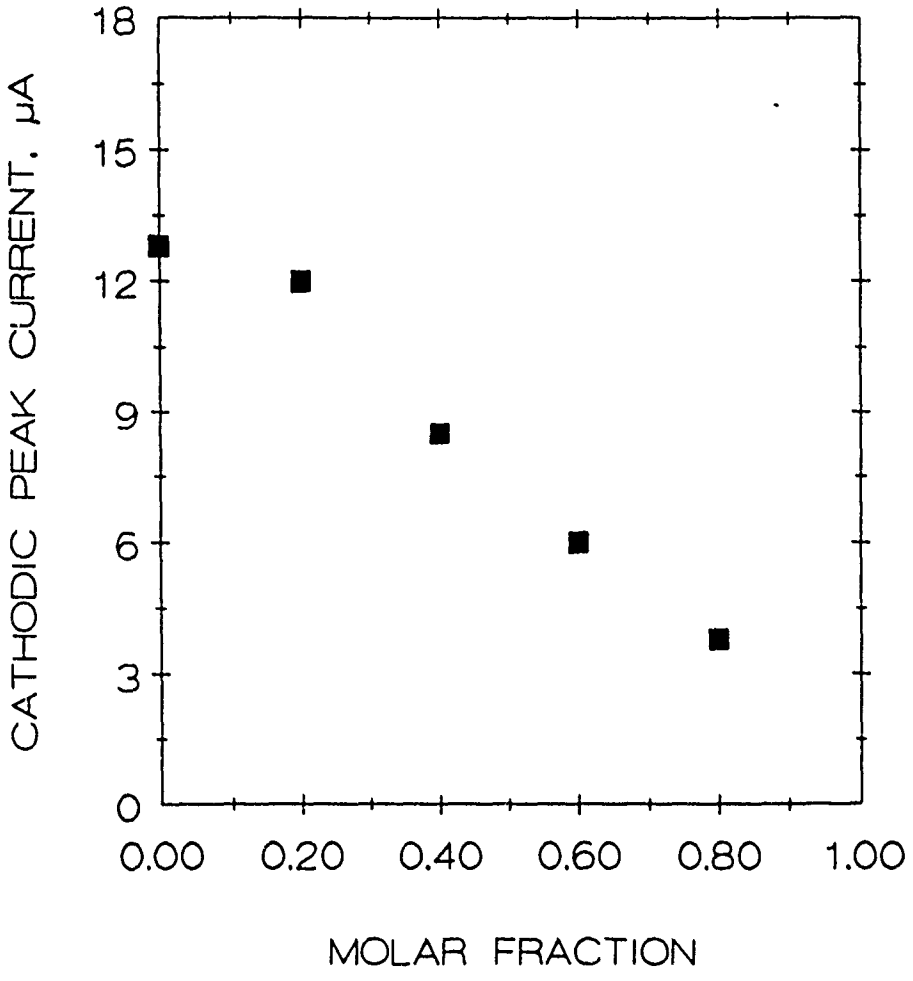

FIG. 5 HAN & KAIFER

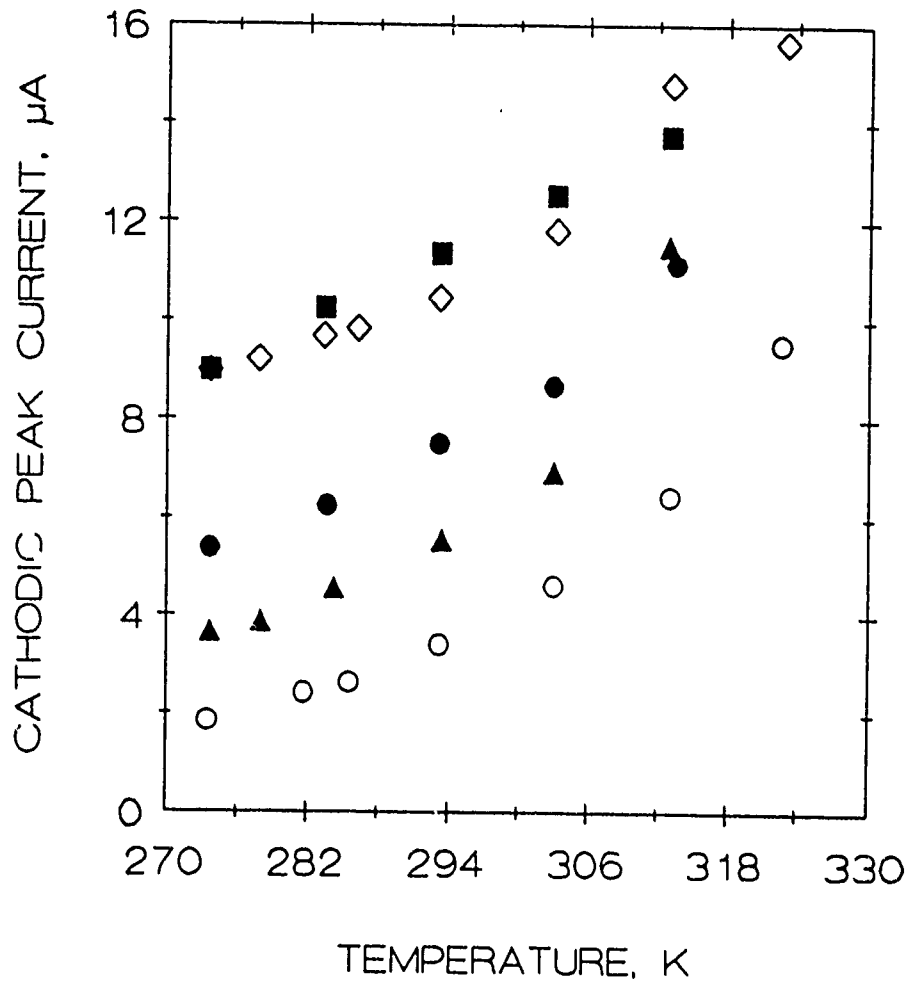

FIG. 6 HAN { KAIFER

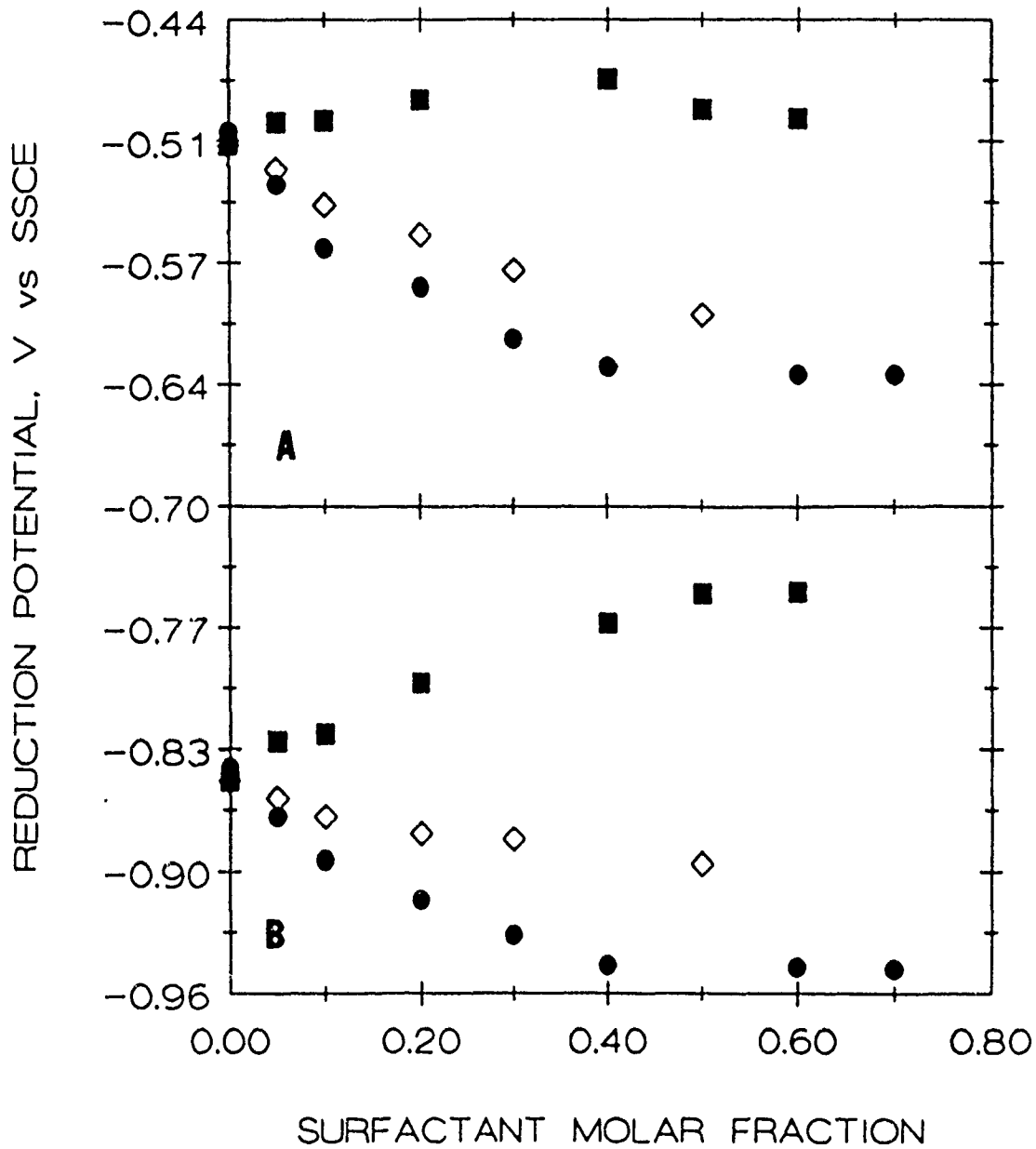

FIG. 7 HAN & KAIFER

II-64

(14)

Electrochemical Methods and Physicochemical Structures of Liquid Disperse Systems

Alain Berthod

Laboratoire des Sciences Analytiques, UA CNRS 435, Université de Lyon 1
69622 Villeurbanne cedex, FRANCE.

ABSTRACT

Electroanalytical techniques can provide valuable information on the physico-chemical structures of liquid disperse systems. micellar solutions, emulsions, and microemulsions. In micellar media, the partition coefficient of an electroactive solute can be determined from its polarographic apparent diffusion coefficient. Equations show that micelle size can be estimated from diffusion coefficients only at high surfactant concentration and with solute having a high partition coefficient (P > 10,000). In emulsion, the droplet size act on the kinetic of an oil-soluble electroactive compound release in aqueous phase. In coarse dodecane emulsions, ferrocene voltammograms depict an irreversible electrochemical process which becomes more reversible in fine emulsions. Polarographic fist kind maxima on oxygen reduction waves may allow to delineate the L2 zone in a ternary phase diagram.

The liquid disperse systems considered in this paper are micellar solutions, emulsions and microemulsions. Micellar solutions contains micelles which result from the aggregation of surfactant molecules above the appropriate concentration termed critical micelle concentration (CMC) (1). Emulsions are heterogeneous systems made of two immiscible liquids. One of the liquids is dispersed in the other in the form of droplets of microscopic size (>0.1 μm). Surfactants stabilize the system greatly slowing down droplet coalescence (2). Microemulsions are isotropic, spontaneous forming and microstructured liquid phases. They are composed of water or brine, an oil and a blend of surfactant and cosurfactant (3).

Physicochemical structures of such liquid systems were investigated using quasi-elastic light scattering (4), radioactive tracers (5), conductivity and viscosity measurements (6), small angle neutron scattering spectroscopy (7), microwave dielectric measurements (8) or high resolution NMR (9, 10). Electrochemical methods, such as polarography or cyclic voltammetry, are other ways to obtain physicochemical information on liquid disperse system (10).

In this work, we go a little deeper into the solute partition coefficient determination obtained using the diffusion current of polarography in micellar media. Emulsion particle size is shown to affect oil-soluble solute cyclic voltammograms. The possibility of L2 microemulsion-zone-delineation using polarography is proposed and discussed.

EXPERIMENTAL SECTION

Chemicals. The surfactant used were sodium dodecylsulfate (SDS, $C_{12}H_{25}OSO_3^- Na^+$), an anionic water-soluble surfactant; sodium bis-ethylhexylsulfosuccinate (AOT, $C_8H_{17}OOC-CH_2-CH(COO-C_8H_{17})-SO_3^- Na^+$), an anionic reverse micelle-forming surfactant; cetyltrimethylammonium bromide (CTAB, $C_{16}H_{33}N(CH_3)_3^+ Br^-$), a water-soluble cationic surfactant, polyoxyethylene 23 dodecyl ether (Brij® 35, $C_{12}H_{25}(OCH_2CH_2)_{23}OH$), a nonionic water-soluble surfactant. They were supplied by Merck (Darmsdadt, Germany) Table I lists some physicochemical properties of the four surfactants used. Dodecane and heptane were obtained from Merck. Water was deionized and glass-distilled.

Electrochemical system. A polarograph PRG-5 (Tacussel Electronics, Villeurbanne, France) was used with a three electrode arrangement. Two working electrode were used. a dropping mercury electrode for polarography and a platinum rotating disk for cyclic voltammograms. The counter-electrode was a platinum wire and the reference electrode was a Ag/AgCl/saturated KCl electrode with a protecting sheath filled with a gel of agar-agar ($LiClO_4$, 1M).

Emulsions. Dodecane in water emulsion composition was 30–70% v/v. They were oil in water (o/w) emulsions prepared with a high speed mixer (20,000 rpm, Ultra–Turax, Cole Palmer) or a Manton–Gaulin homogeneizer, for coarse emulsions (particle diameter ± 1.8 μm) or fine emulsions (diameter ≤ 0.4 μm), respectively (**11**). Particle size were estimated by laser light–scattering correlation spectroscopy (Coulter Nanosizer, Coultronics). The Nanosizer gave an average diameter of about 1.8 μm with a high polydispersity index for every emulsion prepared with the mixer. Microemulsion systems were prepared by simply mixing the appropriate weight of water, oil, surfactant and cosurfactant (**3**).

DIFFUSION COEFFICIENTS AND MICELLAR PARTITION COEFFICIENTS

A micellar media can solubilize an apolar solute into the apolar micelle core. Using the pseudo–phase model, the apolar micellar phase is considered as a separated phase whose volume fraction is CV, with the concentration of micellized surfactant, C (= surfactant bulk concentration – CMC), and the molar volume of the surfactant, V (Table I). A solute partitions between the aqueous phase and the micellar pseudo–phase. A partition coefficient, P_{mw}, is introduced to quantify the solute affinity for the micellar pseudo–phase. The inverse, $1/P_{mw}$, is noted P_{wm}. P_{wm} is the partition coefficient of the solute between the aqueous and micelle phases.

The observed diffusion coefficient of a solute in micellar solution, D_{obsd}, is given by

$$D_{obsd} = \alpha D_m + (1 - \alpha) D_{aq} \quad (1)$$

where D_m is the diffusion coefficient of the micelle, D_{aq} is the diffusion coefficient of the solute in aqueous surfactant solution just below the CMC (no micelle nearby) and α is the mole percent of solute in the micelle. We demonstrated that eq. 1 can be developed

$$D_{obsd} = (D_m + \psi D_{aq})/(1 + \psi) \quad (2)$$

with

$$\psi = N (1 - CV)/(P_{mw} CV) = P_{wm} N (1 - CV)/CV \quad (3)$$

where N is the micelle aggregation number. Eqs 1 and 2 were first used by Stilbs (**12**) and Ohsawa (**13**) with $\psi = P_{wm}$.

If the micelle diffusion coefficient, D_m, is known, the solute diffusion coefficient, D_{aq}, can be measured in a water solution containing a surfactant concentration just below the CMC. Then, the

solute diffusion coefficient, D_{obsd}, can be measured in micellar solutions. Figure 1 shows the effect on increasing micellar concentrations on the solute polarographic wave. The limiting diffusion current decreases as the micellar concentration increases. A minimum limiting diffusion current is observed when the solute is almost completely located inside the micelles and diffuses with the micelles. In this case, $\alpha \approx 1$ and $D_{obsd} \approx D_m$.

For the Figure 1 conditions, Figure 2 shows the evolution of the ratio of the limiting diffusion current in micellar media over the limiting diffusion current without micelles, I/I_o, versus the concentration of micellized surfactant for different solute partition coefficients, P. It is clearly showed that D_{obsd} can be matched with D_m only for high surfactant concentrations (C>0.1M) **and** high partition coefficients (P>10,000).

2 Methyl 1,4 naphthoquinone (vitamin K3) is poorly soluble in water (max. sol. 8.6×10^{-4}M, 0.15 g/L or 150 ppm). Its solubility is greatly enhanced by micelles. Vitamin K3 needs two electrons and two protons to be reduced to the corresponding diphenol. The half-wave potential is pH-depending. Vitamin K3 polarographic reduction was studied in three different micellar media, at differing surfactant concentrations and pHs, as listed in Table II. The measured P_{mw} coefficients were 34000, 32500 and 20500 in SDS, CTAB and Brij 35 micellar solutions, respectively. The relative standard deviations were 12%, 28% and 34% in the three micellar solutions, respectively. the main source of error was the poor precision of the micelle aggregation number. The solute partition coefficients per surfactant molecule, namely P_{mw}/N, were 380, 270 and 82 for SDS, CTAB and Brij 35 surfactants, respectively. The relative standard deviation were only 5%, 15% and 12%, respectively. In the three micellar media, the log P_{mw} values were close to 4.5.

In ionic micellar solutions, the supporting electrolyte greatly affects the partition coefficient of charged solutes (15). In this case, the solute-micelle interaction is due to partition and ion-exchange. However, experimental polarograms resembling Figure 1's and experimental I versus log C plots resembling Figure 2's were obtained with Cd^{2+}, Tl^{+} and Zn^{2+} ions in SDS and CTAB solutions (16). The half-wave potentials are often affected by micellar solubilization. This was discussed by Pelizzetti (17).

CYCLIC VOLTAMMOGRAMS AND EMULSION PARTICLE SIZE

Electrochemistry in water in oil emulsions is difficult or impossible with classical methods due to the low conductivity of such media. We worked in oil in water systems. Very hydrophobic molecules can be solubilized in oil in water emulsions. They are located inside the oil droplets. On

the opposite, polar molecules and/or ions are located in the continuous water phase. We showed that the mechanism of the electrochemical oxidation of ferrocene in a dodecane–in–water emulsion stabilized with nonionic surfactants could be compared to a CE mechanism (**18**). The nature of the "preceding reaction" was not clearly identified. It could be (i) ferrocene mass transfer from dodecane droplets to the aqueous phase, (ii) droplet rupture near the electrode surface, or (iii) surfactant wetting mechanism.

Ferrocene oxidation was performed in 30–70% v/v dodecane in water emulsions stabilized with SDS, CTAB and Brij. The emulsification was done with two different energy levels, a medium energy level (mixer at 20,000 rpm) and a high energy level (homogenizer working at pressures higher than 300 bars or 4300 p.s.i.). The emulsion particle size ranged from 0.12 μm to 1.8 μm. Figure 3 shows the cyclic voltammograms of ferrocene in a 1.8 μm emulsion (3–1), a 0.45 μm emulsion (3–2) and a micellar nonionic solution (3–3). The electrochemical oxidation of ferrocene is reversible. The ratio of the cathodic peak current over the anodic peak current, i_{pc}/i_{pa}, gives information on kinetic, or other, complications in the electrode process (**19, 20**). Its value was 1.7 and 1.13 in the coarse and fine emulsions, Figures 3–1 and 3–2, respectively.

Table III lists the average particle size, viscosity and i_{pc}/i_{pa} ratio for dodecane–in–water emulsions stabilized by SDS, CTAB and Brij. The i_{pc}/i_{pa} ratio decreased from 1.75 in coarse emulsions to 1.05 in fine emulsions regardless to the surfactant used to stabilize the emulsion (**11**). There is no relationship between the i_{pc}/i_{pa} ratio and viscosity. In fine emulsions, the value of the peak current ratio is close to unity indicating that the weight of the kinetic term decreased. The current seems mainly controlled by the motion of the fine droplets whose size can be roughly estimated from the ferrocene diffusion coefficients. The value 2.5×10^{-7} cm^2/s, obtained for the ferrocene diffusion coefficient in the fine Brij emulsion (Figure 3–2) corresponds to a Stoke–Einstein droplet size of 30 nm diameter. In this emulsion, the Nanosizer average particle diameter was 450 nm (Table III) which a large polydispersity index. The very fine emulsion droplets seems to control the ferrocene transport at the electrode surface. In o/w microemulsions, the droplet polydispersity is much lower than in emulsion. Mackay et al. (**21**) showed that the ferrocene diffusion coefficient reflected the size of droplets of a hexadecane–water o/w microemulsion system.

Today it exists apparatuses able to give the accurate mean droplet diameter of any emulsion in minutes. A particle size distribution histogram is also produced by such particle meters. Cyclic voltammetry will not be used to make this measurement. However, cyclic voltammetry shows that the solubilization of an electroactive compound in emulsion droplets complicates its electrochemical reaction at the electrode surface. The particle size distribution of an o/w emulsion affects the general shape of the voltammogram of the oil–soluble electroactive compound.

II-70

OXYGEN POLAROGRAMS AND MICROEMULSION STRUCTURE

Some microemulsion systems have a physico-chemical structure easy to determine. For example, the oil-in-water area, named L1 structure, can be well separated in the phase diagram from the water-in-oil area, named L2 structure. For example, the SDS-hexanol-dodecane system, the SDS-heptanol or SDS-octanol-oil-water systems present phase diagrams with tiny L1 area well-differentiated from large L2 area (22). A number of interesting microemulsion systems presents a large domain of stable microemulsions whose composition can change continuously from the L1 structure with water-rich compositions to L2 structure with oil-rich compositions. Between the L1 and L2 structures, there is an intermediate structure, the bicontinuous structure (3).

The polarographic study of oxygen reduction in microemulsion was showed to be a possible way to obtain structural information (23). Oxygen is an interesting electroactive solute which is water and oil soluble. It dissolves naturally in microemulsion without changing neither the microemulsion structure nor the ionic strength. The two steps of its reduction process are pH-sensitive. In several anionic microemulsion system, a first kind polarographic maximum was observed on the first reduction wave of oxygen. It was demonstrated that surfactant adsorption onto the mercury electrode was not responsible for the current changes observed (23, 24). The polarographic maximum appeared suddenly at a precise microemulsion composition. Given the characteristics of polarographic maxima and the surfactant adsorption on electrode surface (studied by ac-polarography), it was assumed that the maxima could only exist in presence of a non-aqueous continuous phase, i.e. L2 structure, with an oil-mercury interface without adsorbed surfactant (23). The area of the phase diagram of the system SDS-pentanol-dodecane-water, in which a polarographic maxima was observed, corresponded to the L2 area determined independently by conductivity measurements (24).

Figure 4 presents the phase diagram of the system CTAB-butanol-heptane-water. The CTAB/butanol mass ratio was 1. Water contained 0.1M NaCl electrolyte. In this cationic microemulsion system, a first kind maximum was observed inside the area limited by a dashed line. Points indicate the microemulsion composition corresponding to the polarograms presented on the figure. The delineated area of this system is much larger than the ones obtained in anionic systems. It would be very interesting to confirm that microemulsion compositions with more than 55% water still have a L2 structure (Figure 4) Unfortunately we did not find such a confirmation in the literature.

Figure 5 shows the AOT-heptane-water system which does not contain a cosurfactant. It is known that this system has a large L2 area well separated from the L1 area (23). In the horizontally hatched area, sudden current changes were observed at a reproducible potential as shown by the two

polarograms shown on the right of the figure. The area is not exactly limited because difficulties to perform polarography in this system interrupted the polarographic measurements in many compositions. The complications were (i) a too high viscosity in water and surfactant–rich compositions, (ii) a very high resistivity in heptane–rich compositions, (iii) surfactant adsorption–desorption in intermediate compositions. This shows the limitation of the method. The microemulsion composition should have a suitable electrical conductivity, a low viscosity and no surfactant adsorption sharp changes in the potential range of the polarographic maximum.

LITERATURE CITED

1. Hinze, W.L. In *Solution Chemistry of Surfactants*; Mittal, K.L., Ed.; Plenum Press, New York, 1979, Vol. 1; pp. 79–101.
2. Becher, P. *Encyclopedia of Emulsion Technology*, Marcel Dekker, New York, 1983.
3. Robb, I.D. *Microemulsions*; Plenum Press, New York, 1982.
4. Cazabat, A.M.; Langevin, D. *J. Chem. Phys.* 1981, 74, 3148–3155.
5. Lindman, B.; Kamenka, N.; Brun, B.; Nilson, P.G. *J. Phys. Chem.* 1980, 84, 2485–2491.
6. Boned, C.; Peyrelasse, J.; Zradba, A.; Clausse, M. *J. Colloid Interface Sci.* 1982, 88, 602–604.
7. Cabane, B. In *Surfactant Solutions, New Methods of Investigations*; Zana, R., Ed., Marcel Dekker; New York, 1987, Surfactant Science Series, Vol. 22, Ch. 3.
8. Epstein, B.R.; Foster, K.R.; Mackay, R.A. *J. Colloid Interface Sci.* 1983, 95, 218–227.
9. Lindman, B.; Stilbs, P. In *Microemulsion Systems*, Rosano, H.L.; Clausse, M., Eds; Marcel Dekker; New York, 1987, Surfactant Science Series, Vol. 24, Ch. 7.
10. Dayalan, E.; Qutubuddin, S.; Texter, J. *This symposium* 1991, paper III–1.
11. Georges, J.; Desmettre, S. *Electrochim. Acta* 1986, 31, 1519–1524.
12. Armstrong, D.W.; Ward, T.J.; Berthod, A. *Anal. Chem.* 1986, 58, 579–582.
13. Stilbs, P. *J. Colloid Interface Sci.* 1981, 80, 608–610.
14. Ohsawa, Y.; Aoyagui, S. *J. Electroanal. Chem.*, 1982, 136, 353–360.
15. Berthod, A.; Georges, J. *Nouv. J. Chim.* 1985, 9, 101–108.
16. Moorthy, P.N.; Kishore, K. In *Surfactants in Solution*, Mittal, K.L. Ed.; Plenum Press, New York, 1989, Vol. 9; pp.135–147.
17. Pelizzetti, E.; Minero, C.; Fisicaro, E. *This symposium* 1991, paper I–1.
18. Georges, G.; Berthod, A. *J. Electroanal Chem* 1984, 175, 143–152.
19. Nicholson, R.S.; Shain, I. *Anal Chem.* 1964, 37, 706–710.
20. Bard, A.J , Faulkner, L.R. *Electrochemical Methods*, J. Wiley, New York, 1980, pp 229 and 447–451.

21. Mackay, R.A.; Myers, S.A.; Bodalbhai, L.; Brajter–Toth, A. *Anal. Chem.* 1990, 62, 1084–1090.

22. Georges, J.; Berthod, A.; Arnaud, H. In *Surfactants in Solution*; Mittal, K.L.; Bothorel, P., Eds.; Plenum Press, New York, 1986, Vol. 1; pp.1457–1472.

23. Berthod, A.; Georges, J. *J. Colloid Interface Sci.* 1985, 106, 194–202.

24. Berthod, A. In *Microemulsion Systems*, Rosano, H.L.; Clausse, M., Eds; Marcel Dekker; New York, 1987, Surfactant Science Series, Vol. 20, Ch. 20.

25. Berthod, A.; Nicolas, O.; Porthault, M. *Anal. Chem.* 1990, 62, 1402–1407.

Table I : Physicochemical Properties of the Surfactants Used

Surfactant	m.w.	V L/mol	CMC mM		R nm		N		D_m 10^{-7} cm^2/s	
			water	0.1 M NaCl	water	0.1 M NaCl	water	0.1 M NaCl	water	0.1 M NaCl
SDS	288.4	.246	8.2	1.4	2.5	2.9	62	80–100	5.7	5.3
AOT	444.6	.383	oil	soluble	reverse	micelle	size dep	ends on	water	cont.
CTAB	364.5	.364	.9	.19	2.2	2.6	90	100–140	6.8	6.5
Brij 35	1200	1.064	.17	.17	4.8	4.8	200–300	200–300	4.7	4.7

V = molar volume, R = average micelle radius, N = average micelle aggregation number, from Refs. 15, 23 and 25 and references therein.

Table II: Polarographic Measurement of the Partition Coefficient of Vitamin K3

Surfactant	concentration M	pH	$E_{1/2}$ $V_{Ag/AgCl}$	D_{obsd} 10^6 cm^2/s	α %	Pmw / N	Pmw	log P
SDS	0.0336	1.6	+.03	2.5	75	380	30000–38000	4.5
D_{aq} = 8.5 10^{-6}	0.0340	6.5	−.28	2.5	75	380	30000–38000	±.05
CTAB	0.0263	3.2	−.04	2.4	75	310	31000–43000	
D_{aq} = 7.6 10^{-6} cm^2/s	0.130	3.2	−.04	1.2	92	240	24000–34000	4.5
	0.267	3.6	−.05	0.88	97	280	28000–39000	±.15
	0.126	7.3	−.24	1.2	92	250	25000–35000	
Brij 35	0.00783	3.1	−.04	5.1	43	92	18400–28000	
D_{aq} = 8.6 10^{-6} cm^2/s	0.0393	3.1	−.04	2.5	75	69	14000–21000	4.3
	0.080	4.2	−.09	1.4	89	84	17000–25000	±.15
	0.0383	7.0	−.23	2.3	77	82	16500–24500	

NaCl 0.1 M supporting electrolyte; pH adjusted with HCl or NaOH..

Table III: Particle size, viscosity and Ferrocene current ratio in different emulsions

surfactant	conc. %w/w	Emulsifier	d_p μm	ν cP	i_{pc}/i_{pa}
SDS	1.65	M	1.8	2.3	1.7
CTAB	1.1	M	1.8	2.3	1.5
	1.1	H	0.21	2.4	1.3
	1.65	M	1.8	2.8	1.7
	1.65	H	0.15	3.0	1.05
	5.15	M	1.8	3.6	1.75
	5.15	H	0.12	3.9	1.09
BRIJs	1.1	M	1.8	2.3	1.7
	1.1	H	0.45	2.4	1.13

Surfactant concentration in % w/w added to a 30-70 w/w dodecane-water mixture; ferrocene concentration 5_n10^{-3} M; scan rate 50 mV/s; M = mixer; H = homogenizer; viscosity data from Ref. 11 and 18; Brijs means a blend of 50% Brij 78 and 50% Brij 72 w/w (HLB = 10).

FIGURE CAPTIONS

Figure 1: Effect of surfactant concentration and partition coefficient on the appearance of the polarographic wave of a hypothetical solute. Polarograms calculated using the Heyrovski equation and Eqs. 2 and 3 with D_{aq} = 2.6 10^{-6} cm^2/s, D_m = 5.7 10^{-7} cm^2/s, $E_{1/2}$ = 0.6 V, α n = 1, N = 62 molecules/micelle, V = 0.248 L/mol, thin solid line C = 0.001M, dashed line C = 0.01M, dotted line C = 0.1M, thick solid line C = 1M.

Figure 2: Plots of the ratio I/I_o versus the micellized surfactant concentration. Same data as Figure 1's. CMC = 1.4 10^{-3}M.

Figure 3: Voltammograms of ferrocene. 1- 5*10^{-3}M in a 30-70 v/v dodecane-in-water emulsion with d_p = 1.8 μm. 2- 5*10^{-3}M in a 30-70 v/v dodecane-in-water emulsion with d_p = 0.45 μm. 3- 2.5*10^{-3}M in a Brij 35 12 % w/v micellar solution. Temperature = 22°C, electrode area 3 mm^2, scan rate 50 mV/s.

Figure 4: Oxygen polarograms obtained in the CTAB-butanol-heptane-water microemulsion system. The dashed line delineates the area in which a first kind polarographic maximum can be observed. Points locate the composition of the corresponding polarograms. Sampled dc polarography, drop time 1.5 s, scan rate 10 mV/s, horizontal scale 0.5 V, vertical scale 10 μA. Dotted area: liquid crystal, black area: biphasic turbid systems.

Figure 5: Oxygen polarograms in the AOT-heptane-water system. In the horizontally hatched area, some current perturbations, as illustrated by the polarograms was observed. Natural drop time, scan rate 10 mV/s. LC = liquid crystal, dotted area: highly viscous biphasic mixtures of LC and L2 systems.

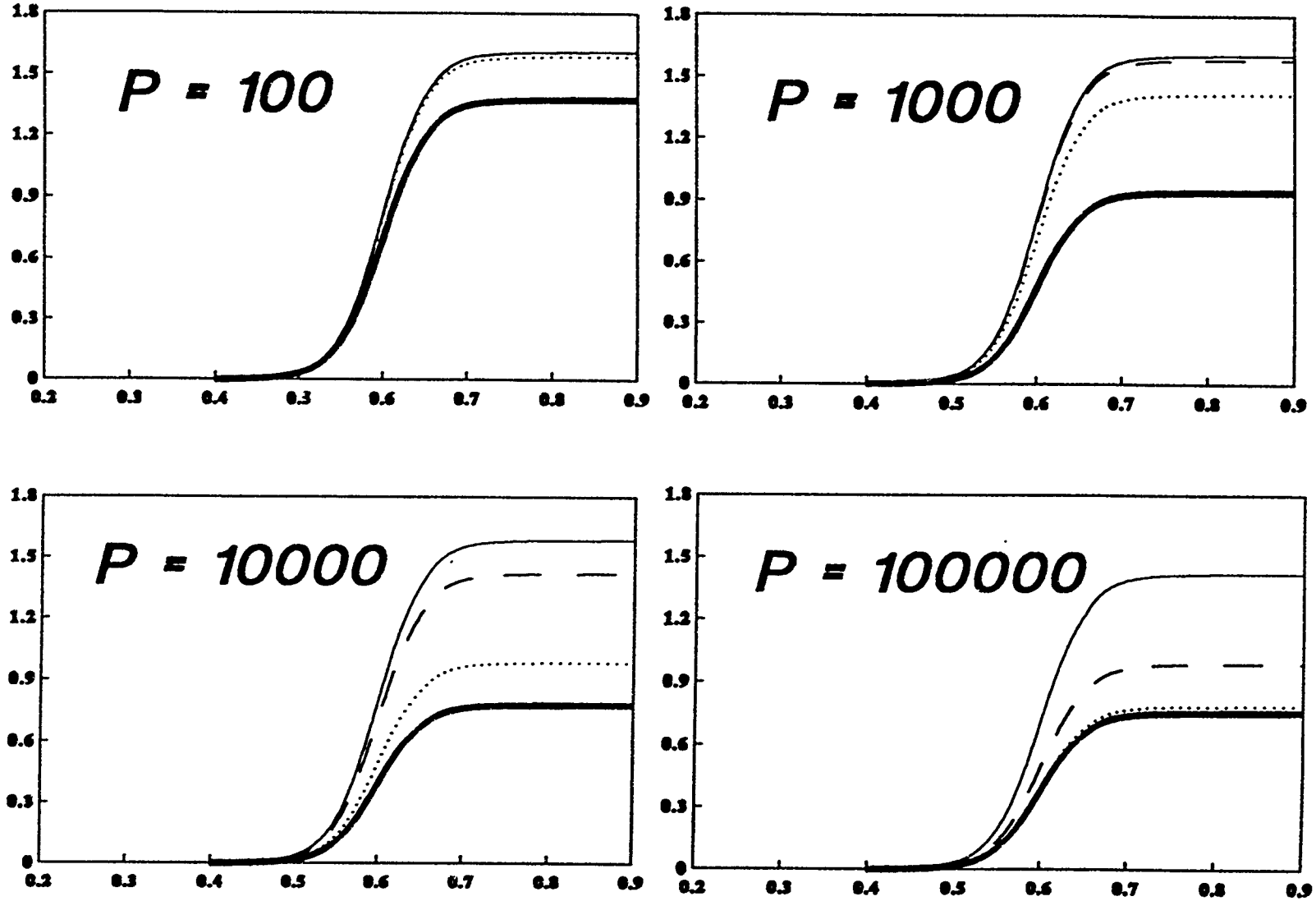

II-77

Berthod Figure 1

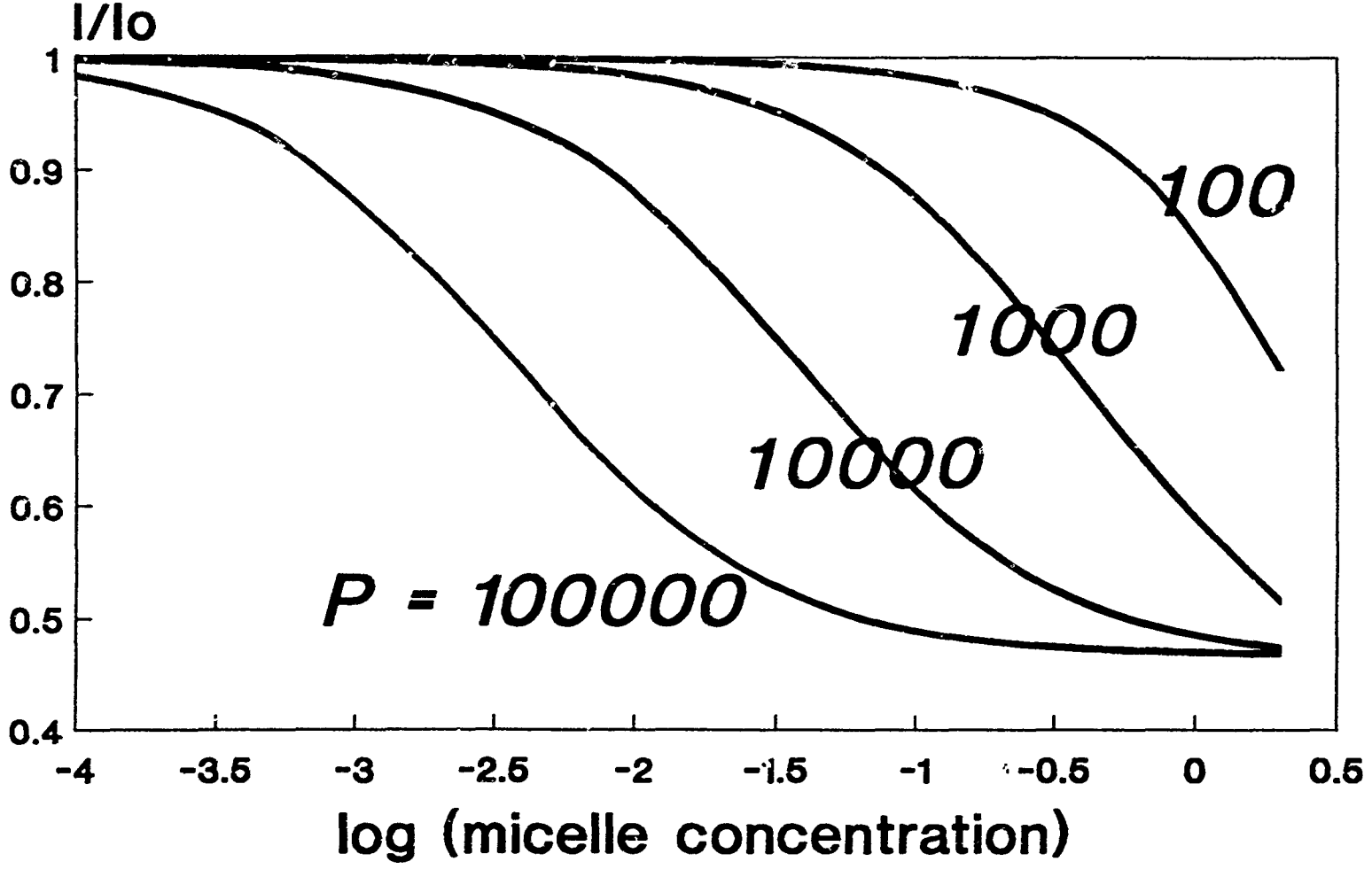

R - II

Berthod - Figure

Figure 3. Electr

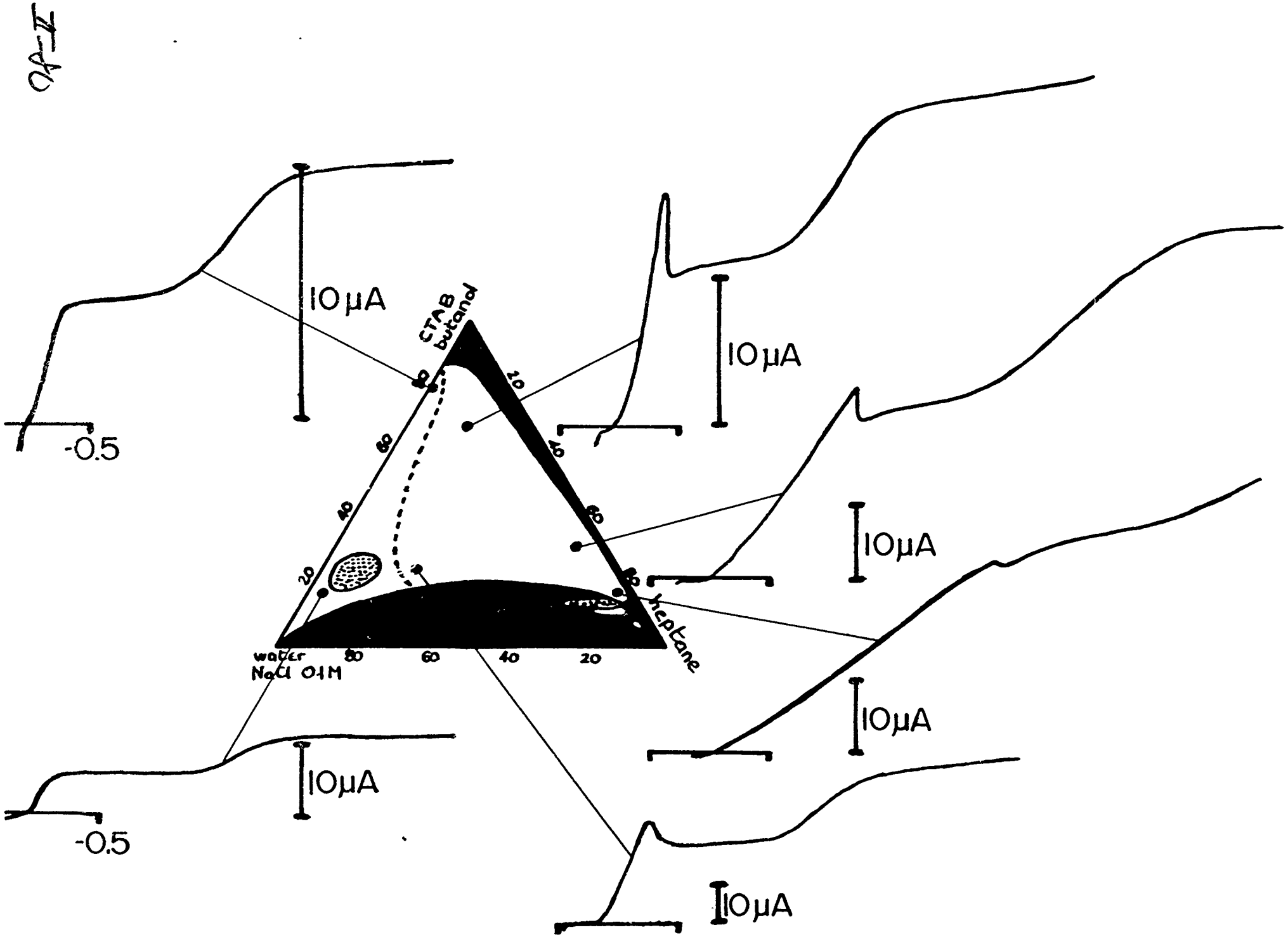
CTAB
butanol
heptane
water
NaCl 0.1M
80
60
40
20
10
40
60
80
10μA
-0.5

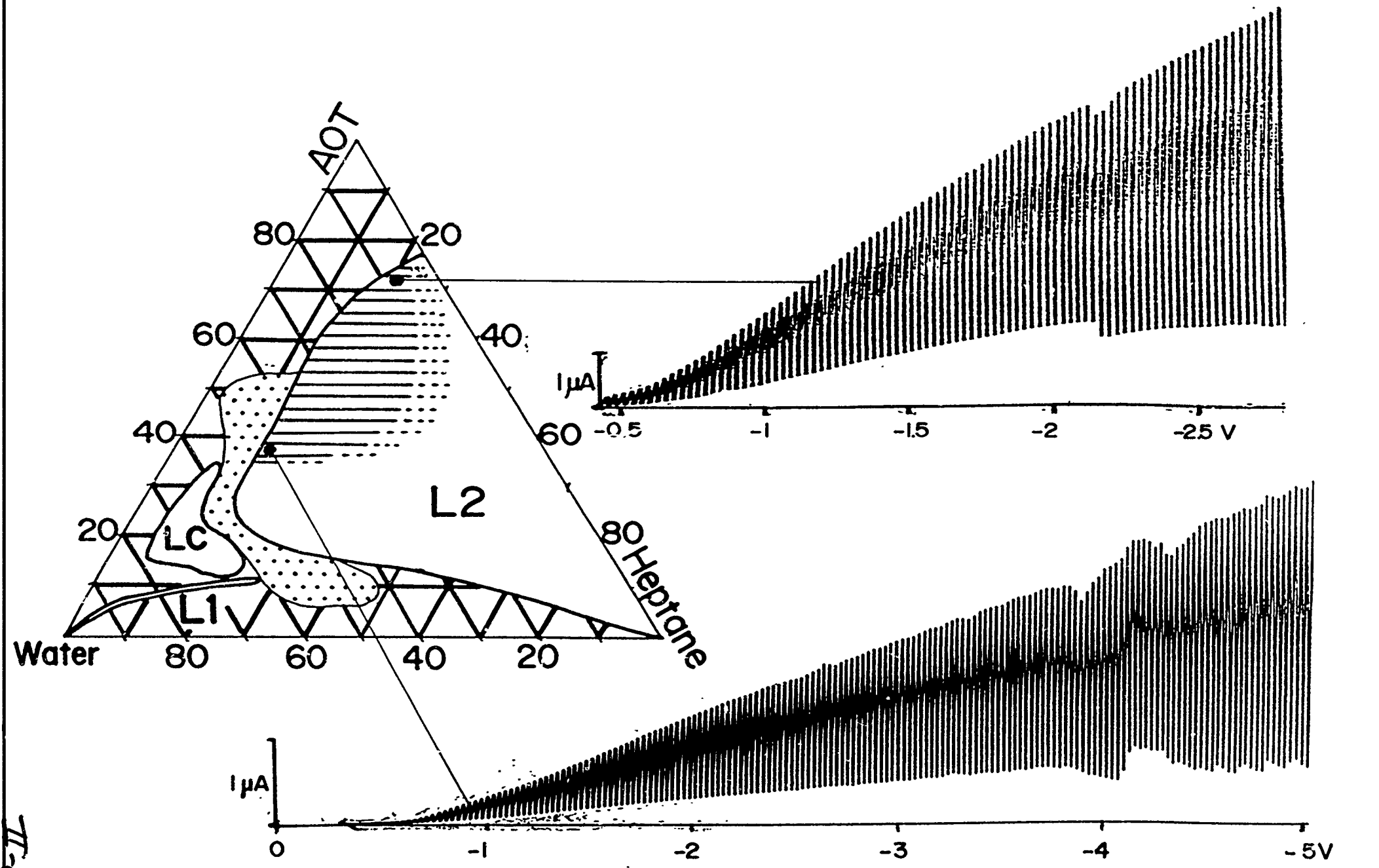
AOT
80
20
60
40
40
60
20
LC
L2
80
Heptane
L1
Water
80
60
40
20
1 μA
-0.5
-1
-1.5
-2
-2.5 V
1 μA
0
-1
-2
-3
-4
-5V

II-8

(15) ELECTROCHEMICAL INSIGHTS INTO MICROEMULSION STRUCTURE AND THE EFFECT OF MICROSTRUCTURE ON ELECTROCHEMICAL REACTIONS

By

Stephanie A. Myers, Liakatali Bodalbhai, Anna Brajter-Toth
Department of Chemistry
University of Florida
Gainesville, FL 32611-2046

and

Raymond A. Mackay
CRDEC, U.S. Army
Aberdeen Proving Ground, MD 21020-5423

INTRODUCTION

A microemulsion (μE) is thermodynamically stable mixtures of oil, water and surfactant [1]. Often it also contains a cosurfactant, which is usually a medium chain alcohol. Inorganic electrolytes, such as NaCl, may also be included in the mixture. Besides being thermodynamically stable, μEs are microscopically heterogeneous with distinct oil and water regions. This microstructure has made them of interest for many applications. For example, they provide an attractive alternative to conventional solvents [2-4]. Being microscopically heterogeneous, μEs can solubilize both oil-soluble and water-soluble compounds. Since the reagents are localized in either the oil or water phase, the effective local concentrations are increased. This can increase the reaction rates [4-7]. Reactions can be followed spectroscopically, since μEs are optically isotropic [3,4].

On the microscopic level, μEs organize into specific structures [1]. In mixtures with high water content, i.e. oil-in-water (O/W) μEs, oil is confined to discrete droplets and water acts as a continuous phase. The oil droplets are surrounded by a well-defined layer of surfactant and cosurfactant [8], which is often referred to as the membrane phase. Similarly, water-in-oil (W/O) μEs have high oil content, and water droplets, surrounded by the membrane phase, exist in a continuous phase of oil. If both oil and water content of the solution are significant, the so-called bicontinuous μE is formed. In such systems, both oil and water act as continuous phases, with a sponge-like organization [9]. As with droplet μEs, the membrane phase separates oil from water.

Many techniques have been used to determine microstructure of μEs. Quasielastic light scattering (QELS) [10,11] and small angle neutron scattering (SANS) [9,12] have been used to determine droplet size in both O/W and W/O systems. Fluorescence quenching [13,14] has been used to determine the surfactant aggregation number, i.e the number of surfactant monomers attached to the droplet. From this number, droplet size can be determined.

The techniques mentioned above are used only to determine droplet size. Consequently, they provide little useful information about bicontinuous μEs. Fourier transform pulsed gradient spin echo NMR

II-84

may be used to determine the microstructure of both droplet and bicontinuous μEs [4,15] through measurement of the self-diffusion coefficient of each μE component. If the diffusing species is attached to the μE droplet, it cannot diffuse over macroscopic distances and, therefore, the diffusion coefficient measured is the diffusion coefficient of the droplet [10,16,17]. For example, in O/W μE, the species confined to the droplet would be either oil or surfactant. The diffusion coefficient can then be related to the size of the droplet by the Stokes-Einstein equation. Typical diffusion coefficients of species confined to μE droplets are on the order of 10^{-7} cm^2/s [18]. On the other hand, the self-diffusion coefficient of the continuous phase is lowered from its value in neat liquid by the obstruction effect [8,19-21]. The obstruction effect slows the self-diffusion coefficient of a component in a continuous phase by lengthening its diffusion path. For example, the volume excluded by oil and surfactant in an O/W μE will lengthen the diffusion path of water, since water will not penetrate the oil droplets [8]. In bicontinuous μEs, the volume of excluded phase will be larger and the self-diffusion coefficient of both oil and water lower than if they had been the continuous phase in a droplet μE. Typical self-diffusion coefficient values of water and oil in bicontinuous μEs are on the order of 10^{-6} cm^2/s. These values of self-diffusion coefficient are lower than values in neat liquid, which are typically about 10^{-5} cm^2/s, and higher than typical values of 10^{-7} cm^2/s for droplets. Since the diffusion path of the surfactant is restricted by both oil and water, its self-diffusion coefficient in bicontinuous μEs is lower than that of either oil or water, typically ca. 1×10^{-6} cm^2/s [18,22].

Electrochemical methods offer a simple and convenient method to determine μE structure with the same versatility as NMR. With electrochemical techniques, the diffusion coefficient of an electroactive probe will reflect the self-diffusion of the phase in which the probe resides [10,23,24]. Consequently, electrochemical diffusion coefficients reflect μE structure in the same manner as self-diffusion coefficients from NMR. In addition, electrochemical techniques can also be used to study redox and related chemical reactivity in the microheterogeneous environment of μEs [23-26].

In this work, electrochemical methods are used to determine the microstructure of an anionic μE of sodium dodecylsulfate (SDS)/1-pentanol/dodecane/0.1 M $NaCl_{(aq)}$. The large μE region [27] of this

system allows changes in structure to be observed over a wide range of compositions. Since the droplet region of this μE has been characterized previously, there is sufficient data for comparison of electrochemical techniques to other methods. Ferrocene (Fc) is used to probe the oil phase of the μE. Because of its low solubility in water compared to dodecane, Fc resides almost completely in the oil phase. The diffusion coefficient (D_0) of water-soluble ferricyanide ($Fe(CN)_6^{-3}$) is used to probe the aqueous phase. Since $Fe(CN)_6^{-3}$ is negatively charged, it does not interact with the anionic surfactant. Methyl viologen (MV^{+2}) is used to probe the membrane phase. MV^{+2}, as a cationic, water-soluble probe, associates with the anionic surfactant layer.

The effect of μE structure/composition on the redox reactivity of the probes was also investigated. Microemulsion composition was shown to affect both formal potential (reactivity) and reversibility (kinetics). Effect of composition on structure and reactivity were also demonstrated by comparing the electrochemical results of this study to a similar study of a cationic cetyltrimethylammonium bromide (CTAB)/1-butanol/hexadecane/water μE [23].

EXPERIMENTAL

Materials. Sodium dodecylsulfate (SDS), NaCl, KCl and potassium ferricyanide ($Fe(CN)_6^{-3}$) were obtained from Fisher. 1-Pentanol and methyl viologen dichloride hydrate (MV^{+2}) were obtained from Aldrich. Ferrocene (Fc) was from Arapahoe Chemicals. n-Dodecane was from Alfa products. All chemicals were used without further purification. Water used was deionized and then distilled.

Apparatus. For cyclic voltammetry (CV) and chronocoulometry a Bioanalytical Systems Electrochemical Analyzer, BAS-100, was used. In the electrochemical measurements, which were conducted in a three electrode configuration, the working electrode was glassy carbon (High Performance, Englewood, CA, or Electrosynthesis). The working electrode was made by sealing a glassy carbon rod in a glass tube with epoxy cement [28]. Electrical contact was established with a mercury contact between the glassy carbon and a copper wire lead. The auxiliary electrode was platinum wire and the reference was a saturated calomel electrode (SCE). Before each measurement, glassy carbon working electrodes were polished with Gamal gamma alumina/water slurry (Fisher) on a microcloth using Ecomet 1 polishing wheel (Beuhler). After polishing, the electrodes were ultrasonicated in distilled water for about five minutes immediately before use.

Methods. The working electrode areas were determined by chronocoulometry in 3.1×10^{-3} M solution of $Fe(CN)_6^{-3}$ in 0.5 M KCl. Using the diffusion coefficient, $D_0 = 7.6 \times 10^{-6}$ cm^2/s [29], the glassy carbon electrode areas were 0.07 ± 0.01 cm^2. In the measurements of electrode area, the pulse width was 250 ms and the potential was stepped from +0.400 to -0.100 V.

In CV measurements in μEs, typical resistances were between 100 to 500 ohms before compensation and were compensated to less than 50 ohms using the BAS-100. Peak potentials and peak currents were measured after iR compensation.

Diffusion coefficients for the reduced, D_R, or the oxidized, D_O, forms of the probes were calculated from the slopes of the chronocoulometric plots of Q vs $(t)^{1/2}$ [30]. The potential step window for chronocoulometry was chosen following CV experiments. The pulse widths were 250 ms. All measurements were carried out at 25 ± 2°C and all potentials are cited versus SCE.

Preparation of Microemulsion Solutions. The phase diagram of the SDS microemulsion (μE) used in this study (Figure 1) has been reported [27]. The pseudo three-component system represents aqueous 0.1 M NaCl, oil (dodecane) and emulsifier with a 1:2 ratio of surfactant (SDS) to cosurfactant (1-pentanol). The composition of the μE was varied along the two straight, solid lines shown in Figure 1. This corresponds to keeping the ratio of oil to emulsifier constant at 1:10 or 2:10, while changing the ratio of oil to water. This range of compositions corresponds to a relatively low oil content (< 10% oil) and a range of water content from 89% to 34%. Specific compositions are summarized in Table 1. In the text, μEs are referred to by their ratio of water to oil. F. r example, a μE with 89% water, 1% oil and 10% emulsifier is an 89/1 SDS μE. Since % water was varied over a wide range, results in figures are plotted versus %water. It is apparent that in this investigation changes in μE composition show the effect of dilution by water.

In preparing μEs, each component was added by weight and the solution was mechanically stirred until clear and homogeneous. The μEs were stable for several months and could be frozen and thawed. Ultrasonication was used to aid in dissolving the electrochemical probes in μEs. Since the reduction of oxygen interferes with the reduction peak of MV^{+2}, solutions of MV^{+2} were deaerated with N_2 before measurements. The solution was purged with N_2 using a bubbler containing μE which was first deaerated for at least 30 minutes. The composition of μE used in the bubbler was the same as that used to make the solution of MV^{+2}. Deoxygenation was confirmed by CV which showed disappearance of the oxygen peak at -0.550 V. A positive pressure of N_2 was maintained throughout CV and chronocoulometric measurements of MV^{+2}.

II-88

RESULTS

Ferrocene. Fc is a hydrophobic probe with a reported solubility in water of 0.05 mM [24] and a solubility in dodecane of 0.15 M [31]. Since Fc concentrations in μE were typically 3 mM, which is significantly greater than water solubility, the probe is expected to reside primarily in the oil phase. The concentration was limited to 3 mM by solubility in the μE. In SDS μE with Fc concentrations from 1-3 mM, diffusion coefficients (D_R) and formal potentials ($E_{1/2}$ = (Epa + Epc)/2 ≈ E°') were not dependent on the concentration of the probe (Table 2). In CTAB μE, dependence of D_R on probe concentration was observed at concentrations less than 5 mM [23]. The oxidation product of Fc, ferricinium cation (Fc^+), is water soluble. Water solubility of Fc^+ has been demonstrated in micellar solutions, where $D_O \approx D_{aq}$ = 6.7 X 10^{-6} cm^2/s [24,26], rather than a slower D_O (≈10^{-7} cm^2/s) typical of the electroactive probe interacting with micelles.

In water rich 89/1 SDS μE, Fc D_R = 5.8 X 10^{-7} cm^2/s (Table 3) ca. an order of magnitude lower than in aqueous solutions ($D_{R,aq}$ = 6.7 X 10^{-6} cm^2/s [24]) or in dodecane ($D_{R,oil}$ = 4.4 X 10^{-6} cm^2/s [32]). Therefore, D_R must reflect a different process and not Fc diffusion through a continuous phase. As water content decreases, D_R of Fc increases to a value of 3.87 X 10^{-6} cm^2/s in a 34/6 SDS μE, close to $D_{R,oil}$.

The $E_{1/2}$ of Fc was determined from CV. In an 89/1 μE, Fc $E_{1/2}$ = +0.219 V (Table 3) which is more positive than aqueous formal potential ($E°'_{aq}$ = +0.160 V [26]) and less positive than E°' in acetonitrile ($E°'_{CH3CN}$ = +415 [33]). As the amount of water decreases, the $E_{1/2}$ becomes more positive, changing to +0.311±3 V in a 36/4 μE.

In 0.1 M $NaCl_{(aq)}$ [24], in acetonitrile [33] and in CTAB μE [23], the oxidation of Fc is reversible. In SDS μE, the oxidation also shows reversible behavior as indicated by the separation of the anodic and cathodic peak potentials (ΔEp), which is ca. 60 mV (Table 3). The ratio of peak currents (i_{pa}/i_{pc}) is slightly greater than unity (Table 3).

Ferricyanide. $Fe(CN)_6^{-3}$ and its reduction product, $Fe(CN)_6^{-4}$, are both water soluble anions and reside in the aqueous phase of SDS μE, due electrostatic repulsion from the membrane. Concentrations

of $Fe(CN)_6^{-3}$ were typically 1 mM, since at higher concentrations the μE became turbid. This demonstrates that the structure is sensitive to salt concentration where changes in concentration can result in a solution which does not form a μE.

In an 89/1 SDS μE, the diffusion coefficient of $Fe(CN)_6^{-3}$, $D_0 = 5.9 \times 10^{-6}$ cm^2/s, is comparable to $D_{0,NaCl(aq)} = 6.7(\pm 0.1) \times 10^{-6}$ cm^2/s and $D_{0,KCl(aq)} = 7.6 \times 10^{-6}$ cm^2/s [29]. As the water content is decreased, D_0 decreases (Table 4). In CTAB μE, $Fe(CN)_6^{-3}$ is electrostatically associated with the surfactant and no dependence of D_0 on μE composition is observed [23].

In SDS μE, the $E_{1/2}$ of $Fe(CN)_6^{-3}$ is within experimental error of the $E^{o'}_{aq} = +0.172 \pm 25$ in 0.1 M $NaCl_{(aq)}$ (Table 4). The kinetics of the reduction become faster as the water content of the μE decreases, with ΔEp changing from 885±45 mV in 89/1 to 81±22 mV in a 34/6 μE and the ratio of peak currents (i_{pc}/i_{pa}) also decreases (Table 4).

Methyl Viologen. MV^{+2} is a water soluble dication which is reduced through a stable cation radical, $MV^{+\bullet}$, to water insoluble MV^0:

$$MV^{+2} + e^- \rightleftharpoons MV^{+\bullet} \quad (1)$$

$$MV^{+\bullet} + e^- \rightleftharpoons MV^0 \quad (2)$$

MV^{+2} is expected to associate with the anionic SDS in the membrane layer. Typical MV^{+2} concentrations were 1 mM; similar to the effect of $Fe(CN)_6^{-3}$, higher concentrations were found to cause turbidity

The diffusion coefficient of MV^{+2} in SDS μE, $D_0 = 2.0(\pm 0.5) \times 10^{-6}$ cm^2/s, is significantly lower than in aqueous solutions, where $D_{0,aq} = 6.56 \times 10^{-6}$ cm^2/s [34]. In the μE, D_0 does not change with composition (Table 5). This behavior is similar to that of $Fe(CN)_6^{-3}$ in CTAB μE, where $D_0 = 1.0(\pm 0.5) \times 10^{-6}$ cm^2/s [23] and where $Fe(CN)_6^{-3}$ associates with the surfactant in the interface.

CV of MV^{+2} in 0.1 M $NaCl_{(aq)}$, shows 2 peaks corresponding to the reactions described by equations 1 and 2 (Figure 2). The symmetrical shape of peak (2a) indicates adsorption of MV^0. CV shows that adsorption of MV^0 is eliminated in the μE (Figure 2).

$E_{1/2}$ of MV^{+2} is less negative than in aqueous solutions for both redox couples ($E_{1/2,1,aq} = -0.683 \pm 3$ V and $E_{1/2,2,aq} = -1.025 \pm 7$ V) (Table 5). $E_{1/2}$ of each couple becomes less negative with

decreasing water content (Table 5). For $MV^{+2}/MV^{+\bullet}$, $E_{1/2}$ changes about 30 mV, by going from 89/1 to 36/4 μE (Table 5). A somewhat larger change of $E_{1/2}$ is observed for the $MV^{+\bullet}/MV^{0}$ couple (Table 5).

For the first reduction (equation 1), both ΔEp and $(i_{pc}/i_{pa})_1$ remain constant at all μE compositions (Table 5). Plots of log $i_{pc,1}$ versus log scan rate (ν) have a slope of 0.5 at all compositions, indicating that the system is primarily diffusion controlled and that the reactant, MV^{+2}, does not adsorb. However, $(i_{pc}/i_{pa})_1$ decreases with increasing scan rate which indicates that there is weak adsorption of the product, $MV^{+\bullet}$ [35]. ΔEp is ca. 60 mV which is consistent with reversible kinetics for this system.

For the second step (equation 2), the ratio of peak currents $(i_{pc}/i_{pa})_2$ is greater than unity and increases slightly at high (≈ 500 mV/s) ν. This is also consistent with weak adsorption of $MV^{+\bullet}$. The ratio $(i_{pc}/i_{pa})_2$ increases with a decrease in μE water content (Table 5) due to changes in adsorption with composition. Plots of log $i_{pc,2}$ versus log ν have a slope of ca. 0.5, indicating that the system is primarily diffusion controlled. ΔEp is ca. 60 mV, indicating reversible kinetics for this system.

DISCUSSION

Microemulsion Structure from Diffusion Coefficients

As shown in the results section, in water rich SDS μE, D_R of oil-soluble Fc is an order of magnitude lower than in water or oil. D_R of Fc does not reflect diffusion through the continuous aqueous or oil phase but is consistent with the expected droplet diffusion [36]. The self-diffusion coefficient of oil in O/W μE measured by NMR is typically $D_{oil} \approx 10^{-7}$ cm^2/s [18], in agreement with this model [15,16,21]. QELS measurements also give $D_{drop} \approx 10^{-7}$ cm^2/s [17]. Diffusion coefficient can be related to droplet size by the Stokes-Einstein equation:

$$D = kT/6\pi\eta r \qquad (3)$$

where D is the diffusion coefficient (cm^2/s), k is the Boltzman constant (J/K), T is the temperature (K), η is the viscosity of the solvent (P), and r is the radius of the diffusing species (cm). Since D_R of Fc reflects diffusion of the droplet, it can be used to calculate its size from equation 3. From such calculations, typical droplet sizes correspond well to typical droplet sizes determined by techniques such as QELS and SANS [11,12]. Calculations of droplet sizes from electrochemical D_R are discussed in detail later.

MV^{+2} should be electrostatically attached to the anionic membrane layer of the droplet and, therefore, also reflect droplet diffusion. The electrochemical D_0 of MV^{+2} is considerably lower than $D_{0,aq}$, indicating that the probe moves with the aggregates. However, D_0 of MV^{+2} is not as low as D_{drop} [10,17,18,22,23], nor D_{surf} [18], both of which are ca. 10^{-7} cm^2/s. Partitioning of MV^{+2} between the membrane and aqueous phases may contribute to higher electrochemical D_0. Since water-soluble $Fe(CN)_6^{-3}$ is electrostatically repulsed from the droplet, its D_0 should reflect diffusion in water. In fact, D_0 of $Fe(CN)_6^{-3}$ is only slightly lower than $D_{0,0.1\ M\ NaCl}$. The small decrease in D_0, can be attributed to the obstruction effect. A similar obstruction effect reduces the self-diffusion coefficient of water. For example, in a O/W SDS/1-butanol/toluene/water μE, $D_{water} = 1.5 \times 10^{-5}$ cm^2/s, compared to neat water, $D^{\circ}_{water} = 2.27 \times 10^{-5}$ cm^2/s [18].

Probe Partitioning. As is apparent for MV^{+2}, probe partitioning affects diffusion coefficients. However, partitioning will also occur with other probes, as demonstrated with Fc in CTAB μE [23]. In a

multicomponent system, such as μE, diffusion coefficients measured electrochemically are determined by probe partitioning [37] which create multiple diffusional paths. These paths are a result of place (mass) or electron exchange across phases and contribute to higher diffusion coefficient values. In the μE system studied in this work, electron exchange is unlikely since it requires similar formal potentials in the hydrophobic and hydrophilic phases [37,38]. Low concentrations and large differences in $E^{o'}$ decrease the driving force of the electron-exchange reaction [38]. As shown in Tables 3 and 5, $E_{1/2}$ of Fc and of MV^{+2} in μE are significantly different from the $E^{o'}_{aq}$. However, residence times of probes in μE are ca. 10^{-5} to 10^{-3} s [4]. This is faster than the time scale of chronocoulometry, which was used to measure diffusion coefficients and, therefore, cross-phase place exchange may be considered rapid.

Since exchange between phases is fast in O/W μE, the measured or apparent diffusion coefficient, D', may be expressed as:

$$D' = D_1 f_1 + D_2 f_2 \qquad (4)$$

where $D_1 = D_{aq}$, and f_1 is the fraction of probe in the aqueous phase. $D_2 = D_{drop}$ and f_2 is the fraction of the probe in the droplet [37]. For bicontinuous μE, $D_1 = D_{aq}$ and D_2 = diffusion of probe through the continuous oil phase. If more than one probe is bound to a droplet, D' may depend on probe concentration, C_x. The dependence of D' on C_x for fast exchange of probe between two phases has been described by Rusling et al. [39] where:

$$D' = D_1/(1 + C_M K^n C_x^{n-1}) + D_2 C_M K^n C_x^{n-1}/(1 + C_M K^n C_x^{n-1}) \qquad (5)$$

C_M = total droplet concentration, n = the number of probe molecules bound to a droplet, and K^n describes the equilibrium constant for the binding of n solute molecules to a droplet:

$$M + nX \rightleftharpoons MX_n \qquad (6)$$

where M = droplet and X = probe. More specifically, $K^n = nK'_n$, where K'_n is :

$$K'_n = [MX_n]/([M][X]^n) \qquad (7)$$

According to equation 5, if n = 1 D' does not depend on C_x and equation 5 reduces to equation 4. Since μE is capable of solubilizing large amounts of probes such as Fc, and if high concentrations, such as are used in this work, it is reasonable that n > 1. If K^n, C_M, or C_x^{n-1} is very low, $D' \approx D_1 = D_{aq}$.

If K^n, C_H or C_x^{n-1} is high, $D' \approx D_2 = D_{drop}$. Since in droplet μE, D_R of Fc << D_{aq}, K^n is reasonably high. In SDS unlike in CTAB μE [23], D' does not depend on [Fc] (Table 2). Since C_x and C_M are similar in both SDS and CTAB μEs, differences in the dependence of D' on C_x must be due to differences in K^n. A higher K^n in SDS μE will account for D' approaching D_2 at lower C_x than in CTAB μE and the resulting independence of D' on C_x.

Droplet Size. As discussed already, diffusion coefficient of the oil soluble Fc is ca. D_{drop}. However, partitioning has to be considered. In this work, the concentration of Fc is close to its solubility limit in μE, therefore, the solubility of Fc in water (5×10^{-3} mM [24]) can be used to calculate f_1 and f_2. $D_{drop} = D_2$ can then be calculated from equation 4. Using this calculated $D_{drop} = 3.6 \times 10^{-7}$ cm^2/s for an 89/1 SDS μE, and assuming $\eta_{water} = 0.0089$ P as the viscosity of the continuous phase, the droplet radius, r = 68 Å from equation 3. The r values were calculated for several O/W μEs with the results listed in Table 6. The values are consistent with those obtained by other methods which are also listed in Table 6.

From QELS it has been shown that if the oil content increases, the droplet size increases [11]. This is confirmed by electrochemical results obtained here, where r = 68 Å for and 89/1 SDS μE while in an 88/2 SDS μE, where oil content is doubled, r = 82 Å (Table 6). Increasing the surfactant to cosurfactant ratio (s:c) decreases the hydrophilicity of the μE to a lesser extent than changes in oil content. For and 89/1 SDS μE with s:c = 1:2, r = 68 Å but if s:c = 2:1, r = 72 Å (Table 6).

Structural Changes with Composition. Results in Figure 3 for Fc show that as the water content decreases, D_R increases. According to equation 3, this increase should reflect a decrease in droplet size if Fc continues to diffuse with the oil droplets. However, the decrease in water content, oil content increases and, therefore, size and/or number of oil droplets should increase not decrease [2,11,27,40,41]. Therefore, changes in size cannot explain the increase in D_R. However, when the size and/or number of droplets increases coalescence of droplets is more likely forming a continuous path through the oil phase and making diffusion through this phase important. This in turn can increase D_R. From results in Figure 3, it can be concluded that with decreasing water content, this form of diffusion becomes more important.

Significantly, this also reflects transition from droplet to bicontinuous structures. This is confirmed by comparing electrochemical values with NMR results where changes in D_R of Fc with composition follow D_{oil} values from NMR. For example, when water content is high, D_{oil} and D_R of Fc are ca. 10^{-7} cm^2/s [15,18,21,42-45], consistent with a droplet structure of μE. From NMR, as water content decreases, D_{oil} increases, approaching $D°_{oil}$ (neat liquid) but not achieving it [42-44]. This is consistent with a transition from discrete oil droplets to a bicontinuous structure with oil as a pseudo-continuous phase. For example, in a bicontinuous SDS/1-butanol/toluene/water μE, $D_{toluene} = 8 \times 10^{-6}$ cm^2/s, while $D°_{toluene} = 2.4 \times 10^{-5}$ cm^2/s [18]. Similarly, electrochemically determined D_R of Fc increases as the water content decreases, without reaching the value of $D_{R,oil} = 4.4 \times 10^{-6}$ cm^2/s [32] (Figure 3).

While D_R of Fc reflects oil diffusion, D_0 of $Fe(CN)_6^{-3}$ reflects self-diffusion of water. In μE with high water content, D_0 is slightly less than $D_{0,0.1\ M\ NaCl}$. Similarly from NMR, D_{water} is slightly less than $D°_{water}$ [18]. D_0, like D_{water}, is reduced because of obstruction of water diffusion by oil droplets [16,21,42-46]. The changes in D_0 follow changes in D_{water} (Figure 4), with D_0 decreasing as water content decreases. The obstruction of $Fe(CN)_6^{-3}$ due to increasing amount of oil phase increases as water content decreases.

The D_0 of MV^{+2} reflects the diffusion of the membrane or surfactant phase. D_0 is significantly lower than $D_{0,aq}$ and changes little with composition (Table 5). Similarly, the low D_{surf} form NMR does not change significantly with composition [15,18], since the movement of surfactant is restricted at all compositions. In droplet μE, the surfactant, like oil, diffuses with the droplets. In bicontinuous systems, diffusion of surfactant is confined to the interface and thus slow, typically $D_{surf} = 1 \times 10^{-6}$ cm^2/s [15,42,43]. The D_0 of MV^{+2}, which is ca. 2×10^{-6} cm^2/s, is larger than D_{surf}, probably due to a contribution to D_0 from diffusion of MV^{+2} in the aqueous phase as a result of MV^{+2} partitioning between the membrane and aqueous phase.

As shown for Fc, diffusion of the probe through the oil phase is significant in bicontinuous systems. As shown by electrochemical and NMR results, diffusion is slower than in neat liquid due to obstruction by the surfactant phase [42-44]. Consequently, bicontinuous μEs with higher oil to emulsifier (o:e) ratio will have less obstruction and, therefore, higher diffusion coefficients. This is shown for Fc in

a system with a ratio of o:e = 2:10, where D_R of Fc is higher than in comparable systems where the o:e = 1:10 (Figure 5).

The transition to bicontinuous structure depends on μE components. For example, Figure 3 compares the changes in D_R of Fc with μE composition which reflect the transition from droplet to bicontinuous structures in CTAB and SDS μE. The change is more pronounced in SDS μE. Shielding of the droplet charge by NaCl electrolyte in SDS μE may lead to more facile droplet merging [14] favoring a bicontinuous microstructure at lower oil content than in CTAB μE which does not contain NaCl. This effect can also be seen when an SDS μE lacks electrolyte. In a 79/5 SDS μE in the absence of 0.1 M $NaCl_{(aq)}$, Fc $D_R = 2.2 \times 10^{-7}$ cm^2/s, typical of D_{drop}. However for the same 79/5 system in the presence of 0.1 M $NaCl_{(aq)}$, Fc $D_R = 1.2 \times 10^{-6}$ cm^2/s. The higher D_R in the presence of NaCl must reflect bicontinuous structure since the value is typical of diffusion in a continuous phase and is significantly larger than D_{drop}, which is typically ca. 10^{-7} cm^2/s. Other studies have shown that droplet size increases with when electrolyte is added to the aqueous phase [2,47], which should correspond to a decrease in D_R (equation 3). Since experimentally, D_R with added NaCl is larger, it must reflect a facile transition of large droplets to a bicontinuous structure. Both NMR [18] and electrochemical results (Figures 3 and 4) show gradual changes in diffusion coefficient with composition indicating that the transition from droplet to bicontinuous structures is a gradual one [48]. Neither Fc nor $Fe(CN)_6^{-3}$ D values show an abrupt change, which would be expected if a distinct change in structure from droplets to bicontinuous occurs

Role of Electroactive Probe in Structure Determination. As is clear from the results, electrochemical diffusion coefficients can be used to determine microstructure by appropriate choice of probes. In both CTAB and SDS μEs, Fc D_R reflects diffusion of oil and is comparable to D_{oil} from NMR. D_0 of $Fe(CN)_6^{-3}$ in SDS μE and MV^{+2} in CTAB μE reflect diffusion in the aqueous phase, since both are water soluble and do not associate with the surfactant in the membrane due to electrostatic repulsion. For this reason, D_0 values for MV^{+2} in CTAB μE are comparable to values of D_0 for $Fe(CN)_6^{-3}$ in SDS μE and D_{water} from NMR. Consistent with this, the decrease in MV^{+2} D_0 with decreasing water content [23]

is due to obstruction. In SDS μE, D_0 of MV^{+2}, like D_0 of $Fe(CN)_6^{-3}$ in CTAB μE, reflect D_{surf} [18] showing little change in D_0 with composition.

D_R of Fc in bicontinuous SDS μEs is larger than in CTAB μEs of similar compositions (Figure 3). This is probably due to differences in the viscosity of the oil phase of each μE. Viscosity (η) of hexadecane in CTAB μE is ca. twice that of dodecane in SDS μE ($\eta_{hexadecane}$ = 3.34 cP [32], $\eta_{dodecane}$ = 1.35 cP [32]). It follows that diffusion will be slower in hexadecane and consequently D_R of Fc will be lower in CTAB μE.

Formal Potentials

Effect of Diffusion Coefficients and Partitioning Constants on Reactivity of Ferrocene. In droplet 89/1 SDS μE, $E_{1/2}$ of Fc = +0.219±3 V, which is 59 mV more positive than its $E^{o'}_{aq}$ = +0.160 V [26]. Since Fc is solubilized primarily in oil, and ferricinium ion (Fc^+) is solubilized in water [24,26], their diffusion coefficients, D_R and D_0 respectively, are not equal. The difference between D_R and D_0 will cause a shift in $E_{1/2}$ vs. $E^{o'}_{aq}$ [49] where:

$$E_{1/2} = E^{o'}_{aq} + (RT/nF) \ln (D_R/D_0)^{1/2} \qquad (8)$$

$E^{o'}_{aq}$ (V) is the formal potential in water and the other constants have their usual meaning. In this system, Fc $D_R = 5.8 \times 10^{-7}$ cm^2/s from chronocoulometry, and Fc^+ $D_0 = 6.7 \times 10^{-6}$ cm^2/s [24,26] i.e. equal to $D_{0,aq}$. With these values, a negative 31 mV shift versus $E^{o'}_{aq}$ is predicted from equation 8. Since the experimental $E_{1/2}$ is 59 mV more positive than the $E^{o'}_{aq}$, differences between D_R and D_0 cannot account for the experimental shift in $E_{1/2}$. Changes in $E_{1/2}$ will also result from partitioning. Considering the membrane and oil phase as one, the relevant equilibria can be expressed as [24,25]:

$$\begin{array}{ccccc} Fc^+_{(aq)} & + & e^- & \rightleftharpoons & Fc_{(aq)} \\ \uparrow\downarrow K_0 & & & & \uparrow\downarrow K_R \\ Fc^+_{(oil)} & + & e^- & \rightleftharpoons & Fc_{(oil)} \end{array} \qquad (9)$$

aq and oil represent the aqueous and oil/membrane phases, respectively where K_0 and K_R are defined as:

$$K_0 = [Ox_{(aq)}]/[Ox_{(oil)}] = [Fc^+_{(aq)}]/[Fc^+_{(oil)}] \qquad (10)$$

and

$$K_R = [Red_{(aq)}]/[Red_{(oil)}] = [Fc_{(aq)}]/[Fc_{(oil)}] \quad (11)$$

K_O and K_R are partitioning constants for the oxidized and reduced forms of the probe, respectively. In aggregate systems such as droplet μEs, partitioning constants measured experimentally will be:

$$K_O' = [Ox_{(aq)}]C_M/[[Ox_{(oil)}] = K_O C_M \quad (12)$$

and

$$K_R' = [Red_{(aq)}]C_M/[Red_{(oil)}] = K_R C_M \quad (13)$$

where C_M is the concentration of aggregates, i.e. droplets in a droplet μE. In micellar solutions containing aggregates, typical C_M values are in the mM range [13,39]. If Poisson distribution is assumed, C_M represents total aggregate concentration [50]. Ohsawa and Aoyagui have shown that for systems as in equation 9, $E_{1/2}$ dependence on K_R and K_O can be described by [25]:

$$E_{1/2} = E^{o'}_{aq} + RT/nF \ln (D_R/D_O)^{1/2} + RT/nF \ln \{K_O(1+K_R)/K_R(1+K_O)\} \quad (12)$$

Because of the water solubility of Fc^+, $K_O >> 1$. Therefore, equation 12 reduces to:

$$E_{1/2} = E^{o'}_{aq} + RT/nF \ln (D_R/D_O)^{1/2} + RT/nF \ln \{(1+K_R)/K_R\} \quad (13)$$

Using in equation 13, Fc $D_R = 5.8 \times 10^{-7}$ cm^2/s determined from chronocoulometry, the aqueous diffusion coefficient of Fc^+, $D_O = 6.7 \times 10^{-6}$ cm^2/s [24,26], $E^{o'}_{aq} = +0.160$ V [26] and $E_{1/2} = +0.219$ V from CV, K_R is estimated to be 3×10^{-2}. This is consistent with literature values for micelle binding of hydrophobic probes [47] supporting effective partitioning of Fc into the μE droplet.

With decreasing water content of the μE, the $E_{1/2}$ of Fc increases (Figure 3, Table 3). In a 34/6 SDS μE, Fc $E_{1/2} = +0.311$ V, 151 mV more positive than $E^{o'}_{aq}$. In this system, D_R has increased to 3.9 $\times 10^{-6}$ cm^2/s (Table 3) and D_O of Fc^+ will lower than in the 89/1 system because of the increased obstruction effect. In a μE of similar composition, $D_O = 5.4 \times 10^{-7}$ cm^2/s for $Fe(CN)_6^{-3}$, $D_R = 3 \times 10^{-7}$ cm^2/s for hydroquinone [27], and $D_{water} = 2 \times 10^{-6}$ cm^2/s [18]. Therefore, with $D_R = 3.9 \times 10^{-6}$ cm^2/s and assuming 3×10^{-7} cm^2/s as a minimum D_O value, the maximum shift in $E_{1/2}$ is +0.123 V from equation 12. While the direction of the shift is correct, the magnitude is not sufficient to account for the observed 151 mV shift vs. $E^{o'}$. K_R and/or K_O must, therefore, be a function of μE composition.

As shown in Figure 6, throughout the range of compositions studied $E_{1/2}$ of Fc is more positive in CTAB than in SDS μE of similar composition. Differences in D_R do not account for differences in $E_{1/2}$. For example, D_R is about the same in droplet SDS (Table 3) and CTAB μE [23]. To obtain the more positive $E_{1/2}$, D_0 would have to be much lower in CTAB than in the SDS system. This is unlikely since electrostatic attraction of Fc^+ to the SDS predicts lower D_0 in SDS μE. It is more likely that K_R is smaller in the CTAB μE and leads to more positive $E_{1/2}$ shifts. Smaller K_R in CTAB μE is consistent with larger solubility of Fc in hexadecane than in the dodecane oil phase of SDS μE.

Effect of Equal Partitioning Constants and Diffusion Coefficients. For $Fe(CN)_6^{-3/-4}$ in SDS μE, there should be little difference between K_R and K_0 since neither form is associated with either oil or surfactant phase. Since the partitioning constants and diffusion coefficients of both forms must be approximately equal at any composition ($K_R \approx K_0$ and $D_R \approx D_0$), little change in $E_{1/2}$ is expected based on equation 12. In fact, $E_{1/2}$ of $Fe(CN)_6^{-3}$ in SDS μE is within experimental error of $E^{\circ\prime}_{aq}$ (Table 4).

In CTAB μE, the $Fe(CN)_6^{-3/-4}$ couple is strongly bound to the surfactant interface [23]. As a result, both forms of the probe are equally affected by composition and $K_R \approx K_0$ and $D_R \approx D_0$. Consequently, as observed in SDS μE (Table 4), $E_{1/2}$ also does not change with composition in CTAB μE [23], although the probe is in a different environment.

Partitioning Constants for $MV^{+2}/MV^{+\cdot}$ Redox Couple. Interactions of $MV^{+2/+\cdot}$ with SDS surfactant in a μE should be similar to interactions with SDS micelles. The couple associates with SDS micelles through a combination of electrostatic and hydrophobic interactions [34]. In SDS micelles, MV^{+2} $K_0 = 1.15 \times 10^{-3}$ and $MV^{+\cdot}$ $K_R = 2.4 \times 10^{-4}$ [34]. Therefore, it can be expected that K_0 and $K_R << 1$ in SDS μE. Consequently, equation 12 may be reduced to:

$$E_{1/2} = E^{\circ\prime}_{aq} + RT/nF \ln (D_R/D_0)^{1/2} + RT/nF \ln K_0/K_R \qquad (14)$$

From values of K_0 and K_R, the $MV^{+2/+\cdot}$ couple is predominately in the oil phase, $D_R \approx D_0$, and equation 14 reduces even further:

$$E_{1/2} = E^{\circ\prime}_{aq} + RT/nF \ln K_0/K_R \qquad (15)$$

From equation 15 and experimental $E_{1/2}$ = -0.664 V and $E^{o'}_{aq}$ = -0.690 V for $MV^{+2/+\cdot}$, the ratio of K_O/K_R in the 89/1 SDS μE is estimated to be 2.8. This indicates that the partitioning of $MV^{+\cdot}$ into the oil phase of the droplet μE is more favorable than the partitioning of MV^{+2}. This, in turn, suggests that hydrophobic interactions between the probe and the oil/membrane phase may be more important than electrostatic interactions. Based solely on electrostatics, MV^{+2} should be more strongly associated with the surfactant layer. The predominance of hydrophobic interactions was also observed by Kaifer and Bard in SDS micelles where K_O is about 5 times greater than K_R [34].

The effect of a possible of difference between D_R and D_O on $E_{1/2}$ can be analyzed with equation 14. D_R will reach a maximum value when $MV^{+\cdot}$ is not associated with the oil/membrane phase, $D_{R,max} = D_{O,aq}$ = 6.6 X 10^{-6} cm^2/s [34]. The minimum value of $D_{R,min} = D_{drop} \approx 6 \times 10^{-7}$ $cm^2/s \approx D_R$ of Fc in 89/1 SDS μE if $MV^{+\cdot}$ is strongly associated with the oil phase. With experimental D_O = 3.3 X 10^{-6} cm^2/s, $E_{1/2}$ = -0.664 V, $E^{o'}_{aq}$ = -0.690 V [34] and assuming $D_{R,max}$ = 6.6 X 10^{-6} cm^2/s, $K_O/K_R \approx 2$ from equation 14. Using the same values of D_O, $E_{1/2}$, $E^{o'}_{aq}$ and $D_{R,min}$ in equation 14, $K_O/K_R \approx 7$. Consequently, regardless of possible differences between D_R and D_O, the association of $MV^{+\cdot}$ with the oil phase is always stronger than of MV^{+2} ($K_O > K_R$). Therefore, $D_{R,min}$ reflects better $MV^{+\cdot}$ D_R than $D_{R,max}$. The estimation of K_O/K_R from equation 15, i.e. when $D_O = D_R$, will have ≤60% error.

As the water content of the μE decreases, $E_{1/2}$ becomes less negative but D_O remains constant (Table 5). Since as shown above, $MV^{+\cdot}$ associates more strongly with the oil/membrane phase than MV^{+2}, its $D_{R,max}$ will follow the D_R of Fc. In a 34/6 SDS μE, $MV^{+2/+\cdot}$ $E_{1/2}$ = -0.632 V, D_O = 2 X 10^{-6} cm^2/s and $D_{R,max}$ = 6.6 X 10^{-6} cm^2/s, thus $K_O/K_R \approx 6$ from equation 14. With $D_{R,min} \approx D_O$ = 2 X 10^{-6} cm^2/s, K_O/K_R = 10 from equation 14. K_O/K_R in 34/6 SDS μE may be as much as 3 times K_O/K_R in the 89/1 system. However, if $MV^{+\cdot}$ is very strongly associated with the oil phase, changes D_R alone may be sufficient to account for the shift in $E_{1/2}$.

Partitioning Constants for the $MV^{+\cdot}/MV^0$ Redox Couple. $E_{1/2}$ for the $MV^{+\cdot/0}$ couple is less negative than its $E^{o'}_{aq}$ = -1.020 V. Since both reside primarily in the oil phase, equation 15 can be used to describe shifts in $E_{1/2}$. For an 89/1 SDS μE, $E_{1/2}$ = -1.015 V, and according to equation 15, $K_O/K_R \approx$

1.2. In a 34/6 SDS μE, $E_{1/2}$ = -944 and so $K_O/K_R \approx 19$. Therefore, MV^0 is more strongly associated with oil phase than $MV^{+\cdot}$ for all μE compositions. Since only hydrophobic interactions will affect the partitioning of MV^0, this is consistent with the predominance of hydrophobic interactions in this system. K_O/K_R of the $MV^{+\cdot/0}$ couple is more affected by composition than the $MV^{+2/+\cdot}$ couple, having a smaller value in 89/1 SDS μE and a larger value in 34/6 μE.

Effect of Surface Interactions on Reactivity.

In aqueous solutions, surfactants adsorb on glassy carbon tail first with the polar head group toward the aqueous solution [51]. The layer on the electrode surface will affect the electrochemical response by partially blocking the surface and through electrostatic and hydrophobic interactions [4,51]. Addition of other compounds to the solution, such as salt or alcohol, will affect the structure of the surfactant layer [51].

Kinetics. There are no hydrophobic interactions between $Fe(CN)_6^{-3}$ and SDS, only electrostatic ones. Consistent with this, repulsion of $Fe(CN)_6^{-3}$ from like-charged SDS results in slower electrochemical kinetics. The slower kinetics are shown by ΔEp = 846 mV in 89/1 SDS μE and ΔEp = 885 mV in SDS micelles compared to ΔEp = 152 mV in 0.1 M $NaCl_{(aq)}$. In CTAB μE, adsorbed cationic surfactant attracts $Fe(CN)_6^{-3}$ to the electrode, and the kinetics improve over 0.1 M $NaCl_{(aq)}$ with ΔEp = 60 mV.

As the water content of the SDS μE decreases, ΔEp of $Fe(CN)_6^{-3}$ decreases (Table 4). It has been shown that the alcohol content in the oil/water interface increases as μE water content decreases [8]. Changes in water content should affect the electrode/solution interface in the same way as the oil/water interface since the surfactant organizes in a similar manner at both interfaces. With more alcohol at the electrode/solution interface, the surfactant head groups will be further apart, decreasing charge per area and, thus, the electrostatic repulsion of the electrode surface toward $Fe(CN)_6^{-3/-4}$. The neutral polar group of the alcohol will also increase the hydrophilicity of the surface [51], which may also improve the kinetics of the $Fe(CN)_6^{-3/-4}$ couple (Table 4).

In SDS μE, the ΔEp of Fc is about 60 mV (Table 3), indicating reversible electron transfer. Hydrophobic Fc easily penetrates the surfactant layer allowing facile electron transfer. ΔEp of 60 mV is also observed for Fc in CTAB μE [23], SDS micelles [24] and CTAB micelles [26], where hydrophobic interactions also occur.

In SDS μE, ΔEp of $MV^{+2/+\cdot}$ is ca. 60 mV (Table 5). MV^{+2} can interact both hydrophobically and electrostatically with the adsorbed surfactant, allowing for facile electron transfer. In CTAB μEs, MV^{+2} will be electrostatically repelled from CTAB but will still interact hydrophobically. Since ΔEp in CTAB μE is ca. 60 mV, hydrophobic interactions must predominate.

Adsorption/Diffusion. In SDS μE the electrochemical behavior of Fc on glassy carbon electrodes is diffusion controlled. This is indicated by plots of log anodic peak current (i_{pa}) versus log scan rate (ν), where the slope is ca. 0.5. The same plots for $Fe(CN)_6^{-3}$ show slopes lower than 0.5 which is attributed to kinetic effects [52]. This is confirmed by the ΔEp which increases with ν.

Plots of log i_{pc} versus log ν for the $MV^{+2/+\cdot}$ couple have a slope of ca. 0.5, indicating that MV^{+2} is not adsorbed. However, the ratio $(i_{pc}/i_{pa})_1 < 1$ and decreases with increasing scan rate. Since ΔEp is ca. 60 mV throughout the range of ν, this behavior indicates weak adsorption of $MV^{+\cdot}$. Kaifer and Bard observed weak adsorption of $MV^{+\cdot}$ in SDS solutions which was eliminated when SDS exceeded its critical micelle concentration [34].

For the $MV^{+\cdot/0}$ couple, plots of log i_{pc} versus log ν have a slope of ca. 0.5, indicating that the system is primarily diffusion controlled. The ratio $(i_{pc}/i_{pa})_2$ is greater than unity and increases slightly at high (≈ 500 mV/s) scan rates. This is consistent with greater adsorption of $MV^{+\cdot}$ than MV^0. This is unlike aqueous solutions where significant adsorption of MV^0 is observed. The decrease of adsorbed MV^0 was attributed to the solubilization of MV^0 in the oil phase of the μE. No adsorption of MV^0 was observed in SDS micelles [34], which also solubilize MV^0.

The adsorbed surfactant layer will affect probe adsorption. If adsorption depended on electrostatic attraction between probe and SDS, adsorption of MV^{+2} would be greater than adsorption of $MV^{+\cdot}$. If adsorption depended on hydrophobic interactions, adsorption of MV^0 would be greater than

adsorption of $MV^{+\cdot}$. Since greater adsorption of $MV^{+\cdot}$ is observed for both $MV^{+2/+\cdot}$ and $MV^{+\cdot/0}$, both electrostatic and hydrophobic interactions must affect adsorption.

Shifts in $E_{1/2}$ indicate that $MV^{+\cdot}$ interacts more with the oil/membrane phase than MV^{+2}. This is consistent with the preferential adsorption of $MV^{+\cdot}$ by the interaction with the adsorbed SDS. However, shifts in $E_{1/2}$ for $MV^{+\cdot/0}$ indicate that MV^0 is more strongly associated with the oil/membrane phase than $MV^{+\cdot}$. Since adsorption, as indicated by $(i_{pc}/i_{pa})_2$, suggests that $MV^{+\cdot}$ preferentially interacts with the adsorbed SDS, MV^0 must be primarily solubilized in the oil rather than in the membrane phase. Since as the oil content increases, the solubilization of MV^0 in the oil phase increases, thus the ratio of $MV^{+\cdot}/MV^0$ at the electrode and $(i_{pc}/i_{pa})_2$ increase. Thus, the increasing $(i_{pc}/i_{pa})_2$ with decreasing water content supports the model of MV^0 solubilization in the oil phase.

CONCLUSIONS

To determine microstructure of μEs from electrochemical diffusion coefficients, electroactive probes should be chosen so that the phase in which the probe resides is known. In choosing probes, both electrostatic and hydrophobic effects must be taken into account. However, if both types of interactions occur, hydrophobic effects have a larger influence on partitioning than electrostatic effects. This is shown by the partitioning of $MV^{+2/+\cdot}$ couple , where $MV^{+\cdot}$ is more strongly associated with the oil/membrane phase than MV^{+2}.

In O/W μEs, a probe residing in the oil droplet will have a diffusion coefficient of ca. 10^{-7} cm^2/s, while a probe residing in the continuous aqueous phase will have a diffusion coefficient only slightly less that its diffusion coefficient in water, i.e. ca. 6×10^{-6} cm^2/s. The lowering of diffusion coefficient in the continuous phase is due to obstruction of the diffusion path by the oil droplets. In bicontinuous μEs, the diffusion coefficient of a probe in the aqueous phase will be on the order of 10^{-6} cm^2/s. It will be than its diffusion coefficient in a droplet μE due to increased obstruction by the larger amount of oil phase. In a bicontinuous μE, an oil soluble probe will diffuse through the now continuous oil phase of the μE. Similar to diffusion through the aqueous phase, obstruction by the aqueous phase causes lower diffusion coefficients than in pure oil. Consequently, in a bicontinuous μE, the oil soluble probe will have a diffusion coefficient similar to that of a probe in the aqueous phase. The diffusion coefficient of a probe attached to the membrane phase will be low, ca. 1×10^{-6} cm^2/s, at all μE compositions.

The electrochemically determined diffusion coefficient of a probe in the oil phase of a O/W μE can be used to determine droplet size. The diffusion coefficient will be larger than the diffusion coefficient of the droplet (D_{drop}), due to the contribution of diffusion in the aqueous phase (D_{aq}). At high probe concentrations and/or high probe partitioning into oil, the effect of D_{aq} is small and can be accounted for. D_{drop} can then be used to determine the droplet radius with the Stokes-Einstein equation.

If the oxidized (Ox) and reduced (Red) forms of the probe partition differently between the aqueous and oil/membrane phases of the μE, the formal potential ($E^{\circ\prime}$) will shift from the formal potential in water ($E^{\circ\prime}_{aq}$). Large differences in partitioning will lead to large shifts in formal potential. For instance,

Fc resides primarily in the oil phase, while its oxidized form (Fc^+) resides in the aqueous phase. For $Fc^{0/+}$, $E^{o'}$ in a 34/6 SDS μE is 100 mV more positive than $E^{o'}_{aq}$. On the other hand, for $Fe(CN)_6^{-3/-4}$, the partitioning constants for both forms of the probe are the same and $E^{o'} \approx E^{o'}_{aq}$ at all μE compositions. The partitioning constants were shown to be a function of μE composition.

The shift in $E^{o'}$ can also be related to differences between D_R and D_O. For droplet μEs, if Ox and Red reside in different phases $D_R \neq D_O$, shifting the formal potential. However, in bicontinuous μEs, $D_R \approx D_O$. Thus, shifts in $E^{o'}$ will be primarily determined by partitioning constants.

Since both partitioning constants and diffusion coefficients are a function of μE composition, $E^{o'}$ may be controlled by choice of μE. Alternatively, if diffusion coefficients are known, partitioning constants may be determined from shifts in potential.

At the hydrophobic glassy carbon surface, surfactant adsorbs tail first onto the electrode. Hydrophobic and electrostatic interactions of the probe with this surfactant layer will affect adsorption and kinetics. As shown for $MV^{+\cdot}$, a combination of electrostatic and hydrophobic interaction can induce weak adsorption. However, purely hydrophobic probes, such as MV^0, may preferentially solubilize in the oil phase rather than the surfactant layer. Probes with a higher charge, like MV^{+2}, may preferentially solubilized in the aqueous phase. Electrostatic interactions can either facilitate or hinder kinetics. For instance, electrostatic attraction to CTAB enhances the kinetics of $Fe(CN)_6^{-3/-4}$, while electrostatic repulsion by SDS hinders the same reaction. Composition of the μE affects the layer of adsorbed surfactant, decreasing the electrostatic repulsion with decreasing water content. Therefore, the kinetics of probes which are electrostatically repulsed by adsorbed surfactant, such as $Fe(CN)_6^{-3/-4}$ in SDS μEs, can be improved by decreasing the μE water content. Hydrophobic interactions between probe and adsorbed surfactant can also improve kinetics. This was observed with $MV^{+2/+\cdot}$ in CTAB μEs, where electron transfer was fast despite electrostatic repulsion.

REFERENCES

1 S.E. Friberg, P. Bothorel, "Microemulsions· Structure and Dynamics", CRC Press, Boca Raton, FL, 1987.

2 M.L. Robbins, J. Bock, J.S. Huang, J. Colloid Interface Sci., 1988, 126, 114.

3 P.L. Luisi, M. Giomini, M.P. Pileni, B.H. Robinson, Biochim. Biophys. Acta, 1988, 947, 229.

4 E. Pelizzetti, E. Pramauro, Anal. Chim. Acta, 1985, 169, 1.

5 J. Burgess, Colloids Surfaces, 1990, 48, 185.

6 R. Schomaecker, B.H. Robinson, P.D.I. Fletcher, J. Chem. Soc. Faraday Trans. I, 1988, 84, 4203.

7 C. Minero, E. Pramauro, E. Pelizzetti, Colloids Surfaces, 1989, 35, 237.

8 J.C. Russell, D.G. Whitten, J. Am. Chem. Soc., 1982, 104, 5937.

9 E.W. Kaler, H.T. Davin, L.E. Scriven, J. Chem. Phys., 1983, 79, 5685.

10 R.A. Mackay, N.S. Dixit, R. Agarwal, R.P. Seiders, J. Dispersion Sci. Techn., 1983, 4, 397.

11 H.M. Cheung, S. Qutubuddin, R.V. Edwards, and J.A. Mann, Jr., Langmuir, 1987, 3, 744.

12 L.J. Magid, R. Triolo, J.S. Johnson, Jr., J. Phys. Chem., 1984, 81, 5161.

13 M. Almgren, J.-E. Löfroth, J. Colloid Interface Sci., 1981, 81, 486.

14 A. Malliaris, J. Lang, J. Sturn, R. Zana, J. Phys. Chem., 1987, 91, 1475.

15 P. Stilbs, K. Rapacki, B. Lindman, J. Colloid Interface Sci., 1983, 85, 583.

16 B. Jönsson, H. Wennerström, P.G. Nilsson, P. Linse, Colloid Polymer Sci., 1986, 264, 77.

17 S. Qutubuddin, K.R. Choshi, A. Bhatia, A. Hussan, "An Electrochemical Investigation of an Oil-in-Water Microemulsion", Symposium on Microemulsions, A.I.Ch.E. Annual Meeting, Chicago, November 1985.

18 B. Lindman, P. Stilbs, M.E. Moseley, J. Colloid Interface Sci., 1981, 83, 569.

19 K. Shinoda, M. Araki, A. Sadaghiani, A. Khan, B. Lindman, J. Phys. Chem., 1991, 95, 989.

20 W.O. Parker, Jr., P. Albonico, E. Borgarello, I. Blute, Colloids Surfaces, 1990, 48, 21.

21 D.M. Anderson, H. Wennerström, J. Phys. Chem., 1990, 94, 8683.

22 H.T. Davis, J.F. Bodet, L.E. Scriven, W.G. Miller, Physica A, 1989, 157, 470.

23 R.A. Mackay, S.A. Myers, L. Bodalbhai, A. Brajter-Toth, Anal. Chem., 1990, 62, 1058.

24 J. Georges, S. Desmettre, Electrochim. Acta, 1984, 29, 521.

25 Y. Ohsawa, Y. Shimazaki, S. Aoyagui, J. Electroanal. Chem., 1980, 114, 235.

26 Y. Ohsawa, S. Aoyagui, J. Electroanal. Chem., 1982, 136, 353

27 J. Georges, J.W. Chen, Colloid Polymer Sci., 1986, 264, 896.

28 P.T. Kissenger, W.R. Heineman, "Laboratory Techniques in Electroanalytical Chemistry", Marcel Dekker, Inc., New York, 1984, p. 308.

29 M. Stackelberg, M. Pilgram, M. Toome, Z. Electrochem. 1953, 57, 342.

30 A.J. Bard. L.R. Faulkner, "Electrochemical Methods: Fundamentals and Applications", J. Wiley and Sons, New York, 1980, p.143.

31 J. Georges, A. Berthod, J. Electroanal. Chem., 1984, 175, 143.

32 at 25°C, calculated from Stokes-Einstein equation (3), radius of ferrocene from reference 24 and viscosity of dodecane and hexadecane from "CRC Handbook of Chemistry and Physics", CRC Press, Boca Raton, FL, 1984, p. F-39.

33 M. Sharp, Electrochim. Acta, 1983, 28, 301.

34 A. Kaifer, A.J. Bard, J. Phys. Chem., 1985, 89, 4876.

35 A.J. Bard, L.R. Faulkner, "Electrochemical Methods: Fundamentals and Applications", J. Wiley and Sons, New York, 1980, pp. 525-531.

36 A. Malliaris, J. Lang, R. Zana, J. Phys. Chem., 1986, 90, 655.

37 D. Evans, J. Electroanal. Chem., 1989, 258, 45.

38 F.C. Anson, J.-M. Savaent, K. Shigehara, J. Am. Chem. Soc., 1983, 105, 1096.

39 J.F. Rusling, C.-N. Shi, T.F. Kumosinski, Anal. Chem., 1988, 60, 1260.

40 P. Lianos, J. Lang, C. Strazielle, R. Zana, J. Phys. Chem., 1982, 86, 1019.

41 A. Roux, G. Roux-Desgranges, J.-P. E. Grolier, A. Viallard, J. Colloid Interfacial Sci., 1981, 84, 250.

42 K. Shinoda, M. Araki, A. Sadaghiani, A. Khan, B. Lindman, J. Phys. Chem., 1991, 95, 989.

43 B. Lindman, K. Shinoda, U. Olsson, D. Anderson, G. Kaelstörm, H. Wennerström, Colloids Surfaces, 1989, 38, 205.

44 B. Lindman, N. Kamenka, T.M. Kathopoulis, B. Frun, P.G. Nilsson, J. Phys. Chem., 1980, 84, 2485.

45 B. Lindman, O. Soderman, H. Wennerström, "Surfactant Solutions: New Methods of Investigation", R. Zana, ed., Marcel Dekker, New York, 1987, pp. 296-352.

46 P.G. Nilsson, B. Lindman, J. Phys. Chem., 1983, 87, 4756.

47 S.E. Boyette, Ph.D. dissertation, University of Florida, Gainesville, FL, 1991.

48 M. Clausse, J. Heil, J. Peyrelasse, C. Bond, J. Colloid Interface Sci., 1982, 87, 584.

49 A.J. Bard, L.R. Faulkner, "Electrochemical Methods: Fundamentals and Applications", J. Wiley and Sons, New York, 1980, p. 160.

50 M. Almgren, F. Grieser, J.K. Thomas, J. Am. Chem. Soc., 1979, 101, 279.

51 M.J. Rosen, "Surfactants and Interfacial Phenomena, J. Wiley and Sons, New York, 1982.

52 A.J. Bard, L.R. Faulkner, "Electrochemical Methods: Fundamentals and Applications", J. Wiley and Sons, New York, 1980, pp. 228-231.

53 R. Adams, "Electrochemistry at Solid Electrodes", Marcel Dekker, New York, 1969, p. 221.

54 P. Yeh, T. Kuwana, J. Electrochem. Soc., 1976, 123, 1334.

FIGURE CAPTIONS

1 Phase diagram of SDS microemulsion used [27]. Units are in weight percent. Aqueous phase is 0.1 M $NaCl_{(aq)}$, oil is dodecane, surfactant is SDS, cosurfactant is 1-pentanol, and the ratio of surfactant to cosurfactant is 1:2. Exact compositions used in these experiments are listed in Table 1.

2 Cyclic voltammogram of MV^{+2} at 100 mV/s.

3 Diffusion coefficient (D_R) of Fc versus weight percent water in the microemulsion.

4 Diffusion coefficient (D_O) versus weight percent water in microemulsion.

5 Diffusion coefficient (D_R) of Fc versus SDS microemulsion composition for different oil to emulsifier ratios.

6 Formal potential ($E_{1/2}$) of Fc versus weight percent water in microemulsion.

TABLE 1

SDS MICROEMULSION COMPOSITIONS[a]

	%brine[b]	%dodecane	%SDS	%1-pentanol
34/6	34.02	5.94	20.09	39.96
45/5	45.53	5.01	16.60	33.27
52/8	52.02	8.00	13.32	26.66
56/4	56.12	4.01	13.27	26.60
64/6	64.00	6.00	10.00	20.00
67/3	67.02	3.00	10.01	19.96
76/4	76.00	4.00	6.66	13.34
88/2	88.02	1.98	3.32	6.68
89/1	89.00	1.00	3.35	6.66

[a]units are weight percent (w/w).

[b]0.1 M $NaCl_{(aq)}$, unbufferred, pH 5.6.

TABLE 2

EFFECT OF CONCENTRATION OF PROBE ON DIFFUSION COEFFICIENT OF PROBE IN SDS MICROEMULSIONS

probe	sol'n[a]	conc (mM)	$D_R' \times 10^6$ (cm^2/s)	$E_{1/2} \times 10^3$ (V)
Fc	89/1	0.77	0.81±0.02	+225±4
		1.84	0.53±0.03	+221±3
		2.25	0.58±0.03	+219±3
Fc	67/3	0.94	3.23±0.06	+275±5
		1.97	2.84±0.04	+267±2
		2.88	2.73±0.04	+273±9
Fc	45/5	0.83	4.31±0.04	+297±16
		1.52	4.06±0.13	+291±3
		2.44	3.36±0.02	+299±11
		3.15	3.46±0.05	+291±4

[a]SDS microemulsion composition %water/%oil. See Table I for exact compositions.

TABLE 3

FERROCENE IN SDS MICROEMULSIONS

conc (mM)	sol'n[a]	$E_{1/2}$[b]X10^3 (V)	ΔEp[b] (mV)	i_{pa}	i_{pa}/i_{pc}[b]	D_R' X 10^6 (cm^2/s)
4.98	MeCN[c]	+419±4	61±8	160±5	0.99±0.09	24[d]
2.11	34/6	+311±3	64±6	24.3±0.1	1.29±0.08	3.87±.11
3.15	45/5	+291±4	67±8	33.6±1.7	1.16±0.09	3.46±.05
3.13	52/8	+292±6	75±6	34.4±0.6	1.31±0.06	3.30±.03
2.80	56/4	+282±1	62±2	30.1±0.6	1.26±0.04	3.04±.06
3.06	64/6	+287±6	68±6	34.1±0.4	1.30±0.02	3.26±.03
2.88	67/3	+273±9	74±18	28.8±0.9	1.14±0.13	2.73±.03
2.98	76/4	+268±7	72±14	27.1±0.7	1.31±0.06	2.38±.07
2.98	78/4	+252±2	63±3	23.9±0.2	1.33±0.02	1.69±.04
2.87	88/2	+220±3	59±9	9.3±0.1	1.15±0.05	0.32±.01
1.54	89/1	+219±3	55±5	9.4±0.2	1.08±0.05	0.58±.03
--	0.28 M SDS[e] in 0.1 M $NaCl_{(aq)}$	+195	--	--	--	0.61
--	aqueous	+160[e]	--	--	--	6.7[e]

[a]SDS microemulsion composition %water/%oil. See Table I for exact compositions.

[b]currents and potentials measured at 100 mV/s. Resistance was compensated to <5Ω.

[c]in 0.5 M tetraethylammonium chloride in acetonitrile

[d]reference [53]

[e]reference [25]

[e]reference [26]

II-112

TABLE 4

FERRICYANIDE IN SDS MICROEMULSIONS

conc (mM)	sol'n[a]	$E_{1/2}$[b] X 10^3 (V)	ΔEp[b] (mV)	i_{pc}[b] (μA)	i_{pc}/i_{pa}[b]	D_o' X 10^6 (cm^2/s)
1.04	34/6	+222±11	81±22	4.4±0.2	1.18±0.06	0.54±.01
1.37	45/5	+200±14	108±28	6.0±0.6	1.13±0.24	0.32±0.01
1.19	52/8	+200±7	157±16	4.8±0.2	1.09±0.07	0.92±0.04
1.05	56/4	+180±13	269±26	2.5±0.3	1.00±0.16	1.0±0.1
1.14	64/6	+171±14	381±27	5.9±0.3	1.59±0.42	1.8±0.1
1.09	67/3	+173±15	364±30	6.1±0.2	1.22±0.06	1.6±0.1
1.05	76/4	+154±36	607±72	4.2±0.1	1.76±0.16	4.0±0.1
1.21	78/4	+168±20	535±40	8.5±0.1	1.66±0.05	3.9±0.1
1.10	88/2	+154±20	308±40	8.9±0.1	2.02±0.21	5.3±0.2
1.17	89/1	+151±5	846±10	9.5±0.2	2.37±0.29	5.9±0.1
2.68	SDS[c]	+140±23	885±45	22.1±.5	2.21±0.20	5.2±0.3
2.46	aq[d]	+172±25	152±60	31.4±2.3	0.98±0.13	6.7±0.1

[a]SDS microemulsion composition %water/%oil. See Table I for exact compositions.

[b]currents and potentials measured at 100 mV/s. Resistance compensated to <50 Ω.

[c]SDS micelles, [SDS] = 2.97 mM in 0.1 M $NaCl_{(aq)}$

[d]measured in 0.1 M $NaCl_{(aq)}$

TABLE 5

METHYL VIOLOGEN IN SDS MICROEMULSIONS

conc (mM)	sol'n[a]	$E_{1/2,1}X10^3$ (V)	ΔEp_1[b] (mV)	i_{pc1}[b] (μA)	i_{pc1}/i_{pa1}[b]	$E_{1/2,2}X10^3$ (V)	ΔEp_2[b] (mV)	i_{pc2}[b] (μA)	i_{pc2}/i_{pa2}[b]	$D_R' \times 10^6$ (cm^2/s)
1.10	34/6	-632±6	55±12	3.4±0.6	0.60±0.14	-944±7	67±14	4.7±0.4	2.35±0.67	1.5±0.1
1.00	40/10	-635±7	56±13	3.6±0.4	0.65±0.15	-937±6	64±12	4.5±0.1	1.66±0.53	1.6±0.1
1.08	45/5	-641±3	52±6	4.0±0.2	0.64±0.06	-954±6	59±11	5.0±0.2	1.67±0.18	1.6±0.1
1.07	52/8	-642±5	57±9	3.7±0.3	0.54±0.08	-948±7	67±13	5.4±0.1	1.64±0.33	1.7±0.1
0.99	56/4	-646±6	49±11	4.7±0.7	0.72±0.17	-958±6	61±11	5.1±0.1	1.50±0.25	2.1±0.1
1.21	64/6	-654±6	57±11	6.3±0.1	0.84±0.02	-962±6	53±12	6.2±0.1	1.29±0.07	2.3±0.1
1.19	67/3	-665±3	59±6	5.5±0.4	0.68±0.07	-983±4	66±8	6.2±0.2	1.47±0.12	1.8±0.2
1.13	88/2	-668±3	60±6	6.3±0.5	0.64±0.06	-1014±4	63±8	6.0±0.2	1.05±0.11	2.5±0.2
1.31	89/1	-664±5	61±10	7.6±0.6	0.70±0.07	-1015±5	62±10	7.1±0.2	1.06±0.06	3.3±0.3
1.0	70 mM SDS[c]	-650	70	4.3	1.23	-1120	40	3.5	1.52	0.95
1.0	aq[c]	-690	60	11.8	1.09	-1020	30	10.3	--	6.56

[a]SDS microemulsion composition %water/%oil. See Table I for exact compositions.
[b]measured at 100 mV/s
[c]in 0.1 M $NaCl_{(aq)}$ [34]

TABLE 6

DROPLET SIZES AS A FUNCTION OF MICROEMULSION COMPOSITION

μe[a]	%aq	%oil	%em	electrolyte	s:c ratio[b]	[Fc] (mM)	D'X10^6 (cm^2/s)	D_{drop}X10^6 [c] (cm^2/s)	radius[d] (Å)
SDS	89.0	1.0	10.0	0.1 M NaCl	1:2	1.54	0.58	0.54-0.36	45-68
SDS	89.0	1.0	10.0	0.1 M NaCl	2:1	1.91	0.52	0.49-0.34	50-72
SDS	88.0	2.0	10.0	0.1 M NaCl	1:2	2.87	0.32	0.30-0.20	82-123
SDS	79.0	5.0	16.0	none	1:2	3.31	0.19	0.17-0.09	144-272
						by fluorescence [13]			52
CTAB	88.6	1.0	10.4	none	1:1	4.93	0.57	0.56-0.50	44-49
CTAB	89.8	2.3	6.9	1% NaBr	1:2	4.09	0.71	0.70-0.63	35-40
						by SANS [12]			35-45
CTAB	91	2	6	1% NaBr	1:2	by QELS [11]			56

[a]microemulsion used, in weight percent unless otherwise noted.
SDS μe: %aq = aqueous phase; %oil = dodecane; %em = SDS (surfactant) + 1-pentanol (cosurfactant); electrolyte = electrolyte in aqueous phase
CTAB μe: %aq = aqueous phase; %oil = hexadecane; %em = CTAB (surfactant) = 1-butanol (cosurfactant); electrolyte = electrolyte in total microemulsion

[b]surfactant to cosurfactant ratio

[c]diffusion coefficient of the droplet calculated from equation 4 and solubility (0.01 mM [54]-0.05 mM [24]) and diffusion coefficient (6.7 X 10^{-6} cm^2/s) of ferrocene in water.

[d]radius calculated from the diffusion coefficient of the droplet and the Stokes-Einstein equation (3), assuming aqueous continuous phase viscosity of 0.0089 P

Fig 1

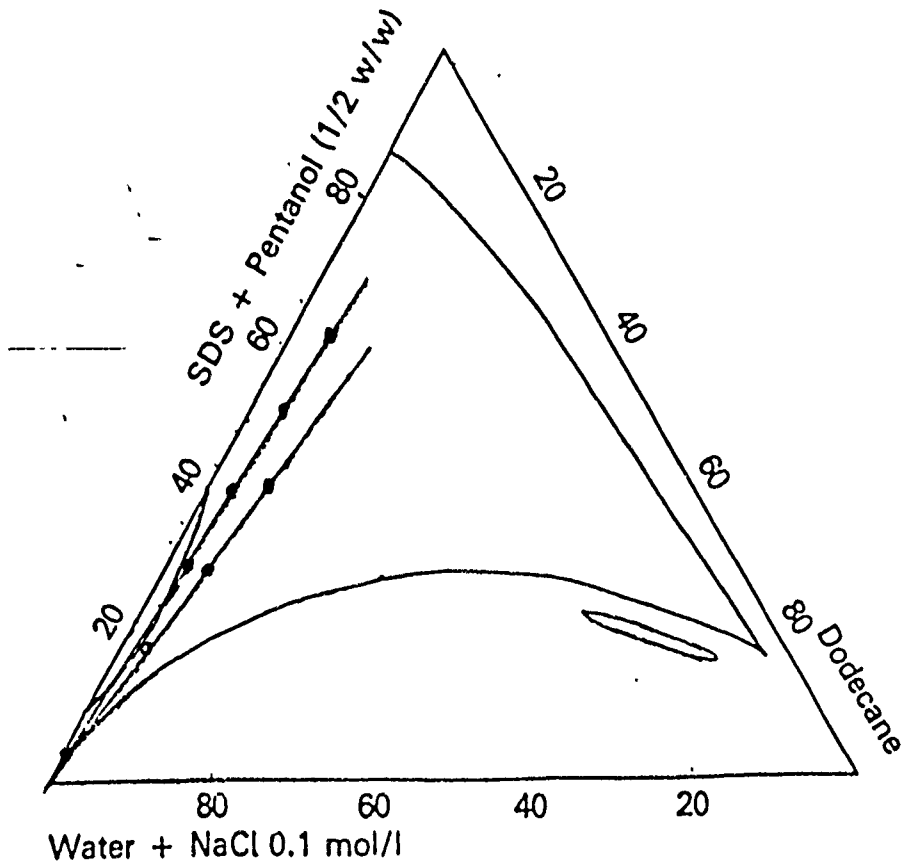
SDS + Pentanol (1/2 w/w)
80
60
40
20
20
40
60
80 Dodecane
80
60
40
20
Water + NaCl 0.1 mol/l

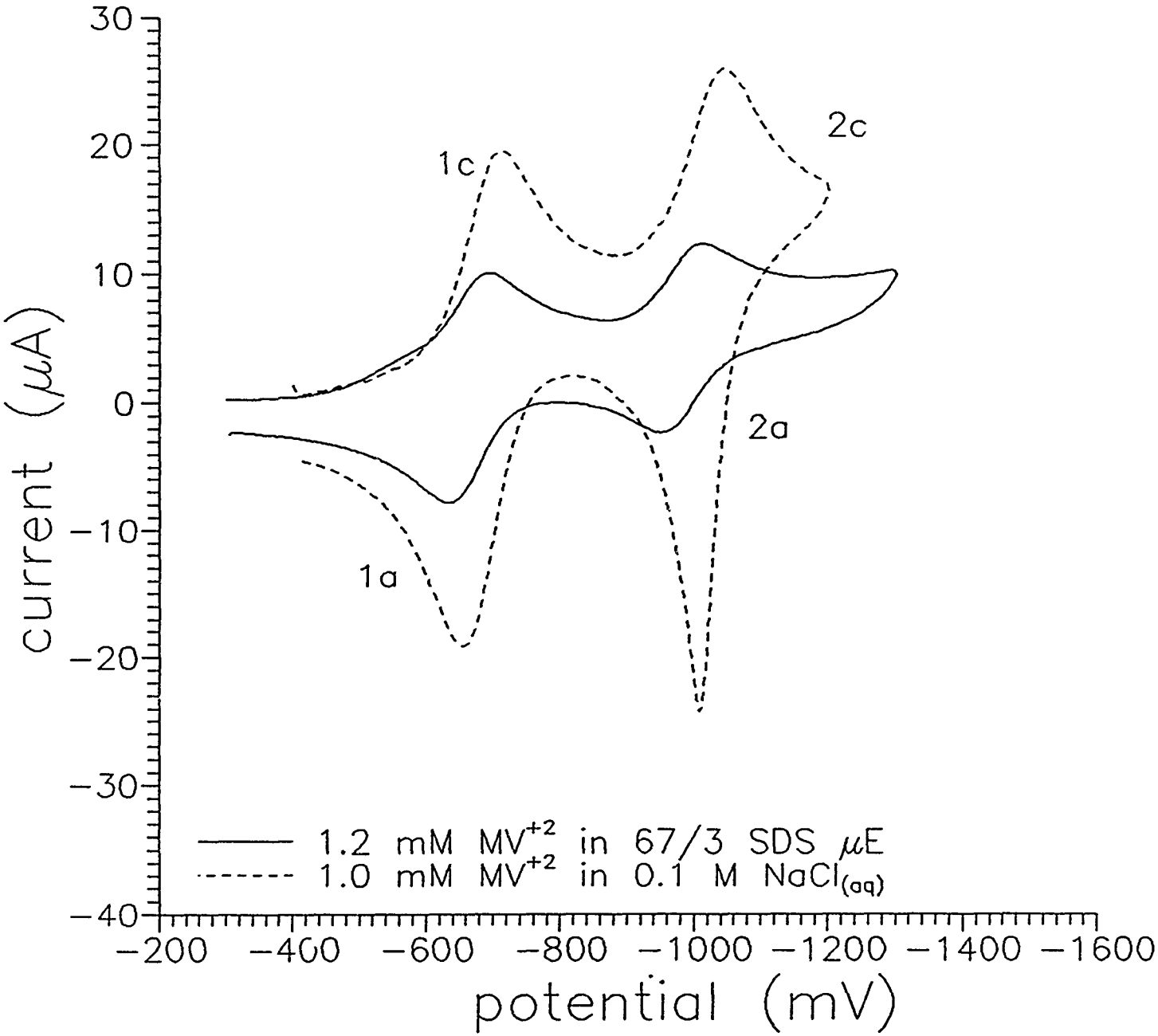
30
20
10
0
−10
−20
−30
−40
current (μA)
−200
−400
−600
−800
−1000
−1200
−1400
−1600
potential (mV)
1c
2c
1a
2a
1.2 mM MV+2 in 67/3 SDS μE
1.0 mM MV+2 in 0.1 M NaCl(aq)

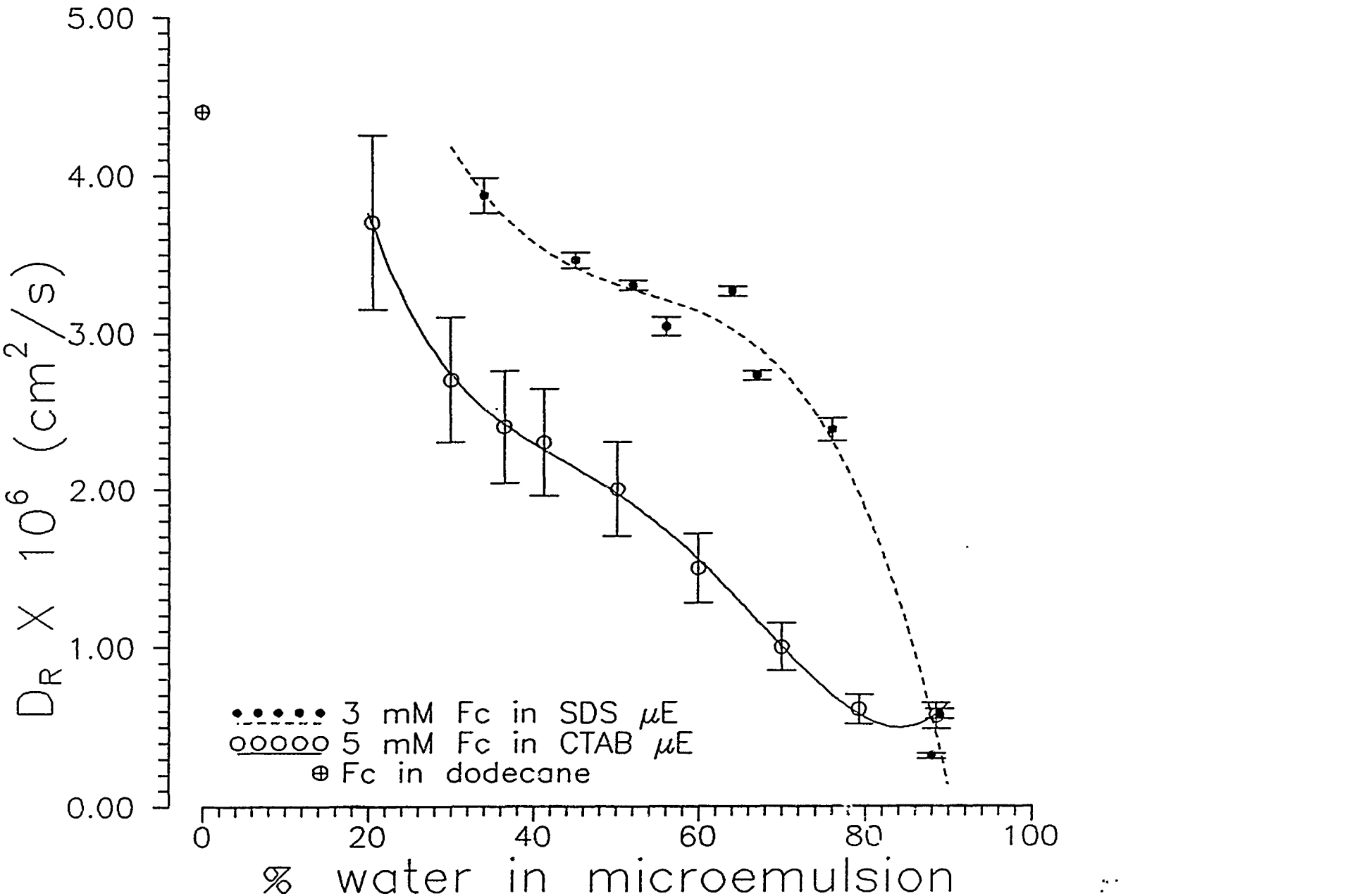
5.00
4.00
3.00
2.00
1.00
0.00
$D_R \times 10^6$ (cm^2/s)
0
20
40
60
80
100
% water in microemulsion
3 mM Fc in SDS μE
5 mM Fc in CTAB μE
Fc in dodecane

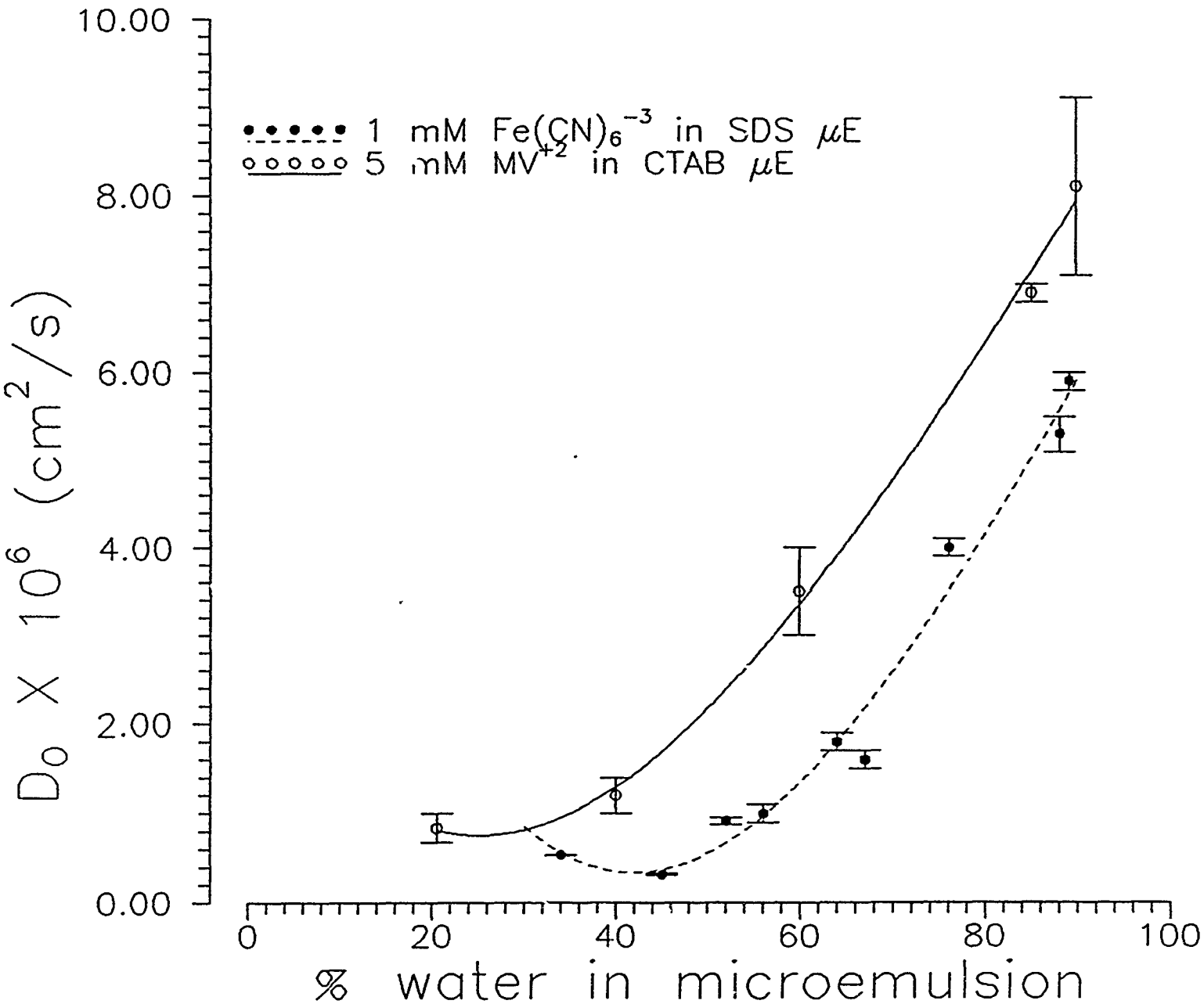
10.00
8.00
6.00
4.00
2.00
0.00
$D_o \times 10^6$ (cm^2/s)
1 mM $Fe(CN)_6^{-3}$ in SDS μE
5 mM MV^{+2} in CTAB μE
0
20
40
60
80
100
% water in microemulsion

6/11-II

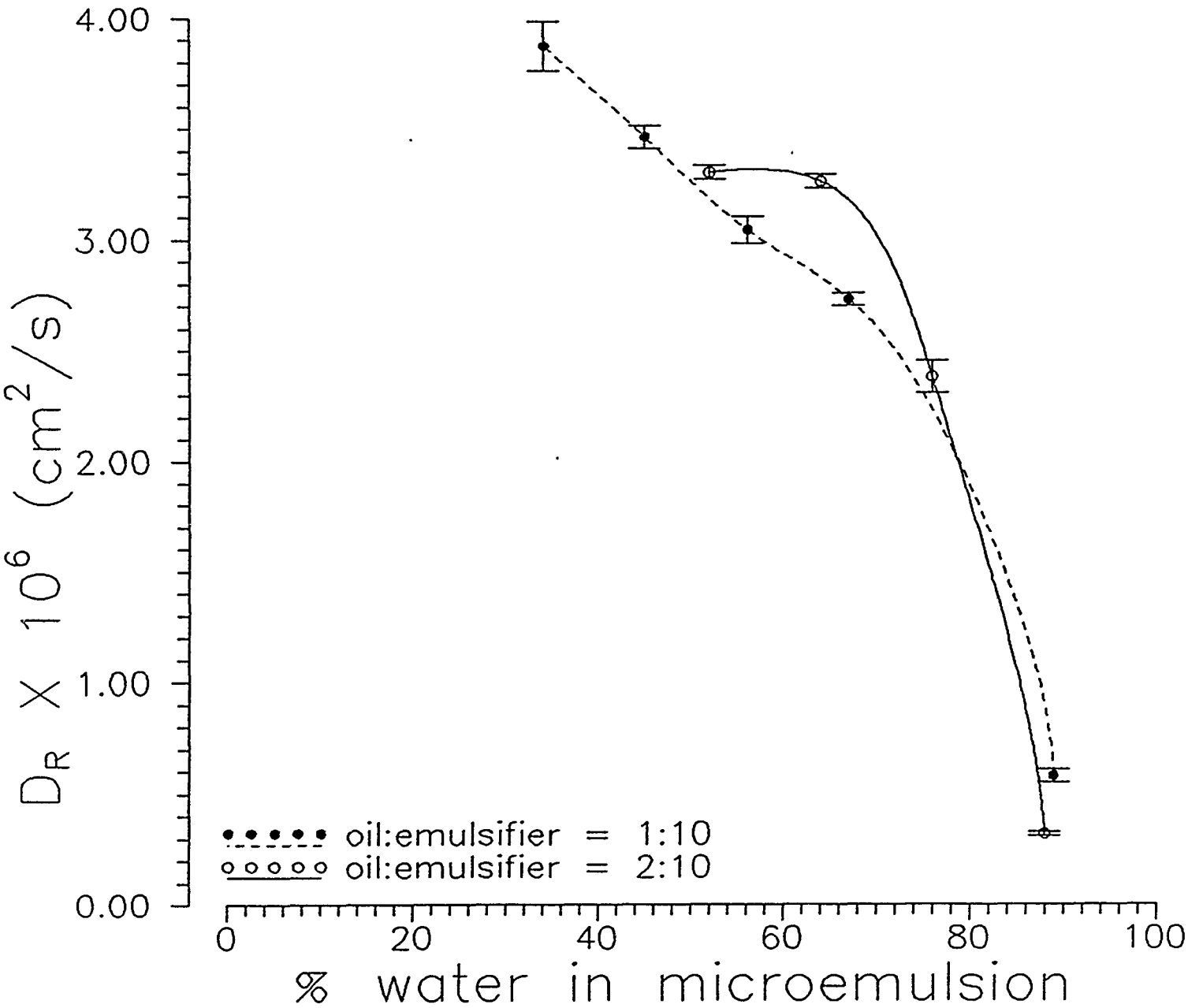
4.00
3.00
2.00
1.00
0.00
$D_R \times 10^6$ (cm^2/s)
oil:emulsifier = 1:10
oil:emulsifier = 2:10
0
20
40
60
80
100
% water in microemulsion

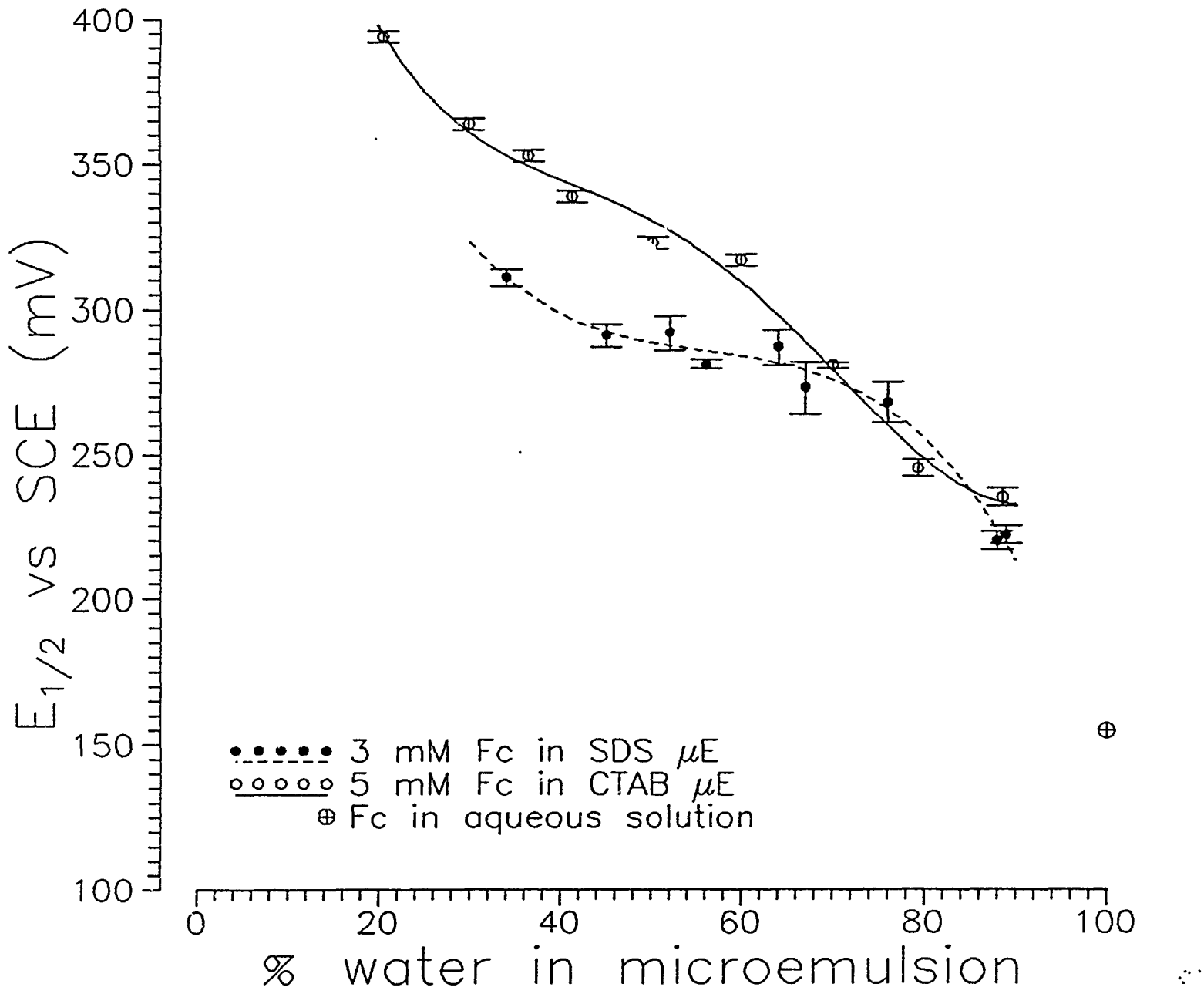
400
350
300
250
200
150
100
$E_{1/2}$ vs SCE (mV)
3 mM Fc in SDS μE
5 mM Fc in CTAB μE
Fc in aqueous solution
0
20
40
60
80
100
% water in microemulsion

ACKNOWLEDGEMENTS

This work was supported by the U.S. Army Research Office through Grant No. DAAA 15-85-C-0034, by the NIH grant R01 GM35451-03 (ABT) and by Battelle, Research Triangle Park office under Scientific Services Agreement DAAL03-86-D-0001.

(16) Luminescence and Electrochemical Studies in Reactive Microemulsions.

F. R. Longo et al.

a U.S. Army Chemical Research, Development and Engineering Center, Aberdeen Proving Ground, MD 21010-5423

b Geo-Centers, Inc., Fort Washington, MD 20744

c Drexel University, Philadelphia, PA 19104

d National Research Council Fellow, U. S. Army CRDEC, Aberdeen Proving Ground, MD 21010-5423

e Lab. IMRCP, Université Paul Sabatier, 31 062 Toulouse, France

ABSTRACT

We have systematically examined microemulsions as possible media for chemical degradation of toxic substances, and we have undertaken a variety of physicochemical studies designed to characterize their microstructure. Luminescence quenching has been used to determine aggregation numbers for CTAB, CTAC, and SDS microemulsion systems. Static luminescence quenching studies are apparently not applicable to most of the microemulsion systems that we have studied. Our data, however, indicate that time-resolved luminescence quenching studies give valid results for solutions with aggregation numbers up to ~400.

Electrchemical techniques, cyclic voltammetry (CV) and chronocoulometry (CC), have been employed to estimate the diffusion coefficients of the aggregates present in these microemulsion media. Our luminescence and electrochemical results appear in fair agreement.

INTRODUCTION

We have examined microemulsions as media for the iodosobenzoate catalyzed degradation of the nerve agent simulant p-nitrophenyldiphenyl

JUN 18 '91 13:27 3016712081 PAGE.002

phosphate (PNDP).[1-6] In order to understand the reactivity control effected by these media, we have initiated studies which will provide information concerning the microproperties (e.g., aggregation numbers, radii, and net charge of the microemulsion droplets) in systems in which we have measured degradation rate constants. In this paper, we report the aggregation numbers which were determined by static and dynamic luminescence quenching techniques and he microaggregate diffusion coefficients which were determined by the electrochemical techniques cyclic voltammetry and chronocoulometry.

Luminescence probes have been used successfully in both steady-state and time-resolved luminescence quenching techniques to measure the mean aggregation number (N , the average number of surfactant molecules per aggregate). In the steady-state or static method developed by Turro and Yekta[7] and by Turro, Yekta and Aikawa[8], luminescence quenching measurements are employed to determine micelle aggregation number. Assumptions inherent in this method include the following: donor and quencher molecules must associate primarily with the micelles; the residence time of the donor and quencher molecules in the micelles must be longer than the unquenched lifetime of the donor; the distribution of donor and quencher molecules in the micelles is Poisson; the immediate deactivation route of excited donor is quenching by an acceptor; the population of micelles is monodisperse; dynamic collisional quenching does not occur, and, therefore, the luminescence lifetime of the donor is independent of the quencher concentration.[9]

When luminescence probe/donor and quencher/acceptor are added to a micellar solution, luminescence is not observed from aggregates containing both excited probe and quencher. The intensity (I) of probe luminescence follows the relationship

$$I = I_0 \exp\frac{[M]}{[Q]} \qquad (1)$$

where I_0 is the luminescence intensity in the absence of quencher (Q) and M is the concentration of aggregates. When static quenching occurs, a plot of ln (I/I_0) vs [Q] yields a straight line whose slope is proportional to N. Lifetime measurements must, therefore, be available to determine the applicability of the steady-state technique as the plot of ln (I/I_0) vs [Q] will continue to be linear and

JUN 18 '91 13:28 3016712081 PAGE.003

appear to yield accurate aggregation numbers even in cases where the technique is not theoretically valid.

A more applicable approach for measuring aggregation numbers is the time-resolved technique developed by Infelta.[10,11] As with the steady-state technique, both probe and quencher must be associated with the aggregate with their distribution following Poisson statistics. Here, however, the lifetime of an excited probe molecule in the micelle depends on the number of quencher molecules present in the micelle. Infelta, Grätzel, and Thomas developed a general equation to describe the kinetics of quenching reactions in micelles.[10]

$$I(t) = I(0) \exp\{-A_2 t - A_3 (1 - \exp(A_4 t)) \qquad (2)$$

When both donor and quencher are immobile A_2 equals $-1/t_o$, A_3 equals $-\eta$, and A_4 equals $-k_q$. $I(0)$ and $I(t)$ are the luminescence intensity at zero time and at time t, τ_o is the lifetime of the donor in the absence of quencher, and k_q is the first order rate constant for luminescence quenching in a micelle containing one quencher, and η is the average number of quencher molecules per aggregate.[11,12] Substitution yields:

$$I(t) = I(0) \exp\{t/t_o + h(1 - \exp(-k_q t)) \qquad (3)$$

The luminescence decay curve of the donor is fit to Equation 3 by adjusting the parameters I_o, k_q, and η.

There are several reports on the application of the static and time-resolved luminescence techniques to micelles.[12-19] Llanos, Lang, and Zana have studied the effects of compositional changes on the aggregation numbers in microemulsions prepared from anionic surfactants.[20-22] Almgren, Grieser, and Thomas[23] have measured aggregation numbers in sodium lauryl sulfate / n-pentanol / dodecane /water microemulsions using the static quenching method.[7] Almgren and Löfroth[12] calculated aggregation numbers and quenching constants from single-photon counting data and steady state

JUN 18 '91 13:29 3016712081 PAGE.004

luminescence measurements in sodium dodecyl sulfate / 1-pentanol microemulsions and swollen micelles.

We have analyzed luminescence quenching data by both static and time-resolved techniques, and present results for six stable microemulsion systems and for three microemulsion systems not apparently at equilibrium. In addition, we include data for two microemulsion systems whose luminescence decay curves appear to follow a single exponential decay, however are not amenable to analysis using either technique.

Diffusion coefficients of electroactive species are obtained from diffusion controlled electrode reactions through the examination of the dependence of the applied potential on the current. Doping a microemulsion with electroactive species that are only soluble in the oily interior of the microdroplet yields a measured current that depends only on the rate at which the microdroplet vehicle moves to the electrode surface. Hence, it is possible to obtain diffusion coefficient and hydrodynamic radius of a microdroplet from electrochemical experiments.

In cyclic voltammetry, CV, the peak current, i_p, is given by the Randles-Sevcik equation:

$$i_p = (2.69 \times 105)n^{3/2}AC_oD_o^{1/2}v^{1/2}$$

where n, A, C_o, D_o, and v are the number of electrons, the electrode area, the concentration of the electroactive species, the diffusion coefficient and the potential scan rate, respectively. A study of the variation of i_p versus $v^{1/2}$ yields the diffusion coefficient.

In chronocoulometry, CC, the trace of charge transferred, Q_d, versus $t^{1/2}$ is linear as predicted by the integrated form of the Cottrell equation:

$$Q_d = (2nFAD_o^{1/2} C_ot^{1/2})/\pi^{1/2}$$

The slope proportional to the diffusion coefficient.

JUN 18 '91 13:29 3016712081 PAGE.005

The choice of the electroactive probe is the key to obtaining meaningful data. According to Qutubuddin[20] who has recently discussed this problem the electroactive probe must not disrupt the nature of the microemulsion aggregate, must undergo diffusion controlled charge transfer at the electrode surface, should be non-polar, and should not be significantly adsorbed onto the electrode surface. Of course, it must be electrochemically reactive within the potential range governed by the electrode material and the microemulsion medium. Ferrocene meets these requirements in many microemulsions and we employ it as the probe in our studies.

Using a polarographic method, Mackay[ref] obtained microdroplet radii (in anionic and cationic microemulsions) comparable to those determined by small angle x-ray scattering, quasi-elastic light scattering and luminescence quenching.[19] Qutubuddin[20] recently reported that diffusion coefficients and microdroplet radii can be obtained from cyclic and rotating disc voltammetry experiments for CTAB/n-butanol microemulsions.

ADD RUSLING REF

We have previously examined the efficacy of numerous microemulsions as media for nucleophilic degradation of phosphate esters. The second order rate constants (25°) for IBA catalyzed degadation were reported for the microemulsions for which we now report luminescence quenching and electrochemical data.

MATERIALS AND EXPERIMENTAL PROCEDURE

Cetyltrimethylammonium bromide (CTAB) was purchased from Aldrich (95 %) or Sigma Chemical Co. (98 %) and used as received. Cetyltrimethyl-ammonium chloride (CTAC) was purchased from Eastman Kodak Co. as a dry chemical (97 %) and was obtained as a 29 % aqueous solution (Arquad 16-29) from Akzo Chemie America. Solid sodium tetraborate decahydrate (0.03 M) was added to the aqueous CTAC solution before use. 1-Methyl-2-pyrrolidinone (MP; 100 %) was received as a gift from BASF Corp. and 1-

JUN 18 '91 13:30 3016712081 PAGE.006

cyclohexyl-2-pyrrolidinone (CHP) was received as experimental material from Virginia Chemicals Inc. Sodium dodecyl sulfate (SDS; 98 %), 1-butanol (1-BuOH, 99 %), N,N-diethylformamide (DEF; 99 %), Adogen® 464 (Ad; 85-90 %), and N,N-diisopropylformamide (DIPF; 98 %) were purchased from Aldrich, and N,N-dimethylformamide (DMF; 99 %) was purchased from Baker and dried over 4 Å molecular sieves before use. Toluene (TOL; Baker; 100%), 4-tert-butyltoluene (t-BuTOL; Aldrich; 95 %), n-dodecane (DDEC; Aldrich; 99 %), and n-hexadecane (HEX; Sigma; 99 %) were used as supplied. Borate buffer

(AQ) was prepared from sodium tetraborate decahydrate (Fischer) and glass-distilled, deionized water. Microemulsions were prepared with 0.03 M, pH 9.4 borate buffer as the aqueous phase.

Three luminescence probes[26] were used in this study: tris(2,2'-bipyridine) ruthenium (2+) chloride hexahydrate (#1), tris(4,7-diphenyl-1,10-phenanthroline -N^1,N^{10}) ruthenium (2+) chloride hexahydrate (#2), and sodium tris [[(4,7-diphenyl-1,10-phenanthroline) (benzenesulfonato)$_x$] -N^1,N^{10}] ruthenate (2-) decahydrate (#3). Probe #2 is insoluble in the aqueous phase and is found almost exclusively in the oil phase of the microemulsion. Probe #3 is soluble not only in the aqueous phase, but in the droplet interface as well, and is strongly attracted to positively-charged microdroplets due to its negative charge. Aggregation numbers determined using the second and the third probes were found to agree within the accuracy of the measurement. Probe #1 was used in an SDS microemulsion to duplicate the measurement reported by Almgren and Löfroth.[12] 9-Methyl-anthracene (MeA; Aldrich; 99 %) was used as the luminescence quencher in all experiments.

Microemulsion cmc's were assumed to be approximately equal to the cmc's for micellar media. This is not exactly correct, but the cmc is small when

JUN 18 '91 13:31 3016712081 PAGE.007

compared to [S] and does not affect the calculated value for N significantly. CTAB, CTAC, and SDS cmc values used were 9.2×10^{-4} M,[27] 1.3×10^{-3} M,[27] and 2×10^{-3} M,[23,28] respectively.[Footnote]

It is assumed that all surfactant is associated with the microdroplets of the microemulsion. This may not be true and some free surfactant and surfactant organized into micelles may co-exist with the microemulsion aggregates. (Unpublished observation T. Kumosinski and R. A. Mackay made while performing sedimentation studies). Although the amount of surfactant in the form of co-existing micelles is not known it must be an extremely small fraction, otherwise, our phosphate ester hydrolysis studies would have yielded much higher rate constants. Second order hydrolysis constants measured in micellar solutions are greater than constants in microemulsion media by a factor of 10^2 to 10^3 .

For time-resolved measurements, 3 ml sample of microemulsion was placed in a fluorimetry cuvette to which 20 µl of a 2.0×10^{-3} M to 7.2×10^{-3} M solution of probe in water (#1, #3) or in MP (#2) were added. The cuvette was capped, mixed thoroughly, and purged with nitrogen for at least 15 minutes. For runs with quencher, a 25 µl sample of 6.16×10^{-2} M solution of MeA in acetonitrile was injected into the cuvette and thoroughly mixed. The solution was then purged with nitrogen for an additional 3 minutes. The doubled output from a Spectra-Physics (Quanta-Ray) Model DCR- 2A Nd:YAG laser provided an excitation wavelength of 532 nm with a pulse width of 6-7 ns. This wavelength, though not at the absorption maxima of the donors (~450 nm), yielded sufficient luminescence intensity for these studies and provided results identical to those obtained with 355 nm excitation. Luminescence emitted at 90° was collected and focused onto the entrance slit of a Spex Model 1403 monochromator equipped with an RCA 31034A photomultiplier tube (PMT).

JUN 18 '91 13:31 3016712081 PAGE.008

The monochromator was set to the wavelength of maximum luminescence intensity (629 nm for #1, 615 nm for #2, 612 nm for #3) and the bandpass was set to approximately 1 nm. A LeCroy Model TR8828C transient recorder digitized the output of the PMT at 20 ns intervals, and the resulting decay curve was stored on floppy disk. The Asyst® software package[29] provided the least squares routines used to fit the data to Equation 2. Because the laser pulse width (6-7 ns) was much shorter than the probe luminescence lifetime, deconvolution of the laser pulse was not necessary. Equation 2 is not a single exponential, and therefore, the time chosen for I_0 is not arbitrary. The Rayleigh scattering from the sample is essentially instantaneous with the incident laser pulse and was used to define t = 0.

Steady-state luminescence measurements were obtained with a Perkin Elmer MPF-66 fluorescence spectrophotometer controlled by a series 7000 computer and with a xenon lamp source. Corrected excitation and emission spectra were collected in the ratio mode at a spectral bandpass of 1.5 to 1.8 ± 0.1 nm. The sample turret was thermostatted at 25.0 °C. An MPF-66 OBEY program, SCOUT, was used to determine the wavelengths of maximum excitation and emission for the donor molecules. The excitation / emission wavelengths used for the donor molecules were 453 / 629 nm (#1), 463 / 615 nm (#2), and 469 / 612 nm (#3).

In the time-resolved measurements the MPF-66 fluorescence spectrophotometer slit widths were adjusted to give an intensity readings of approximately 25 % maximum intensity. A 10 µL sample of a 6.16×10^{-2} M solution of 9-MeA in ACN was then added to the cuvette. The cuvette was capped, mixed thoroughly, and purged with nitrogen for an additional 3 minutes. The cuvette was placed into the spectrofluorimeter and the intensity (I) was read. Additional 10 µL aliquots of 9-MeA in ACN were added to the cuvette

JUN 18 '91 13:32 3016712091 PAGE.009

and the process was repeated. The concentration of 9-MeA, [Q], ranged from 2.033×10^{-4} M to 1.003×10^{-3} M in the cuvette. Steady-state luminescence measurements were collected, minimally, in duplicate for each microemulsion.

Electrochemical measurements were conducted on Microemulsions (mE) 1 to 6, Table 1. We used an M273/96 Potentiostat/Galvanostat interfaced to an IBM PS/2 Model 70-E61 microcomputer, employing EG&G Princeton Applied Research (PAR) M270, v 3.00, Electrochemical Software. The electrochemical cell included a PAR G0197 glassy carbon working electrode, a silver-silver chloride reference electrode and a platinum wire auxiliary electrode. Appropriate IR compensation by positive feedback was applied in all experimental determinations. Temperature was controlled to 26+-0.5°C.

Cyclic voltammetric studies were conducted in the staircase mode. For microemulsions mE's #1 to #5 currents were sampled at 25% of the pulse width and for mE#6 at 50%, since the oxidation of ferrocene had a lower heterogeneous transfer rate constant . Chronocoulometric studies wrere conducted in the double potential step mode with a pulse width of 10 seconds. The data were corrected for background charge before the diffusion coefficients were determined from Q_d vs $t^{1/2}$ plots.

The working electrode electrochemical areas were determined by CV and CC in aqueous solutions which were 1.0 M in KCl and 4.0 mM in $K_4Fe(CN)_6$. The literature value of the diffusion coefficient of $Fe(CN)_6^{4-}$ under these conditions is 0.632(+-0.003) x 10-5 cm^2/s at 25°C. ref********** The areas of the three glassy carbon electrodes used in this study ranged from 0.075 to 0.081 cm^2

JUN 18 '91 13:32 3016712081 PAGE.010

****

M. von Stackelberg, M. Pilgram and V. Toome Z. Elektrochem 57 342 (1953)

****

RESULTS AND DISCUSSION

Luminescence

Mean aggregation numbers for mE's 1 through 11 were measured using time-resolved luminescence. The aggregation data presented in Table 2 are averages of at least 4 different determinations and are reported as the mean ± the standard deviation. Based on the calculated values of N, the microemulsions can be divided into three categories: mE's 1 to 6; 7 to 9; and 10,11.

Microemulsions 1-6 yielded reproducible results (i.e. small standard deviations) with good fits of the data to Equation 3. For mE's 1 thru 6, the excited probe luminescence in the presence of quencher exhibits an apparent double exponential decay: immediately after excitation, the decay from aggregates containing one or more quencher molecules dominates and the luminescence dececreases rapidly. At long times, the luminescence intensity is dominated by emission from aggregates without quencher, and the lifetime approaches τ_0. Luminescence decay traces for mE 4 with different quencher concentrations are shown in Figure 1. Values for the multiple correlation coefficient or total goodness of fit parameter (R^2) are given with $R^2 \approx 1.0$ indicating a perfect fit.

Most microemulsions equilibrate within 24 hours. Several systems require additional time, while others either phase separate or never attain

JUN 18 '91 13:33 3016712081 PAGE.011

equilibrium. Systems 1-6 probably come to equilibrium as evidenced by the fact that measured values of *N* that did not change significantly over time periods of 100 hours.

Microemulsions 7,8, and 9 which were studied 24 hours and 100 hours after preparation were not stable and the apparent mean aggregation numbers changed dramatically over peroiods of 100 hours. The mean aggregation number for μE 9 was reported by Almgren[12] to be 313 which is close to the value of 369 which we found 24 hours after preparation. . Measured again 100 hours after preparation *N* had to increase to 833. The effect of cosurfactant on microemulsion stability is clearly evident as mE 7 is identical to μE's 1, 3, and 5 except for the choice of cosurfactant.

Equation 3 could not be solved satisfactorily with data obtained for μE's 10 and 11 and, in fact, produced single exponential decay curves (Figure 2), which are expected for quenching in homogeneous media without aggregates. Inspection of Equation 2 reveals that it predicts a single exponential decay I(t) for small values of k_q where exp (- k_qt) approximates (1 - k_qt). In other words,

$$I(t) = I(0) \exp(-t/\tau) \quad (3)$$

where

$$1/\tau = 1/\tau_o + \eta k_q \quad (4)$$

and

$$\tau_o/\tau = 1 + k_q \tau_o [Q]/[M] \quad (5)$$

which is the Stern-Volmer relationship for collisional quenching.[30] Plots of τ_o/τ vs [Q] for μE's 10 and 11 do indeed yield straight lines over the range of quencher concentrations used (Figure 3). This is probably indicative of large aggregates containing 1 or more quencher molecules . Assuming a Poisson

JUN 18 '91 13:34 3016712081 PAGE.012

distribution of quenchers among the aggregates, less than 10 % of the aggregates will contain no quenchers ($P_0 \approx 0.08$) in μE 10 if $\eta = 2.5$, and N would have to be ~1375 for $[Q] = 4 \times 10^{-4}$. This approach is obviously not quantitative but it does give some indication of how large the aggregates might be. With an aggregation number of this magnitude, it is reasonable to question whether the aggregates are spherical. For μE's 10 and 11, the time-resolved luminescence data can tell us that the structures are large (i.e. have many surfactant molecules associated with them) but cannot provide us with an aggregation number.

We began our steady state studies by re-examinig a 0.045 M SDS micellar system which had previously been examined by Turro. With Probe #1 as donor and 9-methylanthracene as quencher we measured an aggregation number of 60.5+-3.0, in close agreement with Turro's value of 60 ± 2.[7] In addition, the method was applied to solutions of CTAC in 0.02 M phosphate buffer, pH 8.0, 0.08 M NaCl, with Probe #3 (Table 3). Measured aggregation numbers agree (± 10 %) with aggregation numbers calculated from electrochemical measurements reported by Mackay, Dixit, Agarwal and Selders.[31]

The results of the static measurements in the microemulsions whose compositios are given in Table 1 are presented in Table 2. In all of the systems tested, donor lifetime was a function of quencher concentration, and, in fact, decreases as quencher concentration increases. In addition, duplicate and triplicate measurements of N in larger aggregates lacked precision. These results indicate that the steady-state luminescence quenching technique may not be valid when N > 200 to 250. Results of our studies indicate that this

JUN 18 '91 13:34 3016712081 PAGE.013

method may accurately be applied only to micellar media or to small microemulsion aggregates.

When the time-resolved luminescence quenching technique is employed to determine aggregation number in microemulsion media, precise results, i. e., good fits to Equation 3, are obtained. Decreasing the percentage surfactant and increasing percentage AQ and producing microemulsions with smaller aggregates or swollen micelles are likely to be yield systems, the data from which better fit Equation 3. Aggregation numbers determined from steady-state measurements agree with aggregation numbers determined from time-resolved measurements mE's 1, 2, 3, and 4. The steady-state data would appear to be invalidated, however, since donor lifetime in these microemulsions is a function of quencher concentration. Data obtained in systems containing CHP or DIPF as cosurfactant either could not be fit to Equation 3, or resulted in a value for *N* with a large standard deviation.

Electrochemistry

We have estimated the diffusion coefficients of the microemulsion aggregates by eletrochemical methods. Diffusion coefficients for molecules of ordinary size in aqueous medium are of the order of 10^{-5} to 10^{-6} cm^2/s. For instance, the value of D_o for ferrocene as determined by chronopotentiometry in acetonitrile at 25°C is 2.4×10^{-5} cm^2/s,

ref: T. Kuwana, D. E. Bublitz and G. Hoh, JACS 82 5811 (1960)

JUN 18 '91 13:35 3016712081 PAGE.014

whereas the values of D_o for ferrocene in the microemulsions examined in this study are of the order of $10^{-7}cm^2/s$. The Stokes-Einstein Equation relates diffusion coefficient to the radius of a molecule:

$$radius = kT/(6\pi\eta D) \qquad (4)$$

where k is the Boltzmann constant, T is the absolute temperature, and η is the viscosity coefficient (0.98×10^{-3} Ns/m^2 for pure water at 23°C). As can be seen from examination of Equation 4, this indicates that the radius of the electroactive species and/or the viscosity are different in our microemulsion. We have assumed that the ferrocene, since it is non-polar, is strongly associated with the microaggregates present in the microemulsion and, as a simplification, the aqueous medium retains the viscosity of pure water. The ferrocene has lost its translational degrees of freedom and moves with the microaggregate, thus forming a a giant electroactive species with n = 1. The electrochemical measurements then yield the diffusion coefficients and diameters of the microaggregates.

Ferrocene appears to undergo quasi-reversible electrochemical oxidation in the microemulsions (#1 to #6) which we have studied by cyclic voltammetry and chronocoulometry. This is borne out by examination of a typical CV trace , Figure 4, which represents the the cyclic voltammogram for ferrocene (2 mM) in mE#1 at a scan rate of 50 mV/s. Note that the cathodic peak current is signicantly lower than the anodic peak current, the separation between anodic and cathodic peak potentials is ~110 mV, the anodic peak potential and the separation between the anodic and cathodic peaks increases with sweep rate. These are all characteristics of quasi-reversibility. Figure 5a is a double-potential step chronocoulomogram taken in the same mE (#1) at a

JUN 18 '91 13:35 3016712081 PAGE.015

pulsewidth of 10 seconds. A plot of this data as charge passed ,Q, (in C) vs $(time)^{1/2}$ is linear as shown in Figure 5b. The intercept of this plot is the sum of the capacitive charge on the double layer and the faradaic component involved in the oxidation of adsorbed electroactive species.The Anson plot, Q vs θ, also shown in Figure 5b, is slightly, positively displaced and not co-linear, indicating again that a homogeneous chemical reaction precedes the cathodic reaction.

Figure 6 shows plots of D_o-values derived from CV and from CC measurements vs ferrocene concentration over a range from 0.5 to 2.5 mM. As expected from previous studies[ref]
??????????????????????????????Rusling; Qutubudin
the diffusion coefficients appear to decrease and then level off as the concentration of the probe increases. We take the level-off values as the actual diffusion coefficients. Analogous plots for systems mE#1 to #5 also generally show the same characteristics.

Microemulsion #6 demonstrated interesting behavior; see Figure 7 in which are presented the cyclic voltammograms for sweep rates of 20 and of 500mV/s at 2 mM ferrocene. At 500 mV/s we observe a very prominent anodic peak and no cathodic peak, while at 20 mV/s the cathodic peak is as prominent as the anodic peak. This indicates that the oxidation product undergoes chemical reaction before the working electrode becomes cathodic; when the homogeneous reductant in the system is consumed the anodic product can undergo electrochemical reduction , and, hence, a cathodic peak can be observed at scan rates of 20 to 100mV/s. Examination of the composition of mE#6 (Table 1) shows that it is the only one of our microemulsion systems containing Adogen 464, the synthesis of which could result in an amine contamination; amines can act as sources of homogeneous reductant.

JUN 18 '91 13:36 3016712081 PAGE.016

CONCLUSION

As mentioned, (vida supra) our object is to understand how microemulsion media affect reactivity and we have thorouhly investigated the hydrolysis of phosphate esters in numerous microemulsion systems including those examined in this work. Hence, our luminescence and electrochemical studies represent the initiation of a search for structure/reaction relationships.

Table 2 summarizes all of the relevant results of our studies. As can be seen the diffusion coefficients, D_o, extracted from the CV studies agree very well with those from CC. In addition, the aggregation numbers obtained form static luminescence, N_S, and the dynamic luminescence, N_D, except in a few instances, are in reasonable agreement, even though our experiments demonstrate that luminescence lifetimes are a function of quencher concentration.

In order to test the consistency of the luminescence and the electrochemical data we estimated the diameters of the microemulsion aggregates from the CV-determinated diffusion coefficients using the Stokes-Einstein Equation and compared them with the diameters determined from aggregation numbers N_S and N_D. (To calulate Diam from N_S or N_D assumptions must be made; we assumed that microemulsion aggregates accounted for all of the organic substances present in the microemulsion. In addition, we estimated the density of the microdroplets to be 0.8g/cm^3 and the overall density of the microemulsion to be ~0.95g/cm^3.) Examination of our results shows that the diameters estmated from the three types of

JUN 18 '91 13:37 3016712081 PAGE.017

measurements are fairly consistent, the worst exception being the values obtained from studies in mE#6, in which we have already indicated that an unusual irreversible process occurs .

Although we are fairly certain that the reactivity enhancement of the microemulsions is due to the reagent concentrating effect of the interfacial area, there appears to be no simple correlation between aggregate diameter and aggregation number, on the one hand, and the second order rate constants on the other. The lack of correlation is probably due to the fact the interfacial area is enormous and, therefore, its magnitude is not a rate limiting factor. For instance, our calculations show that for mE#2 the interfacial area available in one dm^3 of microemulsion is ~10^9 cm^2. The fraction of interfacial area occupied in an ordinary hydrolysis study is negligible in comparison. We are now attempting to determine the dependence of the rate constant on on microaggregate charge and zeta potential since it is fairly clear that charge has a pronounced effect on the rate of ester hydrolysis in surfactant systems.

JUN 18 '91 13:37 3016712081 PAGE.018

REFERENCES

1. Mackay, R.A., Longo, F.R., Knier, B.L., and Durst, H.D., J. Phys. Chem., 91, 861 (1987).

2. Knier, B.L., Durst, H.D., Burnside, B.A., Mackay, R.A., and Longo, F.R. J. Solution Chem., 17, 77 (1988).

3. Burnside, B.A., Szafraniec, L.L., Knier, B.L., Durst, H.D., Mackay, R.A., and Longo, F.R., J. Org. Chem., 53, 2009 (1988).

4. Burnside, B.A, Knier, B.L., Mackay, R.A., Durst, H.D., and Longo, F.R., J. Phys. Chem., 92, 4505 (1988).

5. Mackay, R.A., Burnside, B.A., Garlick, S.M., Knier, B.L., Durst, H.D., Nolan, P.M., and Longo, F.R., J. Disp. Sci. Technol., 9, 493 (1989).

6. Garlick, S.M., "Chemical and Physical Studies in Microemulsion Media," University Microfilms International, Ann Arbor, MI, (1990).

7. Turro, N.J. and Yekta, A., J. Am. Chem. Soc., 100, 5951- 5952 (1978).

8. Yekta, A., Aikawa, M., and Turro, N.J., Chem. Phys. Lett., 63, 543-548 (1979).

9. Lofroth, J-E.; Almgren, M. "Surfactants in Solution, Volume 1", edited by Mittal, K. L. and Lindman, B. Ed.; Plenum Press: New York, 1984; pp 627-643.

10. Infelta, P.P., Gratzel, M., and Thomas, J.K., J. Phys. Chem., 78, 190-195 (1974).

11. Infelta, P.P., Chem. Phys. Lett., 61, 88-91 (1979).

12. Almgren, M., Grieser, F., and Thomas, J.K., J. Am. Chem. Soc., 102, 3188-3193 (1980).

13. Almgren, M. and Swarup, S., "The Size of Sodium Dodecyl Micelles With Various Additives: A Fluorescence Quenching Study," In "Surfactants in Solution, Volume 1", edited by Mittal, K.L. and Lindman, B., Plenum Press: New York, 1984; pp. 613-625.

14. Kajiwara, T.; Thomas, J. K. J. Phys. Chem., 76, 1700-1706 (1972).

15. Turro, N. J.; Lee P. C. C. J. Phys. Chem., 86, 3367-3371 (1982).

JUN 18 '91 13:38 3016712081 PAGE.019

16. Aikawa, M.; Yekta, A.; Yurro, N. J. Chem. Phys. Lett., 68, 285-290 (1979).

17. Aikawa, M.; Yekta, A.; Liu, J-M.; Turro, N. J. Photochem. and Photobiol., 32, 297-303 (1980).

18. Atik, S. S.; Nam, M.; Singer, L. A. Chem. Phys. Lett., 67, 75-80 (1979).

19. De Schryver, F. C. 4th Interim Report # DAJA 45-84-C-0012, U. S. Army, European Research Offices of the U. S. Army, 1985.

20. Llanos, P., Lang, J., Strazelle, C., and Zana, R., J. Phys. Chem., 86, 1019-1025(1982).

21. Llanos, P., Lang, J., and Zana, R., J. Phys. Chem., 86, 4809-4814 (1982).

22. Llanos, P., Lang, J., and Zana, R., J. Phys. Chem., 88, 819-822 (1984).

23. Almgren, M. and Lofroth, J-E., J. Coll. Int. Sci., 81, 486-499 (1981).

24. Mackay, R.A. and Hermansky, C., J. Phys. Chem., 85, 739 (1981).

25. Moss, R.A., Scrimin, P., and Rosen, R.T., Tetrahedron Lett., 28, 251-254 (1987).

26. Durst, H.D., Longo, F.R., Garlick, S.M., Haddaway, K.G., U.S. Army CRDESCS Chemical Defense Research, 39-46 (1990).

27. Rosen, M.J., "Surfactants and Interfacial Phenomena," Wiley Interscience, New York, 1978, p 96.

28. Hayase, K. and Hayano, S., J. Coll. Int. Sci., 63, 446-451 (1978).

29. ASYST Software Technology, Inc. 100 Corporate Woods, Rochester, NY 14623.

30. Lakowicz, J.R., "Principles of Fluorescence Spectroscopy," Plenum Press, New York, 1986, pp 257-301.

31. Mackay, R. A.; Dixit, N. S.; Agarwal, R.; Selders, R. P. J. Disp. Sci. Tech., 4, 397-407 (1983).

II-141

FIGURE CAPTIONS

Figure 1. Luminescence decay curves for μE 4: a) [Q] = 0; τ_o = 3.4 μsec; R^2 = .9991; b) [Q] = 6.06 x 10^{-4} M; *N* = 196; R^2 = .9985; c) [Q]= 8.05 x 10^{-4} M; *N* = 184; R^2 = .9995; d) [Q]= 10.03 x 10^{-4} M; *N* = 182; R^2 = .9996.

Figure 2. Luminescence decay curves for μE 10: a) [Q] = 0; τ_o = 4.1 μsec; R^2 = .9983; b) [Q] = 4.05 x 10^{-4} M; τ = 1.6 μsec; R^2 = .9983; c) [Q] = 6.06 x 10^{-4} M; τ = 1.2 μsec; R^2 = .9991; d) [Q] = 10.03 x 10^{-4} M; τ = 1.0 μsec; R^2 = .9987.

Figure 3. Stern-Volmer plots for μE 10 (+) and μE 11 (*). Slopes are 2.04 mM^{-1} (R^2 = .956) for μE 10 and 3.26 mM^{-1} (R^2 = .963) for μE 11.

Figure 4. The cyclic voltammogram of ferrocene (2 mM) in mE#1. Several aspects of this trace indicate that the electrochemical process is quasi-reversible.

Figure 5a. A double-potential step chronocoulomogram, Q vs time, taken in mE#1 at a pulsewidth of 10 seconds.

Figure 5b. A plot of Q vs $(time)^{1/2}$ for the data from the double-potential step chronocoulometry experiment .(See Figure 5a for conditions.)

Figure 6. Plots of D_o-values derived from CV and from CC measurements vs ferrocene concentration over a range from 0.5 to 2.5 mM in mE#6.

Figure 7. Cyclic voltammograms for 2.0 mM ferrocene in mE#6 at sweep rates of 20 and of 500mV/s .

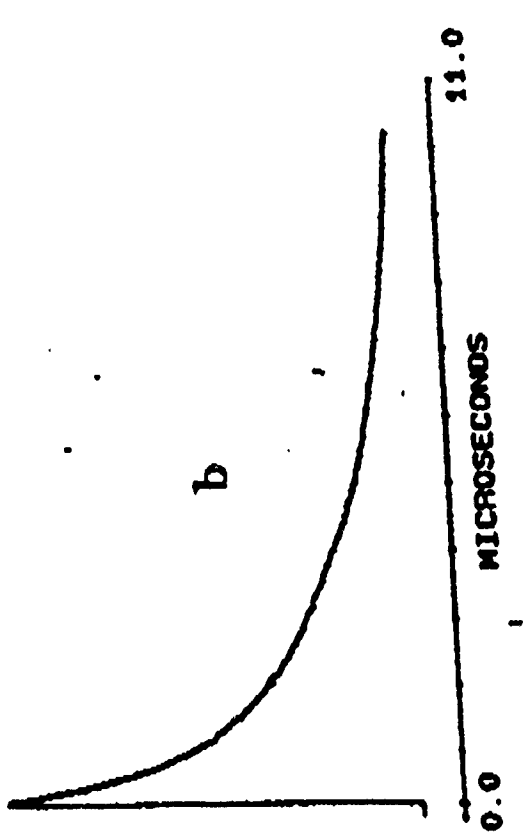
b
11.0
MICROSECONDS
0.0

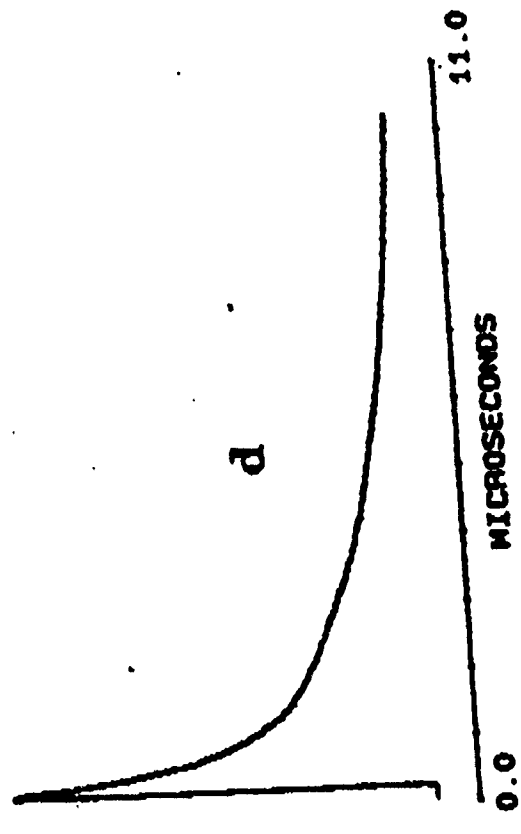
d
11.0
MICROSECONDS
0.0

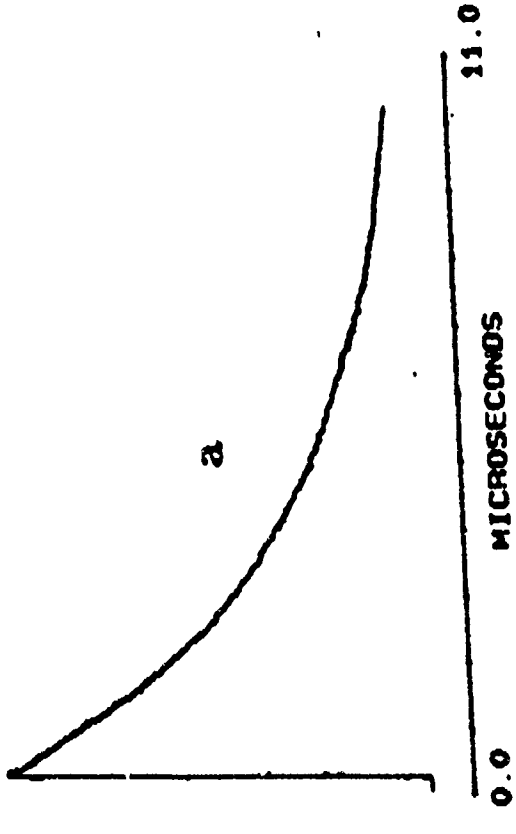
a
11.0
MICROSECONDS
0.0

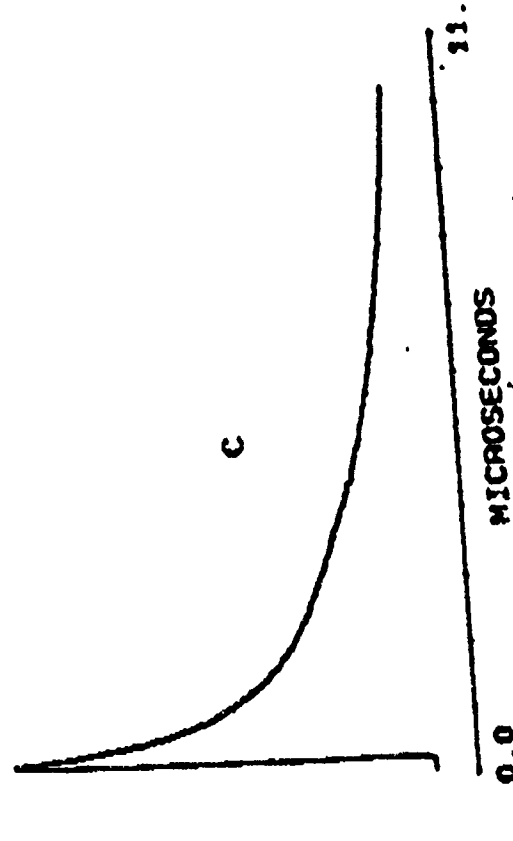
c
11.0
MICROSECONDS
0.0

F2

Legend

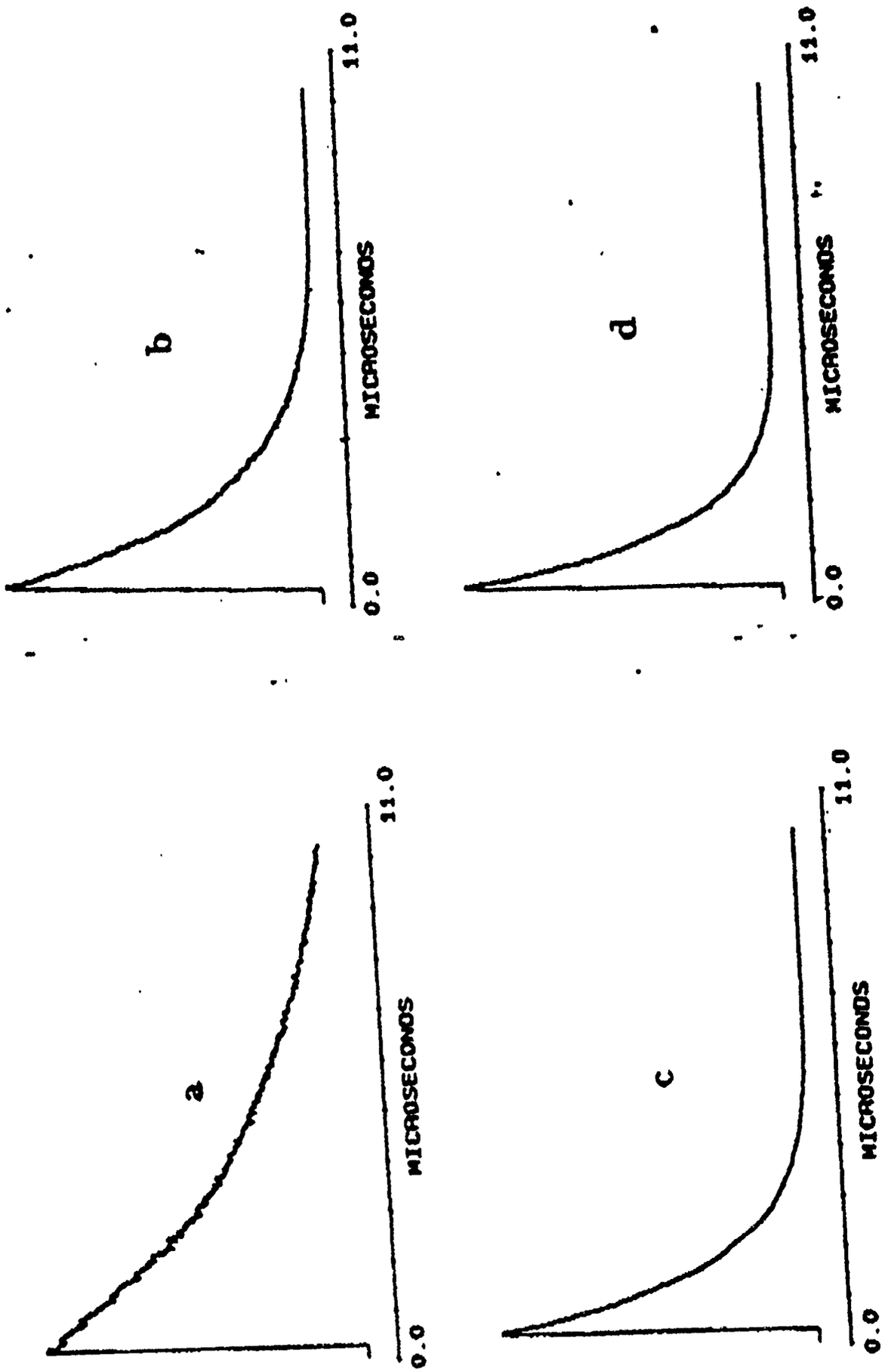

II-141

Figure 3

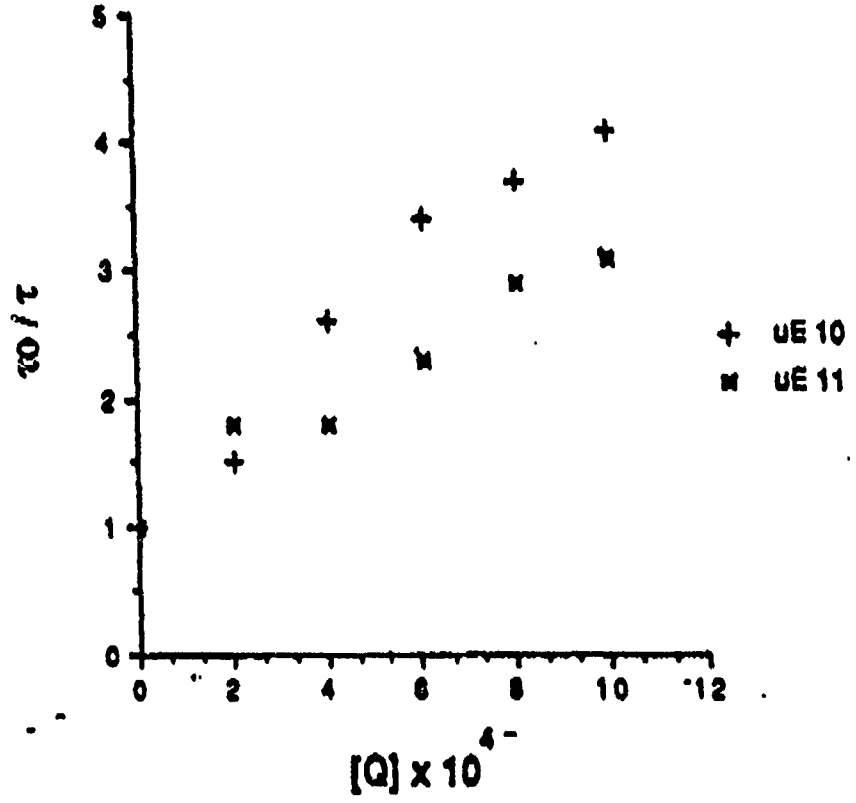

F3

Deduce kg from both traces

JUN 18 '91 13:41

9h/-II

Fig 4

larger version of above

002FC#1.50

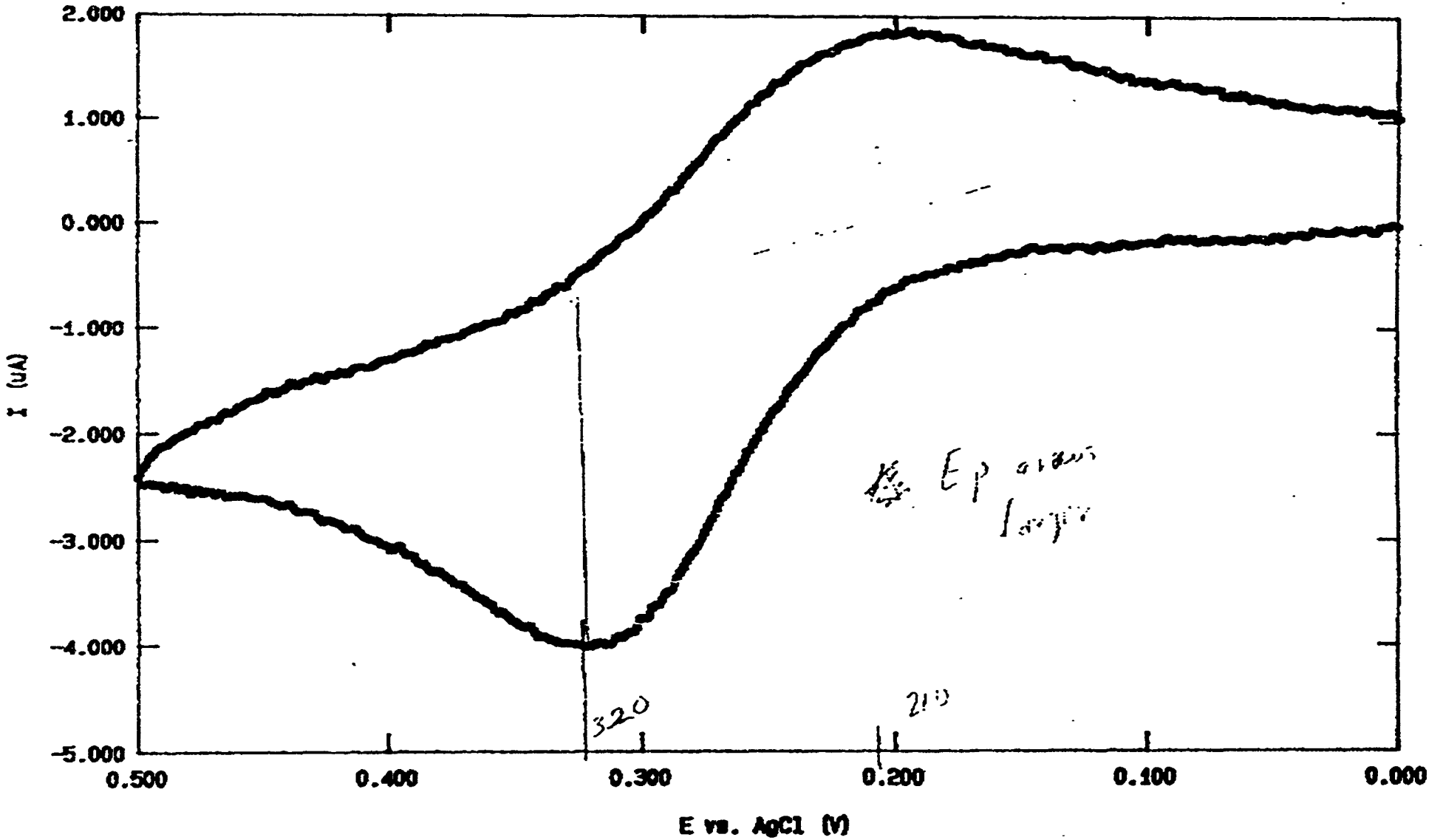

Ep values larger

10 mV

3016712081 PAGE.025

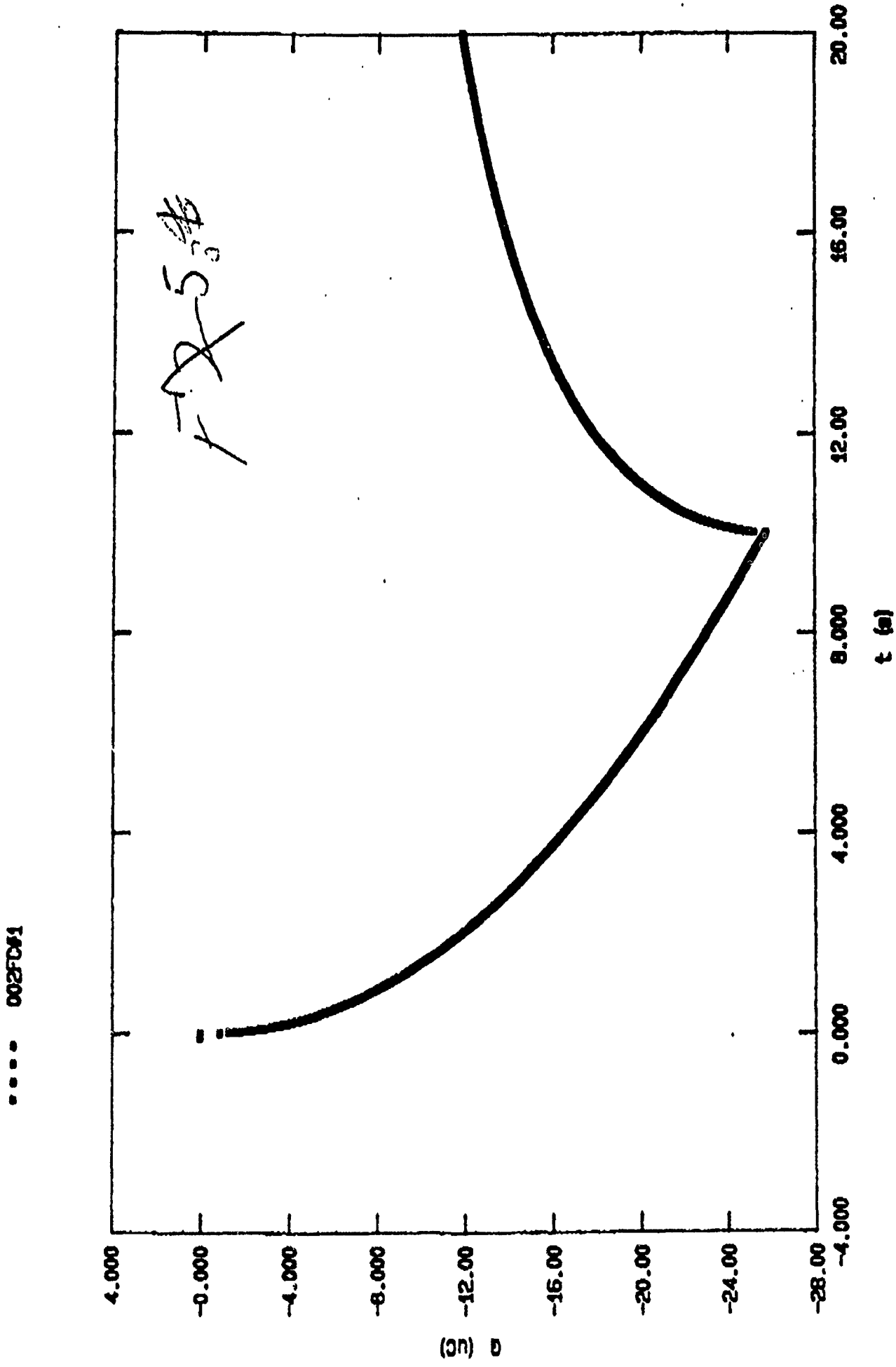
002FCM1
Q (uC)
4.000
-0.000
-4.000
-8.000
-12.00
-16.00
-20.00
-24.00
-28.00
20.00
16.00
12.00
8.000
4.000
0.000
-4.000
t (s)

II-147

PH-II

F 5

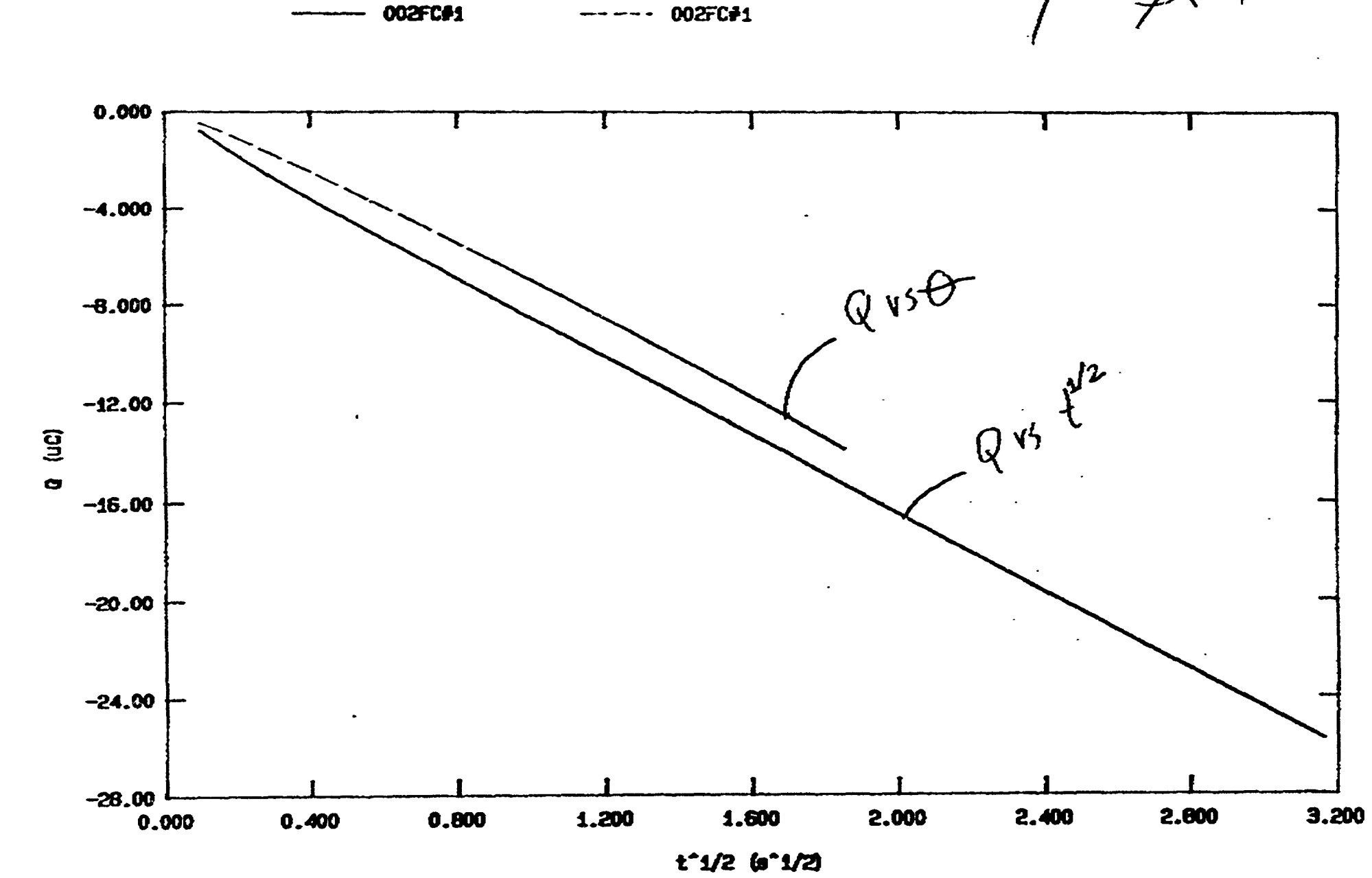
002FC#1
002FC#1
0.000
-4.000
-8.000
-12.00
-16.00
-20.00
-24.00
-28.00
Q (ml)
0.000
0.400
0.800
1.200
1.600
2.000
2.400
2.800
3.200
t^1/2 (s^1/2)
Q vs θ
Q vs t^1/2

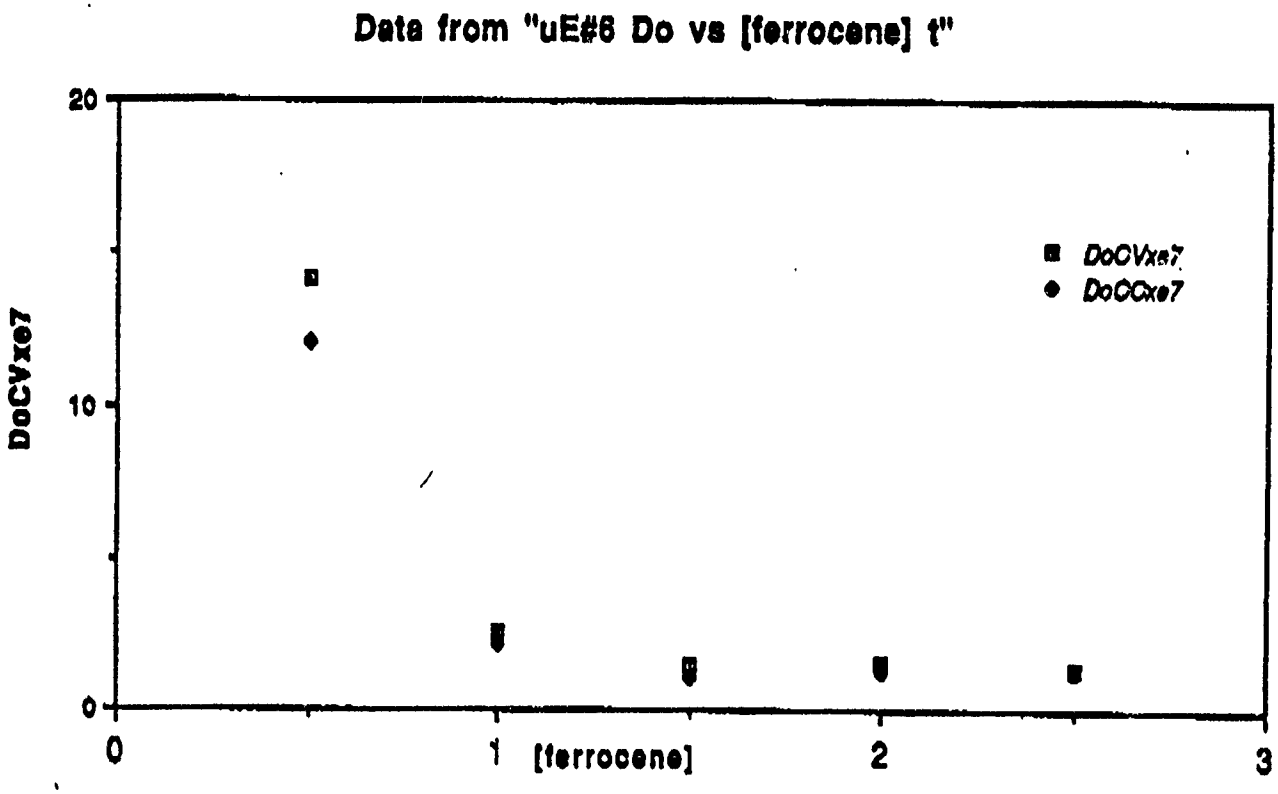
Data from "uE#6 Do vs [ferrocene] t"
20
10
0
DoCVxe7
0
1
[ferrocene]
2
3
DoCVxe7
DoCCxe7

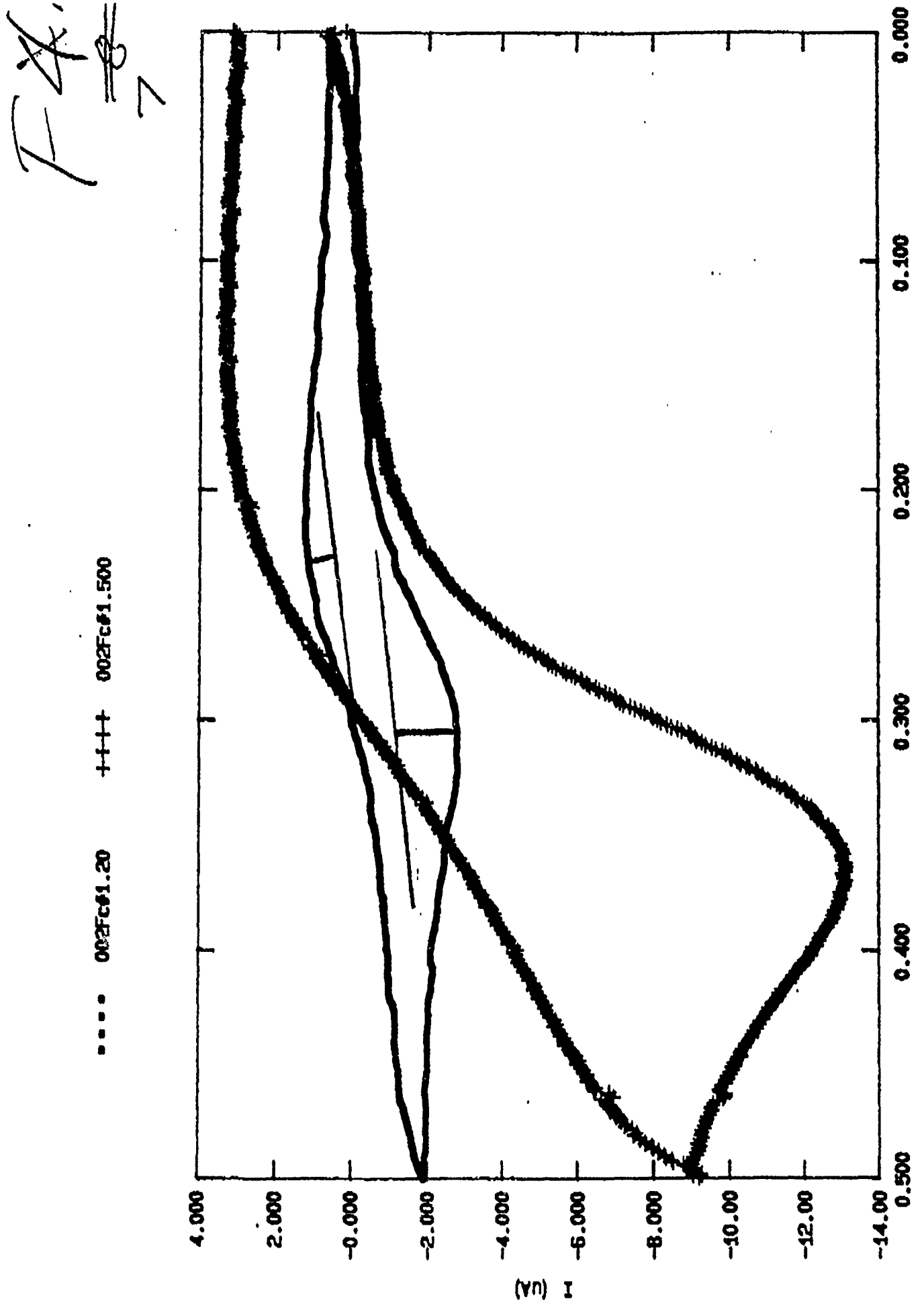
002Fc#1.20
002Fc#1.500
I (uA)
E vs. AgCl (V)
4.000
2.000
-0.000
-2.000
-4.000
-6.000
-8.000
-10.00
-12.00
-14.00
0.000
0.100
0.200
0.300
0.400
0.500

II-150

TABLE 1

Show Composition of μE's only

JUN 18 '91 13:43 3016712081 PAGE.030

JUN 18 '91 13:44

	$D_Q x 10^7$ (cm²/s)						Diameter (Å)		
μE	CV	CC	τ_o	η	$k_q(x10^6)/s$	N_D	CV	N_S	N_D
1	5.05	5.02	3.67±0.22	0.51±0.07	1.39±0.13	118±15	97.2	71.7	723
2	5.93	5.97	3.77±0.36	0.63±0.08	0.94±0.41	153±20	85.0	78.5	78.9
3	7.10 ~~7.7~~	7.13	4.89±0.21	0.72±0.12	1.25±0.31	173±22	68.8	79.4	76.0
4	3.0	4.44	3.36±0.77	0.63±0.15	1.13±0.34	194±39	161	82.6	85.7
5	3.5	4.2	4.50±0.58	1.02±0.05	0.88±0.10	246±16	142	71.2	89.5
6	1.36	1.26	3.72±0.16	1.77	0.31	452±57	363	85.9	109.1
7	—	—	4.10±0.37	1.13±0.56	0.19±0.16	277±166*	—	77.0	97.8*
8	—	—	4.06±0.65	1.11±0.55	0.21±0.18	335±130*	—	71.9	104.2*
9	—	—	0.70±0.01	1.30±0.83	1.29±0.62	489±302*	—	84.8	128.1*
10	—	—	4.30±0.19	—	—	—	—	109.5	—
11	—	—	4.75±0.20	—	—	—	—	107.5	—

*System may not have been at equilibrium

Table 2. Microemulsion aggregation numbers and aggregate diameters determined by static and dynamic luminescence quenching experiments, and by electrochemical techniques of cyclic voltammetry and chronocoulometry.

3016712081 PAGE.031

[CTAC]	N	k_{IBA} (Ms)$^{-1}$
1×10^{-3}	10	54
6×10^{-3}	98 ± 11	156
1×10^{-2}	113 ± 4	180

Table 3. Aggregation numbers for several CTAC / buffer solutions determined by the steady state luminescence quenching technique employing Probe #3. Second order rateconstants for the catalytic hydrolysis of PNDP are included.

(17) # MICELLE AND MICROEMULSION DIFFUSION COEFFICIENTS

Ethirajulu Dayalan[1] and Syed Qutubuddin
Chemical Engineering Department
Case Western Reserve University
Cleveland, OH 44106

and

John Texter[2]
Photographic Research Laboratories
Eastman Kodak Company
Rochester, NY 14650

[1]Present address: Erosion/Corrosion Research Center, The University of Tulsa, Tulsa, OK 74104.

[2]To whom correspondence should be addressed.

II-155

JUN 21 '91 15:35 918 596 1299 PAGE 002

ABSTRACT

INTRODUCTION

Micelles are dynamic aggregates of amphiphilic or surfactant molecules possessing both hydrophilic and hydrophobic character [1]. microemulsions are isotropic dispersions of two immiscible fluids, generally oil and water (with or without electrolyte), which are thermodynamically stabilized by the presence of surfactant molecules at the interface [2,3]. Micelles and microemulsions are the very interesting among various surfactant systems. Their scientific, engineering importance combined with the industrial and biomedical applications warrant a thorough understanding of these systems. Characterization by particle sizing and microstructure determination has been the subject of numerous investigations. The most common tools have been quasi-elastic light scattering (QELS) [4-9], NMR [10,11], small angle X-ray scattering [12,13], neutron scattering [14,15], fluorescence spectroscopy [16,17], and ultracentrifugation [18,19]. Recently electrochemical techniques are being used increasingly for studies in micelles, microemulsions and macroemulsions [16-25]. Determination of critical micelle concentration (CMC), particle sizing and studies on solute partitioning, microstructure, fundamental electrochemistry are some of the examples.

It is a fact that no single technique can lead to complete understanding of micelles and microemulsions. Sometimes a technique which yields very important and reliable information can even produce results under different experimental conditions which are difficult to interpret. For e.g., QELS is the most widely used technique for measuring diffusion coefficients in micelles and microemulsions. Very good results are obtained at low concentrations of surfactants and added salts. Difficulties arise at high concentrations of surfactants and in the presence of added salts due to thermodynamic and hydrodynamic interactions. Therefore

measurements from more than one technique are used for a proper understanding of these systems. Most of the techniques mentioned above require costly and sophisticated instrumentation. Electrochemical techniques are are simple and inexpensive and the results are easy to interpret.

In this article the principle of measuring diffusion coefficients in micelles and microemulsions using various electrochemical techniques will be briefly reviewed. The results of diffusion coefficient measurements using rotating disk electrode technique in various surfactant systems will be discussed. The electrochemical results will be compared with the QELS and NMR results where applicable.

In principle any electrochemical technique which allows the determination of the diffusion coefficient of an electroactive substance can be used for measuring diffusion in surfactant systems. A known concentration of an electroactive probe is dissolved in the micelle or microemulsion system. The apparent diffusion coefficient is then measured using one of the electrochemical methods. The information obtained depends on the nature of the electroactive probe. For e.g. using a probe like ferrocene which is predominantly soluble in nonaqueous phase the diffusion coefficients of micelles and that of the oil droplets (nonaqueous pseudo phase) in oil-in-water microemulsions can be determined. Water soluble and water/oil soluble probes yield CMCs and information on probe partitioning and microstructure. Different electrochemical techniques which have been in use are polarography, cyclic voltammetry (CV), rotating disk voltammetry (RDV), chronoamperometry and chronopotentiometry. The relationships which are applicable for each of these techniques are as follows:

Polarography (Illkovic equation)

$$i_d = 708\, D^{1/2}\, C\, m^{2/3}\, t^{1/6} \qquad (1)$$

Cyclicvoltammetry (Randles-Sevcik equation)

$$i_p = 2.69 \times 10^5 n^{3/2} A D^{1/2} C v^{1/2} \quad (2)$$

Rotating disk voltammetry (Levich equation)

$$i_l = 0.62 n F A D^{2/3} w^{1/2} v^{-1/6} C \quad (3)$$

Chronoamperometry (Cottrell equation)

$$i(t) = \frac{n F A D^{1/2} C}{n^{1/2} t^{1/2}} \quad (4)$$

Chronopotentiometry (Sand equation)

$$\frac{i T^{1/2}}{C} = \frac{n F A D^{1/2} n^{1/}}{2} \quad (5)$$

where

CV and RDV techniques were extensively used by the authors for measuring diffusion coefficients in micelles and mic: emulsions of different types of surfactants. The results from both the techniques are essentially same in most of the cases and as expected. But differences arise in some cases and the authors prefer the results from RDV over CV results for the following reasons. When the number of probes per micelle or microemulsion droplet is more than one CV yields an apparently increased value. This is due the increase of the value of $Cn^{3/2}$ in equation (2). In RDV the value of nC do not change due to an increase in the number of probes. The CV diffusion coefficients can also involve errors due to (i) any quasi reversibility of the electron transfer reaction in the medium at high scan rates, (ii) effects due to any small adsorption of probe/surfactant on the electrode surfactant, and (iii) the difficulties in correctly estimating the peak currents. These effects are minimum in RDV measurements.

The surfactants studied are CTAB (cetyltrimethyl ammonium bromide, cationic), SDS (sodium dodecylsulfate, anionic), DTINS (di-/triisopropyl naphthalene sulfonate, anionic), C_{18}DMB (octadecyl dimethyl betaine, zwitterionic), Triton X-100 (octyl phenoxy polyethoxy ethanol, nonionic) and Neodol 91-6 (C_9 - C_{11} linear primary alcohol ethoxylate, nonionic). The probes used are ferrocene (oil soluble), methylviologen dichloride trihydrate (MV^{2+}) (water soluble), potassium ferrocyanide (water soluble) and substituted paraphenylene diamines (PPDs) (water and oil soluble).

MATERIALS AND METHODS

CTAB, SDS and MV^{2+} were obtained from Sigma. Triton X-100 and Neodol 91-6 were free samples from Rohm and Haas Co., and Shell Chemical Co., respectively. DTINS and PPDs were provided by Kodak Research Laboratories. C_{18}DMB was prepared by reacting octadecyl dimethylamine with sodium chloroacetate. The alcohols (1-pentanol and 1-butanol) and ferrocene were from Aldrich, the oils (octane and dodecane) were from Humphrey. NaCl, NaBr and K_2CO_3 were certified ACS reagents from Fisher. $KHCO_3$ was a guaranteed reagent from Fluka AG. $K_4[Fe(CN)_6]$ was ACS reagent from Mallinckrodt, Inc. The chemicals were used as received. All the solutions were prepared in triple-distilled water.

Electrochemical experiments were performed by using an electrochemical analyzer (BAS model 100). A Pine Instrument Co. rotating assembly was used for rotating the electrode. A digital plotter (Bausch and Lomb DMP-40 series) was used for recording the voltammograms. A three electrode arrangement in a conventional three compartment cell was used. A glassy carbon working electrode, a platinum foil counter electrode and a SCE reference electrode were used. All the solutions were deoxygenated by bubbling nitrogen or argon. The temperature was maintained at 25°C or 40°C and to within ± 1°C. Viscosity measurements were made with Brookfield Digital Viscometer and Ubbelohde viscometers.

QELS experiments were performed by using the apparatus described in ref. 7. An argon ion laser (Lexel 95-4) equipped with an etalon provided the incident radiation. Measurements were made at 90^{o} scattering angle.

RESULTS

Micelles:

The diffusion coefficients of CTAB, SDS and DTINS micelles were measured in 0.1 M NaCl solution, pH adjusted to 10 with NaOH. The apparent diffusion coefficient values determined using ferrocene probe were corrected to account for the ferrocene present in the aqueous phase. The solubility of ferrocene in the micellar solutions at these surfactant concentrations is very low. The concentration of ferrocene used in this investigation was very close to the saturation concentration. Under these conditions ferrocene is also present in the aqueous phase to the extent of its solubility in 0.1 M NaCl ~ mM/liter). The diffusion coefficient of ferrocene in 0.1 M NaCl is 6.7×10^{-6} cm^2 sec^{-1} which is an order of magnitude higher than the micelles. So, the limiting current measured in micellar solutions using RDV has significant contribution due to the ferrocene present in aqueous part. The corrections were made using the relationship developed for partitioning solutes (ref , equation). The measured and the corrected diffusion coefficient values for CTAB and SDS micelles are shown in Table I. The corrected values are in agreement with the values reported in by Georges and Desmettre for similar systems. The diffusion coefficients measured by QELS in the present investigation and from literature in similar systems are also shown in the table. The diffusion coefficient values of CTAB micelles show a slight increase as the concentration is increased from 10 mM to 50 mM showing the increase in micelle size. The QELS values (from our measurement as well as from literature) also show the same trend.

The measured and corrected diffusion coefficient values for DTINS at various concentrations are shown in Table II along with the QELS values. The corrections are very considerable at low concentrations of surfactant as expected. As the surfactant concentration is increased the fraction of ferrocene in the micelles is very high compared to aqueous phase concentration and the correction also becomes less. The corrected diffusion coefficient values show that the size of the micelles does not increase as the concentration of DTINS is increased. The corrected electrochemical values and QELS values are compared in figure 1. The QELS values are higher compared to electrochemical values. The concentrations of DTINS used in this study are well above CMC and the diffusions are affected by interactions between micelles.

The results of diffusion measurements in nonionic surfactants are shown in Table III. The concentrations of the surfactants used here are very high and so the ferrocene is present mostly in the micelles. The corrections made in the CTAB, SDS and TINS micelles were not required here. The diffusion coefficients in Neodol 91-6 micelles in 0.1 M NaCl solution decreases with increasing concentration of surfactant. This shows that the micelle size increases with concentration in this system. The results of Triton X-100 system also shows the same trend. Table III also shows the diffusion coefficients measured with the water and oil soluble probe PPD. These values do not directly represent the diffusion coefficient values of the micelles. The decrease in the diffusion coefficient values with increasing surfactant concentration indicate the micelle size increase as well as the presence of increased amount of probe in the micelles.

Microemulsions:

The diffusion coefficients were measured in microemulsions of the anionic surfactant, SDS. The oil phase is toluene and the cosurfactant is n-butanol with NaCl as the electrolyte. The measurements were made as a function of added salt concentration. The microemulsion changes from lower phase to middle and then to upper phase as the salt concentration is increased.

Diffusion coefficients were measured with ferrocene probe in the lower phase as well as middle phase microemulsions. Potassium ferrocyanide was used as the water soluble probe for measurements in the middle phase.

Comparison with NMR values.

SDS micelles and microemulsion values using ferrocene and QELS (Table IV).

References:

1. Fendler, J.H.; Fendler, E.J. "Catalysis in Micellar and Macromolecular Systems"; Academic Press: New York, 1975.
2. Healy, R.N.; Reed, R.L. Soc. Pet. Eng. J. 1977,17,129.
3. Miller, C.A.; Qutubuddin. S. In "Interfacial Phenomena in Apolar Media"; Eicke, H.F.; Parfitt, G.D. Eds; Marcel Dekker: 1987; pp. 177-185.
4. Vrij, A., Nieuwenhuis, N.M., Fignaut, and Agerof, W.G.H., Faraday Discuss. Chem. Soc. 65, 101 (1978).
5. Cazabat, A.M., Langevin, D.F., and Poudhelon, A., J. Colloid Interface Sci. 73, 324 (1980)
6. Dorshow, R.B., and Nicoli, D.F., in "Measurement of Suspended Particles by Quasi-elastic Light Scattering"; B.E. Dahneke, Ed., Wiley, New York, 1983.
7. Cheung, H.M.,
8. Gulari, E., Bedwell, B., and Alkhafaji, S., J. Colloid. Interface Sci. 77, 202 (1980).
9. Cazabat, A.M., Chatency, D., Langevin, D., and Meuiner, J., in "Surfactants in Solution," Vol. 1. Plenum, New York, 1982.
10. (a) Lindman, B., Kamenka, N., Puyal, M., Bru, B., amnd Jonsson, B., J. Phys. Chem. 88, 53 (1984); (b) Lindman, B., Puyal, M., Kamenka, N., Rymden, R., and Stilbs, P., J. Phys. Chem. 88, 5048 (1984).
11. Nilson, P., and Lindman, B., J. Phys. Chem. 86,271 (1982).
12.

Table I. Diffusion coefficients of CTAB and SDS micelles.

Surfactant	Conc.	Diffusion coefficient ($Dx10^7$ cm^2 sec^{-1})				
		Electrochemical			Light scattering	
	mM	Meas.	Corr.	Lit.	Present	Lit.
CTAB	50	8.1	6.6	7.9/55mM	-	-
	20	11.2	6.7		7.4	7.0
	10	15.4	7.1		9.7	10
SDS	50	9.9	7.3	7.3/69mM	-	12

II-164

918 596 1299 PAGE 011

Table II. Diffusion coefficients of DTINS micelles.

Conc.	Diffusion Coefficient ($Dx10^7$ cm^2 sec^{-1})		
	Electrochemical		Light scattering
mM	Measured	Corrected	
200	8.7	8.0	16.2
150	9.0	8.1	15.9
100	-	-	14.9
80	9.7	7.9	14.3
50	10.4	7.9	12.6
30	13.3	8.1	-

111

Table IV. Diffusion coefficients of nonionic systems.

System	Diffusion Coefficient ($Dx10^7$ cm^2sec^{-1}) Ferrocene probe	PPD2 probe
Neodol 91-6 micelles (in 0.1 M NaCl, 25°C)		
1%	5.9	-
2%	6.7	-
4%	4.4	-
6%	3.3	-
8%	3.1	-
10%	3.0	-
Triton X-100 micelles (in pH 10 buffer, 40°C)		
4%	1.5	9.2
6%	1.3	7.2
8%	0.92	6.1
10%	0.91	5.4
Triton X-100 microemulsions (8% Triton X-100, pH 10buffer, dodecane, 40°C)		
0.5% dodecane	1.6	6.2
1.0% dodecane	2.6	6.7
1.5% dodecane	2.4	6.4

11

II-166

IV

Table ~~III~~. Diffusion coefficients of SDS systems.

System	Diffusion Coefficient ($Dx10^7$ cm^2sec^{-1}) Electrochemical	Light scattering
Micelles (70 mM SDS + 100 mM NaBr)	14.1	9.6
Mixed micelles (70 mM SDS + 100 mM NaBr + 3% 1-pentanol)	10.4	7.8
Microemulsion -1 (190 mM SDS + 100 mM NaBr + 10.3% 1-pentanol + 5.1% dodecane)	4.6	7.2
Microemulsion -2 (70 mM SDS + 100 mM NaBr + 5.5% 1-pentanol + 2.0% dodecane)	4.1	2.0

FIG. 1

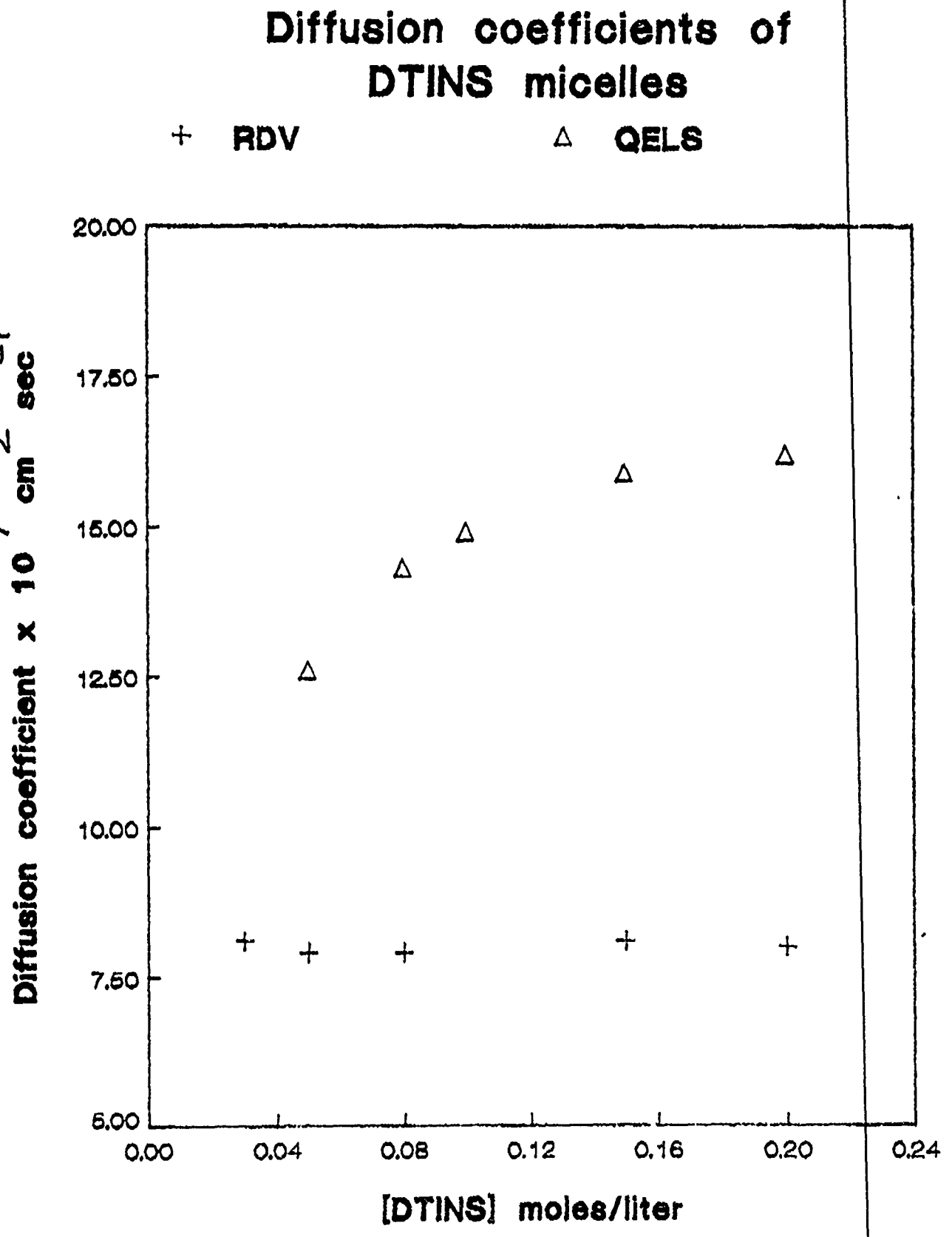
Diffusion coefficients of DTINS micelles
+ RDV
Δ QELS
Diffusion coefficient x 10^7 cm^2 sec^-1
20.00
17.50
15.00
12.50
10.00
7.50
5.00
0.00
0.04
0.08
0.12
0.16
0.20
0.24
[DTINS] moles/liter

SDS microemulsion
Comparison of diff. coeff. data

△ RDV ○ NMR-Clarkson ▲ NMR-Lindman

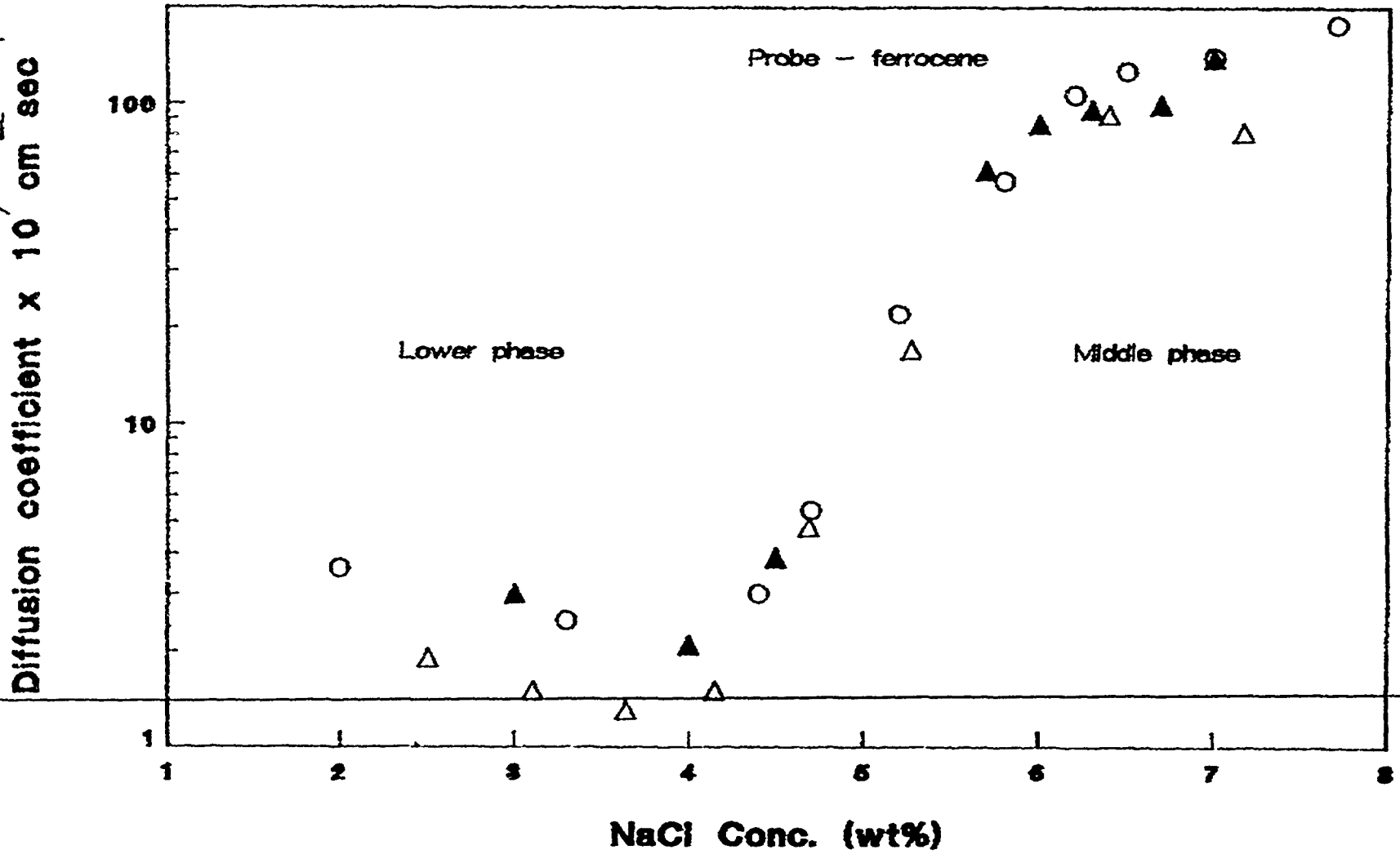

(91)

611-II

Fig. 2

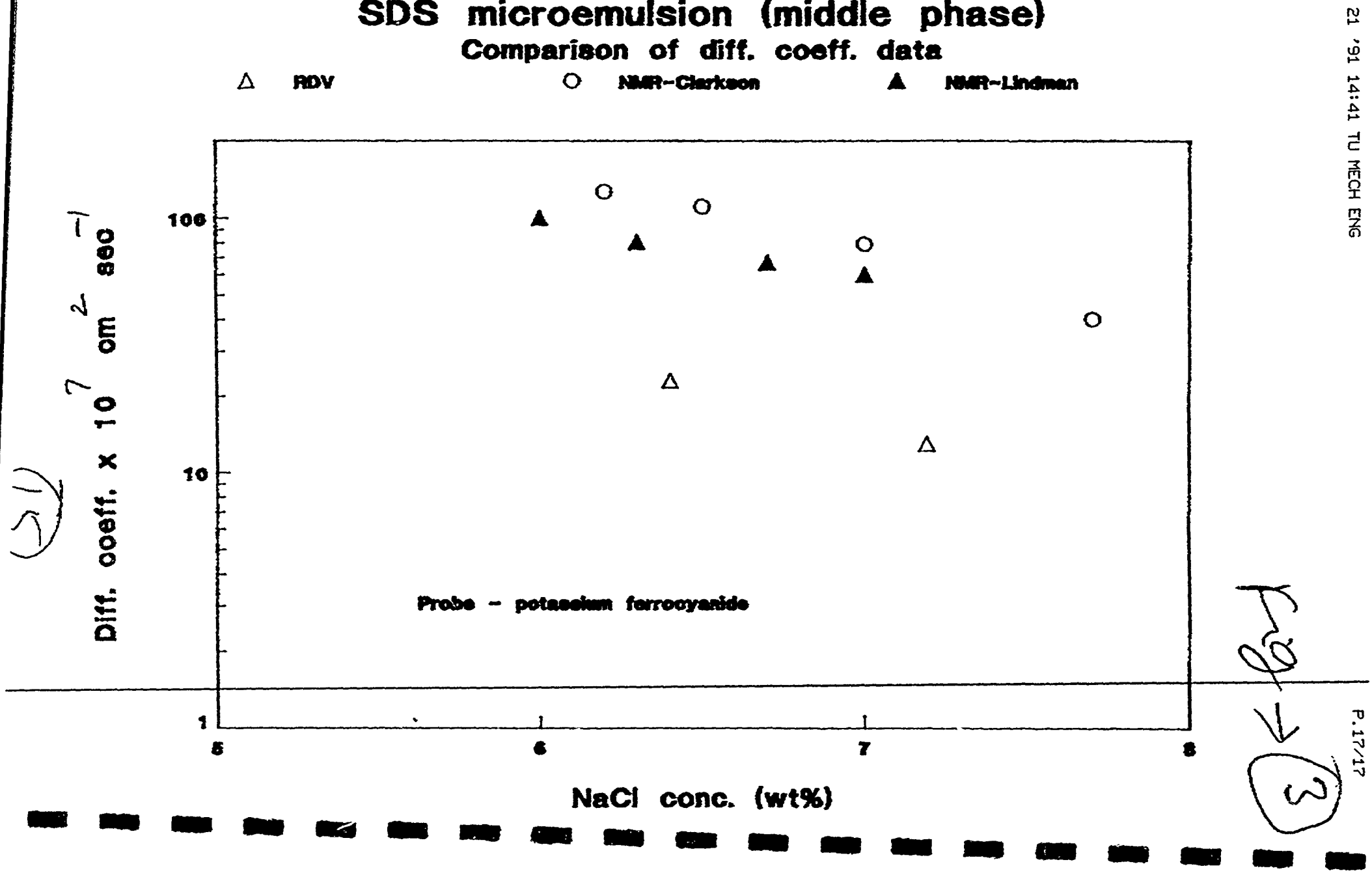
SDS microemulsion (middle phase)
Comparison of diff. coeff. data
RDV
NMR-Clarkson
NMR-Lindman
Diff. coeff. x 10^7 cm^2 sec^-1
100
10
1
Probe - potassium ferrocyanide
5
6
7
8
NaCl conc. (wt%)

(18) The mechanism of particulate enhanced mass transport in shearing fluids

David Roha
ALCOA Technical Center
Alcoa Center, PA 15069

It is well known that inert particles suspended in flowing fluids tend to increase the rate of mass transport from the bulk fluid to solid walls in contact with the fluid. However, the hydrodynamic and convective mechanisms through which this enhancement takes place is not agreed upon. In addition some workers have observed a maximum effect at some optimum particle diameter while others have not. The particle size effect can be explained by a boundary layer which clings to the surface of the particle and is scaled to its diameter. The velocity shear of the bulk fluid induces the particle and its boundary layer to rotate. In a bulk concentration gradient a region in the boundary layer is alternately exposed to layers of high and low concentration. Transient diffusion between the particle boundary layer and the surrounding bulk fluid is responsible for the enhancement of mass transfer.

The Particle film model

The particle film model is illustrated in Fig. 1 and Fig. 2 below. A velocity gradient γ exists in the bulk solution which causes the particle to rotate at $\gamma/2$ radians/s. Next to the particle a liquid film of thickness Δ is postulated, which clings to the particle surface and rotates with it.

There are two sub-cases of this model: the solid boundary model and the continuum model. In the solid boundary model (Fig. 1) first put forward by Roha [1], the particle film serves to transfer mass between a solid boundary and the solution. As the film rotates with its particle, it absorbs mass through diffusion from the surrounding solution. As the film comes in contact with the boundary mass is transferred to it by diffusion out of the particle film.

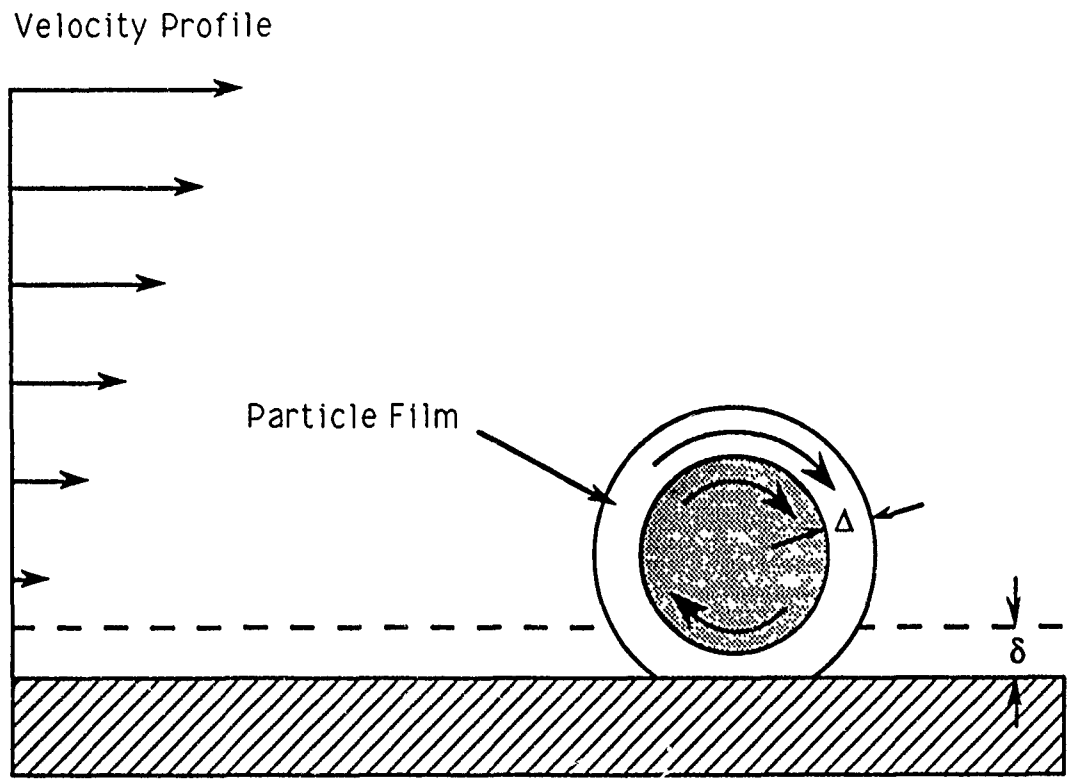

Solid Boundary Particle Film Model

Fig. 1

The second variant of the model is the continuum model as analyzed by P.J. Sonneveld, W. Visscher and E. Barendrecht [2]. No solid boundary exists outside of the particle. The particle rotates inside a macroscopic concentration gradient. Mass is transferred into and out of the particle film by diffusion. Thus material is transfer from regions of high concentration to regions of low concentration through the microconvection of the particle.

Concentration Profile: Velocity Profile

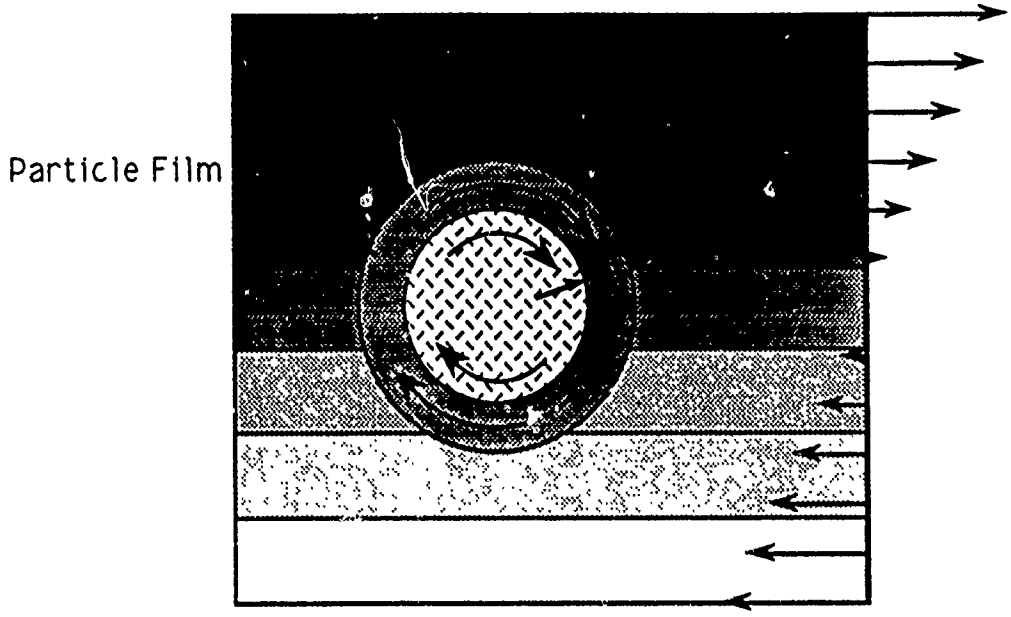

Continuum
Particle Film Model

Fig. 2

Both variants are similar in their basic assumptions. The solid boundary model is more appropriate when the particle diameter is equal to or greater than the boundary layer thickness A sphere rolling over a plane is more hydrodynamically complex. Both the particle film and the diffusion layer of the solid boundary are squeez' 'ogether in some unknown fashion. However it is at this point o' constriction that the greatest mass transport takes place.

The continuum model is most applicable when the particles are much smaller than the boundary layer thickness. The boundary layer can then be modeled as a continuum of inter-dispersed particles. Sonneveld et. al utilized an analytical solution from Batchelor [3,4] for creeping flow around a sphere in a shearing fluid. The velocity is expressed as the sum of a disturbance velocity u and the overall shear velocity v. The disturbance velocity is given by:

$$\mathbf{u} = -(\omega_0 \times \mathbf{r})\left(\frac{a}{r}\right)^5 \cos\psi \qquad \text{[Eq. 1]}$$

where a is the particle radius, r the radial distance to a point in the fluid, ψ the angle to the point from the plane of symmetry and ω_0 the angular velocity of the particle. The magnitude of the angular velocity is

$$|\omega_0| = \frac{\gamma}{2} \qquad \text{[Eq. 2]}$$

where γ is the local shear rate of the fluid. Roha's earlier assumption that $\omega_0 = \gamma$ is erroneous.

Sonneveld et. al. also prove that when a particle enters the boundary layer it approaches it's steady-state rotational velocity, ω_0, with a time constant τ:

$$\tau = \frac{\rho a^2}{120\mu} \qquad \text{[Eq. 3]}$$

where ρ is the particle density and μ is the fluid dynamic viscosity. For a typical particle of radius less than 20 μm, the tie constant is less than 10μs. Therefore the assumption of steady-state hydrodynamics is essentially valid.

However, in their mass transport model Sonneveld et. al. make the assumption that the solution of the particle film is well mixed. It therefore becomes a region of constant concentration and consequently reduces the thickness of the boundary layer.

This appears to be only true in the asymptotic sense. Finite element advection-diffusion simulations of a 1 μm radius sphere, freely rotating in a shear field were performed. The diffusivity was 7.2 x10^{-6} cm^2/s and the dynamic viscosity 0.01 cm^2/s. The concentration profiles obtained are shown in Fig. 6 through Fig. 11. It can be seen that a well mixed condition is just beginning to be achieved at a shear rate of 10^6 s^{-1}. However, the highest shear rates achieved by Sonneveld et. al. at the outer edge of their disks is at most 53,000 s^{-1}. It appears then that the particle film is

really a very dynamic region, with its concentration profile changing considerably as it rotates between regions.

A Dynamic Particle Film Model

Roha developed a particle film model which accounted for dynamic concentration changes in the particle film in a simplistic fashion. It was originally developed for a solid boundary model, but its basic concepts could easily be applied to a continuum model.

As shown in Fig. 1 above the particle film is assumed to rotate with the particle uniformly with an angular velocity of Ω. As the film turns around to the surface, mass diffuses out of the film to the surface. This transfer continues until the film finally pulls away form the surface and mass transfer stops.

This momentary transfer of mass is treated as a one-dimensional transient diffusion problem governed by Fick's second law:

$$\frac{\partial C}{\partial t} = D\frac{\partial^2 C}{\partial y^2} \qquad \text{[Eq. 4]}$$

and subject to the boundary conditions:

$$C = 0 \qquad y = 0 \qquad \text{[Eq. 5]}$$

$$\frac{\partial C}{\partial y} = 0 \qquad y = y_o \qquad \text{[Eq. 6]}$$

The distance, y, is zero at the solid boundary and y_0 at the surface of the particle. The diffusivity of the transported species is represented by D. Some initial concentration profile C_0 exists in the film before it contacts the solid boundary. Elapsed time, t, is measured from the moment of contact. The general solution of this problem is well known and is given by

$$C = b_1 e^{-\alpha t}\sin\left(\frac{\pi y}{2y_o}\right) + b_2 e^{-9\alpha t}\sin\left(\frac{3\pi y}{2y_o}\right) + b_3 e^{-25\alpha t}\sin\left(\frac{5\pi y}{2y_o}\right) + \ldots \qquad \text{[Eq. 7]}$$

where

$$\alpha \equiv \frac{\pi^2 D}{4y_o^2} \qquad \text{[Eq. 8]}$$

and b_n are the Fourier coefficients used to describe the concentration profile at t=0.

Roha arbitrarily choose the first four terms of this series to express the concentration profile as

$$C = \frac{C_0}{(1-C_2+C_3-C_4)}\left[e^{-\alpha t}\sin\left(\frac{\pi y}{2y_0}\right) + C_2 e^{-9\alpha t}\sin\left(\frac{3\pi y}{2y_0}\right) + C_3 e^{-25\alpha t}\sin\left(\frac{5\pi y}{2y_0}\right) + C_4 e^{-49\alpha t}\sin\left(\frac{7\pi y}{2y_0}\right)\right]$$

[Eq. 9]

Here C_0 is the initial concentration at the particle surface and the coefficients C_2, C_3, and C_4 are treated as adjustable parameters to be determined by regression with experimental data.

The amount of species contained in the gap between the particle and the solid boundary, M(t), expressed as moles per unit area is

$$M(t) = \int_0^{y_0} C\,dy$$

[Eq. 10]

$$M(t) = \frac{C_0}{(1-C_2+C_3-C_4)}\left(\frac{2y_0}{\pi}\right)\left[e^{-\alpha t} + \frac{C_2}{3}e^{-9\alpha t} + \frac{C_3}{5}e^{-25\alpha t} + \frac{C_4}{7}e^{-49\alpha t}\right]$$

[Eq. 11]

The amount of material transferred to the surface is equal to the amount lost from the particle film or M(0)-M(t)

$$M(0) - M(t) = \frac{C_0}{(1-C_2+C_3-C_4)}\left(\frac{2y_0}{\pi}\right)\left[(1-e^{-\alpha t}) + \frac{C_2}{3}(1-e^{-9\alpha t}) + \frac{C_3}{5}(1-e^{-25\alpha t}) + \frac{C_4}{7}(1-e^{-49\alpha t})\right]$$

[Eq. 12]

A model based solely on Eq. 12 was previously run by Roha [1]. Although it showed a maximum in the limiting current as a function of particle size very similar in shape to the experimental data, the peak of the experimental data was much broader.

One need not use much imagination to think of phenomena which might broaden and smear out the peak. Although only one separation distance, y_0, and only one contact time, t, are assumed in Eq. 12, there is in fact a distribution of these variables. A point on the planar surface, depending on its location in relation to a particle drifting by, will either experience a short interaction at long y_0 or a long interaction with y_0 changing from long to short to long again. There is a distribution of particle distances from the wall. There is reason to believe the particles are not uniformly dispersed but are less numerous close to the wall. The distribution of particle sizes must be taken into account. There may be a significant distribution of particle velocities about some mean at any given point on the cathode. However, the radial distribution of mean particle velocity is taken into account by this model.

In many instances the distribution functions needed to solve the real problem are not known. If they were known then one would be presented with a very tedious mathematical integration problem which most likely could not be solved analytically. Roha finessed this problem by introducing two variants of this model the multi-level variant and the Peclet dependent y_0 variant. Both models involve additional parameters which are adjusted to fit the experimental data.

Multi-Level Variant

To account for the distribution in separation distance, y_0, three discrete separation distances are used, y_0, $y_0/9$, and $y_0/81$. Eq. 12 then becomes:

$$M(0) - M(t) = \frac{C_0}{(1-C_2+C_3-C_4)}\left(\frac{2y_0}{\pi a_T}\right)\sum_0^2 \frac{a_m}{9^m}$$
$$\left[\left(1-e^{-81^m\beta}\right) + \frac{C_2}{3}\left(1-e^{-81^m 9\beta}\right) + \frac{C_3}{5}\left(1-e^{-81^m 25\beta}\right) + \frac{C_4}{7}\left(1-e^{-81^m 49\beta}\right)\right] \qquad \text{[Eq. 13]}$$

where β is αt

$$\beta \equiv \frac{\pi^2 Dt}{4y_0^2} \qquad \text{[Eq. 14]}$$

a_m is the surface area of the mth level and a_T is the total area

$$a_T = a_0 + a_1 + a_2 \qquad \text{[Eq. 15]}$$

The transient component of the limiting current, i_{LT}, caused by the particles is

$$i_{LT} = nFN_p wV[M(0) - M(t)] \qquad \text{[Eq. 16]}$$

where N_p is the number of particles per unit area within Δ of the electrode, w, the width of the particle's interaction with the surface and V is the speed of the particle relative to the surface. The interaction time, t, was set equal to w/V, under the assumption that the particle is as long as it is wide. The height of the highest level y_0, was set equal to the height of the center of the mean interacting particle.

$$y_0 = a + \frac{\Delta}{2} \qquad \text{[Eq. 17]}$$

The initial concentration at the surface of the particle, C_0, was assumed to be the average concentration across the diameter of all spheres interacting with the solid boundary. The thickness of the particle film, Δ, was postulated to be proportional to the particle radius.

$$\Delta = c_1 a \qquad \text{[Eq. 18]}$$

The steady state component of the limiting current density, i_{LS}, is the Levich limiting current density taking into account the increase in bulk viscosity and decrease in diffusivity and bulk concentration, multiplied by the fraction of the surface not interacting with particle films.

$$i_{LS} = (1-N_p a_T)\, 0.620\, nFD^{2/3}\Omega^{1/2}v^{-1/6}C_1 \qquad \text{[Eq. 19]}$$

where D is the bulk effective diffusivity of the species, C_B is the its bulk concentration, Ω is the rotation rate of the disk and v is the effective kinematic viscosity.

The overall limiting current density is given as the sum of the transient and steady state components.

$$i_L = i_{LS} + i_{LT} \qquad \text{[Eq. 20]}$$

Peclet dependent y_0 variant

This variant is much more arbitrary but also simpler. We take our cue from the observation that under a given set of conditions, one separation distance y_0 seems to dominate micro-convective transport. An attempt is made to describe this dominate separation distance, denoted y_L, by

$$\left(\frac{y_L}{a}\right) = k_2 = k_{2,0}\left(\frac{aV}{D}\right)^b \qquad \text{[Eq. 21]}$$

where $k_{2,0}$ and b are to be determined empirically. The dimensionless group (aV/D) is a Peclet number for the particle which indicates the extent of discharge of the particle film. When the Peclet number is large only a small fraction of the mass available in the film has been transferred and the predominant level distance is very small. When the Peclet number is small most of the film's solute has reacted with the surface and y_L is large.

The concentration profile is assumed to be a simple 1/4 wave sine function. In this case Eq. 12 reduces to

$$M(0) - M(t) = C_0\left(\frac{2y_0}{\pi}\right)(1 - e^{-\alpha t}) \qquad \text{[Eq. 22]}$$

In this variant, y_0 is a measure of the amount of solution in the gap available for transfer and is assumed equal to Δ. As before Δ is assumed to be proportional to the particle thickness.

$$y_0 = \Delta = C_1 a \qquad \text{[Eq. 23]}$$

Eq. 16 becomes

$$i_{LT} = nFN_p wVC_0\left(\frac{2y_0}{\pi}\right)\left[1 - \exp\left(-\frac{\pi^2 D}{4y_0^2}\left(\frac{w}{V}\right)\right)\right] \qquad \text{[Eq. 24]}$$

Except for the above changes, the limiting current density was calculated as in the multi-level variant. From a nonlinear regression with experimental data the unknown parameters were found to be

$C_1 = 1.183$
$k_{2,0} = 2.478$
$b = -0.1829$

If one wishes one can cast Eq. 24 in dimensionless form. In this instance the Sherwood and Peclet numbers are defined

$$Sh = \left(\frac{i_{LT}\, a}{nFDC_0}\right) \qquad \text{[Eq. 25]}$$

$$Pe = \left(\frac{aV}{D}\right) \qquad \text{[Eq. 26]}$$

The width of the particle interaction, w, was judged to be proportional to its radius by

$$w = k_w a = \left[\pi\left(C_1 - \tfrac{2}{3}C_1^2\right)\right]^{\frac{1}{2}} a \qquad \text{[Eq. 27]}$$

The number of particles on the surface, N_p, is given by

$$N_p = \frac{3\phi_s C_1}{4\pi a^2} \qquad \text{[Eq. 28]}$$

where ϕ_s is the volume fraction of particles actually in contact with the surface. Eq. 24 then becomes

$$Sh = \left(\frac{3k_w C_1^2}{2\pi^2}\right)\phi_s Pe\left[1 - \exp\left(-\frac{\frac{\pi^2 k_w}{(2k_{2,0})^2}}{Pe^{1+2b}}\right)\right] \qquad \text{[Eq. 29]}$$

for the best fit parameters it becomes

$$Sh = 0.1885\ \phi_s Pe\left[1 - \exp\left(-\frac{0.3561}{Pe^{0.6342}}\right)\right] \qquad \text{[Eq. 30]}$$

Finite Element Analysis

Hydrodynamics

To help resolve some of the uncertainties concerning the hydrodynamics and convection around a spherical particle in a shear field, some finite element simulations were performed. The FIDAP computational fluid dynamics program from Fluid Dynamics International was used. The domain of the simulation is shown in Fig. 3. Since the problem is symmetrical, only half of the sphere is used. The sphere rotates about an axis parallel to the z-axis. Along the boundaries fluid is constrained to flow in the x-direction only.

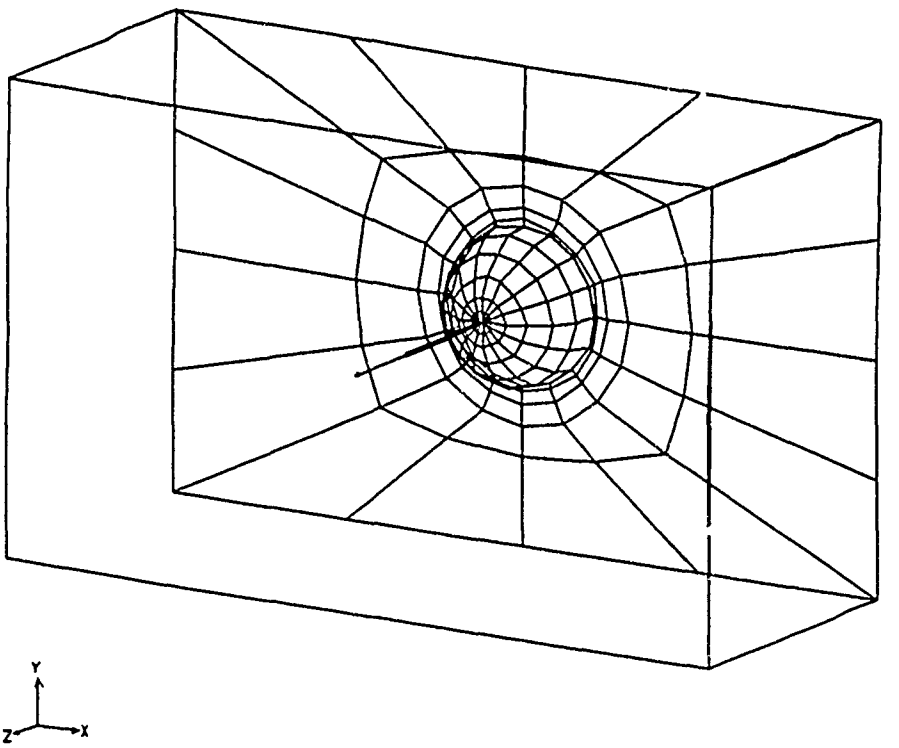

Fig. 3

The shear rate,

$$\gamma = \frac{\partial U_x}{\partial y} \qquad \text{[Eq. 31]}$$

is constant. Stokes or creeping flow is assumed. If the particle has a radius of 1 μm, then the domain is 6 μm tall (y-direction), 10 μm long (x-direction) and 4 μm deep(z-direction). When the particle size was increased, the domain was expanded proportionately. The bottom xz plane has an x velocity of -3γ and the top xz plane 3γ. The hemisphere rotates about its axis at $\omega = \gamma/2$. Although the entire 3-D domain was meshed with 3-D hexahedral elements, for clarity only the surface mesh on the hemisphere and plane of symmetry is shown.

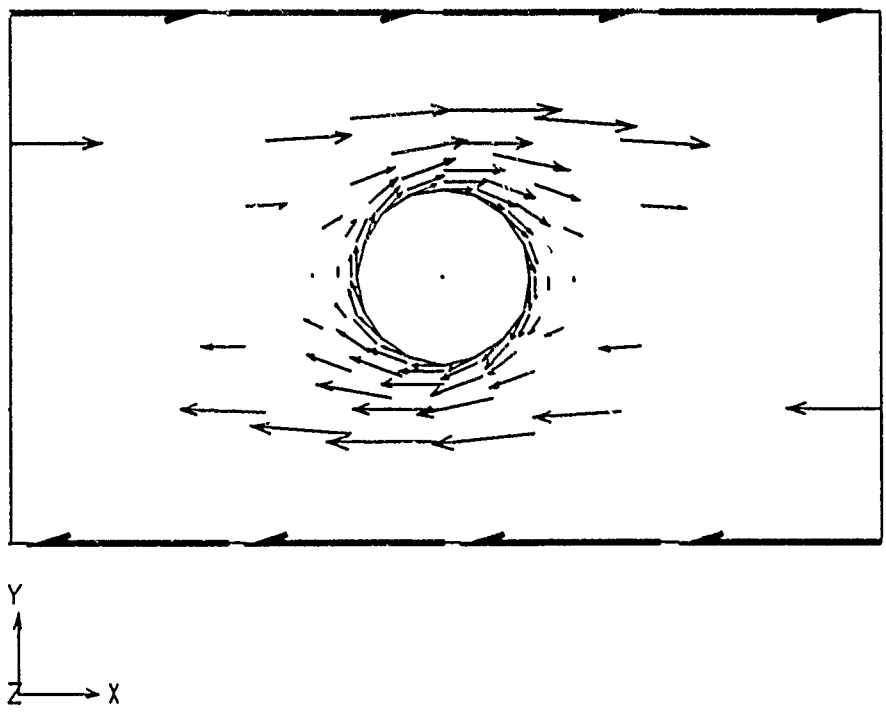

[Fig. 4]

A velocity vector plot is shown in Fig. 4 for the plane of symmetry. It is not apparent from Fig. 4 what the extent of recirculating fluid is around the particle. To better visualize the shape of the recirculation zone, we simulate the release of six particles, evenly spaced along a line from 1.04

to 1.26 radii, and track their paths over time, Fig. 5.

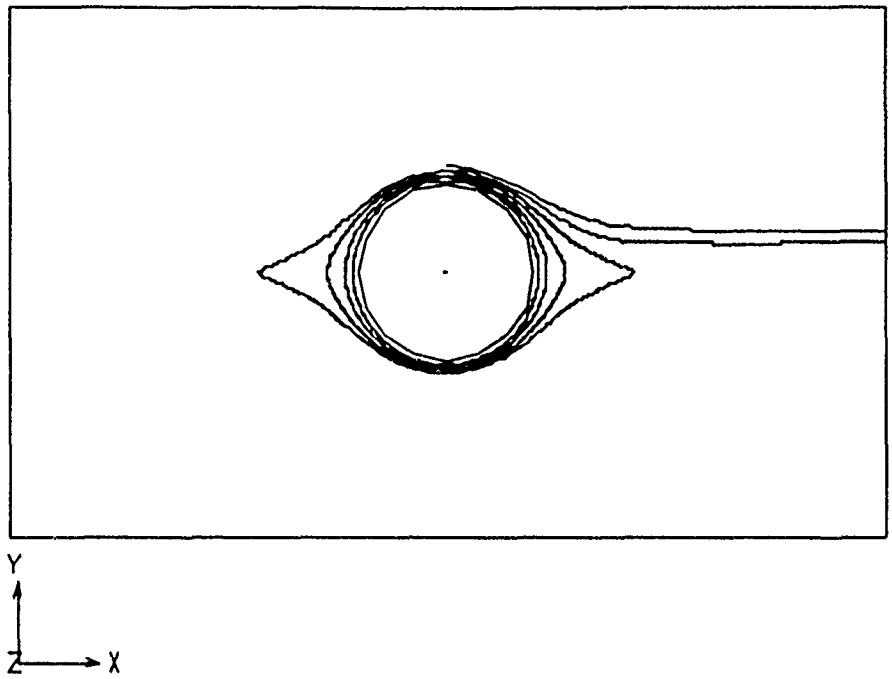

[Fig. 5]

The recirculation zone appears as a "lens" or an "eye" shaped region. The fluid layers close to the particle move with it at more or less constant velocity coupled to the particle's rotation. The outside layers move very rapidly above and below (y-direction) the particle. However, in the lobes to the right and left the fluid velocity is extremely slow.

The circular particle film postulated by Roha [1] is only approximately correct. The velocity profile calculated by Batchelor [3],[4] is confirmed.

Concentration Profiles

A linear concentration profile was imposed in the y-direction along the boundaries of the domain. The xz plane on the bottom of the domain was set to a concentration of zero. The xz plane on top of the domain was set to a constant concentration consistent with the imposed concentration gradient. The four other boundary planes had a constant concentration gradient:

$$\frac{\partial C}{\partial y} = 1 \qquad \text{[Eq. 32]}$$

The steady-state advective-diffusion equation

$$D\nabla^2 C - \mathbf{V} \cdot \nabla C = 0 \qquad \text{[Eq. 33]}$$

was solved together with the Navier-Stokes equation for the sphere in the velocity gradient. The diffusivity was arbitrarily set to 7.2×10^{-6} cm^2/s. In this analysis the Peclet Number is defined.

$$Pe = \frac{a^2\gamma}{D} \qquad \text{[Eq. 34]}$$

The concentration profiles on the plane of symmetry for various Peclet numbers are shown in Fig. 6 through Fig. 11.

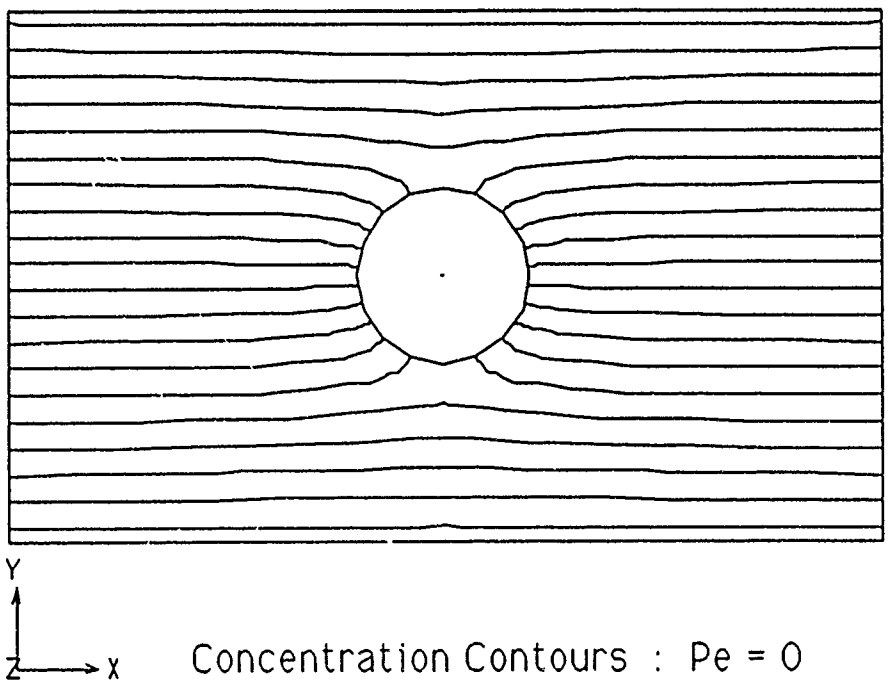

Concentration Contours : Pe = 0

[Fig. 6]

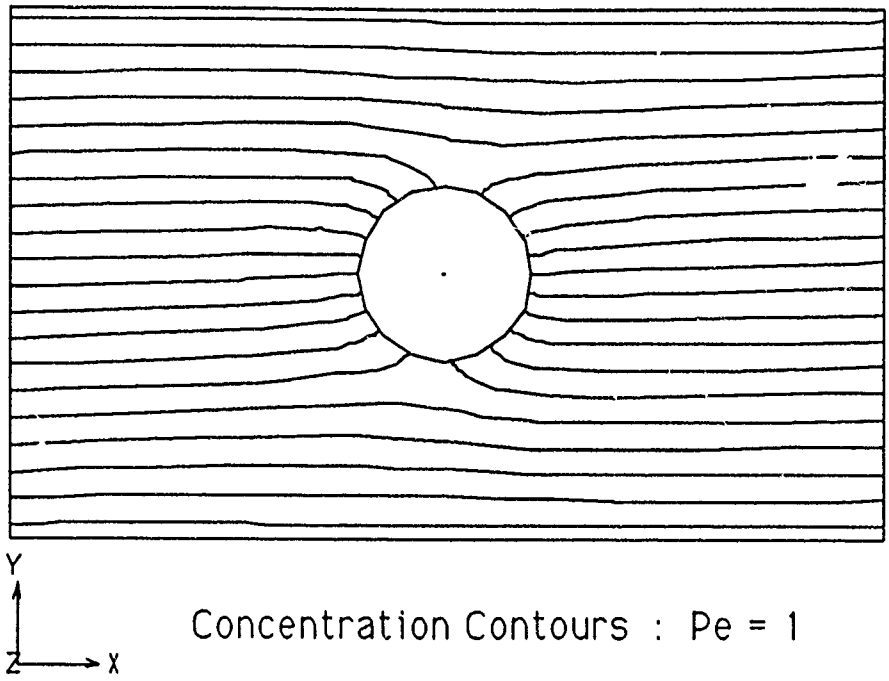

Concentration Contours : Pe = 1

[Fig. 7]

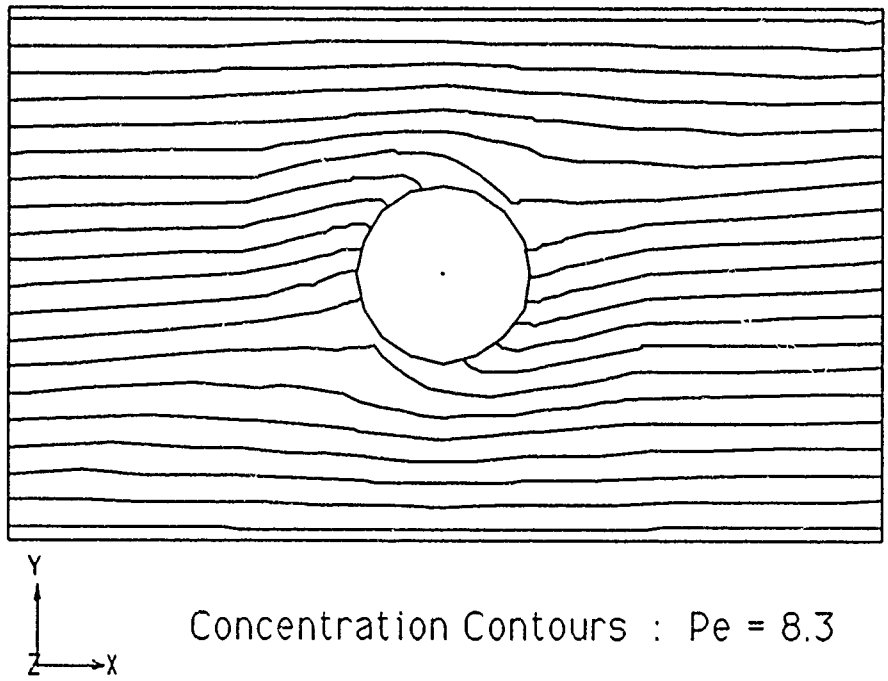

Concentration Contours : Pe = 8.3

[Fig. 8]

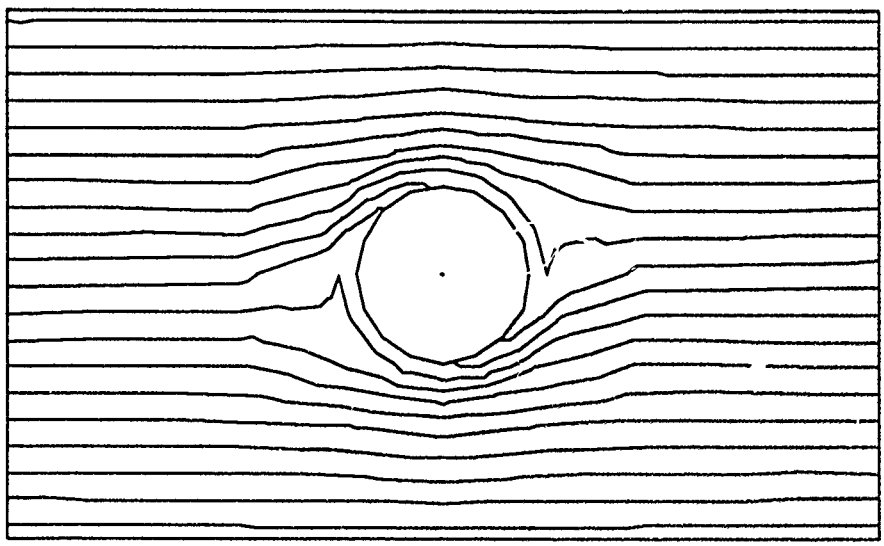

Concentration Contours : Pe = 28

[Fig. 9]

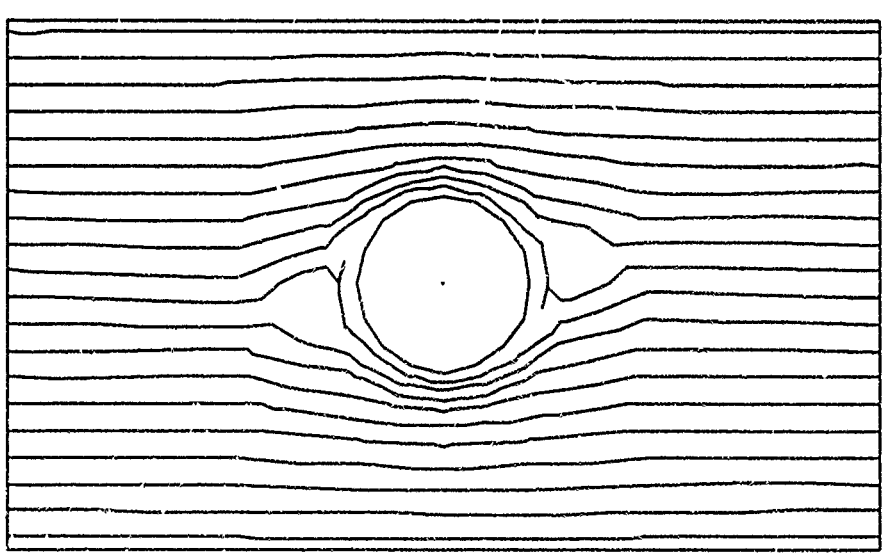

Concentration Contours : Pe = 417

[Fig. 10]

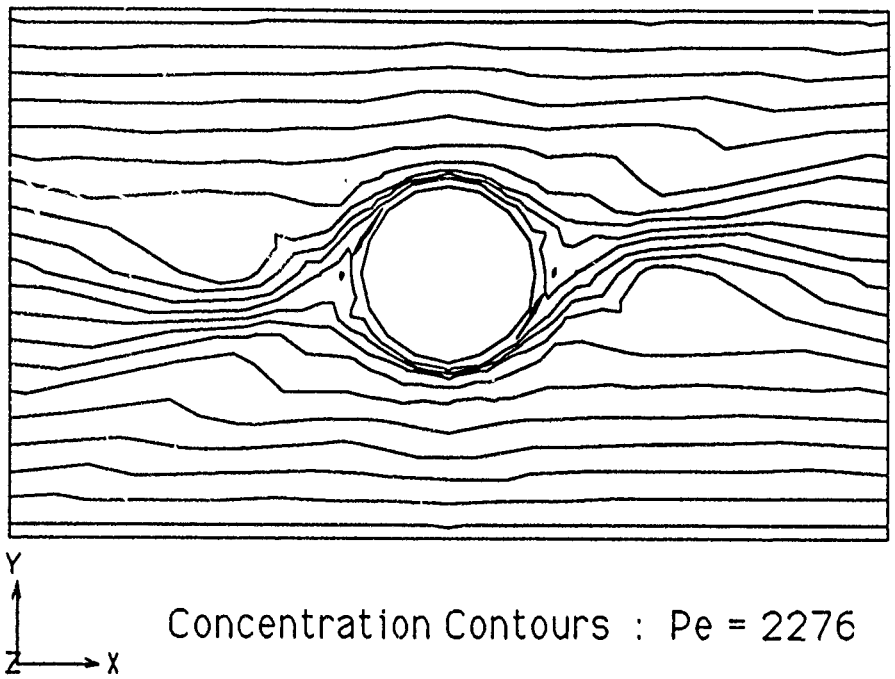

[Fig. 11]

Fig. 6 depicts to a fixed sphere with no fluid motion. The species simply diffuses around it. This constitutes the base case in the measure of micro-convection. As the particle begins to rotate and the Peclet number increases, convection around the sphere starts to supplement diffusion. As Pe increases still further, the film around the sphere becomes better mixed and fewer and fewer contour lines intersect the sphere. Eventually the film has essentially a constant concentration.

The average mass flux was calculated by the FIDAP post-processor program. A measure of the effectiveness of micro-convection is the Specific Enhancement, SE, defined as

$$SE = \frac{N_{Pe}-N_0}{\phi N_0} \qquad \text{[Eq. 35]}$$

N_{Pe} is the mean mass flux at a given Peclet number. N_0 is the flux at zero Peclet number or the purely diffusive flux. The volume fraction solids is denoted by ϕ, 1.7 % in this case.

Runs were made keeping the particle radius constant at 1 μm and varying the shear rate from 0 to 10^6 s^{-1}, and then keeping the shear

constant at 100 s^{-1} and varying the particle radius from 1 to 128 μm. The results of both runs are shown in Fig. 12.

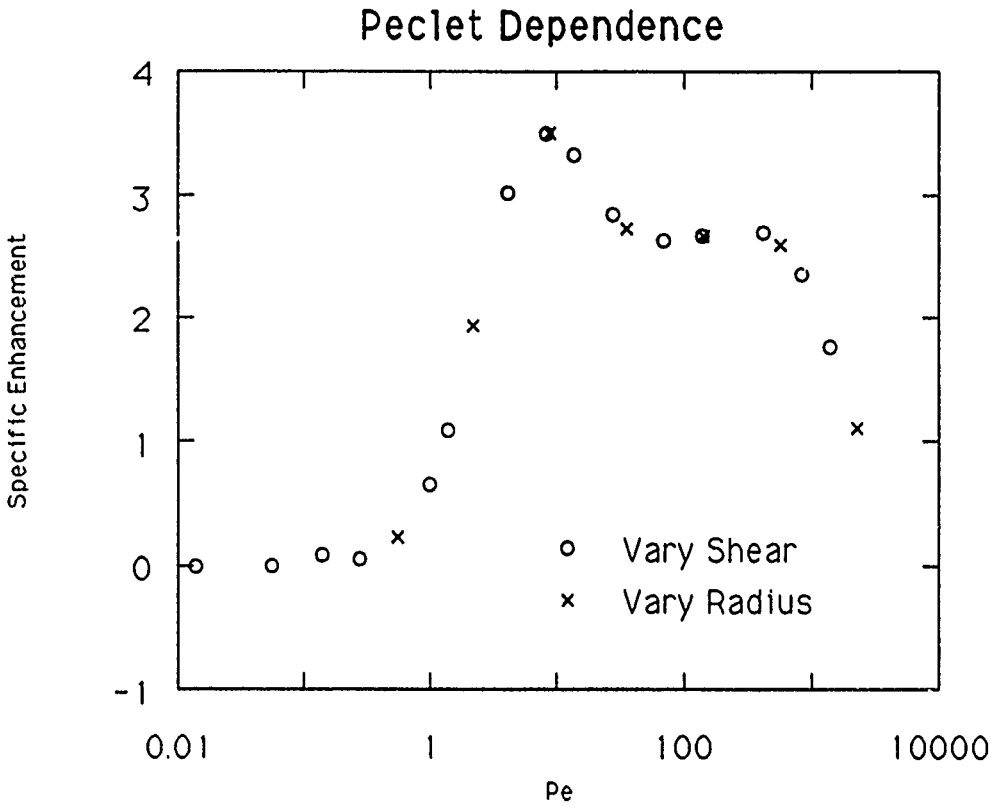

[Fig. 12]

It can be seen that when expressed as functions of Pe, the results of both runs lie along the same line. Although the effect of diffusivity hasn't been investigated, it seems apparent that the degree of mass transfer enhancement is a function of Peclet number alone.

Let us adapt Eq. 30 and search for a relation in the form:

$$SE = A\,Pe^{a}(1 - \exp(-BPe^{b})) \qquad \text{[Eq. 36]}$$

A least squares fit to the data is shown in Fig. 13.

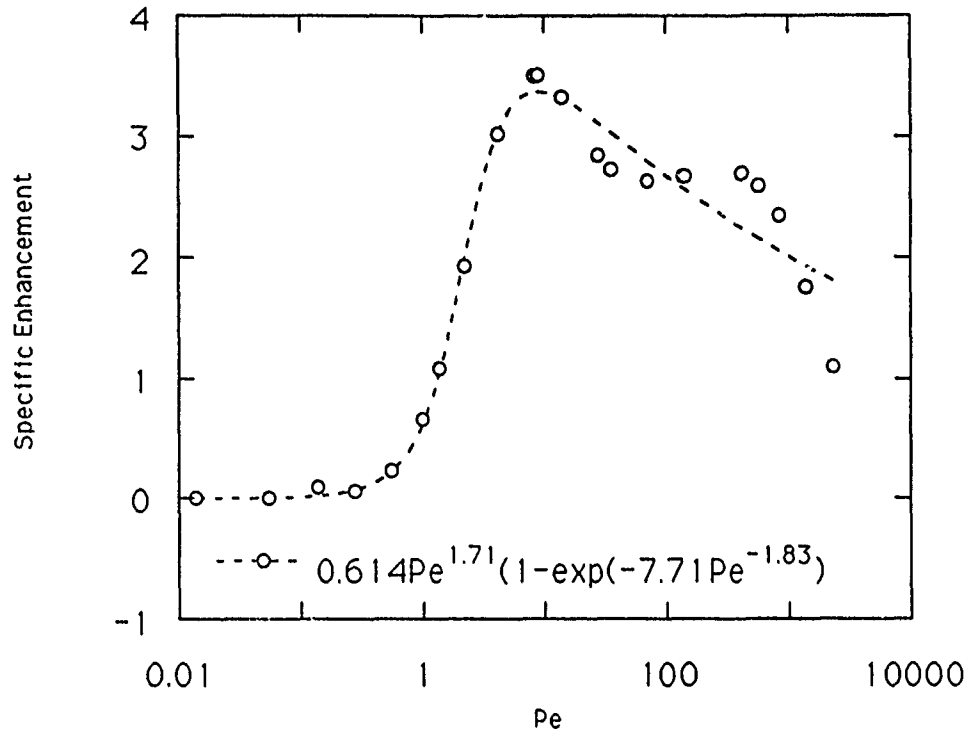

Fig. 13

The best parameters and their standard errors are:

A = 0.6142 ± 0.1545
a = 1.708 ± 0.360
B = 7.707 ± 1.799
b = -1.838 ± 0.191

At high Peclet numbers there seems to be an oscillation of the data about the line of Eq. 36. To more closely examine this phenomenon, the residuals (data minus the function) are plotted in Fig. 14

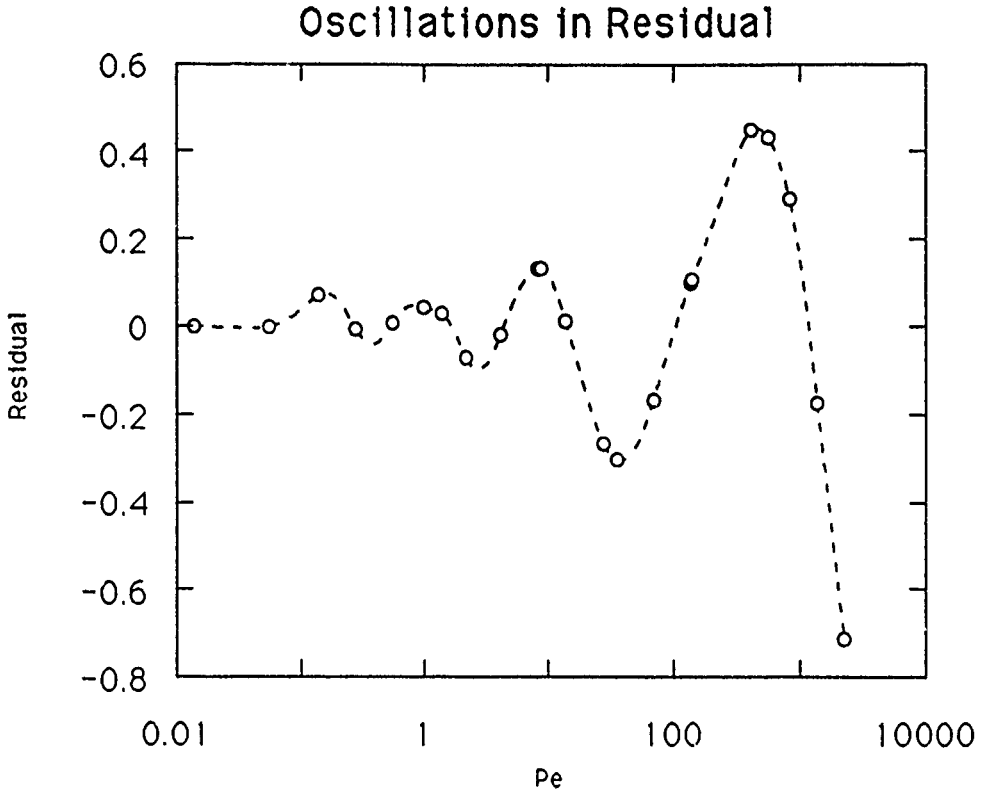

Fig. 14

The deviation from Eq. 36 is not random but appears to be periodic on the semi-log plot. The cause of this phenomenon is not known at this time. It may be a numerical instability from the finite element problem. It may also be a naturally occurring resonance phenomenon, which doesn't appear in rotating disk experiments since the wide distribution of local Peclet number smears out such fine detail.

[1] David J. Roha, M.S. Thesis, U.C. Berkeley, 1981

[2] P.J. Sonneveld, W. Visscher, E. Barendrecht, *J. Appl. Electrochem.*, **20** (1990) 563-574

[3] G.K. Batchelor, 'An introduction to fluid dynamics', Cambridge University Press (1970) p. 248

[4] G.I. Batchelor, *J. Fluid Mech.* **56** (1972) 375

(19)

Preparation of colloidal metals by reduction or precipitation in microheterogeneous fluids

Jerzy Kizling[1], Magali Boutonnet-Kizling[1], Per Stenius[1], Raymonde Touroude[2] and Gilbert Maire[2]

1)Institute for Surface Chemistry, Box 5607, S-11486 Stockholm, Sweden
2) Laboratoire de Catalyse et Cinie des Surfaces, U.A. 423 du CNRS, 4 Rue Blaise Pascal, F-67070 Strasbourg, France

Abstract

Several methods of preparing colloidal particles of metals or metal oxides by reduction of salts dissoved in the water pools of microemulsions have been reported. These are briefly reviewed. In many cases the reduction is followed by aggregation of the precipitated material to colloidal particles that contain much larger numbers of metal atoms than those contained in each water pool. However, by judicious choice of systems and reaction conditions it appears possible to limit the initial reaction to each water pool. In such cases, the method offers the possibility to carry out the reduction under conditions corresponding to relatively concentrated electrolyte concentrations in spite of the system as a whole being very dilute. Using this method it is also possible to prepare alloys of metals directly by reduction. This has been demonstrated for H_2PtCl_6 and $PdCl_2$ in $C_{12}E_5$-hydrocarbon-water micro-emulsions. The state of the metal ions in the water pools was investigated by EXAFS. The results show that Pt and Pd do indeed form an alloy and that the coordination number for Pt and Pd in particles is lower than it is in bulk metal.

Introduction

Colloidal dispersions essentially are prepared by two different methods: by comminution of large pieces of material or by association or precipitation (condensation) of ions, atoms or small molecules. The former method is extensively used for large-scale preparation of emulsions, pigment dispersions etc. In general, due to the increasing importance of surface forces compared to shearing forces as the particle size decreases, it is not possible to prepare colloids with mean particle sizes smaller than about 0.1 μm by the former method. Moreover, due to the difficulty to achieve precise control the factors

governing comminution the resulting dispersions often show a rather broad particle size distribution.

Therefore, for the preparation of dispersions with low polydispersity and/or very small particle sizes the condensation method is generally utilized. As originally clarified by La Mer (1), two consequtive stages in the process of particle formation by condensation are essential for the formation of such particles. A rapid nucleation process leading to the formation of as many particles as possible when a critical nucleation concentration is reached should be followed by a particle growth controlled by diffusion. Monodispersity is achieved if the firs stage is as rapid as possible while no additional nucleation takes place during the second stage. This obviously requires that once the nuclei have been formed the rate of capture of additional material by these should be considerably faster than any formation of additional nuclei. Since diffusion-controlled particle growth will increase with increasing area/volume ratio of the particles, small particles will tend to grow faster than larger ones, leading to monodispersity.

The formation of extremely small colloidal particles is of particular interest in heterogeneous catalysis. For efficient utilization of the catalytic material one is interested in achieving as high area/volume areas as possible, in particular in the case of expensive transition metal catalysts. Controlled functioning and durability of the catalyst requires that it should be prepared in a reproducible way and that the particles formed should remain dispersed. of particular interest is the possibility that in the preparation of very small particles, the formation of some crystalline planes might be preferred to others.

With these ideas as a background, microemulsions appear to offer particularly favourable reaction media for the formation of monodisperse metal particles. With suitably chosen composition, such systems, which are thermodynamically stable, will contain micellar aggregates (typically of size around 0.5 - 20 nm) consisting of water pools surrounded by amphiphiles in a continuous non-polar medium. By dissolving material that is subsequently precipitated in the water pools, a situation is created where particle nucleation can be initiated simultaneously at a very large number of spots in the solution, with the nucleation sites well isolated from one another and in close contact with surfactants that may act as stabilizers of the particles formed.

This idea has been utilized by us (2) and others to prepare particles of several materials. Thus, particles have been prepared consisting of catalytically active

transition metals (2) and their alloys (3), magnetite (4, 5), calcium and barium carbonate (6-8), silver halogenides (9,10) and Ni-, Co- and Fe borides (11, 12). Precipitation was initiated by reacting dissolved salts with gases bubbled through the microemulsions (2, 3, 6-8) or by direct reaction in solution (9-13), utilizing microemulsions containing anionic, cationic as well as nonionic surfactants. In this paper we give an overview of our studies of the preparation of metal particles from nonionic microemulsions, with emphasis on microemulsion structure and the fact that an additional advantage of using microemulsions is that it is possible to achieve high reactivity by creating local isolated environments of very high concentration of the reactants dissolved in the micellar interior.

Experimental

Systems studied

In our studies, we have focused on the preparation of particles of transition metals used as catalysts in hydrocarbon reactions and for the oxidation of automotive exhausts: Pt, Pd, Ir and Rh salts as well as mixtures of Pt and Pd salts. Unsuccessful attempts were made to dissolve these in microemulsions based on anionic surfactants. Hexachloroplatinic acid is soluble i microemulsions based on a cationic surfactant (cetyl trimethyl ammonium bromide) and an aliphatic alcohol (octanol) but it was found it was found that the most useful microemulsions were those formed by polyethene oxide alkyl ethers and water in aliphatic hydrocarbons. Such microemulsions were able to dissolve the metal salts and did not break when the salts were reduced to metal. As a model system we have used penta(ethene oxide) dodecyl ether ($C_{12}EO_5$) and water dissolved in different n-alkanes.

Figure 1 shows the phase diagram for $C_{12}EO_5$/hexadecane/water at 25°C with typical compositions which were used for particle preparation indicated. Within a relatively narrow temperature range Which has been termed the "phase inversion temperature", PIT), the solubility of water in these systems is strongly enhanced; the location of the range depends on the chain length of the hydrocarbon (as shown in figure 2) and also, of course, on the lengths of the hydrocarbon moiety and the polyethene oxide chain of the surfactant. These relationships have been studied extensively; for reviews see, e.g. ref. 14-16. Thermodynamically, the occurrence of the PIT may be regarded as a property of the three-component system resulting from the immiscibility of water and hydrocarbon, the occurrence of a lower consolute solution temperature in the

water/surfactant system and the occurrence of an upper consolute solution temperature in the hydrocarbon/surfactant system (1/).

Addition of H_2PtCl_6, $IrCl_3$, $RhCl_3$, $PdCl_2$ or $AuCl_3$ to to the microemulsions lowers the PIT but in other respects the stability of the microemulsion is not much affected.

Preparation of particles

Metal particles were formed in the microemulsions by reduction of the dissolved salts with hydrogen or hydrazine. Total concentrations were typically of the order 0.1%. Details are given in (1). Note that these concentrations correspond to considerably larger larger local concentrations of the metal ions. Successful particle preparation was obtained in systems typically containing about 10% $C_{12}EO_5$ and 4% water (by weight); from the sizes of the reverse micelles formed in these systems it may be inferred that there will initially be on the average 5-10 metal ions in each micelle.

The reduction of the ions could generally be achieved under conditions less severe (e.g., lower temperatures) than those required for reduction of the corresponding ions in dilute aqueous solution. Resulting particle sizes are given in table 1. The particle dispersions were colloidally stable. The particles could be deposited on different materials (for example, alumina, silica or silicon carbide for catalytic purposes) without extensive aggregation by destabilizing the dispersions by adding suitable solvents (e.g. tetrahydrofurane).

Investigation of the microemulsions

Aggregate formation in the microemulsions was investigated by calorimetry, using the equipment at the Laboratory for Thermochemistry, University of Lund and by dynamic light scattering. For details on the calorimetry, see (18). The light scattering experiments are described in (19). The structure of Pt and Pd ions when dissolved in the microemulsions was investigated using equipment at the LURE-DCI storage ring at Orsay, France, and at the Laboratory of Catalysis and Surface Chemistry at Strasbourg, France (20). The structure of the particles was studied by electron microscopy (2). Their chemical composition was verified using a Leybold-Heraeus ESCA equipment .

Results and discussion

Aggregate size in the microemulsions

Figure 3 shows the temperature dependence of the size of the reverse micelles formed in systems containing hexadecane and $C_{12}EO_5$ in the weight ratio 9:1 and increasing amounts of water (19). Note that investigations were made in the PIT range for this solvent (cf figure 2). Similar results were obtained for dodecane in the PIT range corresponding to this solvent. Figure 4 shows results for systems containing 3% water to which was added different amounts of H_4PtCl_6 (20).

Figure 3 shows

(i) Micelles are formed by the nonionic surfactants in the aliphatic solvents when water is added. The concentration at which micelles begin to occur are determined by the water/$C_{12}EO_5$ ratio which must exceed about 2 mol water/EO unit. In addition, a minimum total concentration of $C_{12}EO_5$ is required to obtain micelle formation. Both observations indicate that association is a weakly cooperative process, probably due to the the geometric requirement that the water incorporated into the swelling aggregates is to be shielded from hydrocarbon contact.

(ii) The size of the micellar aggregates increases linearly with water concentration at constant temperature but decreases with temperature at constant water content. At a given temperature the total number of aggregates is independent of total water concentration.

Comparison of fig 4 with these results shows

(i) the general dependence of aggregate size on temperature does not change when the metal salt is added. At constant temperature the size of the aggregates increases linearly with the amount of aqueous H_4PtCl_6 solution added (figure 5), and the apparent hydrodynamic radius of the aggregates decreases sharply with temperature.

(ii) The whole PIT range of this system is shifted downwards by the addition of hexachloroplatinic acid (as has been observed in many similar systems when large anions are added) (figure 6). Thus, the increase in aggregate size shown by figure 5 is due to general effects of anions on the hydrophilic/lipophilic

balance of the surfactant, not on any specific interaction of the hexachloroplatinic ion with the surfactant.

(iii) H_4PtCl_6 could not be dissolved in any appreciable amounts at all unless sufficient amounts of surfactant and water were present for reverse micelles to occur. This is immediate evidence that the acid is solubilized in the micellar interior and that the concentrations of acid outside the aggregates must be negligible. Thus, indeed, the microemulsion does offer the possibility to create pools with locally high concentrations of ions well isolated from one another.

Aggregate sizes were not investigated for other salts. However, their effect on PIT appears to be similar to that of H_4PtCl_6 an it seems highly probable that their effects on aggregate size will also be similar.

The binding of water in the micelles

Figure 7 shows the differential enthalpy of solution of water in the $C_{12}EO_5$ system at two different temperatures. The enthalpy profiles at other concentrations of $C_{12}EO_5$, for a surfactant with shorter EO chain length ($C_{12}EO_4$) and for decane as solvent are very similar (18).

The differential enthalpies first decrease steeply, i.e. binding of the first molecules of water to the EO chain (solubility of water in the aliphatic solvent as such is negligible) is strongly exothermic. A relatively sharp minimum occurs and then as the water concentration increases the differential enthalpy gradually approaches zero.

As detailed in ref. (18), the calorimetric investigations also indicate that $C_{12}EO_5$ dimerizes in dry aliphatic solvents.

The interpretation of the results exemplified in figure 7 is relatively straightforward (18). The binding of the first molecules of water to monomeric $C_{12}EO_5$ is strongly exothermic; at very low concentrations of water this effect predominates over binding of water to associated $C_{12}EO_5$. As the water concentration increases, the binding of water to associated surfactant progressively becomes more important. When the concentration increases beyond the concentration giving maximum exothermicity the surfactant aggregates gradually grow and the partial molar enthalpy approaches zero as the water eventually will dissolve in an environment quite similar to pure water.

The light scattering results indicate indicate that in systems containing 10% $C_{12}EO_5$ micelles are formed only when the water concentration exceed 2%. This association does not give rise to any abrupt changes in the partial molar enthalpies of water (figure 7) or $C_{12}EO_5$ (18). Rather, there is a smooth transition to enthalpies that are almost zero for water at the concentrations where micelles can be detected.

Appreciable solubilization of the metal salts requires the presence of reverse micelles. Thus, the salts will be solubilized only when sufficient water has been added so that the strong primary hydration of the EO chains does not compete with the solvation of the metal ions. Specific EO/metal ion interactions are apparently not strong enough to compete with the tendency of the chains to bind water. However, the primary binding of water to the EO chains is relatively small (the minimum in the enthalpies occurs at around 0.1 mol water/mol ethene oxide) and even at the solubility limit the concentration of water is only about 2 mol water/EO unit.

EXAFS studies of ions in solution

The radial distribution of nearest neighbours of Pt and Pd atoms in the microemulsions, in crystals and in water was determined by EXAFS. Results are given in tables 2 and 3, taken from ref. (3). They show that chloroplatinic acid is not much influenced by the environment in which it is dissolved. The acid retains its octahedral structure in which the Pt^{4+} ion is surrounded by 6 chloride ions (21). The bond distances between the central atom and the ligands is the same irrespectively of the acid concentration or the environment. Moreover X-ray diffraction analysis has shown that the distances are equivalent to the distance in the crystal (22,23).

However, a closer investigation of the radial distribution functions, reveals some differences between the arrangement of the $PtCl_6^{2-}$ ions in the concentrated aqueous solution and in the microemulsion; the amplitude of the radial distribution corresponding to the second neighbours of central metal atom is higher in the microemulsion than in water. From this observation it can be deduced that the $PtCl_6^{2-}$ species are more densely packed when dissolved in the micellar aggregates than in the concentrated water solution. This could explain why the Pt ions, as pointed out above, are more reactive in the microemulsion than in water (1).

Comparison of the results in table 3 shows the Pd-Cl bond length in water and in microemulsion is the same. However it is shorter than in the crystal by 0.5Å. It should be noted that in the crystal Pd atoms are surrounded by four chlorine ligands and the structure is stabilized by bridging ligands. Such a bridging leads probably to a stretching of Pd-Cl bonds which is not the case in the single $PdCl_4^{2-}$ species that occurs in solution.

Although the bond lengths in water and in the microemulsion is the same, the reactivity of this salt is also higher in microemulsion than in the concentrated water solution (1).

Characterization of particles formed from microemulsions

Electron microscopy reveals that the particles can be prepared from the microemulsions in a well dispersed form with a narrow size distribution (standard deviation about ± 10%). 100 % of the material is reduced to these very small and well.dispersed particles, which indicates that they may be very efficiently stabilized by adsorption of the nonionic surfactant. This is an important observation in view of the potential use of these expensive materials for catalytic purposes. The exact shape of the particles has not been clarified; we thus have no direct information of whether the growth of certain crystalline planes are preferred under the rather special conditions of reaction obtaining in the microemulsions. The particle sizes observed imply that the particles contain 500-1500 atoms. Thus, it is obvious that although nucleation may take place in individual reverse micelles, a secondary aggregation process takes place leading to the formation of the final particles.

ESCA studies

ESCA analysis of particles deposited on different supports revealed that they are indeed reduced to metal and that it is possible to remove the surfactant from the particles by washing once the particles have been deposited. The particles remain attached to the support, presumably due to the rather strong van der Waals forces expected between the small metal particles an solid supports. The Pt particles remain as metal even when exposed to air while the surface of Pd particles is easily oxidized; they may be reduced to metal by treatment with hydrogen.

Mechanism of particle formation

As already mentioned, typical metal concentrations used in the experiments correspond to 5-10 ions per aggregate. attempts to use much higher concentrations resulted in destabilization of the initial microemulsion or to complete instability of the particles formed. Thus it is obvious that formation of final particles of the size finally obtained requires that metal atoms from several different reverse micelles aggregate. From the final size it can be estimated that the amount of ions initially dissolved will produce about 10^{14} particles/cm^3, which is about 30 times lower than the n umber of micelles in the same volume.

The two-step mechanism has been corroborated by studies of the kinetics of the formation of gold particles by pulse radiolysis (24), with particle formation initiated by flash photolysis. The concentration of gold in the $C_{12}EO_5$ system was very low and it may of course be questioned whether the reduction initiated in this ay is really comparable to reduction by a chemical reactant. The results, however, are consistent with the indirect conclusions drawn from the other studies. The initial step appears to be the formation of hydroxy radicals and a hydrated electron:

$$H_2O \rightarrow e^-(aq) + \cdot H + \cdot OH + H_2O_2 + H_2 + H_3O^+$$

followed by reduction of the gold ions:

$$Au^{3+} + e^-(aq) \rightarrow Au^{2+}$$
$$2Au^{2+} \rightarrow Au^{3+} + Au^+$$
$$Au^{++} \cdot R \rightarrow Au^0$$

These reactions take limited to the interior of the micellar aggregates due to the relatively slow exchange of water with the surroundings compared to their reaction rates. The next step then is the formation of gold particles

$$nAu^0 \rightarrow (Au^0)_n$$

The actual process by which this aggregation takes place has not been investigated either in this case or for the formation of platinum metal particles. However, Nagy, Derouane et al (11,12) have interpreted extensive studies of the formation of boride particles by precipitation from microemulsions based on cetyl trimethyl ammonium bromide and hexanol in terms of similar notions.

References

1. La Mer, V.K. and Dineger, R.H., *J. Am. Chem. Soc.* 72 (1950) 4847.

2. Boutonnet, M., Kizling, J., Stenius P. and Maire, G., *Colloids Surfaces* 5 (1982) 209).

3. Touroude, R, Maire, G., Kizling, J., Kizling M. and Stenius, P., *submitted for publication*.

4. Gobe, M., Kandori, K., Kon-No, K., and Kitahara, A., *J. Colloid Interface Sci.*, 93 (1983) 293.

5. Esumi, K., Tano, T., Torigoe, K. and Meguro, K., *Chem. Mater.* 2 (1990) 564.

6. Kandori, K., Kon-No, K., and Kitahara, A., *J. Colloid Interface Sci.*, 122 (1988).

7. Kandori, K., Kon-No, K., and Kitahara, A., *J. Colloid Interface Sci.*, 115 (1987) 579.

8. Kandori, K., Shizuka, N., Kon-No, K., and Kitahara, A., *J. Disp.Sci. technol.*, 8 (1987) 477.

9. Chew, C.H., Gan, L.M. and shah, D.O., *J. Disp.Sci. technol.* , 11 (1990) 593.

10. Hou, M. and Shah, D.O. in "*Interfacial Phenomena in Biotechnology and Material Processing*", Y.A. Attia, B.M. Muodgil, S. Chander, (eds), Elsevier, Amsterdam, 1988.

11. Ravet, J., Nagy, J.B., and Derouane, E. in "*Preparation of Catalysts IV*"", B. Delmon, P. Grange, P. A. Jacobs and G. Poncelet, (eds), Elsevier, Amsterdam 1987 p. 505.

12. Nagy, J.B., Bodart-Ravet, J. and Derouane, E.G., *J. Chem. Soc. Farad. Disc.* 87 (1989) 189.

13. Lewis, L.N. and Lewis, N., *Chem. Mater.* 1 (1989) 106.

46 8 108180 PAGE.010
JUN 21 '91 7:36

14. Sjöblom, J. Danielsson, I. and Stenius P., in *"Nonionic Surfactants"*, M. J. Shick, ed., Marcel Dekker, 1988.

15. Kahlweit, M and Lessner, E., in *Surfactants in Solution* (K.L. Mittal and B. Lindman, eds), Plenum, New York, 1984, vol. 1, p. 23.

16. Shinoda, K. and Friberg, S., *"Emulsions and Solubilization"*, Interscience, New York 1986.

17. Kahlweit, M., Strey, R., Firman, P. and Haase, D., *Langmuir*, 1 (1985) 282.

18. Olofsson, G., Kizling, J. and Stenius, P., *J. Colloid Interface Sci.* 111 (1986) 213.

19. Kizling, J. and Stenius, P., *J. Colloid Interface Sci.* 118 (1987) 482.

20. Touroude, R, Bernhardts, P., Maire, G., Kizling, J., Kizling M. and Stenius, P., *Colloids Surfaces*, accepted for publication (1991).

21. Hartley, F.R., *"The Chemistry of Platinum and Palladium"*, Apllide

JUN.21 '91 7:36 46 8 108180 PAGE.011

Tables.

Table 1. Sizes of particles prepared by reduction of metal salts in microemulsions consisting of $C_{12}EO_5$, hexane and water.

Metal salt	Particle size nm
H_4PtCl_6	2.7±0.3
$PdCl_2$	4.5±0.5
$IrCl_3$	2.5±0.3
$RhCl_3$	3±0.3
$AuCl_3$	~4

II-206

46 8 108180 PAGE.012
JUN 21 '91 7:37

Table 2. Coordination numbers and nearest neighbour distances for Pt^{IV} ions in $C_{12}E_5$/hexadecane/water microemulsions. The results were obtained by analysis of the L_{III} edge of platinum using the equipment at the Laboratory of Catalysis in Strasbourg.

Pt edge	Microemulsion composition weight%			Pt^{IV} conc g/l	Neighbour	Coord. number (from amplitude)	R Å ±0.002	D-W factor
	Hexadecane	$C_{12}E_5$	H_2O					
L_{III}			100	40.0	Cl^-	6	2.32	0.060
	90.0	10.0		1.0	Cl^-	6	2.31	0.066
	89.0	10.0	1.0	1.0	Cl^-	6	2.31	0.066
	88.0	10.0	2.0	1.0	Cl^-	6	2.30	0.074
	85.0	15.0		3.0	Cl^-	6	2.31	0.060

JUN 21 '91 7:37 46 8 108180 PAGE.013

Table 3. Coordination numbers and nearest neighbour distances for crystalline $PdCl_2$ and for $PdCl_2$ dissolved in $C_{12}E_5$/hexadecane/water microemulsions. The results were obtained by analysis of the K edge of platinum using the LURE equipment.

Pd edge	Microemulsion composition weight%			Pd^{II} conc g/l	Neighbour	Coord. number (from amplitude)	R Å ±0.02	D-W factor
	Hexadecane	$C_{12}E_5$	H_2O					
K^{α}				Cryst.	Cl^-	4	2.31	0.082
			100.0	84	Cl^-	4	2.27	0.070
	87.0	10.0	3.0	1.0	Cl^-	4	2.27	0.055

46 8 108180 PAGE.014
JUN 21 '91 7:38

Figure legends

Figure 1. The phase diagram of $C_{12}EO_5$, water and hesadecane at 20 C. At this temperature, $C_{12}EO_5$ and hexadecane are completely miscible; the maximum amount of water can be solubilized corresponds to a relatively constant $C_{12}EO_5$/water ratio. Lamellar liquid crystalline phase is formed in a relatively extensive composition domain; this will not be further discussed (1).

Figure 2. Solubilization of water in a mixture of $C_{12}EO_5$ and solvent in the weight ratio 1/9. (19)

Figure 3. Equivalent hydrodynamic diameters for aggregates formed in solutions containting hexadecane and $C_{12}EO_5$ in the weigt ratio 9:1 and different amounts of water as a functioin of temperature. (19)

Figure 4. The temperature dependence of the aggregate size in microemulsions consisting of $C_{12}EO_5$ and hexadecane (in the weight ratio 1:9), 8 % water and varying amounts of H_2PtCl_6. (2)

Figure 5. Dependence of aggregate size on the concentration of H_2PtCl_6 at different temperatures. Compositions as in figure 4.(2)

Figure 6. Solubilization of water in hexadecane containing 10 % $C_{12}E_5$ compared with solubilization of water in the same system to which was added 0.1 mg/cm^3 Pt^{IV} (as H_2PtCl_6). The shape of the solubility region (to the left of the curves) is not changed, but adding the acid lowers the temperature profile by about 5 °C. (2)

Figure 7. Differential enthalpy of solution of water in ternary solutions cotaining 10.1 % $C_{12}EO_5$ and varying amounts of water in hexadecane at 27.0 and 37.0 °C (18)

46 8 1081801 PAGE.015

JUN 21 '91 7:39

Figure 1.

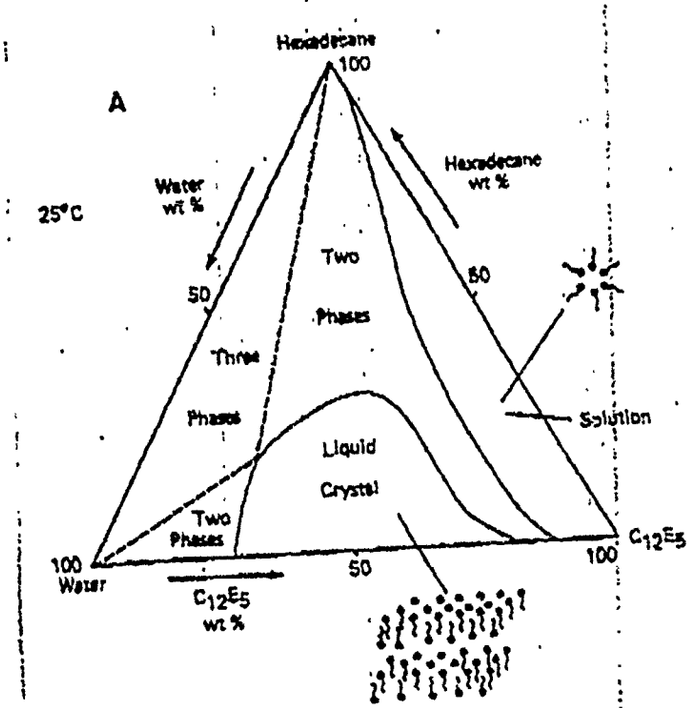

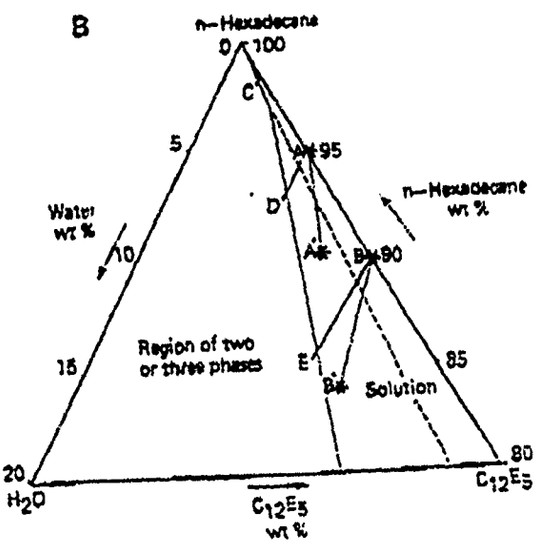

II-210

Figure 2.

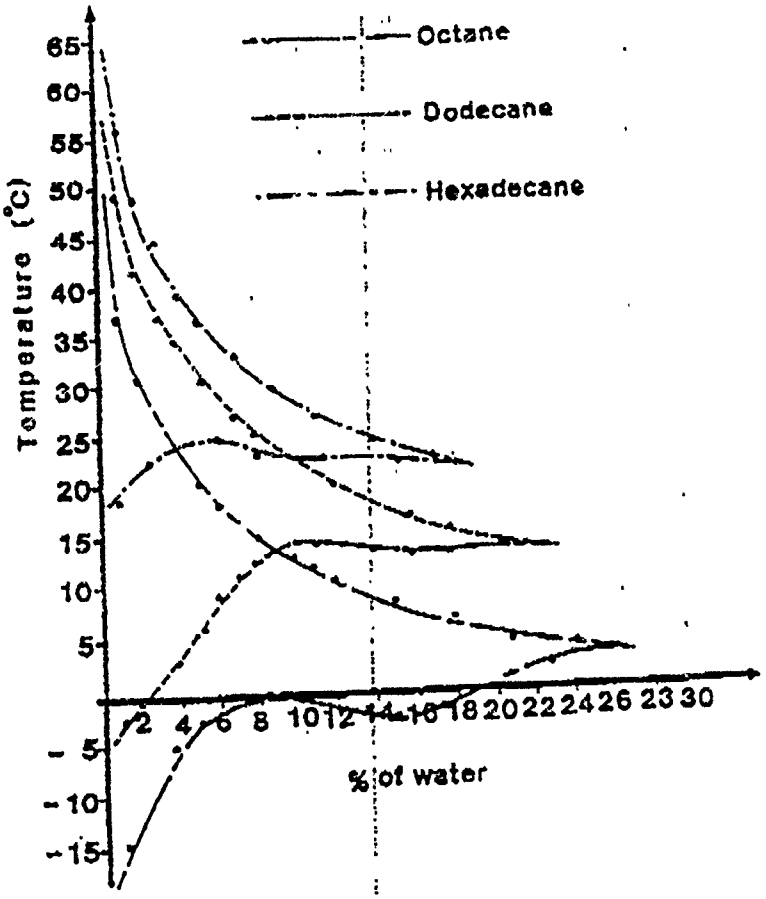
Octane
Dodecane
Hexadecane
Temperature (°C)
65
60
55
50
45
40
35
30
25
20
15
10
5
- 5
- 10
- 15
2 4 6 8 10 12 14 16 18 20 22 24 26 23 30
% of water

JUN 21 '91 7:40 46 8 108180 PAGE.017

Figure 3.

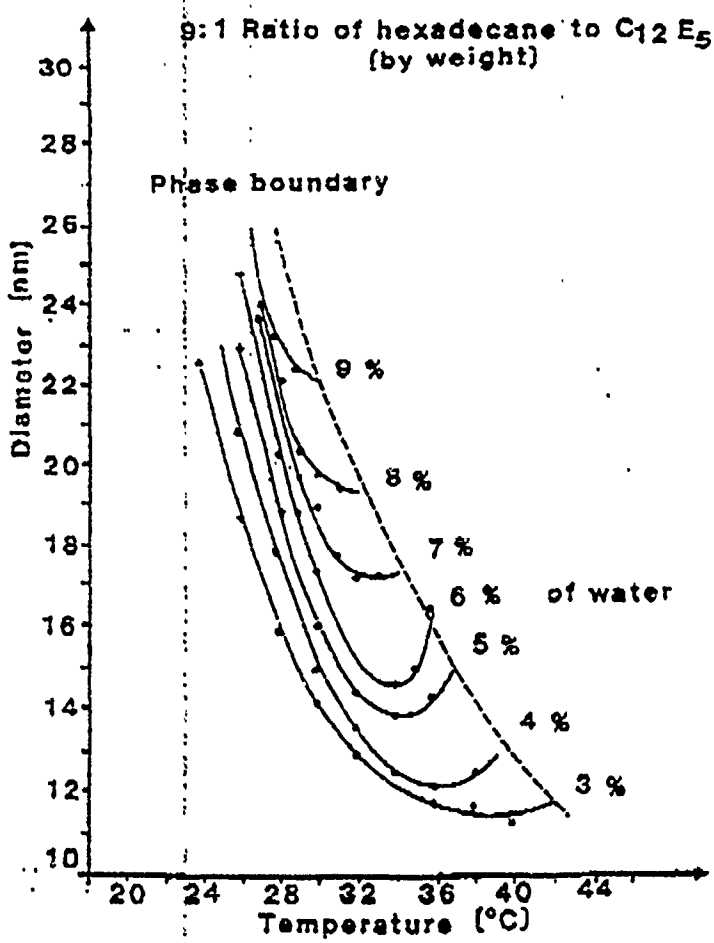

Figure 4

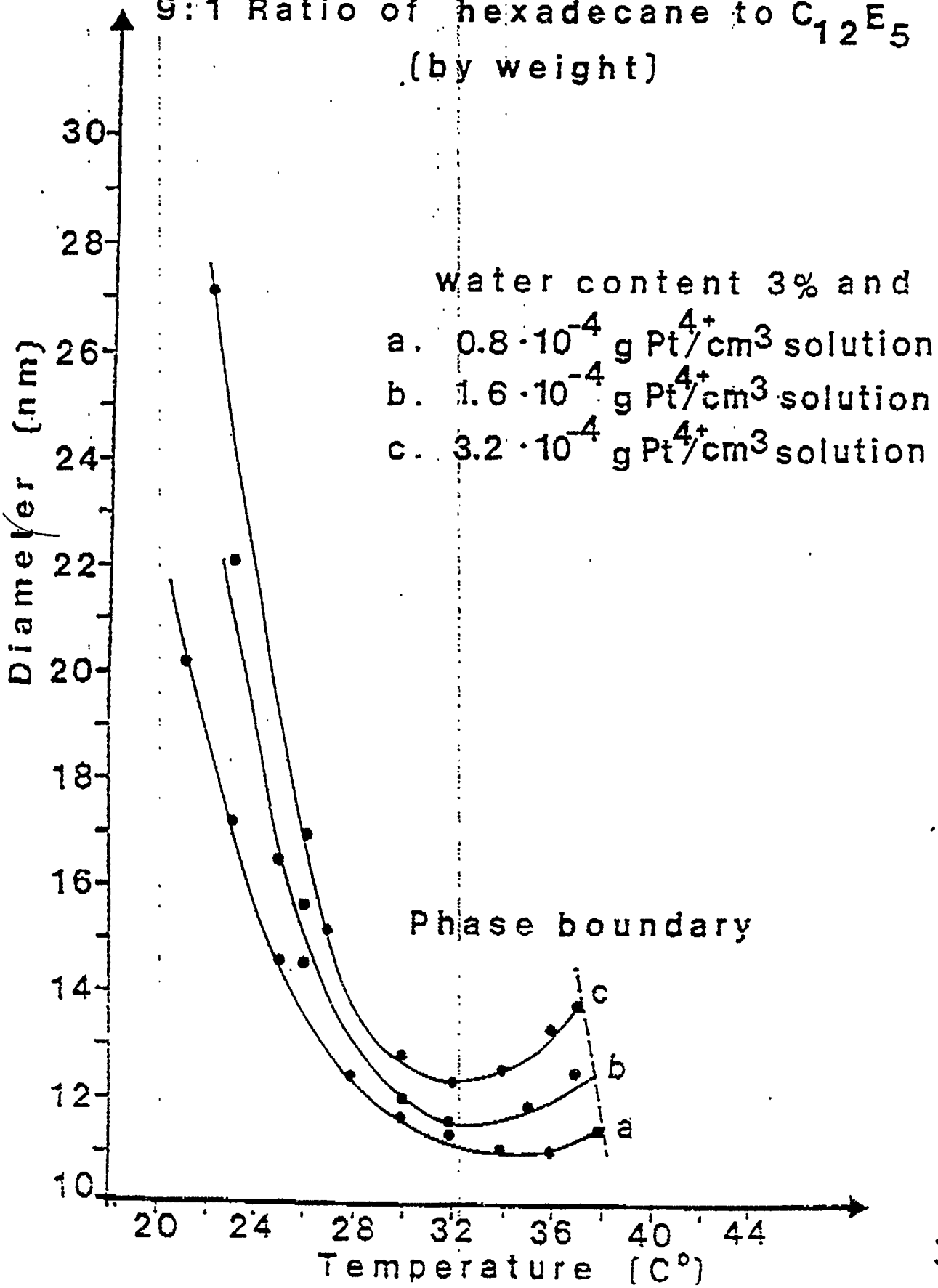
9:1 Ratio of hexadecane to $C_{12}E_5$
(by weight)
water content 3% and
a. $0.8 \cdot 10^{-4}$ g Pt^{4+}/cm^3 solution
b. $1.6 \cdot 10^{-4}$ g Pt^{4+}/cm^3 solution
c. $3.2 \cdot 10^{-4}$ g Pt^{4+}/cm^3 solution
Phase boundary
Diameter (nm)
30
28
26
24
22
20
18
16
14
12
10
20
24
28
32
36
40
44
Temperature (C°)
a
b
c

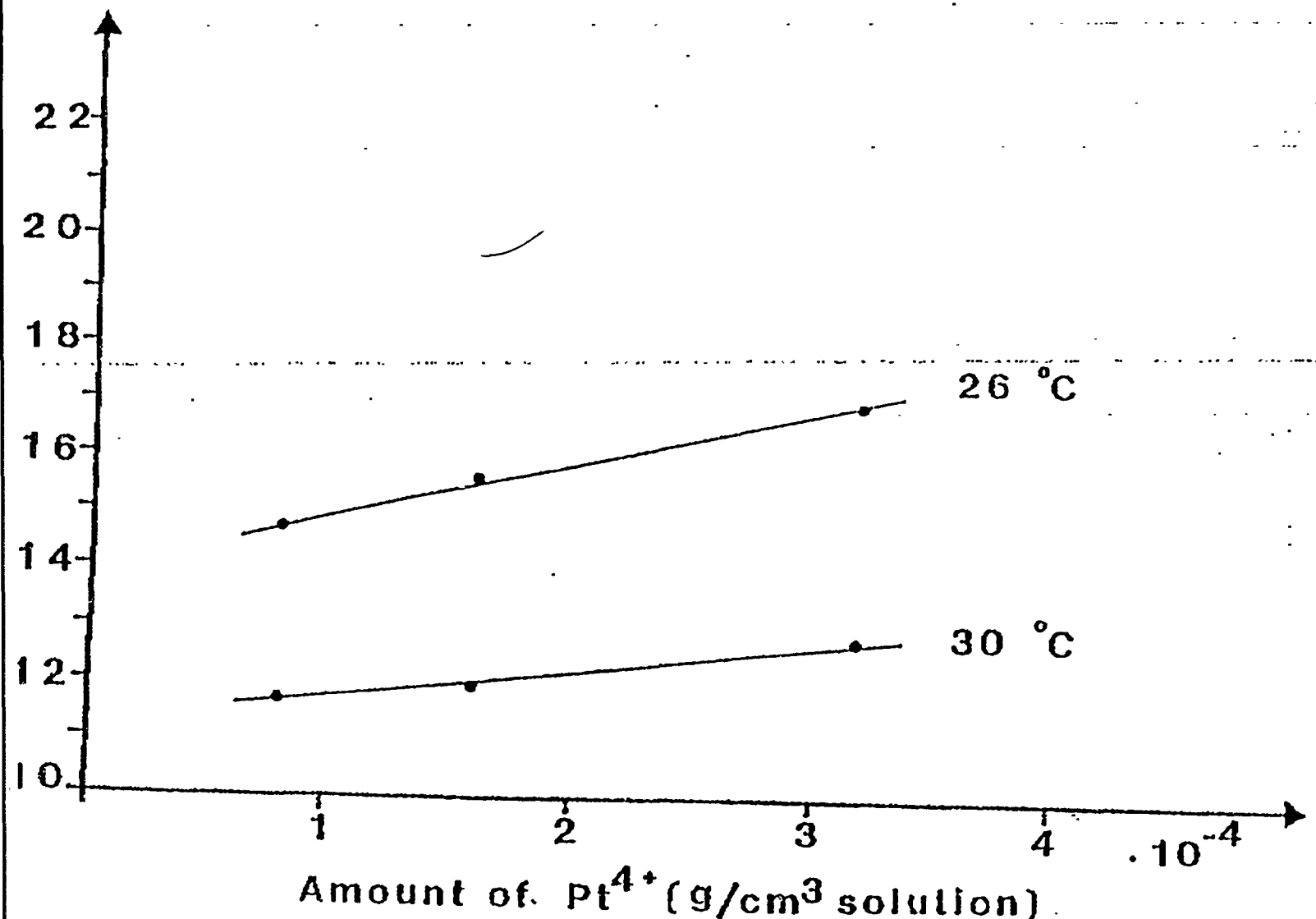
22
20
18
16
14
12
10
26 °C
30 °C
1
2
3
4
·10⁻⁴
Amount of Pt4+ (g/cm3 solution)

Figure 6

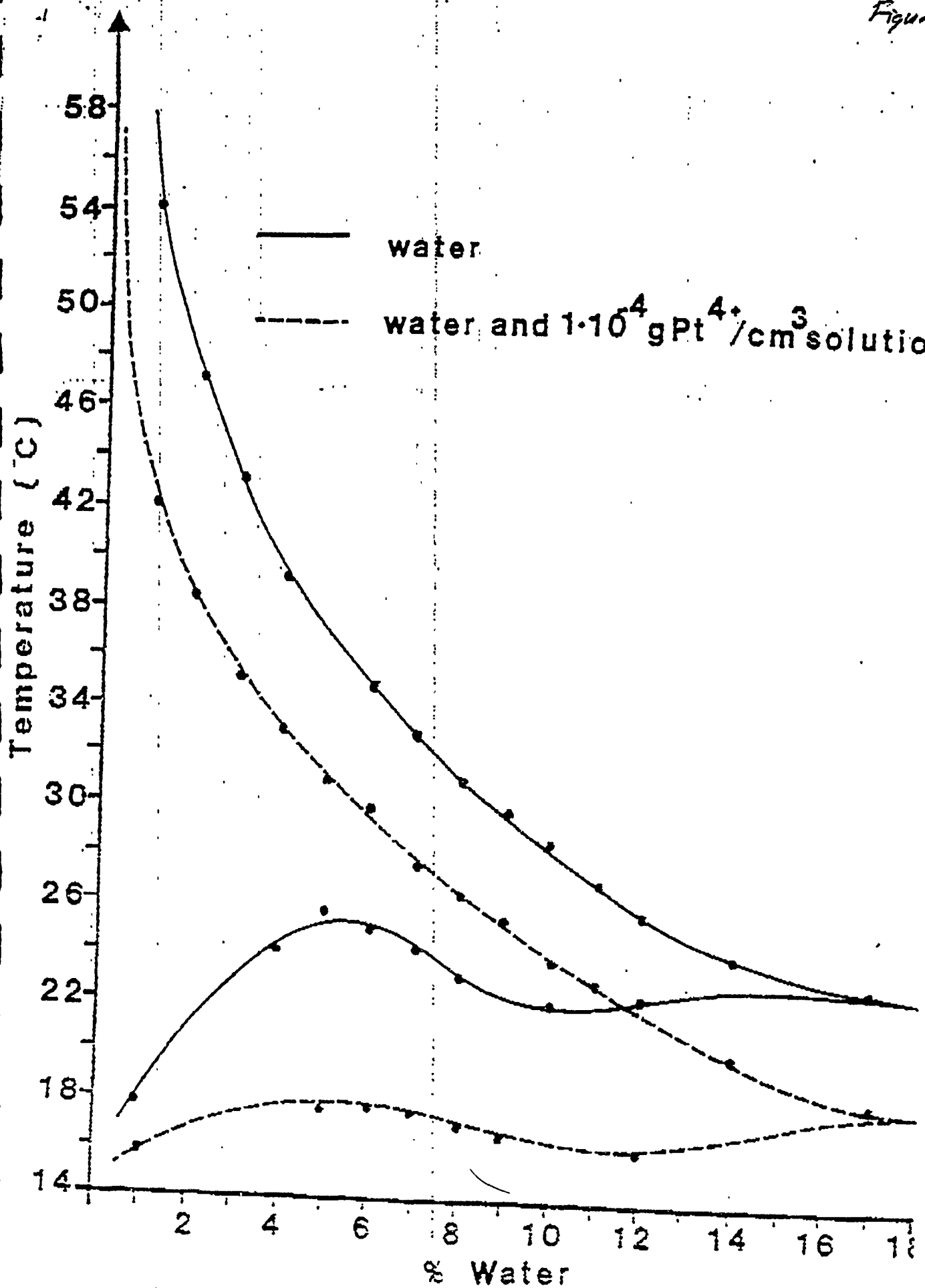
water
water and $1 \cdot 10^{-4}$ g Pt^{4+}/cm^3 solution
Temperature (°C)
58
54
50
46
42
38
34
30
26
22
18
14
2
4
6
8
10
12
14
16
% Water

Figur 7

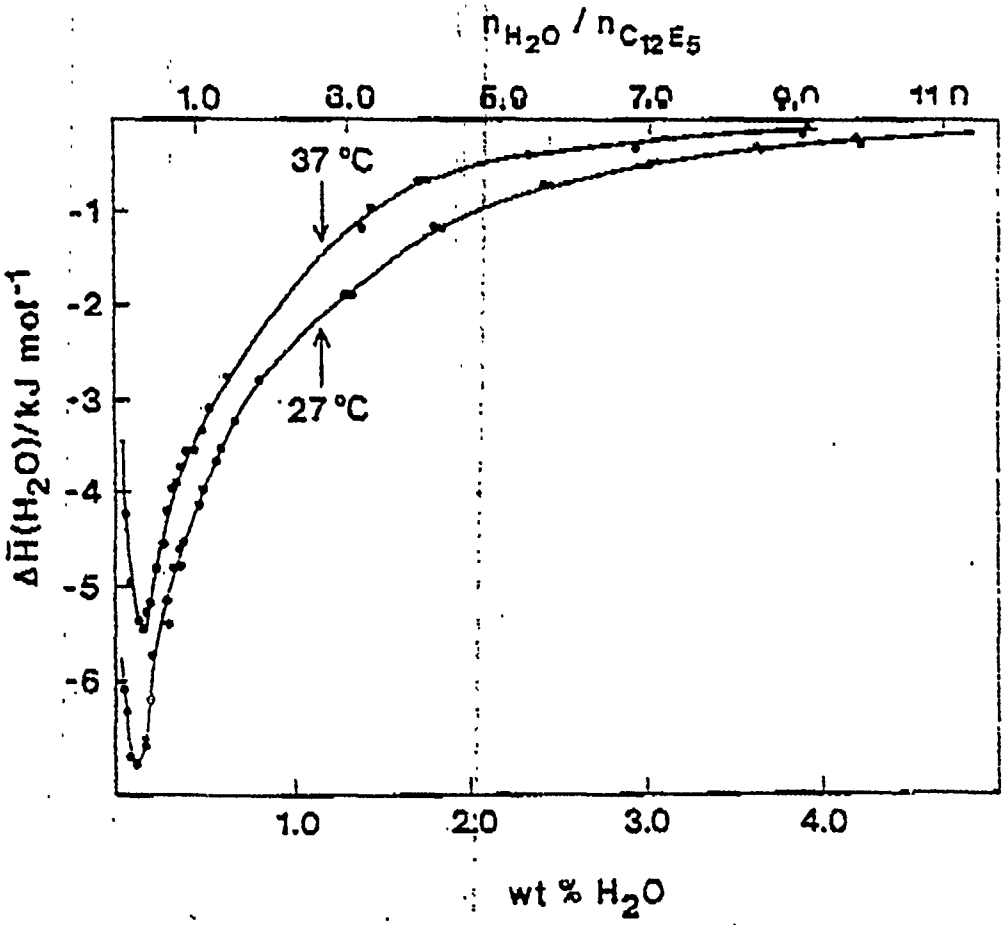

II-216

(20) Modern Aspects of Colloidal Metal Catalysis

Paul Mulvaney, Arnim Henglein and Thomas Linnert
Hahn-Meitner Institut, D-1000, Berlin, 39
Germany.

(1) Introduction:

The catalytic properties of colloidal metals have attracted interest ever since Faraday produced the first gold sols in 1856-57. Colloidal Pt has long been used as a hydrogenation catalyst, and is also well known for its efficacious catalysis of peroxide and hydrazine decomposition. In recent years, attention has focussed on the possible role of colloidal metals as catalysts in water splitting systems (1-3), and currently there is growing interest in the size-dependence of metal cluster redox potentials (4-7).

In this chapter, however, we will concentrate primarily on summarizing some of the salient features of colloidal metal catalysis, which have been elucidated over the last ten years or so. Detailed reviews on the preparation and characterization of catalytically active metal colloids are presented elsewhere in this book. We also present some of our own results which hopefully demonstrate some new aspects of the field of small metal particle research.

(2) Mixed Potential vs. Specific Site Model

The intervention of colloidal metals as catalysts is due to their ability to store reducing agents, and to modify reaction pathways through stabilization of intermediates which would in aqueous solution have very positive formation enthalpies. This ability arises primarily from the unsaturated surface coordination of the surface atoms, which allows strong, primarily dative, bonding from adsorbed substrates to the surface metal atoms, which is facilitated by the large density of unoccupied states just above the Fermi level.

In principle, metal catalysis of electron transfer processes can proceed by two intrinsically different mechanisms. According to the specific-site model, reactants experience higher rates of reaction because of preferential accumulation at the interface. This mechanism is useful for explaining micelle-catalyzed reactions, where both electric field effects and hydrophobicity lead to selectivity, as well as acceleration or inhibition of reactions (8). The effects of reduced dimensionality on reaction kinetics have also been discussed extensively (9). Generally, the reaction pathway is not altered during catalysis in micellar or microemulsion systems, just the rate of product formation.

In metal colloid systems the products themselves are often different. The metal particles stabilize surface intermediates, allowing them to build up to a high enough concentration that they can initiate new product pathways, particularly, it enables a variety of second order reactions to occur, which would not take place in bulk solution. Of particular importance are those involving H atoms. For example, hydroxyalkyl or benzophenyl radicals in bulk solution usually dimerize or disproportionate, by a simple, single H atom transfer.

$$2ROH\cdot \longrightarrow RO + RHOH \quad [1]$$

or $$2ROH\cdot \longrightarrow HO\text{-}RR\text{-}OH \quad [2]$$

In the presence of colloidal Pt, hydrogen is formed (10-12).

$$2ROH\cdot \xrightarrow{Pt} 2RO + H_2 \quad [3]$$

Spiro and coworkers extensive investigations of mixed potentials at Pt electrodes and colloids have clearly demonstrated that the mixed-potential (MP) mechanism is most apt for explaining colloidal metal catalysis (13). Particularly convincing is the fact that catalysis is strongly correlated to the exchange currents of the individual reactants, when measured directly using an electrochemical cell with the metal in question. The MP model assumes that a short, conducting path exists between oxidation and reduction sites; this implies they will be at the same electric potential. Catalysis is then not limited to specific sites on the surface, but occurs homogeneously over the surface. When a macroscopic distance is involved, then an ohmic drop may exist between the reaction sites, as is often the case during corrosion of metal surfaces, and as is generally the case in enzyme catalysis (14).

In the following we derive the mixed potential of a metal particle in aqueous solution during a simple redox reaction. Unlike the conventional electrochemical method we choose as our reference potential, the potential in the bulk aqueous solution. The potential at the surface of the particle is then measured with respect to the potential of zero charge (pzc) of the particle, which would be found at a potential E_{pzc} (NHE).

The primary reason for this modification is that the majority of colloidal catalysis experiments are carried out under conditions where no electrochemical measurements are possible. Furthermore, very few radicals possess reversible redox potentials. Unless the electrochemical rate constants are at least 1 cm s^{-1} or greater then a redox potential will not be established by a radical before recombination in solution takes place ($t_{1/2}$~10μs) (15). Only a few reduction potentials have been measured directly, using the technique of pulse-radiolysis-polarography

(PRP) (15), and by flash-photolysis-polarography (FPP) (16). These generally reveal irreversibility, which in many cases is due to strong changes in reorganization energy and also to hydrolysis reactions, especially in the case of organic radicals.

We consider a simple one electron redox reaction, in which a donor species D reduces an acceptor A. The two species have a low rate of reaction, so that electron transfer occurs via the Pt colloid particles in solution. The net rate of transfer of electrons to unit area of a particular particle (mol cm^{-2} s^{-1}) by the donor couple (couple 1) is given by the Butler-Volmer equation

$$j^1 = k^{f1}_{pzc} [D^+] \exp(-\alpha_1 y) - [D] k^{b1}_{pzc} \exp(\beta_1 y) \qquad [4]$$

where $y=e\psi/kT$ is the reduced potential, α_1 is the cathodic transfer coefficient, and β_1 is the anodic transfer coefficient ($\beta_1=1-\alpha_1$). k_{pzc} is the rate constant for electron transfer to (or from) the particle (cm s^{-1}) when it is uncharged, i.e. at the potential of zero charge. In the presence of D/D^+ alone, equilibrium occurs when $j^1 = 0$, i.e. at a surface potential

$$y^1_{eq} = e\psi^1_{eq}/kT = \ln \{k^{f1}_{pzc}[D^+]/k^{b1}_{pzc}[D]\} \qquad [5]$$

Note that although this is an equilibrium potential, it depends on the metal used, since k_{pzc} depends on the work function of the metal in question. In the presence of a second redox couple A/A^-, the presence of electrons at a potential y will be sufficient to drive the reduction of A at the surface at a net rate given by

$$j^2 = k^{f2}_{pzc} [A] \exp(-\alpha_2 y) - k^{b2}_{pzc} [A^-] \exp(\beta_2 y) \qquad [6]$$

The steady state (or mixed) potential occurs when $j^1 = -j^2$, which is also the rate of catalysis. Assuming $\alpha_1 = \alpha_2 = 1/2$,

$$y_{mix} = \ln \left[\frac{k^{b1}_{pzc} [D] + k^{b2}_{pzc}[A^-]}{k^{f2}_{pzc} [A] + k^{f1}_{pzc} [D^+]} \right] \qquad [7]$$

and the net rate of reaction is found by inserting the mixed potential into either eq.[4] or [6].

Eq.[7] is valid only for the case where the electron transfer is activation controlled. If the rate of reaction at the surface is fast enough, the supply of reactant from the solution becomes rate determining for that transfer step. For a neutral reactant, the rate constant (k_{diff} /$M^{-1}s^{-1}$) under diffusion control (mass transfer limit) is

$$k_{diff} = 4\pi R D N_a \times 10^{-3} \qquad [8]$$

where R is the radius of the colloid particle (cm), D the diffusion coefficient of the donor or acceptor species (cm^2s^{-1}), and N_a is Avogadro's number. The intermediate case of mixed transport and activation control can be treated by noting that at all times the rate of supply to the surface from the bulk must equal the rate of loss at the surface. Integrating Fick's equation, but allowing for a finite surface concentration yields

$$k_{obs}\, c_{bulk} = 4\pi R D N_a (c_{bulk} - c_{OHP}) = 4\pi r^2 k_{et}\, c_{OHP} \qquad [9]$$

where c_{OHP} is the concentration at the Outer Helmholtz Plane, which we assume is the plane of electron transfer. Rearrangement yields

$$k_{obs} = \frac{4\pi R^2}{(1/k_{et} + R / D)} \qquad [10]$$

Noting that $k_{et} = k_{pzc}\exp(-\alpha y)$, inclusion of mass transfer in eq.[4] leads to

$$j^1 = \frac{[D^+]}{(1/k^{f1}_{pzc}\exp(-\alpha_2 y) + R/D)} - \frac{[D]}{(1/k^{f1}_{pzc}\exp(-\alpha_2 y) + R/D)} \qquad [11]$$

A similar equation can be written for the acceptor couple A/A^- in eq.[6], and these two equations solved for the mixed potential for the general case of activation or diffusion control. Semiquantitative agreement with the MP model has been achieved in both kinetic and electrochemical investigations of radical induced hydrogen formation (17-20). The major difference between the derivation here and that presented by Miller et al.(17) is that the final particle potential is measured with respect to the bulk solution. To some extent the potential should therefore be amenable to direct measurement. The early work of Hauffe and coworkers (21) and later that of Bard et al. (22) clearly demonstrated that changes in metal oxide surface charge during photocatalysis could be measured by photoelectrophoresis.

For radical reactions at colloidal metal particles where the reaction is usually driven at comparatively high overpotential, Henglein proposed a simpler, Tafel form, in which the back reactions were neglected (23). By assuming a constant Helmholtz capacitance (K_I), and neglecting diffuse double layer effects, the surface potential can be approximated by $\psi=\sigma/K_I$, where σ is the surface charge density. The

stationary charge density on the particles during hydrogen evolution is then given by

$$\sigma = RTK_I/\alpha F \ln J - RTK_I/\alpha F \ln k_o[H+] \quad [12]$$

where J is the rate of electron transfer to the particle, which at high overpotential is almost independent of the charge already present. The accumulated charge was measured conductometrically. Both the pH and dose-rate dependence of the stationary colloid charge on gold and silver sols were in accord with eq.[12], as shown for the case of a silver sol in figure 1. (23).

The MP model ignores a number of features. Primarily it ignores the role of adsorption (which we will address in the following sections) and the effects of the electrical double layer around the metal particles. The double layer contribution is discussed in detail elsewhere in this book, and leads to further corrections for the effect of ionic strength on the reaction rates. Strictly speaking, the forms used here only apply at high ionic strength. These effects can also be quantified when the point of zero charge is used as the reference point. For Pt electrodes, the pzc has been found from capacitance measurements and charging curves to be 0.15-0.18V NHE. An extensive evaluation of literature values concerning the pzc of Pt is given in ref.24. The Pt electrode is Nernstian at partial pressures of $H_2 > 10^{-6}$atm (25). Below this, the potential is constant.

(3) Electrochemical and Double Layer Effects

The hydrogen evolution reaction is the most extensively studied reaction on colloidal metals. Generally, metals can be categorized according to the free energy of adsorption of hydrogen (ΔG_{ads}) on the metal surface. ΔG_{ads} is generally correlated with the d-band metal character(26,27). For metals with low ΔG_{ads}, reaction 13 the discharge of protons to form adsorbed H atoms - is rate determining. The steady state coverage of H atoms during hydrogen gas evolution on these metals is low (around 2-4% for Au at 0.1-0.2V overpotential) (28). In most other cases, H atoms are formed at a rate which is faster than their discharge at the surface. Two paths for the discharge of H atoms can be envisaged. For Pt and Pd, the dimerization of surface H atoms is the most likely, as demonstrated by numerous electrochemical investigations, whereas the Heyrovsky mechanism is often invoked for intermediate cases (26). The Heyrovsky path in colloidal catalysis is slightly different to the conventional mechanism, since electrons are provided by the solution, not through an external circuit.

$$H^+ + e^- \quad \text{----> } H_{(ads)} \quad \text{Discharge Step} \quad [13]$$

$H_{(ads)} + H^+ + e^- \text{----> } H_{2(ads)}$ Heyrovsky Desorption [14]

$H_{(ads)} + H_{(ads)} \text{----> } H_{2(ads)}$ Surface Recombination [15]

In eq.[14], the adsorbed H atom can react with an electron already on the metal, if the Fermi level is at a sufficiently negative potential, or it can be reduced by an electron donated directly by another radical. At a normal metal electrode, all electrons arrive through the metal. If the electron is donated by a radical to the colloid, it does not have to arrive at the Fermi level but may still be at its own redox potential. If the surface coverage is reasonably high, we may argue that the electron is donated directly to an adsorbed H atom, together with a proton. This would allow the full redox energy of the radical to drive the reaction, since if the electron is transferred to the metal, the electron cascades immediately down to the Fermi energy, via electron-phonon interactions, and the energy is lost as lattice vibrations. Although the H atom is generally considered only as a reductant (-2.0V), or an H atom scavenger, it can be quite easily reduced. Using the PRP technique, it was shown that at a dropping mercury electrode a null current occurs at only -0.2V SCE, and significant partial currents were flowing at this potential (15). Between -0.2 and -0.4V SCE, significant cathodic current was observed, i.e. H atom reduction.

The colloids of the noble metals Pt, Pd and Ir are characterized by low surface charges; the transferred electrons exist primarily as H atoms on the surface. The noble metals start to adsorb hydrogen at potentials anodic of the reversible potential, and this can be directly monitored by capacitance measurements. These show that the fractional surface coverage amounts to 0.59, 0.77, 0.65, 0.69 for Rh, Pt, Ir, and Pd respectively as the potential is gradually shifted from anodic potentials up to around 0V NHE (29). Hydrogen continues to adsorb at more negative potentials but the measurements are complicated by hydrogen evolution. For Pt and Pd, monolayer coverage seems to be the equilibrium case under any cathodic bias. In addition Pd *absorbs* hydrogen. In equilibrium with 1 atm of hydrogen gas, a Pd electrode absorbs 0.69 H atoms per metal atom (30). For small colloidal particles, this contribution is far more important than the adsorbed H atom concentration. The adsorption of H atoms is best described by an electrochemical isotherm, in which the dependence of the coverage on potential is calculated. Generally a modified Langmuir isotherm is necessary, since the free energy of adsorption decreases with coverage due to repulsion between the adsorbed surface H atoms. The Langmuir isotherm assumes a constant adsorption free energy, ΔG^o, whereas the Frumkin isotherm includes a correction which is assumed to depend linearly on the coverage.

$$\Delta G = \Delta G^{o} - gR\theta \qquad [16]$$

Here ΔG^{o} is the free energy of adsorption at a bare surface, and g is a term which reflects either attractive ($g<0$) or repulsive ($g>0$) surface forces between adsorbed H atoms. The coverage as a function of potential is given by

$$\theta/(1-\theta)\exp(\Delta G^{o} - gR\theta) = K\,[H^{+}]\exp(FE/RT). \qquad [17]$$

where K is a constant. At intermediate coverage, an approximately linear dependence on potential is predicted, which is reasonably well borne out by charging curves on Pt electrodes (29). The hydrogenation of a substrate will depend on the amount of coadsorbed reactant. A more negative potential will increase the free energy of hydrogenation, but the adsorption may be reduced by the high H coverage. In order to facilitate reduction of CO_2 or NO_3^-, more polarizable metals maybe better, where a greater range of negative potentials is attainable, and H atom adsorption is smaller. CO_2 has been photocatalytically reduced on Ru and Os sols although significant amounts of hydrogen are also produced concomitantly (30), and nitrate is reduced to NH_3 on silver sols by radiolytically produced radicals (31). In the case of CO_2 reduction on Ru, an interesting inhibition effect has been observed using bipyrazine which minimizes the coproduction of H_2. Conversely CO_2 reduction is eliminated at the expense of increased hydrogen evolution by the presence of surface active dithiothreitol (30). Clearly the key to understanding and controlling these catalytic processes depends on being able to monitor the concentration of surface species. Techniques such as SERS (32) and isotope exchange (33) have been used to detect adsorbed surface intermediates or to determine the mechanism of catalysis. Recently it has been shown that NMR can be used to identify and measure the concentration of CO adsorbed to colloidal Pd (34).

Interestingly, a number of workers have reported that the yield of hydrogen increases almost quadratically with colloid concentration. This result has been observed both by fast kinetic techniques (35,36) and by steady state measurements (11,17b). It is especially surprising in the case of the steady-state measurements because the stationary radical concentration is too small for second-order kinetics to be important. Particle-particle charge transfer, and other possibilities have been invoked to explain this effect. A first-order dependence on [Pt] was found by Rabani et al. for the reaction with $ZV^{\cdot}$, but a second-order dependence for the reaction with MV^{2+} (37). The most likely explanation of these effects is that the radicals react only with the free colloid surface. In the absence of equilibrium (i.e. well-defined pH and

hydrogen pressure) the amount of adsorbed H is not known. Consistent with this is the observation that (a) an increase in the hydrogen pressure leads to a slower rate of reaction of MV^+ with colloidal Pt (19,35), and (b) that pre-saturating a sol with H_2 causes a reversion back to a first-order dependence on [Pt] (19,35).

From these kinetic results it seems clear that a more complete account of the catalysis must include the active surface area in the rate equations in eqs.[4]-[11], instead of the geometric area, since in the case of MV^+ at least, it is clear that electron transfer takes place only at the bare Pt surface. The electrochemical data assimilated using the adsorption isotherm in eq.[17] can in principle be used to determine hydrogen coverage on sols, and to estimate the effective surface area, but only when the electrode potential can be correlated with the pzc of the metal sols.

In view of the non-linear dependence on colloid concentration, it is still interesting to ask whether a bicolloidal catalytic mechanism is possible during catalytic water-splitting. During a Brownian encounter between two colloid particles, the diffuse double layers of the approaching colloid particles overlap. If the colloid particles are negatively charged, then the overlap causes the surface potential and zeta potential to become more negative. The concentration of positively charged donors (e.g. MV^+) and acceptors (H^+) at the Outer Helmholtz Plane is therefore increased, which results in a temporary increase in the rate of H atom formation. The overlap acts like a temporary cathodic pulse. If this reaction step is reversible then as the particles separate again the reaction would also be reversed as the field decays. However if the dimerization of H atoms is at least as fast as the back reaction (in eq.[13]), then the overall rate of reaction may be enhanced. The important criterion is that the overlapping electric fields should drive an irreversible step in the reaction sequence. It is of interest that according to this mechanism, thermal energy would effectively be channelled into chemical energy via the double layer electric field. The lifetime of a Brownian encounter (τ) can be crudely estimated as $\kappa^{-2} \sim 2D\tau$, where κ^{-1} is the double layer thickness ($\sim 10^{-6}$cm at 1mM ionic strength), and, D the colloid diffusion coefficient ($\sim 10^{-7} cm^2 s^{-1}$). This yields $\tau \sim 10\mu s$. If H atom formation is able to compete on this timescale, then bicolloidal catalysis may be possible.

(4) Optical Changes- Electromodulation and Adsorption Effects

The previous sections give a brief overview of the advances made, and difficulties involved, in the study of colloid catalysis. But it is necessary to probe the state of the metal surface to come to a more complete understanding of catalytic mechanisms. A promising technique for examining changes in surface characteristics of colloidal metals

during catalysis may be electromodulation, in which the effect of charge transfer on the optical properties of the metal particles themselves are measured. When electrons are added by reducing radicals to colloidal silver, for example, the surface plasmon absorption band at 380nm is found to be blue-shifted; at the same time, the intensity of the band increases, and the full-width of the absorption band at half-maximum intensity (FWHM) decreases (38). Conversely, when electrons are extracted by OH radicals, a corresponding red shift is found, and the band broadens and decreases in intensity. This is shown in figure 2, where the difference spectrum after electron or hole injection has been measured using pulse radiolysis. These effects can be explained in terms of electromodulation, which was originally observed by Hansen et al. during reflection measurements on silver and gold electrodes (39). A theoretical explanation was given by McIntyre et al. (40). In the case of colloidal materials, the electromodulation model is coupled to theories outlining the optical properties of colloidal metals. The absorption spectrum of colloidal silver can be predicted by combining Mie theory with the Drude model for free electron metals (41). This has been found to give good agreement for silver and gol sols in glasses. The absorption coefficient for the sol is given by

$$A= 9\pi NVn_o3c\lambda^2/\sigma * ((\lambda_m^2-\lambda^2)^2 + \lambda^2\lambda_m^4/\lambda_a^2) \quad [18]$$

where $\lambda_m^2=\lambda_c^2(\varepsilon_o +2n_o^2)$ is the wavelength at which maximum absorption occurs, n_o is the refractive index of the medium, and

$$\lambda_c^2=(2\pi c)^2m/4\pi N_e e^2 \quad [19]$$

is the plasma wavelength, λ_c, of the bulk metal in terms of the effective electron mass ($m=0.997m_o$ for Ag) and the electron density, N_e (cm^{-3}). The absorption is proportional to N, the number of particles per unit volume, and V, their volume.

The plasma frequency depends on the free electron concentration in the particle. When strongly polarized, the plasma frequency is changed, the amount depending on the fractional change in N_e. The actual change in N_e depends on the thickness over which the electrons are spread. This is of the order of the Thomas-Fermi screening length, say 1-3Å. For a sol with r=15Å, this means the electrons are distributed throughout 40% of the particle's volume. i.e. in metal sols the internal double layer volume can constitute a large fraction of the metal. For a narrow Lorentzian band the FWHM of the plasma absorption is given by

$$w=\lambda_m^2/\lambda_a = (\varepsilon_o+2n_o^2)c/2\sigma \quad [20]$$

where σ is the particle's d.c. electrical conductivity ($\sigma=N_e e^2R/mu$), and $\lambda_a = 2\lambda_c^2\sigma/c$. It is important to note that the electrical conductivity influences both the FWHM and the intensity of the band. Since this varies linearly with particle size, the absorption band of silver sols depends on the polydispersity and average size. From eq.[20], it is seen that the band narrows with increasing charge density, and through eq.[19], the position of the absorption band maxima is shifted to shorter wavelengths under cathodic polarization. Thus the optical spectrum can in principle be used to determine whether a silver sol is cathodically or anodically polarized. One difficulty is to determine the null point .i.e. the wavelength of the plasma maximum when the silver colloid is uncharged. The shift of the absorption maximum is monotonic with charge and it simply continues to redshift as the sign of the surface charge switches from negative to positive. Doremus (41) and Kreibig (42) have shown that for silver particles formed in glass matrices (n_0=1.50), the maximum lies at 406±1nm. For an aqueous solution with n_0=1.33, this corresponds to 385±1nm. Thus we assume λ_{max}(pzc) = 385nm. A sol with a maximum at shorter wavelengths is assumed to contain excess electrons, a longer wavelength maximum corresponding to a sol with excess silver ions at the surface. Note, the role of adsorbed or stabilizing ions do not contribute here and to obtain the net charge on the sol, must be added separately. This plasma null potential (pnp) only indicates whether the particles are electron rich or deficient, and does not correspond to a silver electrode biased at the potential of minimum interfacial capacitance, since this corresponds to the potential where the total net charge on the electrode is zero. At the pnp, preferential adsorption of either anions or cations still takes place. Indeed, we will show below that silver sols must be cathodically polarized to induce the desorption of iodide ions.

Cathodically polarized sols can be prepared by using radiolytically or photolytically generated reductants. A simple method consists of photolysing a solution of silver ions and HMP with light at λ<280nm in the presence of acetone and 2-propanol. Initially the radicals reduce the silver ions to form a yellow solution of colloidal silver. The quantum yield is 2.0, after a small induction period. When the silver ions are fully reduced, the radicals continue to add electrons to the colloidal particles. During photolysis, the absorption band builds up at 384nm, and then as the reduction of silver ions finishes, the band shifts to shorter wavelengths. Under optimal conditions, it is found that the plasma band can only be shifted to about 374nm even under extremely strong reducing conditions (38)(reducing radicals produced at about 100μMs^{-1}). This point seems to correspond to the point where hydrogen evolution

prevents further polarization. Similar observations have been made by Kolb et al. during electroreflectance measurements on silver electrodes (43).

At first sight it seems a little extraordinary that the plasma frequency can be so strongly shifted by the addition of solution oxidants and reductants. A shift from 400nm to 375nm corresponds to a difference of 14% in the free electron density. But the mixed potential of a sol is achieved by double layer charging. For small particles the ratio of surface charge to volume charge becomes significant when the double layer charge is of the same order as the colloid aggregation number. A stationary concentration of some 500 electrons per particle (N_{agg} ~10^4) has been determined by conductivity measurements (23). For polarizable metals, the large change in free electron density means that the kinetic Fermi energy is significantly altered during reduction. This will contribute to the value of k_{pzc}, since the density of occupied and unoccupied states around E_f is altered. In the transient difference spectra of figure 2, there is a second bleaching signal observed around 300-330nm when the particle contains excess electrons. This is the wavelength regime where d-band to Fermi surface direct transitions begin to take place. The d-band in silver lies about 4eV below the Fermi energy. The bleaching signal may reflect the effect of band-filling of the metal particles at the Fermi level, which leads to a bleaching of those transitions to states directly above the Fermi level.

Whilst the effect of electron transfer on the plasma absorption of silver is quantifiable, it has been found that adsorbents tend to damp the absorption. This was the case for I^-, CN^-, S^{2-}, thiols and carboxy thiols. This is apparently due to changes in the dielectric constant of the surface layer around the particles, which means the resonance condition for plasma absorption ($\varepsilon_{Ag} = -\varepsilon H_2O$) is no longer fulfilled. Particularly interesting is the fact that the adsorption of I^- on colloidal silver causes the CTTS band at 229nm to disappear, due to the break up of the water structure around the hydrated anion. This allows the measurement of the adsorption of I^- on silver sols. This is shown in figure 3(a). As is seen even adsorption of small amounts of I^- leads to damping of the 380nm band, but no increase at 229nm, until $3.0.10^{-5}$M is added, at which point, the absorption at 229nm suddenly appears (see inset 3(a)). At this point, no further changes in the 380nm band are seen either. From the known particle diameter of 30Å, we readily find that the number of surface atoms is about $2.8.10^{-5}$M, i.e. the I^- adsorption reaches monolayer coverage, after which no further adsorption occurs. The iodide covered silver sols can now be polarized cathodically, by means of photolysis. In the presence of acetone and 2-propanol, illumination with 280nm light leads to

$(CH_3)_2CO$ ---> $(CH_3)_2CO$ (T_1) [16]

$(CH_3)_2CO$ (T_1) + $(CH_3)_2CHOH$ --->2$(CH_3)_2COH$ [17]

2$(CH_3)_2COH$ + Ag_n..(I^-_{ads}) ----> 2$(CH_3)_2CO$ + Ag_n^{2-} + $I^-_{(aq)}$ + 2H^+ [18]

The spectrum of such a solution before and after photolysis at pH 11.8 (to minimize the rate of electron loss by proton reduction) is shown in figure 3b. As can be seen, the plasma band almost completely recovers to its intensity prior to iodide addition (figure 3(b)), and simultaneously, the 229nm band due to $I^-_{(aq)}$ increases rapidly in intensity. About 60% of the I^- could be desorbed by the cathodic charging. The readsorption of I^- takes place very slowly (over an hour or more) once the charging is halted. At pH 4, much smaller amounts of I^- could be removed, and the readsorption took place much more quickly initially (50% in 1 minute,) but then this slows down. Thus even during H_2 evolution on colloidal silver some I^- remains chemisorbed to the surface. Iodide adsorption on Pt at potentials >0V NHE completely suppresses H adsorption (44).A model for the adsorption energetics has been described elsewhere(45).

(5) Photochemistry of Colloidal Metals - Photoelectron Emission and Hot Holes:

Until now, virtually all colloid photocatalysis schemes have focussed on the use of semiconductors as light harvesting units, the metal simply acting as a catalyst to guide the energy of the conduction band electrons towards suitable product pathways. The photochemistry of colloidal metals has been neglected, apparently because of the assumption that electrons and holes would thermalize too quickly to take part in photochemical reactions. However as long ago as 1839, photocurrents were observed when metal electrodes were illuminated - the well-known Becquerel Effect (46). Quantum yields for photoelectron emission into solution of the order of 10^{-5}-10^{-4} were found by Sass et al.(47). For colloidal metals, the particle radius is much smaller than the scattering length of electrons at the Fermi level. An electron at the Fermi energy of silver has a velocity of v_f=1.4.10^8 cms^{-1}, and will reach the surface of a particle within a few femtoseconds (t ~ v_f/r ~1.4.10^8 cms^{-1} /2.10^{-7}cm ~1fs), whereas the thermalization takes 2-3ps, as directly observed recently by thermomodulation experiments with a femtosecond laser (48), and as expected from an electron-phonon collision time of 3.7x10^{-14}s (42). (Assuming a loss of ~0.02eV per collision, this is an energy loss rate of ~1V ps^{-1}). Thus excited electrons and holes may directly reach the surface and may either thermalize,recombine or react with adsorbates if such transfer is rapid on a ps timescale. An enhanced rate of photodissolution was found for colloidal silver (Φ=10^{-3}-10^{-2}) in the presence of N_2O, as shown in figure

4. This can readily be explained by the higher yields of hot electrons that reach the surface of photoexcited, nanosized metal particles. At the present time, it is difficult to distinguish between capture of hot electrons by adsorbed N_2O and capture of hydrated electrons. The quantum yields are therefore interpreted as though due to photoelectron emission and irreversible scavenging in bulk solution.

However, the state of the surface can influence the photoelectron yield. When cyanide ions are present during photolysis, but no nitrous oxide, the colloids still dissolve, but form hydrogen gas and silver cyanide as the corrosion products (49).

$$2Ag + 4CN^- + 2H_2O \xrightarrow{h\nu} 2Ag(CN)_2^- + H_2 + 2OH^- \quad [19]$$

At the present time, the following mechanism can be tentatively proposed to explain the enhanced yields. Cyanide ions remove any excess silver ions from the surface of the silver particles and bind to the colloid surface. Light absorption creates holes which can be captured by cyanide ligated surface silver atoms to yield AgCN molecules. This increases the lifetime of electrons, so that the yield of photoemitted electrons is increased. Hydrated electrons can then react with protons to form H atoms in the solution, which then form hydrogen gas, possibly via a Heyrovsky type reaction, as discussed earlier. The AgCN molecule at the surface reacts with a second CN- and desorbs from the surface. The colloid does not gain additional Ag+ ions this way, which would normally enhance the rate of back electron transfer by e-(aq) in the absence of a complexing agent.

References:

1. Grätzel, M. "Heterogeneous Photochemical Electron Transfer", CRC Press, Bocca Raton, 1989.
2. M.A. Fox ; Topics In Current Chemistry **142,** 71 (1989).
3. M. Kirch; J.M. Lehn; J.P. Sauvage; Helv. Chim. Acta; **62,** 1345 (1979).
4. T.Linnert; P.Mulvaney; A.Henglein; H.Weller; J.Am. Chem. Soc. **112,** 4657 (1990).
5. P.Mulvaney; A.Henglein; J.Phys. Chem. **94,** 4182 (1990).
6. P.Mulvaney; A.Henglein; Chem :phys. Lett. **168,** 391 (1990).
7. M.Mostafavi; N.Keghouche; M. Delcourt; J.Bellioni; Chem.Phys. Lett.**167,** 193 (1990).
8. J.H. Fendler and E.J. Fendler "Catalysis in Micellar and Macromolecular Systems", Academic Press, N.Y., 1975.
9. See chapters 3 and 4 in "Kinetics and Catalysis In Microheterogeneous Systems" vol. 38 in "Surfactant Science Series" (ed. M. Grätzel and K. Kalyansundaraum), Marcel Dekker, N.Y.1991.
10. M. Grätzel and C. Grätzel; J. Am. Chem. Soc. **101,** 7741 (1979).

11. D. Meisel; J. Am. Chem. Soc. **101,** 6133 (1979).
12. B. Lindig; J. Westerhausen; A. Henglein; J. Phys. Chem. **85,**1627 (1981).
13. (a) M. Spiro; J. Chem. Soc. Fara. Trans. 1 **79,** 1507 (1979).
(b) M. Spiro and A. Ravno; J. Chem. Soc. 78 (1965).
(c) M. Spiro and P.L. Freund; J. Electroanal. Chem. and Interfacial Electrochem. **144,** 293 (1983).
14. A.K. Vijh in "Modern Aspects of Electrochemistry" vol.17, p.113, (ed. J.O'M. Bockris, B. E. Conway, R.E. White), Plenum Press, N.Y. 1986.
15. A. Henglein in "Electroanalytical Chemistry". vol.9 (ed. A.J. Bard) p.163, Marcel Dekker, N.Y. (1976).
16. (a) G.C. Barker; A. W. Garner; D.C. Sammon; J. Electrochem. Soc. **113,** 1182 (1966).
(b) G.C. Barker and J.A. Bolzan; J. Electroanal. Chem. and Interfacial Electrochem. **49,** 239 (1974).
17. (a) G. McLendon in Energy Resources through Photochemistry and Photocatalysis (ed. M.Grätzel) Academic Press N.Y. 1983.
(b). D.S.Miller; A.J.Bard; G.McLendon; J.Ferguson; J. Am. Chem. Soc. **103,** 5336 (1981).
(c) D.S.Miller; G.McLendon; J. Am. Chem. Soc.**103,** 5336 (1981).
18.. M. Brandeis; G.S. Nahor; J.Rabani; J.Phys. Chem. **88,** 1615 (1984).
19. T.W. Ebbesen; J.Phys. Chem. **88,** 4131 (1984).
20. M. Venturi; Q. Mulazzanni; M.Z. Hoffman; J.Phys. Chem. **88,** 912 (1984).
21. K.H. Hauffe; ch.9 in "Electrochemistry", (ed. H. Bloom and F. Gutman), Plenum Press, 1977.
22. A.J. Bard; D.S.Miller; J.Am.Chem. Soc. **105,** 27 (1983).
23 A.Henglein and J. Lilie J. Am.Chem. Soc. **103,** 1059 (1981).
24. J.Llopis; I.M. Tordesillas; F. Colom; in "Encyclopedia of Electrochemistry of the Elements" vol.VI, (ed. A.J. Bard), Marcel Dekker, N.Y., 1976.
25. S. Schuldiner; B.Piersma; T.Warner; J. Electrochem. Soc. **113,** 573 (1966).
26. P. Delahay "Double Layer and Electrode Kinetics", J.Wiley and Sons N.Y., 1965.
27. J. O'M. Bockris and A.K. Reddy "Modern Electrochemistry" vol.2., Plenum Press, N.Y. 1970.
28. M. Breiter; C. Knorr; V. Volkl; Z. Elektrochem. **59,** 681 (1955).
29. R. Woods in "Electroanalytical Chemistry" vol.9, (ed. A.J. Bard) p.1, Marcel Dekker N.Y. (1976).
30. (a) I. Willner; R. Maidan; D. Mandler; H.Dürr; G. Dörr; and K. Zengerle; J.Am. Chem. Soc. **109,** 6080 (1987).
(b) Y. Degani; I. Willner; J. Chem. Soc. Perkin Trans. II 37 (1986).

31. (a) A. Henglein; J.Phys. Chem. **83,** 2858 (1979).
(b) A. Henglein; Ber. Bunsenges Phys. Chem. **84,** 253 1980.
32. R. Sobocinski; M.Bryant; J.E. Pemberton; J. Am.Chem. Soc. **112,** 6177 (1990).
33. K.Kopple; D. Meyerstein; D.Meisel; J.Phys. Chem. **84,** 870 (1980).
34. J.S. Bradley; J.M.Millar; E.W.Hill; M. Melchior; J.C.S. Chem. Comm. 705 (1990).
35. M. Delcourt; N. Keghouche; J. Belloni; Nouv. J. Chim. **7,** 131 (1983).
36. M. Matheson; P.C. Lee; D. Meisel; E. Pelizzetti; J.Phys. Chem. **87,** 394 (1983).
37. (a) G.S. Nahor; J.Rabani; J.Phys. Chem. **89,** 4541 (1985).
(b) G.S. Nahor; J.Rabani; Rad.Phys. Chem. **29,** 79 (1987).
38. A.Henglein; P. Mulvaney; T.Linnert; Disc. Fara Soc. 92 (1991).
39. (a) W.Hansen; A.Prostak; Phys. Rev. **160,** 500 (1967).
(b) W.Hansen; A.Prostak; Phys. Rev. **174,** 500 (1968).
40. J.D. McIntyre; Surf. Sci. **37,** 658 (1973).
41. R.H. Doremus; J.Chem. Phys. **42,** 414 (1965).
42. U. Kreibig; J.Phys. F: Metal Phys. **4,** 999 (1974).
43. (a) D.M. Kolb and R.Kötz Surf. Sci. **64,** 96 (1977).
(b) R.Kötz ; D.M. Kolb and J.K. Sass Surf. Sci. **69,** 359 (1977).
44. A.N. Frumkin; in "Advances In Electrochemistry and Electrochemical Engineeering", vol.3 (ed. P.Delahay) Interscience, N.Y., 1963.
45. A.Henglein; T. Linnert; P.Mulvaney; Ber. Bunsenges. Phys. Chem. **94,** 1449 (1990).
46. (a) E. Becquerel; Compt. Rend. **9,** 145 (1839).
(b) E.Becquerel; Ann. Chim. Phys. **56,** 99 (1859).
47. J.K.Sass; R.Sen; E.Meyer; H. Gerischer Surf. Sci. **44,** 515 (1974).
48. (a) G.L. Eshley Phys. Rev. B 33, 2144 (1986).
(b).E.J. Heilweil ; R.M. Hochstrasser; J. Chem. Phys. **82,** 4762 (1985).
49. T.Linnert; P.Mulvaney; A.Henglein; Ber. Bunsenges. Phys. Chem. (in press.)

Fig. 1

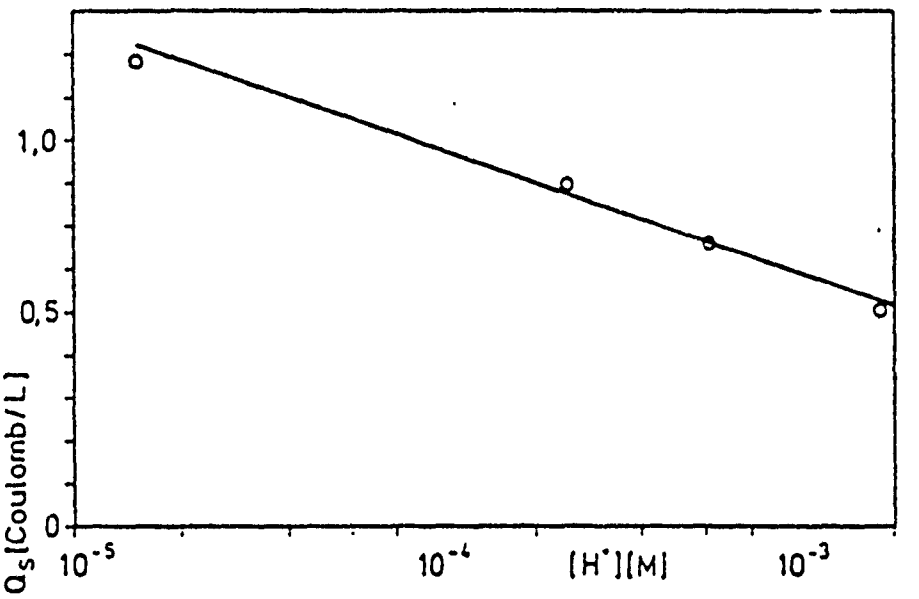

Figure 12. Stationary charge Q_s as a function of the H^+ concentration.

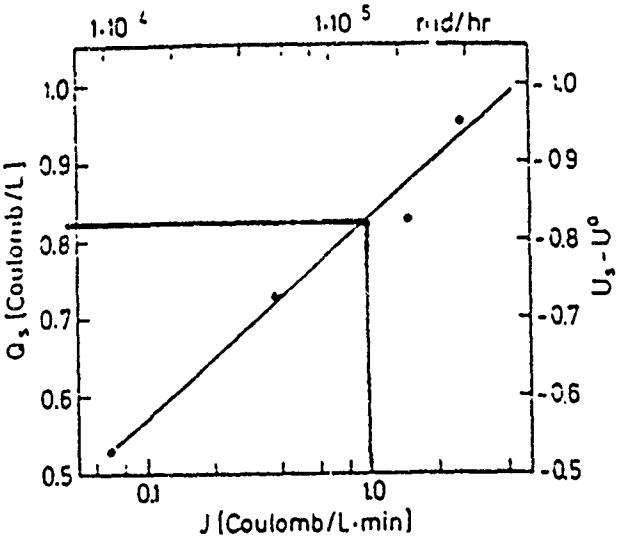

Figure 9. Semilogarithmic plot of the stationary charge Q_s (from the data in Figure 6) vs. the rate J of charge transfer (lower abscissa) or dose rate (upper abscissa). The ordinate scale on the right side gives the calculated potential difference $U - U^0$ (see section 4.3).

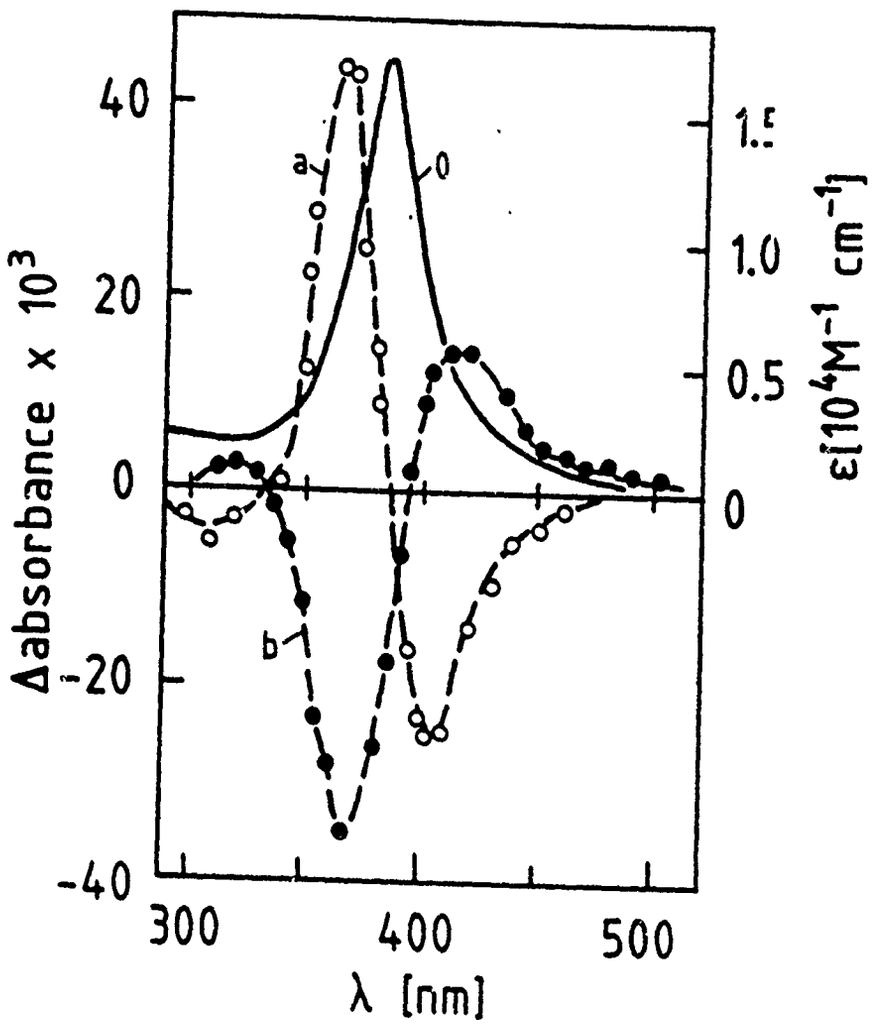
40
20
0
-20
-40
Δabsorbance x 10³
a
b
0
1.5
1.0
0.5
0
ε[10⁴M⁻¹ cm⁻¹]
300
400
500
λ [nm]

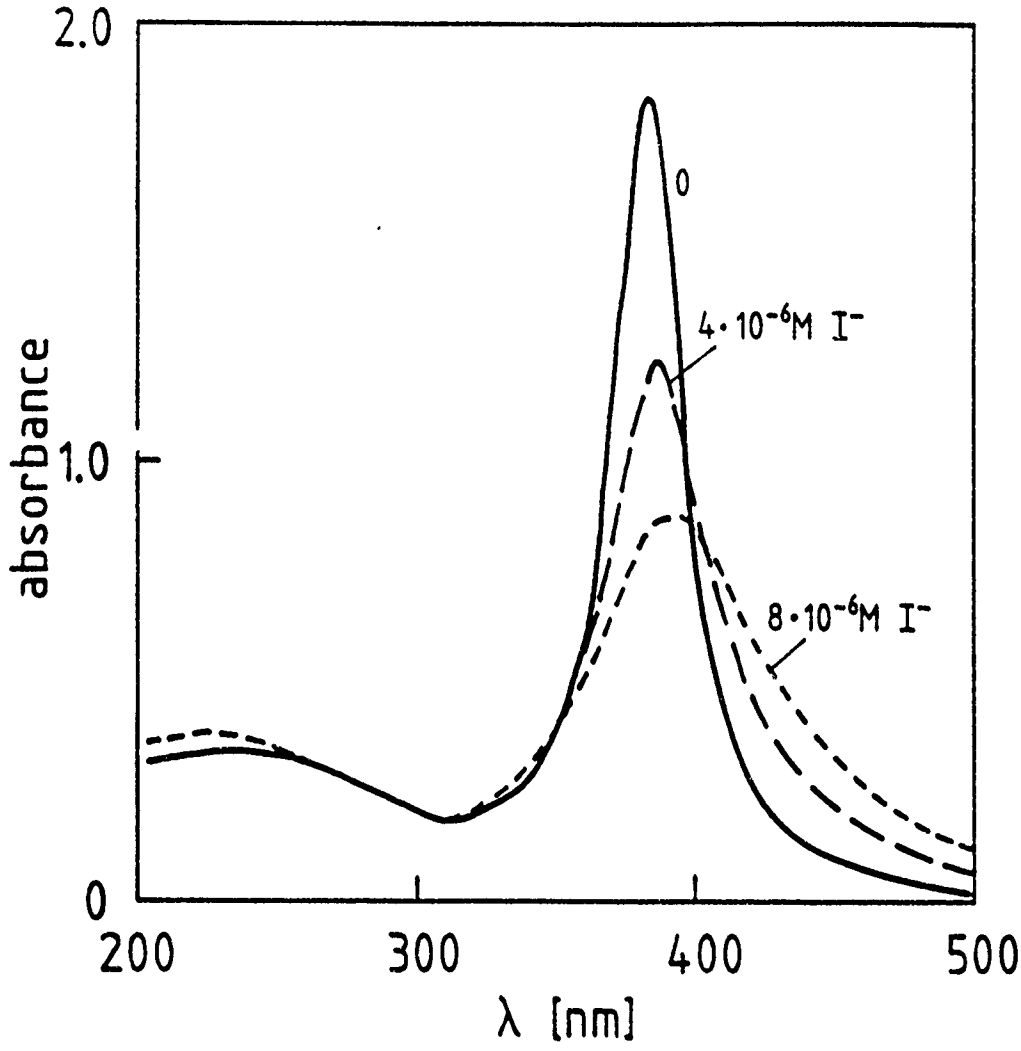
2.0
1.0
0
absorbance
200
300
400
500
λ [nm]
0
4·10⁻⁶M I⁻
8·10⁻⁶M I⁻

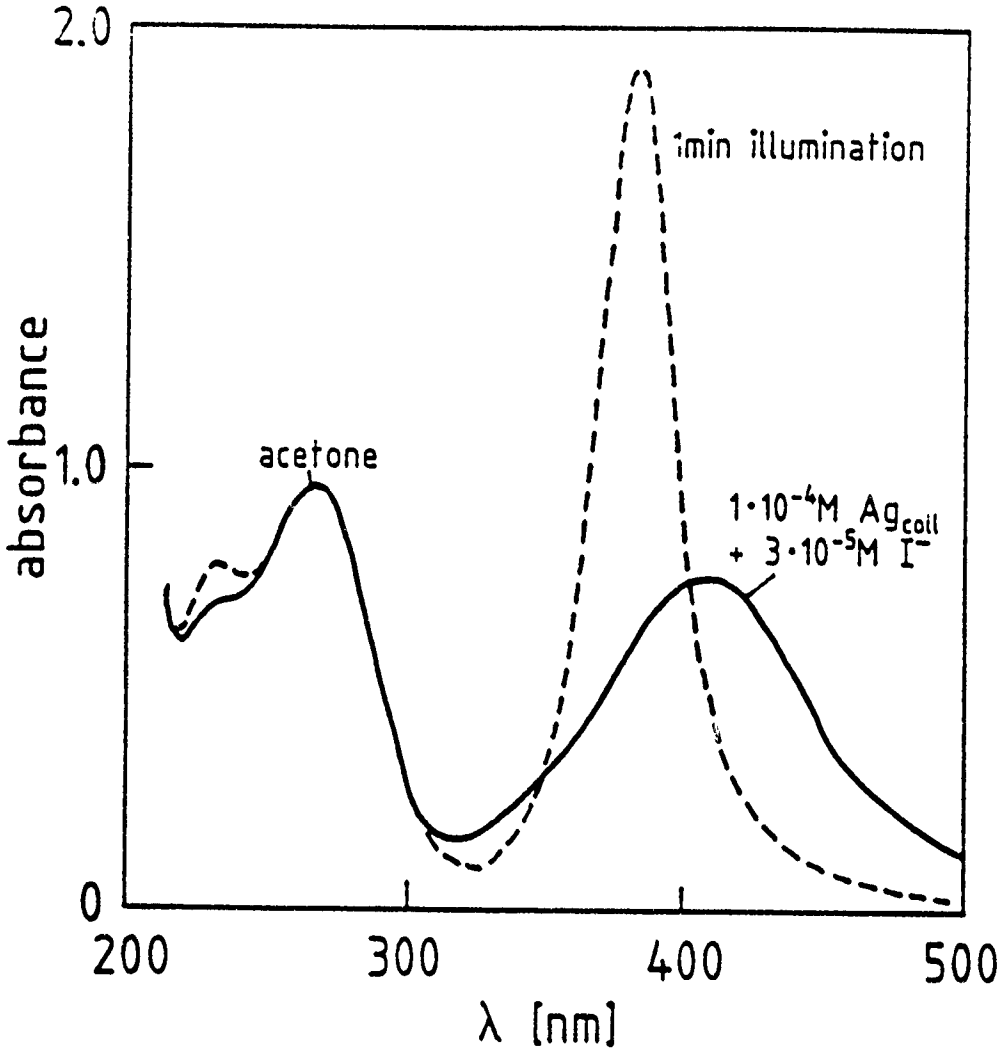
2.0
1.0
0
absorbance
1min illumination
acetone
1·10⁻⁴M Ag coll
+ 3·10⁻⁵M I⁻
200
300
400
500
λ [nm]

fig 3(b)

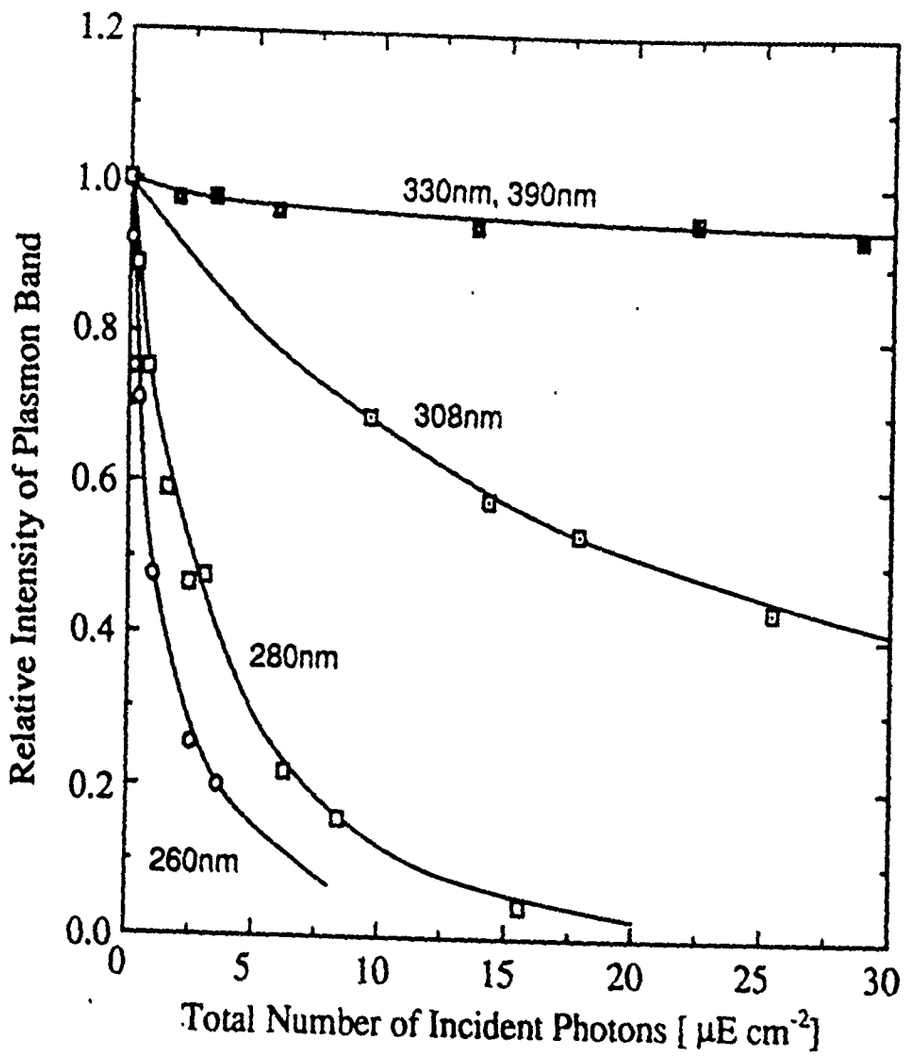
1.2
1.0
0.8
0.6
0.4
0.2
0.0
Relative Intensity of Plasmon Band
330nm, 390nm
308nm
280nm
260nm
0
5
10
15
20
25
30
Total Number of Incident Photons [μE cm-2]

II-236

fig. 4